Title
Bottom-up and Top-down Approaches to a Quantum Theory of Gravity

Author
Murdia, Chitraang

Publication Date
2023

Peer reviewed|Thesis/dissertation

Bottom-up and Top-down Approaches to a Quantum Theory of Gravity

by

Chitraang Murdia

A dissertation submitted in partial satisfaction of the

requirements for the degree of

Doctor of Philosophy

in

Physics

in the

Graduate Division

of the

University of California, Berkeley

Committee in charge:

Professor Yasunori Nomura, Chair
Professor Raphael Bousso
Professor Richard Borcherds

Summer 2023

Bottom-up and Top-down Approaches to a Quantum Theory of Gravity

Abstract

Bottom-up and Top-down Approaches to a Quantum Theory of Gravity

by

Chitraang Murdia

Doctor of Philosophy in Physics

University of California, Berkeley

Professor Yasunori Nomura, Chair

In this dissertation, we explore these two complementary approaches to quantum gravity – holography as a bottom-up perspective and string theory as a top-down framework.

On the holography side, we study two novel extensions of the AdS/CFT duality – TT deformed CFTs and their gravitational duals, and a two-dimensional BCFT with two conformal boundaries dual to AdS spacetime with two End-of-the-World branes that can intersect at a defect. We also develop a bulk flow procedure that can be interpreted as generating a sequence of coarse-grained holographic states. We demonstrate the existence of a novel inside-out entanglement island for the eternally inflating multiverse. We compute the entanglement entropy of free fermions in the presence of a partially transmitting boundary and use it to study entanglement islands for a blackhole with non-trivial graybody factors.

On the string theory side, we study non-perturbative effects in minimal string theory. We compute various instanton contributions like the ZZ cylinder, the ZZ annulus one-point function, and the disk two-point function using string field theory. We also match these to results from the dual matrix model or matrix quantum mechanics.

To my grandparents,

Vimla and Mahendra Singh Murdia,

and

Anita and Dr. Shamsher Chand Bhandari.

Contents

List of Figures

List of Tables

Acknowledgments

First and foremost, I express my deep gratitude and respect for my advisor, Prof. Yasunori Nomura. He has inspired me to become an independent researcher and helped me realize the power of critical reasoning.

I am also very grateful to Prof. Ashoke Sen and Prof. Raphael Bousso for their guidance and support. Collaborating and interacting with them has been extremely enlightening and has helped me navigate my research interests. My sincere thanks also go to Prof. Richard Borcherds for being a member of my dissertation committee and Prof. Holger Muller for being a member of my qualifying exam committee. They generously gave their time to offer me valuable comments toward improving my work.

I thank UC Berkeley's Graduate Division for awarding me the Berkeley Fellowship for Graduate Study which has been instrumental to my research. I also thank the Hearts to Humanity Eternal (H2H8) association for their generous financial support and encouragement.

I would like to especially thank Raghu Mahajan who has been an extremely influential mentor and collaborating with him has been extremely enriching. I would also like to thank my collaborators - Dan Stefan Eniceicu, Masamichi Miyaji, Pratik Rath, Jorrit Kruthoff, Kevin Langhoff, Pronobesh Maity, Kyle Ritchie, and Nico Salzetta.

I have also benefited tremendously from discussions with brilliant friends and colleagues both at BCTP and outside. I would like to extend my gratitude especially to Mykhaylo Usatyuk and to Ning Bao, Andreas Blommaert, Reginald Caginalp, Ven Chandrasekaran, Ben Concepcion, Adam Levine, Hugo Marrochio, Arvin Shahbazi Moghaddam, Ronak Soni, Vincent Su, Marija Tomaševič, Wayne Weng, and Elizabeth Wildenhain.

I thank the administrative and academic staff at Physics Department particularly Joelle Miles, Donna Sakima, and Christian Natividad for all the help and support.

I express my deep gratitude for friends who went through hard times together, cheered me on, and celebrated each accomplishment – Himanshi Mehta, Elizabeth Dresselhaus, Tomohiro Soejima, Jack Spilecki, Adam Frim, Junwen Xiong, Trevor Chistolini, Max Smiley, Daniel Gardeazabal, Scott Eustice, Susan Lee, Benjamin Foster, Jaewon Kim, Madhav Ranka, Raunak Sharma, and Purvanshi Mehta.

I sincerely thank my parents, Manish and Sonali, and my brother Tanay for their unconditional trust, perpetual encouragement, and endless patience. I also thank my grandparents, uncles, aunts, cousins, and other family members for their constant love and support.

Chapter 1

Introduction

Quantum mechanics and general relativity have been the crown jewels of physics in the twentieth century. These theories have been tested to a high degree of accuracy in their respective domains of validity and have led to tremendous amounts of scientific progress. However, the search for a theory of quantum gravity that unifies these theories has been a long-standing problem in theoretical physics. The key issue is that a naive theory of quantum gravity has ultraviolet divergences. When the usual methods of perturbative quantum field theory are applied to gravity, they lead to a nonrenormalizable theory. Historically such ultraviolet divergences have indicated the incompleteness of our current understanding and have necessitated the emergence of new physics at shorter distances. Developing a new, divergence-free fundamental theory represents a bottom-up approach to quantum gravity.

One sharp way the conflict between quantum mechanics and general relativity is realized is through theoretical puzzles such as the black hole information paradox and the firewall paradox [1, 2, 3]. These paradoxes arise from the tension between the equivalence principle in general relativity and unitarity in quantum mechanics. Understanding and resolving these paradoxes is the motivating goal behind a top-down approach to quantum gravity.

In this dissertation, we explore these two complementary approaches – holography as a bottom-up perspective and string theory as a top-down framework towards a quantum theory of gravity.

1.1 Bottom-up Approach

One approach to understanding quantum gravity is through a bottom-up perspective, which seeks to understand the theory from an overarching viewpoint. Holography has been one of the most promising bottom-up approaches to a theory of quantum gravity. The holographic principle is the proposal that the quantum gravitational degrees of freedom in a given region R live on its boundary ∂R like a hologram describing all the physics inside it [4, 5]. The most concrete realization of holography is the AdS/CFT correspondence – a duality between quantum gravity in anti-de Sitter (AdS) spacetime and a conformal field theory (CFT) living

on its boundary [6, 7, 8].

A major advance in our understanding of holography came with the development of the Ryu-Takayanagi (RT) formula and its covariant extension, the Hubeny-Rangamani-Takayanagi (HRT) formula [9, 10, 11]. According to these prescriptions, the entanglement entropy of a subregion in CFT is given by the area of an associated minimal or extremal surface in the bulk. When quantum corrections are included, we get the Quantum Extremal Surface (QES) formula for the entanglement entropy

$$S(R) = S_{\text{gen}}(\gamma_R) := \frac{\mathcal{A}(\gamma_R)}{4G_N} + S_{\text{bulk}}(\Sigma_R) \tag{1.1}$$

where R is a subregion of the CFT and γ_R is the quantum extremal surface (QES), found by extremizing the generalized entropy S_{gen} [12, 13]. Also, Σ_R is a partial bulk Cauchy slice with $\partial\Sigma_R = R \cup \gamma_R$.

Another key aspect of the holographic dictionary is the subregion-subregion duality. This duality tells us that the boundary subregion R has access to all the information about the bulk in the associated entanglement wedge $EW(R)$, the domain of dependence of Σ_R [14, 15]. A major step towards resolving the black hole information puzzle came when the QES prescription was used to study the entanglement wedge of Hawking radiation. After Page time, this entanglement wedge contains a disconnected region that is completely inside the black hole. This disconnected region is called the entanglement island, and including it enables the entanglement entropy of radiation to follow the Page curve [16, 17].

In this work, we focus on holography beyond AdS/CFT and on the applications of entanglement islands to holography.

- Chapter 2 considers $T\bar{T}$ deformed CFTs and their gravitational duals. In this chapter, we refine some recent work demonstrating the success of the RT formula in $T\bar{T}$ deformed theories. We emphasize general arguments that justify the use of the RT formula in general holographic theories that obey a GKPW-like dictionary. In doing so, we clarify subtleties related to holographic counterterms and discuss the implications for holography in general spacetimes. This chapter is based on Ref. [18].

- Chapter 3 focuses on generating a family of bulk-boundary dualities by using a coarse-graining procedure. Motivated by the understanding of holography as realized in tensor networks, we develop a bulk procedure that can be interpreted as generating a sequence of coarse-grained holographic states. This coarse-graining procedure involves identifying degrees of freedom entangled at short distances and disentangling them. This is manifested in the bulk by a flow equation that generates a codimension-1 object, which we refer to as the holographic slice. We generalize an earlier classical construction to include bulk quantum corrections, which naturally involves the generalized entropy as a measure of the number of relevant boundary degrees of freedom. The semiclassical coarse-graining results in a flow that approaches quantum extremal surfaces such as entanglement islands that have appeared in discussions of the black hole information

paradox. We also discuss the relation of the present picture to the view that the holographic dictionary works as quantum error correction. This chapter is based on Ref. [19].

- Chapter 4 studies a novel gravity dual for a 2d BCFT with two conformal boundaries by introducing a defect that connects the two End-of-the-World branes. We demonstrate that the BCFT dual to this bulk model exhibits a richer lowest spectrum. The corresponding lowest energy eigenvalue can continuously interpolate between $-\frac{\pi c}{24\Delta x}$ and 0 where Δx is the distance between the boundaries. This range was inaccessible to the conventional AdS/BCFT model with distinct boundary conditions. We compute the holographic entanglement entropy and find that it exhibits three different phases, one of which breaks the time reflection symmetry. We also construct a wormhole saddle, analogous to a 3d replica wormhole, which connects different boundaries through the AdS bulk. This saddle is present only if the BCFT is non-unitary and is always subdominant compared to the disconnected saddle. This chapter is based on Ref. [20].

- Chapter 5 applies the entanglement islands prescription to the multiverse. We study the redundancies in the global spacetime description of the eternally inflating multiverse using the quantum extremal surface prescription. We argue that a sufficiently large spatial region in a bubble universe has an entanglement island surrounding it. Consequently, the semiclassical physics of the multiverse, which is all we need to make cosmological predictions, can be fully described by the fundamental degrees of freedom associated with certain finite spatial regions. The island arises due to mandatory collisions with collapsing bubbles, whose big crunch singularities indicate redundancies of the global spacetime description. The emergence of the island and the resulting reduction of independent degrees of freedom provides a regularization of infinities which caused the cosmological measure problem. This chapter is based on Ref. [21].

- Chapter 6 studies the entanglement entropy of free fermions in 2 dimensions in the presence of a partially transmitting interface and its application to entanglement islands for a blackhole with non-trivial graybody factors. We focus on the case of a single interval that straddles the defect, and compute its entanglement entropy in three limits: Perturbing away from the fully transmitting and fully reflecting cases, and perturbing in the amount of asymmetry of the interval about the defect. Using these results within the setup of the Poincaré patch of AdS_2 statically coupled to a zero-temperature flat space bath, we calculate the effect of a partially transmitting AdS_2 boundary on the location of the entanglement island region. The partially transmitting boundary is a toy model for black hole graybody factors. Our results indicate that the entanglement island region behaves in a monotonic fashion as a function of the transmission/reflection coefficient at the interface. This chapter is based on Ref. [22].

1.2 Top-down Approach

A complementary approach to understanding quantum gravity is through a top-down perspective, which seeks to understand the theory from a fundamental viewpoint. String theory is currently the best candidate for a top-down theory of quantum gravity. In this theory, one replaces the point particles of quantum field theory with one-dimensional objects called strings. This softens the divergences of gravity and unifies it with quantum field theory. String theory has been extremely successful owing to the capability to describe a wide range of phenomena while simultaneously including gravity. Perturbative string theory has been studied extensively and has led to various exciting results such as consistent quantum gravity amplitudes, grand unified gauge groups, and extra dimensions. However, non-perturbative effects in string theory still need to be understood better.

In this work, we focus on non-perturbative contributions in minimal string theory, a particular model of 2-dimensional gravity.

- Chapter 7 studies one-eigenvalue instantons across this duality. We use insights from string field theory to analyze and cure the divergences in the cylinder diagram in minimal string theory with both boundaries lying on a ZZ brane. We focus on theories with worldsheet matter consisting of the $(2, p)$ minimal model plus Liouville theory, with total central charge 26, together with the usual bc-ghosts. The string field theory procedure gives a finite, purely imaginary normalization constant for non-perturbative effects in minimal string theory, or doubly non-perturbative effects in JT gravity. We find precise agreement with the prediction from the dual double-scaled one-matrix integral. We also make a few remarks about the extension of this result to the more general (p', p) minimal string. This chapter is based on Ref. [23].

- Chapter 8 generalizes our results to multi-instantons. We compute the normalization of a general multi-instanton contribution to the partition function of (p', p) minimal string theory and also to the dual two-matrix integral, and find perfect agreement between these two results. This chapter is based on Ref. [24].

- Chapter 9 studies subleading corrections to these non-perturbative effects. We compute the ZZ annulus one-point function of the cosmological constant operator in non-critical string theory, regulating divergences from the boundaries of moduli space using string field theory. We identify a subtle issue in a previous analysis of these divergences, which was done in the context of the $c = 1$ string theory, and where it had led to a mismatch with the prediction from the dual matrix quantum mechanics [25, 26]. After fixing this issue, we find a precise match to the expected answer in both the $c < 1$ and $c = 1$ cases. We also compute the disk two-point function, which is a quantity of the same order, and show that it too matches with the general prediction. This chapter is based on Ref. [27].

Part I

Bottom-up Approach

Chapter 2

Comments on Holographic Entanglement Entropy in $T\bar{T}$ Deformed CFTs

2.1 Introduction

Gauge-gravity duality, specifically AdS/CFT, is our best known example of a holographic description of quantum gravity [6]. The so-called GKPW dictionary [8, 7] relating bulk physics to boundary dynamics takes the form

$$Z_{\text{CFT}}[\gamma_{ij}] = e^{-I_{\text{bulk}}[g_{\mu\nu}]}, \tag{2.1}$$

where γ_{ij} is the background metric of the space in which the boundary CFT lives, and $g_{\mu\nu}$ is the bulk metric. A particularly consequential holographic correspondence given by this duality is the Ryu-Takayanagi (RT) formula

$$S(A) = \min_{\partial\Gamma=\partial A}\left[\frac{\|\Gamma\|}{4G}\right], \tag{2.2}$$

which relates the entanglement entropy of a subregion A of the boundary space to the area of the bulk extremal surface Γ anchored to the entangling surface ∂A [9, 10, 11]. Throughout, we will work to leading order in the bulk Newton's constant, G, and suppress all bulk fields aside from $g_{\mu\nu}$. Higher order effects are well understood in the context of AdS/CFT [12, 13].

Other holographic dualities with similar features have been proposed. In particular, the TT deformation of 2-dimensional CFTs and its appropriate generalizations to higher dimensions have been argued to have holographic duals [28, 29, 30]. Of crucial importance to our discussion is that the proposed dictionary relating the boundary and bulk observables in these theories takes the same form as Eq. (2.1), except that now Dirichlet boundary conditions are imposed on a cutoff surface in the bulk.

The simple idea we would like to highlight is that Eq. (2.2) was derived in the context of AdS/CFT from Eq. (2.1) under rather tame assumptions [31]. The same argument, therefore, can be used to show that the RT formula holds for all dualities adopting dictionaries of the form of Eq. (2.1). This straightforward result is known in the community; however, careful consideration of it resolves subtleties involving counterterms when calculating entanglement entropy in TT deformed theories.

Note that several calculations of entanglement entropy in TT deformed theories have appeared recently [32, 33, 34, 35, 36, 37, 38]. Our goal is to emphasize the generality of the arguments leading to an agreement between boundary entanglement entropy and the RT formula and clarify some of the calculations performed in these works.

Conventions

The background metric of the space in which the boundary field theory lives is denoted by γ_{ij}, while h_{ij} refers to the bulk induced metric on the cutoff surface at $r = r_c$. These are related by $h_{ij} = r_c^2 \gamma_{ij}$.

Overview

In Section 2.2, we review some aspects of entanglement entropy from a field theory perspective and then proceed to a calculation in the particular case of TT deformed theories. In Section 2.3, we discuss the general holographic argument for the RT formula, which is followed by a sample calculation in cutoff AdS. Along the way, we address some subtleties related to holographic renormalization. We conclude with a discussion about the consequences for holography in general spacetimes in Section 2.4.

2.2 Field Theory Calculation

Preliminaries

Consider a D-dimensional CFT with action $I[\phi] = \int d^D x \sqrt{\gamma}\, \mathcal{L}[\phi]$. One can prepare a density matrix ρ on a spatial slice Σ using an appropriate Euclidean path integral. In order to compute the entanglement entropy $S(A)$ of a subregion A of Σ, one can use the replica trick as follows:

$$\begin{aligned} S(A) &= \lim_{n\to 1} \frac{\log\left(Z^{(b)}\left[M_n\right]\right) - n \log\left(Z^{(b)}\left[M_1\right]\right)}{1-n} \\ &= \left(1 - n\frac{d}{dn}\right) \log\left(Z^{(b)}[M_n]\right)\Big|_{n\to 1}, \end{aligned} \tag{2.3}$$

where

$$Z^{(b)}[M] = \int D\phi \, \exp\left(- \int_M d^D x \sqrt{\gamma} \, \mathcal{L}[\phi] \right) \tag{2.4}$$

is the "bare" partition function computed by the path integral on a given manifold M. M_1 is the manifold used to compute $\mathrm{Tr}\, \rho$, while M_n is an n-sheeted version of M_1 which is a branched cover with a conical excess of angle $\Delta\phi = 2\pi(n-1)$ localized at the $(D-2)$-dimensional submanifold ∂A.

The bare partition function $Z^{(b)}[M]$ typically diverges and takes the form

$$\log\left(Z^{(b)}[M]\right) = c_1(\Lambda a)^D + c_2(\Lambda a)^{D-2} + \ldots, \tag{2.5}$$

where Λ is a UV cutoff and a is the length scale associated with the manifold M [39]. What are the contributions of these divergences to entanglement entropy? These divergence can be expressed as local integrals of background quantities [40, 41, 42]. (In even dimensions, there is a logarithmic divergence which cannot be expressed in this manner.) This implies that their contributions cancel in Eq. (2.4) everywhere away from ∂A, since M_n and n copies of M_1 are identical manifolds except at ∂A. However, M_n has extra divergent contributions coming from curvature invariants localized at ∂A. This leads to

$$S(A) = \sum_{k=1}^{\lfloor D/2 \rfloor} a_k \Lambda^{D-2k} \int_{\partial A} d^{D-2} x \sqrt{H} \left[\mathcal{R}, \mathcal{K}^2\right]^{k-1}, \tag{2.6}$$

where $[\mathcal{R}, \mathcal{K}^2]^{k-1}$ represents all possible scalar intrinsic and extrinsic curvature invariants of ∂A of mass dimension $2k-2$, with their coefficients collectively written as a_k, and H_{ab} is the intrinsic metric of ∂A. Here, we have suppressed possible finite terms to focus on the leading divergences. This is the famous "area law" associated with entanglement entropy, which comes from the short distance correlations between A and $\bar{A}$.

Since the above behavior is sensitive to the cutoff, one often considers a renormalized version of entropy. In particular, the divergences in Eq. (2.5) can be subtracted (except for logarithmic ones) by introducing a counterterm action I_{ct} which involves local integrals of curvature invariants:

$$I_{\mathrm{ct}} = \sum_{k=1}^{\lfloor D/2 \rfloor + 1} b_k \Lambda^{D-2k+2} \int_M d^D x \sqrt{\gamma} \, \mathcal{R}^{k-1}. \tag{2.7}$$

Here, $\mathcal{R}^{k-1}$ represents all possible scalar curvature invariants of M that one can write down at mass dimension $2k-2$, and their coefficients b_k can be tuned exactly to cancel the divergences. The renormalized entropy is then given by

$$S_{\mathrm{ren}}(A) = \lim_{n \to 1} \frac{\log\left(Z_{\mathrm{ren}}[M_n]\right) - n \log\left(Z_{\mathrm{ren}}[M_1]\right)}{1-n}, \tag{2.8}$$

where Z_{ren} is the renormalized partition function which is computed using the action with the counterterms in Eq. (2.7). This renormalized entropy is universal, i.e. UV regulator independent in the continuum limit, and has been discussed previously in the literature [42]. A closely related version of renormalized entropy was discussed in [41]. These two are not identical, but they both extract the appropriate universal behavior in the CFT limit by subtracting the power divergences.

Entanglement Entropy in TT Deformed Theories

We now specialize to the case of a D-dimensional CFT deformed by a particular composite operator X_D of the stress tensor [30]. The presence of this deforming irrelevant operator breaks conformal invariance and gives rise to a QFT that is conjectured to be holographically dual to AdS with a finite cutoff radius, where Dirichlet boundary conditions are imposed.

We will focus on computing the partition function of this TT deformed theory on the manifold S^D of radius R:

$$\gamma_{ij} = R^2 d\Omega_D^2. \tag{2.9}$$

The theory is defined by the flow equation dictated by X_D, and using this we obtain

$$\langle T_i^i \rangle = -D\lambda \langle X_D \rangle, \tag{2.10}$$

where λ is the deformation parameter. T_{ij} is the renormalized stress tensor, whose trace vanishes up to conformal anomalies in the CFT limit $\lambda \to 0$. The bare stress tensor $T_{ij}^{(b)}$ is related to the renormalized one[1] as

$$\langle T_{ij}^{(b)} \rangle = \langle T_{ij} \rangle - C_{ij}, \tag{2.11}$$

where C_{ij} represent various terms involving the background metric γ_{ij} that arise from variation of the counterterm action, which in the CFT limit is given by Eq. (2.7). For finite λ, the cutoff of the theory is provided by the deformation itself, so that Λ is replaced by—or identified with—$\lambda^{-1/D}$ in Eqs. (2.5 – 2.7).

Since S^D is a maximally symmetric space, the one point function of the stress tensor takes the form

$$\langle T_{ij} \rangle = \omega_D(R)\ \gamma_{ij}, \tag{2.12}$$

$$\langle T_{ij}^{(b)} \rangle = \omega_D^{(b)}(R)\ \gamma_{ij}. \tag{2.13}$$

[1]The bare stress tensor is related to the Brown-York stress tensor [43], while the renormalized stress tensor is related to the Balasubramanian-Kraus stress tensor [44] by a factor of r_c^{d-2}.

Using the flow equation, one can solve for $\omega_D(R)$ and $\omega_D^{(b)}(R)$ as has been done in [37], yielding

$$\begin{aligned}\omega_D(R) =& -\frac{D-1}{2D\lambda}\sqrt{1+\frac{L_D^2}{R^2}}+\frac{D-1}{2D\lambda}\\ &+\sum_{k=1}^{\lfloor (D-1)/2\rfloor}\frac{f_{k,D}}{\lambda}\left(\frac{L_D}{R}\right)^{2k},\end{aligned} \tag{2.14}$$

$$\omega_D^{(b)}(R) = -\frac{D-1}{2D\lambda}\sqrt{1+\frac{L_D^2}{R^2}}, \tag{2.15}$$

where $L_D^2 = 2D(D-2)\alpha_D\lambda^{2/D}$ with α_D being quantities related to the central charges of the field theory, and $f_{k,D}$ are dimension dependent constants. (Note that $\alpha_D \propto 1/(D-2)$, so that $L_2 \neq 0$.) We stress that while $\omega_D(R)$ has been represented schematically, the expression for $\omega_D^{(b)}(R)$ is exact. The explicit expressions for $\omega_D(R)$ can be found in [37].

Now using these results, we can compute the bare partition function as

$$\frac{d}{dR}\log Z_{S^D}^{(b)} = -\frac{1}{R}\int_{S^D} d^Dx\sqrt{\gamma}\,\langle T_i^{i(b)}\rangle, \tag{2.16}$$

obtaining

$$\begin{aligned}\log Z_{S^D}^{(b)} &= -D\Omega_D\int_0^R dR\;\omega_D^{(b)}(R)\,R^{D-1}\\ &= \frac{\Omega_D L_D R^{D-1}}{2\lambda}\,{}_2F_1\left[-\frac{1}{2},\frac{D-1}{2};\frac{D+1}{2};-\frac{R^2}{L_D^2}\right],\end{aligned} \tag{2.17}$$

where Ω_D is the volume of a unit S^D. The entanglement entropy of a subregion A which is a hemisphere of the spatial S^{D-1} can then be computed by a simple trick described in [33]:

$$\begin{aligned}S(A) &= \left(1-n\frac{d}{dn}\right)\log\left(Z^{(b)}[S_n^D]\right)\Big|_{n\to 1}\\ &= \left(1-\frac{R}{D}\frac{d}{dR}\right)\log Z_{S^D}^{(b)}.\end{aligned} \tag{2.18}$$

This gives us the answer

$$S(A) = \frac{\pi\Omega_{D-2}L_D R^{D-1}}{D(D-1)\lambda}\,{}_2F_1\left[\frac{1}{2},\frac{D-1}{2};\frac{D+1}{2};-\frac{R^2}{L_D^2}\right]. \tag{2.19}$$

We can also compute the renormalized entanglement entropy in multiple different ways, e.g. using Eq. (2.8), which results in a universal answer in the CFT limit [42]. Alternately, one can use the version employed in [41]. For finite λ these two versions give different

answers, which explains the discrepancy in [38] between the field theory calculation and the renormalized entropy.

We, however, emphasize that the TT deformation provides a particular physical regulator for the entropy, so one need not focus their attention on the renormalized entropy. This regularization has a simple interpretation in field theory, which also has a geometric bulk interpretation. Specifically, on the field theory side one only includes the energy levels below the shock singularity, above which the energies take complex values. The existence of this regularization naturally leads us to consider the bare entanglement entropy in Eq. (2.19), which captures all the information about correlations between A and $\bar{A}$.

2.3 Bulk Calculation

Holographic Duality

Using the holographic dictionary in Eq. (2.1), the entanglement entropy $S(A)$ of a boundary subregion A can be calculated as

$$S(A) = \lim_{n\to 1} \frac{I_{\text{bulk}}[B_n] - nI_{\text{bulk}}[B_1]}{n-1}, \tag{2.20}$$

where B_n and B_1 are the saddle point bulk solutions dual to the boundary conditions dictated by the field theory path integral on M_n and M_1, respectively [31]. Notably, the action I_{bulk} dual to the bare partition function is the usual Einstein-Hilbert action supplemented by the Gibbons-Hawking-York boundary term. Assuming that the solution B_n preserves the $\mathbb{Z}_n$ symmetry of the boundary, [31] showed that the contribution to the above expression is localized to the extremal surface Γ, resulting in the RT formula

$$S(A) = \min_{\partial\Gamma=\partial A} \left[\frac{\|\Gamma\|}{4G}\right]. \tag{2.21}$$

Our simple observation is that this proof carries through unmodified as long as one is computing the bare partition function. The TT theory must then obey the RT formula by construction.

Counterterms added to the boundary action are well understood to correspond to boundary terms added to the bulk action [44, 45]. Per the discussion in Section 2.2, these terms give rise to extra contributions to $S(A)$ localized to the entangling surface ∂A. The saddle point solutions are not modified by the inclusion of these terms, which are pure functionals of the induced metric h_{ij}. This implies that the renormalized entropy can be calculated holographically as

$$S_{\text{ren}}(A) = \min_{\partial\Gamma=\partial A} \left[\frac{\|\Gamma\|}{4G}\right] + \tilde{S}(\partial A), \tag{2.22}$$

where the form of $\tilde{S}(\partial A)$ is discussed in [42].

RT Formula in Cutoff AdS

As a simple check, we now compare the result of the RT formula to the entanglement entropy obtained in Section 2.2. On the bulk side, we need to compute the minimal surface Γ anchored to the entangling surface ∂A on the cutoff surface at $r = r_c$, on which the induced metric is given by

$$h_{ij} = r_c^2 R^2 d\Omega_D^2 \equiv r_0^2 d\Omega_D^2. \tag{2.23}$$

This calculation was performed in [38] and the answer obtained is

$$S(A) = \frac{r_0^{D-1}\Omega_{D-2}}{4G(D-1)}\, {}_2F_1\left[\frac{1}{2}, \frac{D-1}{2}; \frac{D+1}{2}; -\frac{r_0^2}{l^2}\right], \tag{2.24}$$

where l is the AdS radius. By using the holographic identifications

$$\lambda = \frac{4\pi G l}{D r_c^D}, \tag{2.25}$$

$$l^2 = 2D(D-2)\alpha_D \lambda^{2/D} r_c^2 = L_D^2 r_c^2, \tag{2.26}$$

we find that this is identical to Eq. (2.19).

2.4 Discussion

Holographic Dictionary

As emphasized throughout, if there exists a holographic duality between Einstein gravity in the bulk and a quantum field theory on the boundary such that the two are related by Eq. (2.1), then the RT formula will hold. This is true independent of the details of the bulk spacetime and the boundary field theory. Indeed, we have shown that the TT deformed CFT provides an explicit example of the validity of the Lewkowycz-Maldacena (LM) proof beyond AdS/CFT at the conformal boundary.[2] In fact, all the results based only on this dictionary element will hold in any such duality, at least in a perturbative expansion in G. Two salient examples include the prescription for calculating refined Rényi entropies presented in [47] and generalizations of the RT formula in higher curvature gravity [48]. Though the robustness of the LM proof is far from unknown, we hope that highlighting this feature helps solidify the relationship between entanglement entropy and geometry in general spacetimes.

Holographic Renormalization and Counterterms

In CFT calculations, one often considers only renormalized quantities because these are universally well-defined and survive the continuum limit. However, entanglement entropy

[2] An important assumption is the $\mathbb{Z}_n$ symmetry in the bulk. It is plausible that the argument holds after relaxing this assumption; See, e.g., [46].

is not one of these quantities. Nevertheless, since the TT operator implements a particular physical cutoff which has a simple geometric dual, it is sensible to consider bare quantities. In particular, TT deformations with different background geometries would implement different regularizations, leading to different entanglement entropies. On the bulk side, this manifests as different choices of the cutoff surface. This provides a better understanding of the UV-IR correspondence.

The handling of counterterms is the only additional subtlety encountered when calculating entanglement entropy in TT deformed CFTs. For finite deformations, all quantities are automatically regulated and hence the previous distinction between finite and divergent terms becomes muddled. We aimed to clarify the conceptual aspects of these terms and how they are related with the holographic result.

The fundamental idea is that the dictionary relation

$$Z_{\text{CFT}}[\gamma_{ij}] = e^{-I_{\text{bulk}}[g_{\mu\nu}]} \tag{2.27}$$

is precisely between the *bare* CFT on the boundary and Einstein-Hilbert gravity (plus the necessary Gibbons-Hawking-York term) in the bulk, both of which have divergent partition functions. This is the arena in which the RT formula was shown to hold. If one now chooses to introduce specific counterterms to renormalize the CFT stress tensor, then this will correspondingly alter the gravity side of the dictionary (specifically by adding terms localized to the boundary of the bulk). In particular, the addition of counterterms will alter the RT prescription to include terms beyond the standard area piece. This addition manifests as integrals of local geometric invariants at the entangling surface. In the CFT limit these are used to cancel power divergences, but with finite deformations one need not add a counterterm. Indeed, calculations including counterterms [33, 38] would necessarily miss the area law piece for $D > 2$, which is finite for finite deformations.

Holography in General Spacetimes

The explicit verification of the RT formula beyond AdS/CFT at the conformal boundary of AdS provides a strong footing for the surface-state correspondence [49] and related constructions to understand holography in general spacetimes via entanglement entropy [50, 51, 52, 53, 54]. In previous work, the RT formula was used as an assumption to investigate properties of a hypothetical boundary theory, and self-consistency checks provided confidence in that assumption. Now, the evidence that a duality in the form of Eq. (2.1) exists beyond basic AdS/CFT, and the RT formula along with it, suggests that a duality may indeed exist for general spacetimes and bolsters our confidence in previous work.

The results of TT deformations provide a particularly promising avenue to investigate flat space holography, since they hold down to scales below the AdS radius l. This contrasts with the conventional UV-IR correspondence, which would result in a single matrix-like theory describing an AdS volume [55]. It suggests that there is a way to redistribute degrees of freedom on the boundary theory in a way that maintains local factorization, and the TT

deformation implements this. This is explicitly seen in the calculation of entanglement entropy in the fact that it does not face an obstruction when a volume law scaling is reached at $r_0 \approx l$. Volume law scaling of entanglement entropy suggests that the boundary theory for asymptotically flat space is non-local, as is expected from the TT deformation. Corresponding behavior is seen in cosmological spacetimes [53], and investigating properties of highly deformed CFTs may shed light on these theories. Since the TT operator naturally implements some sort of coarse graining, it would be interesting to relate this to the geometric coarse graining procedure developed in [54].

Chapter 3

Coarse-Graining Holographic States: A Semiclassical Flow in General Spacetimes

3.1 Introduction

The holographic principle, as embodied by the AdS/CFT correspondence, has led to a tremendous amount of progress in our understanding of quantum gravity. In particular, the realization that entanglement plays a crucial role in generating bulk spacetime has put the holographic correspondence on much stronger footing [9, 10, 11, 56, 57]. This has led to key insights about bulk reconstruction and subregion duality, culminating in entanglement wedge reconstruction [58, 59, 60, 14, 15, 61]. Interestingly, several of these insights are quite general and do not seem to require an AdS setting in particular, and thus they can be used to understand features of holography in general spacetimes [51, 52, 53, 54].[1]

A particular manifestation of the above ideas can be seen in tensor networks (TNs) that serve as useful toy models of holography [57, 69, 70, 71, 72]. TNs prepare quantum states with a lot of structure and via the process of "pushing" the state generate a sequence of boundary states, each of which satisfies the Ryu-Takayanagi (RT) formula [9, 10].[2] This procedure involves disentangling certain short-distance degrees of freedom and coarse-grains the state by reducing it to one in a smaller effective Hilbert space. Applying this procedure to a general smooth classical spacetime leads to a flow equation in the continuum limit as

[1] An early work in this direction is the so-called surface/state correspondence [49, 62], of which the construction of Refs. [51, 52, 53, 54] can be viewed as a covariant generalization. For other work on holography beyond AdS/CFT, see, e.g., Refs. [63, 64, 65, 66, 67, 35, 68].

[2] We distinguish this from the Hubeny-Rangamani-Takayanagi (HRT) formula [11] which applies in time-dependent spacetimes.

we shall review later [54]. The flow equation takes the form[3]

$$\frac{dx^\mu}{d\lambda} = \frac{1}{2}(\theta_k l^\mu + \theta_l k^\mu),$$

where x^μ are the embedding coordinates of a codimension-2 surface σ on which the holographic states are defined, and $\{k^\mu, l^\mu\}$ are the future-directed null vectors orthogonal to σ, with $\theta_{k,l}$ being the classical expansions in the corresponding directions. This flow satisfies all the required properties for it to be interpreted as a disentangling procedure resulting in a sequence of coarse-grained states.

In this work, we go beyond the classical flow equation by including bulk quantum corrections. In the TN picture, we include these effects by modifying the network such that it includes non-universal tensors/bonds as well as bonds connecting tensors nonlocally. With this picture in mind, we develop a coarse-graining procedure analogous to the classical flow equation which pleasantly fits in with our understanding of holography. In the continuum limit, the procedure leads to a flow equation similar to that in the classical case:

$$\frac{dx^\mu}{d\lambda} = \frac{1}{2}(\Theta_k l^\mu + \Theta_l k^\mu),$$

where $\Theta_{k,l}$ now represent quantum expansions [73].[4] This is our primary result. It is in line with many results in which quantum corrections are included by replacing the area $\mathcal{A}/4G_N$ with the generalized entropy S_{gen} [73, 74, 75, 76, 77]. Though motivated by TNs, which often face issues in describing time-dependent situations, our procedure can be applied quite generally. In fact, we obtain consistent descriptions in general time-dependent spacetimes.

Another important progress in understanding holography is the view that the holographic dictionary works as quantum error correction [3, 78, 79, 80], where a small Hilbert space of semiclassical bulk states is mapped isometrically into a larger boundary Hilbert space. In our framework, this picture arises after considering a collection of states over which we want to build a low energy bulk description. Choosing such a collection is equivalent to erecting a code subspace. We argue that while there is no invariant choice of code subspace in a general time-dependent spacetime, our framework gives a natural choice(s) determined by the coarse-graining procedure. This procedure leads to a one-parameter family of "dualities" depending on the amount of coarse-graining performed, providing an improved understanding of the holographic dictionary in general spacetimes.

Overview

In Sec. 3.2, we first establish the framework in which we are working. We explain how quantum corrections affect the description of holography in general spacetimes and the associated

[3]The sign convention for the flow parameter λ in this paper is opposite to that in Ref. [54].

[4]We use a modified version of the quantum expansion which includes a bulk entropy contribution from an exterior region as described in Sec. 3.5.

HRT formula. In Sec. 3.3, we review the classical flow equation. In Sec. 3.4, we motivate our coarse-graining procedure with a toy model of TNs, elucidating how features of a state relevant for the quantum-level consideration are represented there.

In Sec. 3.5, we present our main result, i.e. the procedure of performing the flow in the bulk at the quantum level, which corresponds to moving the holographic boundary. In Sec. 3.6, we discuss properties of this flow indicating that it corresponds to a coarse-graining of holographic states. We elucidate that the way the flow ends can be used as an indicator of qualitative features of the boundary state describing a given spacetime, using the example of a collapse-formed evaporating black hole. In Sec. 3.7, we discuss how the picture of quantum error correction may be implemented in our framework. Finally, conclusions are given in Sec. 3.8.

3.2 Framework

In this work, we follow and further develop the framework of holography for general spacetimes proposed in Ref. [51]. In this framework, we consider an arbitrary spacetime $\mathcal{M}$ and posit the existence of a dual "boundary" theory that lives on a holographic screen [81], which is a codimension-1 hypersurface H embedded in $\mathcal{M}$. This hypersurface is foliated by marginally trapped/anti-trapped codimension-2 surfaces called leaves, which we denote by σ. A marginally trapped/anti-trapped surface σ is defined by the property that σ has classical expansion $\theta = 0$ in one of the orthogonal null directions. The proposal is that the boundary theory describes everything in the "interior" of H, and states of the theory are naturally defined on the leaves σ, which provide a preferred foliation of H into constant time surfaces. Based on the covariant entropy bound, it is expected that the boundary theory effectively possesses $\mathcal{A}(\sigma)/4G_N$ degrees of freedom, where $\mathcal{A}(\sigma)$ is the area of a leaf. The AdS/CFT correspondence can be viewed as a special case of this duality, where the holographic screen is sent to the conformal boundary of AdS.

Given this setup, it was shown in Ref. [50] that the HRT formula for computing entanglement entropy can be applied consistently using a maximin procedure [59]; i.e., for any subregion A of a leaf

$$S(A) = \frac{\mathcal{A}(\gamma_A)}{4G_N}, \tag{3.1}$$

where $S(A)$ is the von Neumann entropy of the reduced density matrix on subregion A, and $\mathcal{A}(\gamma_A)$ is the area of the HRT surface γ_A of A. The entanglement wedge, denoted by $\mathrm{EW}(A)$, is defined as the bulk domain of dependence of any bulk partial Cauchy slice Σ_A with $\partial\Sigma_A = A \cup \gamma_A$, which is often called the homology surface. The entropies obtained by the above procedure can be shown to satisfy all the basic properties of von Neumann entropy and are consistent with more constraining inequalities satisfied by holographic states in AdS/CFT [82, 83, 84].

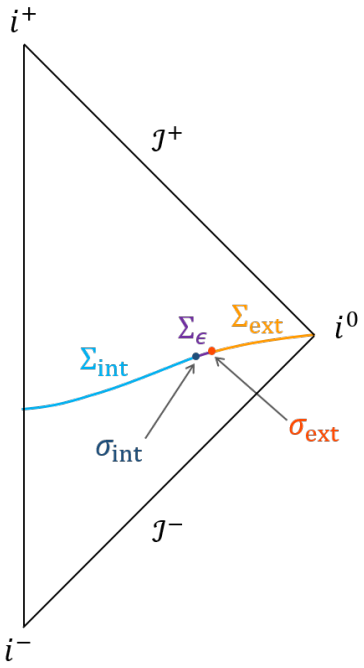

Figure 3.1: The leaf σ is split into $\sigma_{\text{int}} \cup \sigma_{\text{ext}}$ such that σ_{int} and σ_{ext} are separated by a small regulating region Σ_ϵ on a Cauchy slice Σ. This induces a division of the Cauchy slice as $\Sigma = \Sigma_{\text{int}} \cup \Sigma_\epsilon \cup \Sigma_{\text{ext}}$. We define the location of the holographic screen by requiring it is marginally quantum trapped/anti-trapped under variations of σ_{int}.

Now, in order to generalize this framework to the quantum level, we can follow the simple guiding principle of replacing $\mathcal{A}/4G_N$ with the generalized entropy S_{gen} to include quantum corrections in the bulk [12, 13]

$$\frac{\mathcal{A}}{4G_N} \rightarrow S_{\text{gen}} = \frac{\mathcal{A}}{4G_N} + S_{\text{bulk}}, \tag{3.2}$$

where S_{bulk} is the von Neumann entropy of the bulk reduced density matrix on the homology surface which is appropriately modified at the quantum level. This is motivated by various examples in which this naturally works [73, 74, 75, 76, 77]. Furthermore, S_{gen} is a natural quantity because it is a quantity that is renormalization scheme independent, and hence is expected to be associated with fundamental degrees of freedom in the UV theory [85, 86, 75].

The generalization to include bulk quantum corrections requires a refined understanding of the holographic duality which we now turn to. First, we note that the global description of a state involves both the interior and exterior portions of the holographic screen [81]. Although the generalization of the HRT formula we describe applies to the interior region, it will be important to keep track of the exterior as well.

Next, the quantum extension of Eq. (3.2) implies that the location of the screen on which the holographic theory is defined needs to be shifted accordingly. Let us consider a specific global bulk state. We propose that the boundary theory describing the dynamics of this state lives on a modified version of a Q-screen H' [74], rather than a classical holographic screen H. A Q-screen is defined as a codimension-1 hypersurface foliated by quantum marginally trapped/antitrapped surfaces, i.e. surfaces that have the quantum expansion $\Theta = 0$ in one of the orthogonal null directions. Usually the quantum expansion is defined by including a contribution from the von Neumann entropy of the interior or exterior region of a leaf which is a simple codimension-2 surface. In this paper, however, we consider that leaf σ is given by $\sigma_{\rm int} \cup \sigma_{\rm ext}$ such that $\sigma_{\rm int}$ and $\sigma_{\rm ext}$ are split by a small regulating region Σ_ϵ on a Cauchy slice Σ as seen in Fig. 3.1. This induces a division of the Cauchy slice as $\Sigma = \Sigma_{\rm int} \cup \Sigma_\epsilon \cup \Sigma_{\rm ext}$. Now, we define the generalized entropy of σ to be

$$S_{\rm gen}(\sigma) = \frac{\mathcal{A}(\sigma)}{4G_N} + S_{\rm bulk}(\Sigma_{\rm int} \cup \Sigma_{\rm ext}). \tag{3.3}$$

With this definition of generalized entropy, one can define a quantum expansion Θ by the variation of $S_{\rm gen}(\sigma)$ under deformations of $\sigma_{\rm int}$ while holding $\sigma_{\rm ext}$ fixed. Using this definition of Θ, we can locate marginally trapped/anti-trapped surfaces self-consistently for any given ϵ. The location H' of the holographic screen is a Q-screen defined using this definition of Θ in the limit $\epsilon \to 0$.

Generalizing the HRT formula of Eq. (3.1), we postulate that the von Neumann entropy of a subregion A on the leaf σ of a Q-screen can be computed as

$$S(A) = \frac{\mathcal{A}(A \cup \Gamma_A)}{4G_N} + S_{\rm bulk}(\Sigma_A), \tag{3.4}$$

where Γ_A is the minimal quantum extremal surface (QES) [13], and Σ_A is the homology surface with $\partial\Sigma_A = A \cup \Gamma_A$. To find Γ_A, we can use a maximin procedure at the quantum level [87] applied to general spacelike surfaces containing σ. We treat $\sigma_{\rm ext}$ as a single unit that cannot be further divided into subregions, which must be either included in or excluded from A. We assume that the leaf σ is convex where $\sigma_{\rm ext}$ is treated as an indivisible unit. Thus, $S(A)$ obtained by Eq. (3.4) satisfies properties required for it to be interpreted as the von Neumann entropy of the density matrix of subregion A. With this assumption, we will show that the same applies to any renormalized leaf $\sigma(\lambda)$ obtained from σ by our coarse-graining procedure.

In AdS/CFT, the regime of validity of the quantum extremal surface formula, Eq. (3.4), has been suggested to be all orders in G_N [13]. However, there are subtleties with the definition of entanglement entropy for gravitons which have not been completely resolved (see e.g. Ref. [73]). At the least, we expect the formula to hold at $O(1)$, where it can already lead to a surface different from that obtained by using Eq. (3.1) [16, 17, 88, 89, 90]. In order to avoid subtleties with gravitons, one could consider a setup with bulk matter having a large central charge c so that the graviton contribution is subleading in $1/c$ expansion. We expect a similar regime of validity for Eq. (3.4) in general spacetimes.

Note that in Eq. (3.4) we have included the area contribution from A in addition to that from Γ_A. This is required if there is a spacetime region outside the leaf, as is the case in generic spacetimes. In this case, $S_{\text{bulk}}(\Sigma_A)$ receives a contribution from entanglement of bulk fields across A, which is divergent. This divergence is then canceled with that in the area contribution from A in the first term, making $S(A)$ well defined. The same applies to the AdS/CFT case if we impose transparent boundary conditions near the boundary which lead to kinetic terms coupling the interior and exterior of AdS space [16, 17]. In fact, the classical formula in Eq. (3.1) must also have the contribution from the boundary subregion area, $\mathcal{A}(\gamma_A) \to \mathcal{A}(A \cup \gamma_A)$, in these cases, although this does not affect the minimization leading to γ_A and hence the result of Ref. [54].

There are special cases in which the area contribution from A—as well as the corresponding contribution from $S_{\text{bulk}}(\Sigma_A)$—is absent. This occurs when the spacetime outside the leaf is "absent," as is the case if Dirichlet boundary conditions are imposed on the Q-screen, or if reflective boundary conditions are imposed in AdS/CFT. Even in this case, however, our coarse-graining procedure—which corresponds to moving the leaf portion σ_{int} inward—induces the area contribution from A on a moved—i.e. renormalized—leaf $\sigma_{\text{int}}(\lambda)$, reflecting the fact that the spacetime continues across $\sigma_{\text{int}}(\lambda)$.[5]

3.3 Review of Classical Flow

In previous work [54], it was shown that a coarse-graining procedure motivated by TNs can be defined in the bulk at the level of classical geometry. Here we review this construction, which allows us to elucidate a generalization to include bulk quantum corrections.

A key idea is to realize that a TN defines a sequence of states that can be generated by including fewer tensors, layer by layer, as shown in Fig. 3.2. For example, one can consider a state defined on the outermost legs which lives in Hilbert space $\mathcal{H}_\sigma$. A coarse-grained version of this state can then be given by a smaller TN that is obtained by peeling off the outermost layer. This state lives in a smaller Hilbert space $\mathcal{H}_{\sigma_1}$, and the TN provides an isometric map from $\mathcal{H}_{\sigma_1}$ to $\mathcal{H}_\sigma$. The sequence can then continue, giving a series of Hilbert spaces $\mathcal{H}_{\sigma_2}$, $\mathcal{H}_{\sigma_3}$, and so on.

In fact, this peeling-off procedure can be decomposed further into smaller steps. For any subregion A of a given boundary, there is an isometric map from the in-plane legs at the RT surface γ_A to the boundary legs in A [69, 70]. This implies that a particular subspace of the boundary subregion legs, corresponding to the in-plane legs at γ_A, is maximally entangled with the complementary subregion $\overline{A}$ via γ_A, which acts as an entanglement "bottleneck" see Figs. 3.3 and 3.4. All the other subregion legs can be disentangled by applying unitary U_A that acts locally within A.

[5] This is different from what has been done in the AdS/CFT literature in the context of TT deformations [28, 33, 37, 38, 18, 91], which corresponds to (re)imposing Dirichlet boundary conditions at each step in the coarse-graining, i.e. at $\sigma_{\text{int}}(\lambda)$ for all λ.

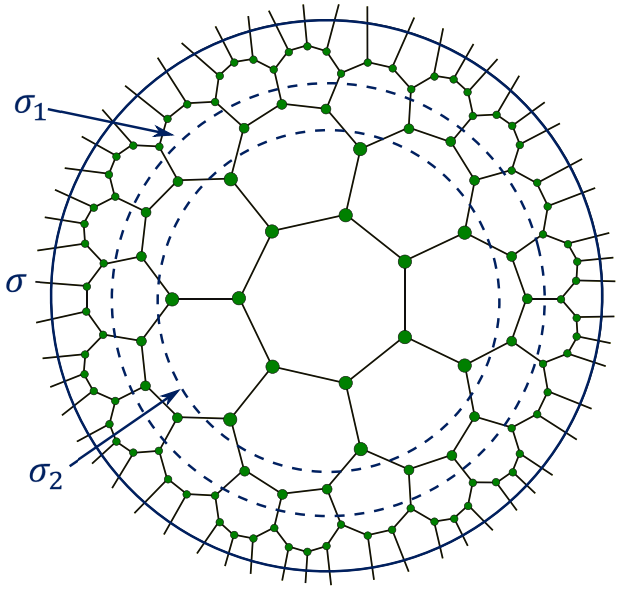

Figure 3.2: A TN defines a boundary state in the Hilbert space $\mathcal{H}_\sigma$ at the outer legs. One can, however, also consider "coarse-grained" states defined at inner layers, e.g. states defined in Hilbert spaces $\mathcal{H}_{\sigma_1}$ and $\mathcal{H}_{\sigma_2}$.

Therefore, if one is to preserve only long range entanglement while getting rid of short range entanglement, one could compress the state down to that defined at the legs of the surface $\sigma' = \gamma_A \cup \overline{A}$. This reduces the size of the effective Hilbert space, mapping a pure state in the larger boundary Hilbert space $\mathcal{H}_\sigma$ to a pure state in a smaller boundary Hilbert space $\mathcal{H}_{\sigma'}$. This can be done by considering small subregions of σ and truncating the TN to end at σ'. One useful way to interpret this step is that we are retaining the complementary entanglement wedge $\mathrm{EW}(\overline{A})$. This step can then be repeated multiple times to generate a sequence of states, all of which are increasingly coarse-grained.[6]

Now, we apply this idea to a general spacetime $\mathcal{M}$ by considering infinitesimal subregions A of size δ ($\to 0$) on the boundary leaf σ. In order to coarse-grain, we find the HRT surface γ_A and reduce the accessible spacetime region to the complementary entanglement wedge, $\mathrm{EW}(\overline{A})$. Repeating this multiple times involves shrinking the domain of dependence at each step by finding new HRT surfaces anchored to infinitesimal subregions as seen in Fig. 3.5.

In the continuum limit, this reduces to the original construction of Ref. [54]; see Fig. 3.6. Here, we consider the intersection of the complementary entanglement wedges $\mathrm{EW}(\overline{A_p})$ for infinitesimal subregions A_p, centered around arbitrary points on the leaf, denoted by p. This

[6]We note that this is similar to the construction suggested in Refs. [92, 93], although here we directly use the TN description and its fine structure, as opposed to constructing the TN using information about the boundary state such as entanglement of purification [94, 95] or reflected entropy [96].

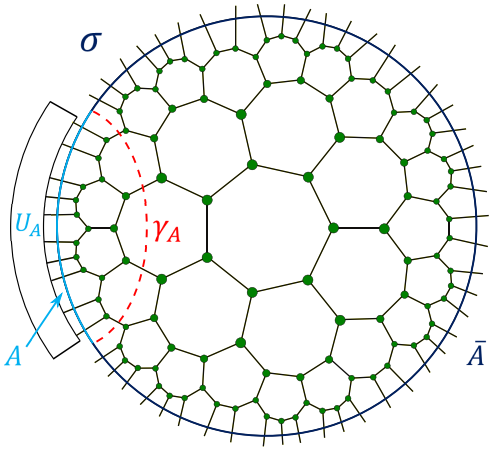

Figure 3.3: The von Neumann entropy of subregion A is computed by the minimal cut γ_A that splits the TN into two parts containing A and $\overline{A}$ respectively.

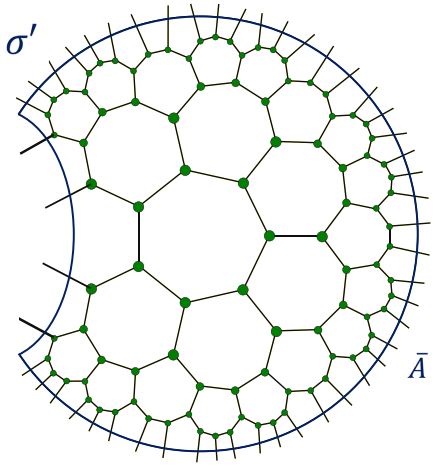

Figure 3.4: By applying a local unitary on A, we can find maximally entangled legs across γ_A, which serve as a bottleneck for the entanglement between A and $\overline{A}$.

leads to a new domain of dependence $R(\sigma)$,

$$R(\sigma) = \cap_p \, \mathrm{EW}(\overline{A_p}), \tag{3.5}$$

which can be interpreted as defining the state on a new "renormalized" leaf σ_1 such that the domain of dependence of σ_1 is $R(\sigma)$, i.e. $D(\sigma_1) = R(\sigma)$.[7] The HRT prescription can be shown to consistently apply for subregions on this renormalized leaf as well, owing to the fact

[7]The domain of dependence of a closed codimension-2 surface is defined as the domain of dependence of a spacelike hypersurface enclosed by the surface.

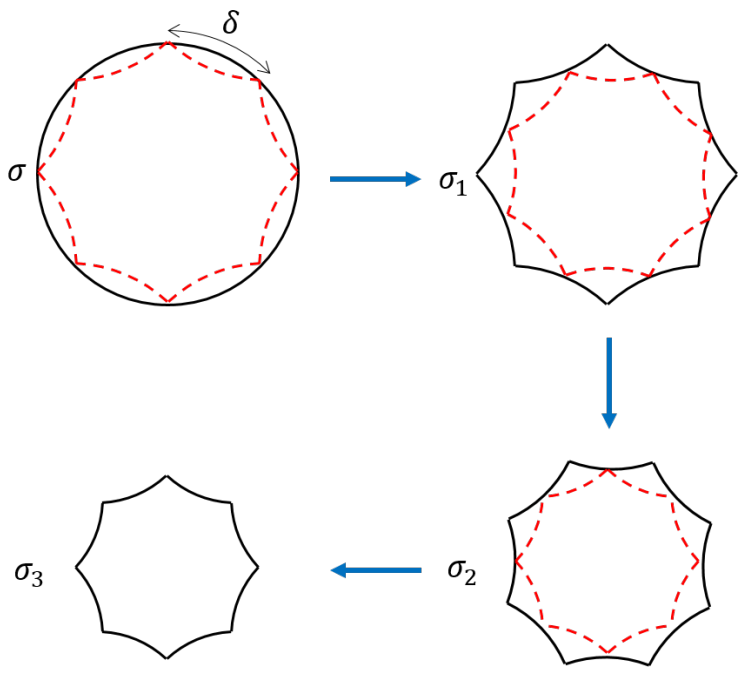

Figure 3.5: A sequence of coarse-graining steps. At each step, we consider infinitesimal subregions of size δ ($\to 0$) and reduce the spacetime region to their respective complementary entanglement wedges.

that it is still a convex surface [54]. Thus, we may interpret this as the spacetime continuum version of the procedure yielding the sequence of states described above using TNs.

This continuum procedure can be written in terms of a flow equation for the leaf $\sigma(\lambda)$, which is interpreted as a Lorentzian mean curvature flow:

$$\frac{dx^\mu}{d\lambda} = \frac{1}{2}(\theta_k l^\mu + \theta_l k^\mu), \tag{3.6}$$

where x^μ are the embedding coordinates of $\sigma(\lambda)$, $\{k^\mu, l^\mu\}$ are the future-directed null vectors orthogonal to $\sigma(\lambda)$, normalized such that $k \cdot l = -2$, and $\theta_{k,l}$ are the classical expansions in the k, l directions, respectively. The sequence of renormalized leaves span a codimension-1 hypersurface, which was termed the holographic slice. In particular, it is a partial Cauchy slice of the bulk domain of dependence, $D(\sigma)$, of the original leaf σ.

It was shown that the flow described above satisfies various interesting properties that are consistent with the coarse-graining interpretation. These include the fact that the area of the leaf $\sigma(\lambda)$ decreases monotonically with λ, implying that the number of degrees of freedom in the effective Hilbert space $\mathcal{H}_{\text{eff}}(\sigma(\lambda))$ decreases as we flow. By choosing statistically isotropic subregions with random shapes, one can obtain a preferred holographic slice that preserves the symmetries of the system. Alternatively, by varying flow rates along the transverse directions, one could get a range of different, but gauge equivalent, slices of $D(\sigma)$.

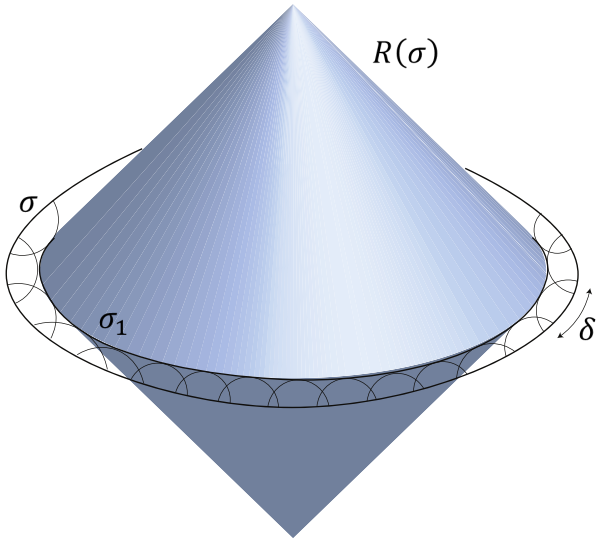

Figure 3.6: Coarse-graining over infinitesimal subregions on σ can be performed by considering the intersection of complementary entanglement wedges. This leads to a domain of dependence $R(\sigma)$ which corresponds to a new renormalized leaf σ_1.

3.4 Motivation from Tensor Networks

Having the classical construction in hand, we now describe how to generalize it to include bulk quantum corrections. Let us take a specific state defined on a leaf of a Q-screen. We want to understand how coarse-graining of this state works using the TN picture.

We expect that the state is still modeled by a TN at the quantum level. In order to represent the effect of bulk quantum corrections appropriately, this TN must include two additional features compared with the classical case. First, tensors and bonds used in the network should in general not be all "featureless," i.e. all the tensors being the same and connected by maximally entangling bonds, as was the case in simple perfect tensor [69] or random tensor [70] networks. Reflecting the existence of excitations of bulk low-energy fields, tensors and/or bonds must have a non-universal structure representing such excitations. This generally makes the network not fully isometric. Second, since bulk low-energy quantum fields can have long-range entanglement, corresponding to S_{bulk} in S_{gen}, there should be longer bonds connecting non-nearest-neighbor tensors, although the number of such nonlocal bonds (or more precisely, the total dimension associated with them) is suppressed generally as the bonds become longer. A typical TN of this sort is depicted in Fig. 3.7.

Once we have a TN representation of the state, the scenario in Sec. 3.3 can be generalized in a relatively simple manner. To do so, we must first establish how to compute the entropy of a boundary subregion, following the formula in Eq. (3.4). In general, the boundary legs consist of both the shortest, local bonds and longer, nonlocal bonds cut by the boundary. When we compute the entropy of subregion A of σ_{int}, i.e. a subset of these legs, we must

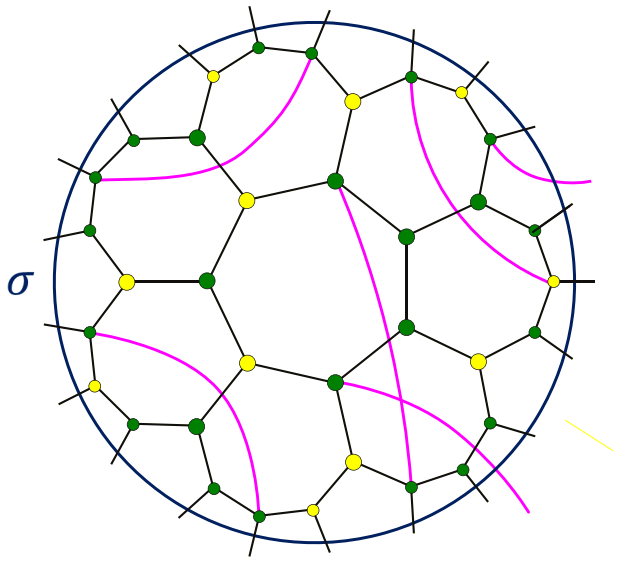

Figure 3.7: A TN representing a state at the quantum level has tensors that are not universal (yellow) and bonds that connect tensors nonlocally (pink).

minimize

$$\tilde{S}_{\rm gen}(A, X_A) = \frac{\mathcal{A}(A \cup X_A)}{4G_N} + S_{\rm bulk}(\Xi_A) \tag{3.7}$$

over all surfaces X_A anchored to the boundary of A, where Ξ_A is the homology surface with $\partial\Xi_A = A \cup X_A$. In this expression, the area term represents the contribution from the shortest bonds, while $S_{\rm bulk}(\Xi_A)$ from longer bonds, cut by $\partial\Xi_A$. In short, $\tilde{S}_{\rm gen}(A, X_A)$ is given by the entropy of all the bonds connecting tensors inside and outside $\partial\Xi_A$, regardless of their lengths; see Fig. 3.8. (This reflects the fact that the precise way to separate the contributions from local and nonlocal bonds is arbitrary and does not have an invariant meaning.)

With this prescription, we can follow the analysis in Sec. 3.3 and coarse-grain the region A of the boundary state by removing the bulk regions that are entangled with A, i.e. by reducing the TN to a smaller one giving a state on

$$\sigma' = \overline{A} \cup \Gamma_{\overline{A}}. \tag{3.8}$$

Note that here the complement $\overline{A}$ of A is defined as that on the entire leaf $\sigma = \sigma_{\rm int} \cup \sigma_{\rm ext}$, not on $\sigma_{\rm int}$. The QES $\Gamma_{\overline{A}}$ is given by the surface $X_{\overline{A}}$ minimizing

$$\tilde{S}_{\rm gen}(\overline{A}, X_{\overline{A}}) = \frac{\mathcal{A}(\overline{A} \cup X_{\overline{A}})}{4G_N} + S_{\rm bulk}(\Xi_{\overline{A}}), \tag{3.9}$$

where

$$\partial X_{\overline{A}} = \partial\overline{A} = \partial\overline{A}_{\rm int} \tag{3.10}$$

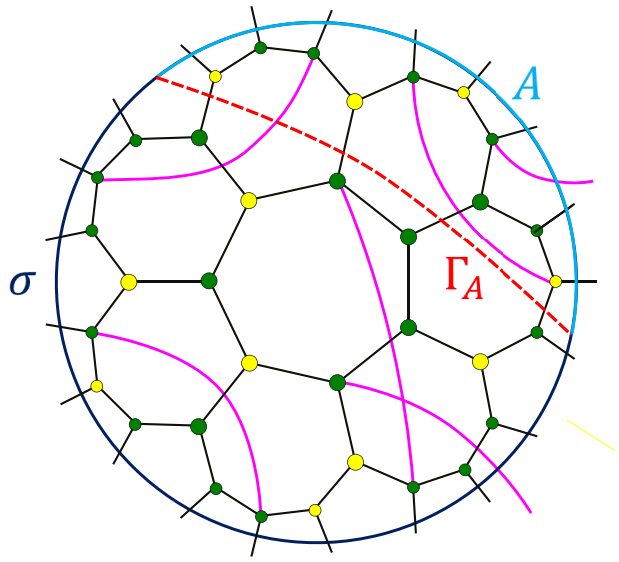

Figure 3.8: The minimal QES Γ_A of subregion A is determined by minimizing the entropy of all bonds connecting tensors inside and outside $A \cup \Gamma_A$ (consisting of 12 black and 2 pink bonds in the figure).

with $\overline{A}_{\text{int}}$ the complement of A on σ_{int} (i.e. $\overline{A} = \overline{A}_{\text{int}} \cup \sigma_{\text{ext}}$, and $\partial \Xi_{\overline{A}} = \overline{A} \cup X_{\overline{A}}$, meaning that

$$\Xi_{\overline{A}} = \Xi_{\overline{A},\text{int}} \cup \Sigma_{\text{ext}}. \tag{3.11}$$

Here, $\partial \Xi_{\overline{A},\text{int}} = \overline{A}_{\text{int}} \cup X_{\overline{A}}$, and Σ_{ext} is a spacelike hypersurface exterior to σ_{ext}. Note that here we have defined that for σ_{ext}, the surface "enclosed" by σ_{ext} to be the exterior of σ_{ext}:

$$\partial \Sigma_{\text{ext}} = \sigma_{\text{ext}}. \tag{3.12}$$

This procedure gives the interior portion of the new leaf to be

$$\sigma'_{\text{int}} = \overline{A}_{\text{int}} \cup \Gamma_{\overline{A}}. \tag{3.13}$$

We assume that for a TN representing a state with a semiclassical bulk, the RT formula with quantum corrections can be applied to the state on this new surface as well. The process described here can be repeated multiple times, leading to a similar sequence of coarse-grained states as before.

Note that the assumption of the RT formula continuing to hold is nontrivial given that generic bulk states break the isometric property of the TN. However, we will only need to assume that the RT formula holds for infinitesimal subregions and their complements, which gives results that are consistent with the coarse-graining interpretation suggested here. As discussed in Sec. 3.2, one could also consider bulk matter with large central charge so that the non-isometric behavior appears only at subleading order in $1/c$ for reasonable bulk states [92, 93].

3.5 Coarse-Graining and Quantum Flow

Definition

Having found the procedure in TNs, we can now look for a continuum version in semiclassical gravity. Given the framework established in Sec. 3.2, we can locate the Q-screen for a given state and start a coarse-graining procedure analogous to that discussed in Sec. 3.4.

As described in Sec. 3.3, we consider an infinitesimal subregion on the interior portion σ_{int} of the original leaf σ and reduce the accessible spacetime region to the complementary quantum entanglement wedge $\text{QEW}(\overline{A})$, which is determined by the minimal QES $\Gamma_{\overline{A}}$ of $\overline{A}$ such that $\text{QEW}(\overline{A}) = D(\Sigma_{\overline{A}})$, where $\partial\Sigma_{\overline{A}} = \overline{A} \cup \Gamma_{\overline{A}}$. Note that in a general spacetime, the global description includes an exterior portion outside σ_{ext}. Thus, the complement of an infinitesimal subregion $A \subset \sigma_{\text{int}}$ on the leaf is $\overline{A} = \overline{A}_{\text{int}} \cup \sigma_{\text{ext}}$, and the bulk entropy term S_{bulk} of the generalized entropy is given by the von Neumann entropy of $\Sigma_{\overline{A}} = \Sigma_{\overline{A},\text{int}} \cup \Sigma_{\text{ext}}$. The necessity of including the region exterior to σ_{ext} can be argued from complementary recovery in pure states.

Considering many such infinitesimal subregions A_p on σ_{int} centered around points p as in Eq. (3.5), we can sequentially reduce the accessible spacetime region to

$$R(\sigma) = \cap_p \, \text{QEW}(\overline{A_p}), \tag{3.14}$$

which leads to a renormalized leaf σ_1 such that $D(\Sigma_1) = R(\sigma)$, where $\partial\Sigma_1 = \sigma_1$. This yields a new boundary state in a smaller effective Hilbert space defined on σ_1. As we show later, the convexity of the original leaf implies that the corresponding renormalized leaf is also convex, which ensures that the coarse-graining prescription can be repeatedly applied to get a family of leaves. This describes what we call the quantum flow. The preservation of convexity also means that $S(A)$ of a subregion A of a renormalized leaf obtained by Eq. (3.4) satisfies properties needed for it to be interpreted as the von Neumann entropy of the density matrix of the region.

Possibility of appearance of disconnected leaf portions

While performing the coarse-graining as described above, it may occur that the minimal QES $\Gamma_{\overline{A_p}}$ for $\overline{A_p}$ in Eq. (3.14) becomes non-infinitesimal. In particular, if there is a bulk region surrounded by a surface X of area $\mathcal{A}(X)$ and whose entanglement with the exterior of σ_{ext} exceeds $\mathcal{A}(X)/4G_N$ on a given spacelike slice containing $\sigma_i = \sigma_{\text{int},i} \cup \sigma_{\text{ext}}$, then the quantum minimal surface $\chi(\overline{A_p})$ on it has a disconnected component surrounding the region. If such a disconnected component remains after the maximization over all the spacelike slices, then the minimal QES $\Gamma(\overline{A_p})$ does have a disconnected component, and as a consequence $R(\sigma)$ will have a "hole" such that $\partial R(\sigma) \supset X$. This makes the new leaf $\sigma_{\text{int},i+1}$ have a disconnected component X ($\subset \sigma_{\text{int},i+1}$), in addition to the portion infinitesimally close to $\sigma_{\text{int},i}$. The region surrounded by X is thus excluded from the flow afterward.

When it first appears, an excluded region, and hence the disconnected component of the leaf associated with it, is small. This appearance cannot be seen just by solving the flow equation, although our coarse-graining procedure itself captures the occurrence of this phenomenon. After its appearance, the disconnected component of the leaf also flows generally, following the flow equation. This makes the hole of the spacetime larger, which may eventually collide with the component arising from the continuous inward motion of the original leaf portion σ_{int}.

The Flow Equation

In the continuum limit, the behavior of QESs anchored to small subregions can be studied analytically. While the von Neumann entropy can in general show complicated behaviors as the subregion is varied, for an infinitesimal subregion we may expect that such behaviors arise only from physics at scales much larger than the size of the subregion. It is then reasonable to assume that the change of the entropy of the subregion, as well as that of the complement, can be approximated by the volume integral of some density function. With this assumption, and reasonable smoothness assumptions about the spacetime and subregions, we show later that the resulting QESs are such that the deepest point lies in a universal normal direction to the leaf given by

$$s = \frac{1}{2}\left(\Theta_k l + \Theta_l k\right), \tag{3.15}$$

as long as the relevant QESs exist. Here, $\{k^\mu, l^\mu\}$ are the future-directed null vectors orthogonal to σ_{int}, normalized such that $k \cdot l = -2$, and $\Theta_{k,l}$ are the corresponding quantum expansions. Here, $\Theta_{k,l}$ are computed by varying S_{gen} as defined in Eq. (3.9). This is sufficient to find the location of $\sigma_{1,\text{int}}$, and hence of σ_1, after fixing relative normalizations for the size of subregions considered on different portions of the leaf. For convenience, we will choose the normalizations such that the resulting flow equation takes the simplest form. Other possibilities will be discussed in later.

Following the procedure described above, we can derive a flow equation, which generalizes the Lorentzian mean curvature flow in Eq. (3.6) to include bulk quantum corrections:

$$\frac{dx^\mu}{d\lambda} = \frac{1}{2}(\Theta_k l^\mu + \Theta_l k^\mu), \tag{3.16}$$

where x^μ are the embedding coordinates of the interior portion $\sigma_{\text{int}}(\lambda)$ of the renormalized leaves $\sigma(\lambda) = \sigma_{\text{int}}(\lambda) \cup \sigma_{\text{ext}}$, parameterized by λ, and $\Theta_{k,l}$ represent the quantum expansions of $\sigma(\lambda)$ at x^μ. The resulting sequence of $\sigma_{\text{int}}(\lambda)$ spans a codimension-1 quantum-corrected holographic slice as shown in Fig. 3.9.

Derivation of the Flow Equation

Consider a codimension-2, closed, achronal surface σ in an arbitrary $(d+1)$-dimensional spacetime M. Suppose σ is a convex boundary. We assume that both M and σ are sufficiently

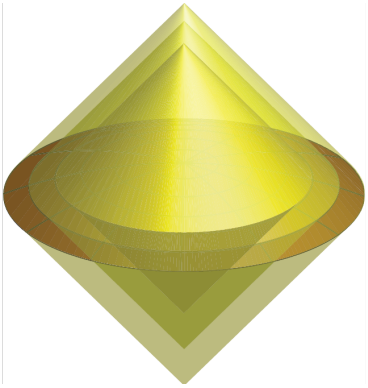

Figure 3.9: A sequence of renormalized leaves $\sigma_{\text{int}}(\lambda)$ obtained by solving the flow equation in Eq. (3.16) spans a codimension-1 quantum-corrected holographic slice. Each leaf represents the domain of dependence of a spacelike surface $\Sigma_{\text{int}}(\lambda)$ with $\partial\Sigma_{\text{int}}(\lambda) = \sigma_{\text{int}}(\lambda)$.

smooth so that variations in the spacetime metric $g_{\mu\nu}$ and induced metric on σ, denoted by h_{ij}, occur on characteristic length scales L_g and L_σ, respectively. We also assume that the changes of the variational entropy current density $J^\mu(x)$, discussed below, occur on a characteristic length scale L_S.

Consider subregion A of characteristic length $\delta \ll L_g, L_\sigma, L_S$ on the surface σ. This subregion A is chosen to be a $(d-1)$-dimensional ellipsoid on σ at order $O(\delta)$. Then, at the leading order, the QES anchored to ∂A lives on the hypersurface generated by the evolution vector[8]

$$s = \frac{1}{2}(\Theta_k l + \Theta_l k) = \Theta_t t - \Theta_z z \tag{3.17}$$

normal to σ. Here, k and l are future-directed null vectors orthogonal to σ normalized as $k \cdot l = -2$, and t and z are vectors related to these by

$$k = (t + z), \quad l = (t - z). \tag{3.18}$$

Let us now prove this claim. Since the subregion A is assumed to be an ellipsoid, we label its center point as p. We can then set up Riemann normal coordinates in the local neighborhood of p:

$$g_{\mu\nu}(x) = \eta_{\mu\nu} - \frac{1}{3}R_{\mu\nu\rho\sigma}x^\rho x^\sigma + O(x^3). \tag{3.19}$$

In these coordinates, we are considering a patch of size $O(\delta)$ around the origin p with $R_{\mu\nu\rho\sigma} \sim O(1/L_g^2)$, so at any point in this patch

$$g_{\mu\nu}(x) = \eta_{\mu\nu} + O\left(\frac{\delta^2}{L_g^2}\right). \tag{3.20}$$

[8]We ignore the possibility that there is no QES infinitesimally close to A as $\delta \to 0$, i.e. the possibility (iii) for the end of flow.

Since there is still a remaining $SO(d,1)$ symmetry that preserves the Riemann normal coordinate form of the metric, we can use these local Lorentz boosts and rotations to set t and z as the coordinates in the normal direction to σ at p while y^i parameterize the tangential directions. At order $O(\delta)$, the subregion A is then an ellipsoid in the y^i coordinates centered at the origin p.

In a small region around p, we can define a variational entropy current density that measures how S_{bulk} changes. More formally, let X_A be a surface anchored to the boundary of A, or equivalently of $\overline{A}$: $X_A = X_{\overline{A}}$. Let $\Xi_{\overline{A}}$ be the homology surface with $\partial\Xi_{\overline{A}} = \overline{A} \cup X_{\overline{A}}$, then

$$S_{\text{bulk}}(\Xi_{\overline{A}}) = S_0 - \int_{\mathcal{S}} J_\mu(x) da^\mu. \tag{3.21}$$

where S_0 is the S_{bulk} associated with the full σ, so it is independent of the choice of subregion A or the surface X_R. $J_\mu(x)$ is the aforementioned variational entropy current density which upon integrating over $\mathcal{S}$, a homology surface with boundary $\partial\mathcal{S} = A \cup X_{\overline{A}}$, determines how $S_{\text{bulk}}(\Xi_{\overline{A}})$ differs from S_0.

We now Taylor expand the entropy current density about p, so for any point within $O(\delta)$ distance of p

$$J_\mu(x) = \mathcal{J}_\mu \left(1 + O\left(\frac{\delta}{L_S}\right)\right), \tag{3.22}$$

where $\mathcal{J}_\mu = J_\mu(0)$. Recall that L_S is the length scale of the variations of corresponding entropy variations.

Let K^t_{ij} , K^z_{ij} denote the extrinsic curvature tensors of σ for the t and z normals, respectively. It follows that $K^t_{ij}, K^z_{ij} \sim O(1/L_\sigma)$. Since t and z are normal to σ, the equations for the surface σ, described by $t_L(y^i)$ and $z_L(y^i)$, can be Taylor expanded in the region A as

$$t_L(y^i) = -\frac{1}{2} K^t_{ij} y^i y^j + O\left(\frac{\delta^3}{L_\sigma^2}\right), \tag{3.23}$$

$$z_L(y^i) = \frac{1}{2} K^z_{ij} y^i y^j + O\left(\frac{\delta^3}{L_\sigma^2}\right), \tag{3.24}$$

where the negative sign in the first line is due to the time-like signature of the t normal.

From Eqs. (3.23) and (3.24), it follows that at the leading order in δ,

$$\nabla^2 t_L = -\eta^{ij} K^t_{ij}, \tag{3.25}$$

$$\nabla^2 z_L = \eta^{ij} K^z_{ij}, \tag{3.26}$$

where $\nabla^2 = \partial^i \partial_i$. Note that $h_{ij} = \eta_{ij}$ at this order.

It follows that the ratio of quantum null expansions on the surface σ is

$$\frac{\Theta_k}{\Theta_l} = \frac{\eta^{ij}(K^t_{ij} + K^z_{ij}) + 4G_N(\mathcal{J}_t - \mathcal{J}_z)}{\eta^{ij}(K^t_{ij} - K^z_{ij}) + 4G_N(-\mathcal{J}_t - \mathcal{J}_z)}, \tag{3.27}$$

or equivalently

$$\frac{\Theta_t}{\Theta_z} = \frac{\Theta_k + \Theta_l}{\Theta_k - \Theta_l} = \frac{\eta^{ij} K^t_{ij} - 4G_N \mathcal{J}_z}{\eta^{ij} K^z_{ij} + 4G_N \mathcal{J}_t}. \tag{3.28}$$

Here, we have used that bulk entropy is given by Eq. (3.21) along with the Taylor expansion in Eq. (3.22).

The QES $\Gamma_{\overline{A}}$ can be parameterized in a similar way using $t_E(y^i)$ and $z_E(y^i)$. The boundary conditions satisfied by the QES are

$$t_E(\partial A) = t_L(\partial A), \tag{3.29}$$
$$z_E(\partial A) = z_L(\partial A). \tag{3.30}$$

Since the region A is chosen to be an ellipsoidal region in the y^i coordinates at $O(\delta)$, we have symmetry under $y^i \to -y^i$ at this order. Consequently, the t and z directions are normal to the QES at the center point $(t_E(0), z_E(0), 0)$.

Let $\widetilde{K}^t_{ij}$, $\widetilde{K}^z_{ij}$ denote the extrinsic curvature tensors of the QES for the t and z normals, respectively. We assume that the QES is approximately flat at lengthscale δ, i.e. $\widetilde{K}^t_{ij}, \widetilde{K}^z_{ij} \ll 1/\delta$. We will show that this assumption is self-consistent as long as the entropy current density is not too large.

We can Taylor expand $t_E(y^i)$ and $z_E(y^i)$ as

$$t_E(y^i) = t_E(0) - \frac{1}{2}\widetilde{K}^t_{ij} y^i y^j, \tag{3.31}$$
$$z_E(y^i) = z_E(0) + \frac{1}{2}\widetilde{K}^z_{ij} y^i y^j. \tag{3.32}$$

Since the QES has vanishing quantum null expansion, we have at the leading order

$$\eta^{ij}(\widetilde{K}^t_{ij} + \widetilde{K}^z_{ij}) + 4G_N(\mathcal{J}_t - \mathcal{J}_z) = 0, \tag{3.33}$$
$$\eta^{ij}(\widetilde{K}^t_{ij} - \widetilde{K}^z_{ij}) + 4G_N(-\mathcal{J}_t - \mathcal{J}_z) = 0. \tag{3.34}$$

Here, we have used the expansion in Eq. (3.22) because any point on the QES is at most $O(\delta)$ distant from the origin p.

These equations, along with Eqs. (3.31) and (3.32), result in the following differential equations for $t_E(y^i)$ and $z_E(y^i)$ at the leading order

$$\nabla^2 t_E = -\eta^{ij}\widetilde{K}^t_{ij} = -4G_N \mathcal{J}_z, \tag{3.35}$$
$$\nabla^2 z_E = \eta^{ij}\widetilde{K}^z_{ij} = -4G_N \mathcal{J}_t. \tag{3.36}$$

Earlier, we assumed that $\widetilde{K}^t_{ij}, \widetilde{K}^z_{ij} \ll 1/\delta$, which is justified as long as $\mathcal{J}_t, \mathcal{J}_z \ll 1/(4G_N\delta)$, which is the case if $\mathcal{J}_t, \mathcal{J}_z$ do not diverge as $\delta \to 0$.

Let us consider the quantities $\delta t = t_E - t_L$ and $\delta z = z_E - z_L$. These satisfy the following differential equations at the leading order

$$\nabla^2 \delta t = \eta^{ij} K^t_{ij} - 4G_N \mathcal{J}_z, \tag{3.37}$$

$$\nabla^2 \delta z = -\eta^{ij} K^z_{ij} - 4G_N \mathcal{J}_t. \tag{3.38}$$

The boundary conditions are given by

$$\delta t(\partial A) = \delta z(\partial A) = 0. \tag{3.39}$$

It is now clear that at the leading order, $\delta t/\Theta_t$ and $-\delta z/\Theta_z$ satisfy the same differential equation with the same boundary conditions, since Θ_t and Θ_z can be regarded as constant at this order. Thus,

$$\frac{\delta t}{\Theta_t} = -\frac{\delta z}{\Theta_z}\left(1 + O(\delta)\right) \tag{3.40}$$

for all points on the extremal surface. Rewritten, the extremal surface lives on the hypersurface generated by the evolution vector $s = \Theta_t t - \Theta_z z$ normal to σ.

In making the claim above, we have assumed that the subregion A is a $(d-1)$-dimensional ellipsoid on the surface σ. Nonetheless, the proof goes through if the subregion R has a reflection symmetry $(y^1, y^2, ..., y^{d-1}) \to (-y^1, -y^2, ..., -y^{d-1})$ about the center point p at order $O(\delta)$.

In fact, we expect this theorem to hold for a more general subregion A because the above proof works if we can find any point $p \in A$ such that the normal vectors to σ at p match with the normal vectors to the QES at the point corresponding to p at order $O(\delta)$. Under the condition that $\delta \ll L_g, L_\sigma, L_S$, such a point lies at the "center," in the sense that the leading-order treatment here works; for example, the QES of the form of Eqs. (3.31) and (3.32) is correctly "anchored" to ∂A at the leading order in δ.

Finally, our discussion here applies in the context of the main text to the interior portion of the leaf, σ_{int}. The existence of the exterior portion σ_{ext} does not change the fact that the QES of $\overline{A}$ lies on the hypersurface given by Eq. (3.40).

3.6 Features of the Quantum Flow

Convexity of Renormalized Leaves

Let us begin by defining convexity in the context of this chapter. Consider a compact set S on spacelike slice Σ. This set is defined to be convex if the quantum minimal surface χ_A anchored to the boundary ∂A of a codimension-2 region $A \subset S$ is such that $\forall A$, $\chi_A \subset S$. Here, the quantum minimal surface χ_A is defined as the surface on Σ which minimizes the generalized entropy S_{gen} for the region on Σ bounded by $\chi_A \cup A$. A codimension-2 compact surface σ is called a convex boundary if on every codimension-1 spacelike slice Σ such that $\sigma \subset \Sigma$, the closure of the interior of σ is a convex set.

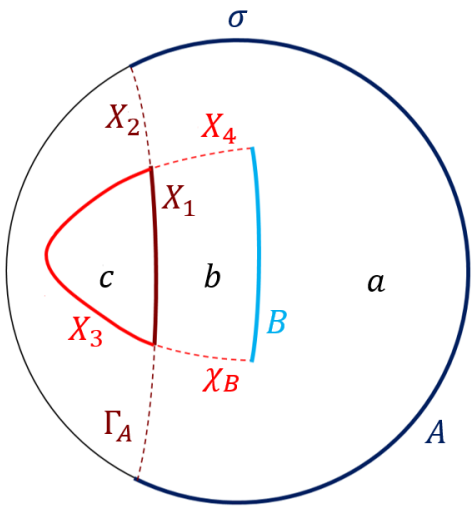

Figure 3.10: The quantum minimal surface χ_B crossing the quantum minimal surface Γ_A.

Theorem. If σ is a convex boundary, then for any subregion $A \subset \sigma$, $A \cup \Gamma_A$ is also a convex boundary.

Proof. Suppose that for some spacelike slice Σ, which contains $A \cup \Gamma_A$, there is B in the closure of the interior of $A \cup \Gamma_A$ such that the unique quantum minimal surface χ_B goes outside $A \cup \Gamma_A$.

Since σ is assumed to be a convex boundary, χ_B cannot go outside σ, i.e. it cannot cross A. Thus, χ_B must cross Γ_A as shown in Fig. 3.10.

As $\Gamma_A = X_1 \cup X_2$ is the quantum minimal surface for A,

$$\frac{\mathcal{A}(X_1)}{4G} + \frac{\mathcal{A}(X_2)}{4G} + \frac{\mathcal{A}(A)}{4G} + S_{\text{bulk}}(ab) \leq \frac{\mathcal{A}(X_2)}{4G} + \frac{\mathcal{A}(X_3)}{4G} + \frac{\mathcal{A}(A)}{4G} + S_{\text{bulk}}(abc), \quad (3.41)$$

where the right hand side corresponds to the surface $X_A = X_2 \cup X_3$.

Also, $\chi_B = X_3 \cup X_4$ is the unique quantum minimal surface for B, so

$$\frac{\mathcal{A}(X_3)}{4G} + \frac{\mathcal{A}(X_4)}{4G} + \frac{\mathcal{A}(B)}{4G} + S_{\text{bulk}}(bc) < \frac{\mathcal{A}(X_1)}{4G} + \frac{\mathcal{A}(X_4)}{4G} + \frac{\mathcal{A}(B)}{4G} + S_{\text{bulk}}(b), \quad (3.42)$$

where the right hand side corresponds to the surface $X_B = X_1 \cup X_4$.

Combining Eqs. (3.41) and (3.42), we have

$$S_{\text{bulk}}(ab) + S_{\text{bulk}}(bc) < S_{\text{bulk}}(b) + S_{\text{bulk}}(abc) \quad (3.43)$$

which contradicts strong subadditivity. Thus, the quantum minimal surface χ_B crossing the quantum minimal surface Γ_A results in a contradiction. □

By repeatedly applying this theorem, we can show that if the initial leaf has the interior portion σ_{int} that is convex, then a sequential quantum flow procedure results in a convex interior portion at each step. In the continuum limit, this sequential procedure gives us the same renormalized leaves that were obtained using the flow equation. Thus, we conclude that if the initial leaf portion $\sigma_{\text{int}}(0)$ is a convex boundary, then the renormalized leaf portion $\sigma_{\text{int}}(\lambda)$ is also a convex boundary for all $\lambda > 0$.

Lemma. Consider a slice Σ and a compact set $S \subset \Sigma$. If S is convex then $\Theta_\Sigma(\partial S) \leq 0$. Here, $\Theta_\Sigma(\partial S)$ is the trace of the quantum extrinsic curvature of ∂S embedded in Σ for the normal pointing inward.

Proof. Suppose that $\Theta_\Sigma(\partial S) > 0$ somewhere on ∂S. One can explicitly construct minimal surfaces that are outside S by considering small enough subregions anchored to this portion of ∂S. □

Let the future-directed null vectors orthogonal to a codimension-2 spacelike surface σ be k and l, which we normalize as $k \cdot l = -2$.

When we discuss the convexity of the leaf $\sigma(\lambda) = \sigma_{\text{int}}(\lambda) \cup \sigma_{\text{ext}}$, we treat σ_{ext} as a single unit on σ which cannot be further divided into subregions. Thus, σ_{ext} is included or excluded as a whole when we consider any boundary subregion A.

Properties of the Flow

We now illustrate some of the salient properties of the flow, showing the consistency of it being interpreted as coarse-graining.

Monotonicity of generalized entropy of renormalized leaves

In order to interpret our procedure as coarse-graining, the number of degrees of freedom must decrease monotonically with λ. The dimension of the effective Hilbert space $\mathcal{H}_{\text{eff}}(\sigma(\lambda))$ associated with leaf $\sigma(\lambda)$ can be defined as the amount of entropy the boundary legs carry in the TN picture, implying

$$\begin{aligned} \ln |\mathcal{H}_{\text{eff}}(\sigma(\lambda))| &= \frac{\mathcal{A}(\sigma(\lambda))}{4G_N} + S_{\text{bulk}}(\Sigma(\lambda)) \\ &= S_{\text{gen}}(\sigma(\lambda)), \end{aligned} \tag{3.44}$$

where $|\mathcal{H}|$ represents the dimension of $\mathcal{H}$, and $\Sigma(\lambda)$ is a bulk codimension-1 spacelike surface bounded by $\sigma(\lambda) = \sigma_{\text{int}}(\lambda) \cup \sigma_{\text{ext}}$, i.e. $\Sigma(\lambda) = \Sigma_{\text{int}}(\lambda) \cup \Sigma_{\text{ext}}$. We thus find that the condition for the decrease of the degrees of freedom is the same as the statement that the generalized entropy of the renormalized leaf $\sigma(\lambda)$ decreases monotonically with λ. We now prove this in a manner similar to Ref. [54].

We have defined the evolution vector s, which is tangent to the holographic slice Υ and radially evolves the interior leaf portion inward:

$$s = \frac{1}{2}\left(\Theta_k l + \Theta_l k\right), \tag{3.45}$$

where the associated quantum expansions satisfy

$$\Theta_s = \Theta_k \Theta_l \leq 0. \tag{3.46}$$

This follows from Θ_k, Θ_{-l} being non-positive. To show this non-positivity property, consider some spacelike slice Σ with boundary σ. The inward normal n on Σ is given by

$$n = \alpha k - \beta l \tag{3.47}$$

with $\alpha, \beta \geq 0$. Suppose $\Theta_k > 0$. Now we can choose a slice Σ such that $\Theta_\Sigma(\sigma) > 0$ by taking $\alpha \gg \beta$. Thus, σ is not a convex boundary because the closure of its interior is not convex on Σ due to the lemma above and we arrive at a contradiction. A similar argument holds if $\Theta_l < 0$.

Next, consider a point p on the leaf portion $\sigma_{\text{int}}(\lambda)$ and the s vector orthogonal to $\sigma_{\text{int}}(\lambda)$ at p. Next consider an infinitesimal patch of area δA around p. As we flow along s by a small amount, the rate at which $S_{\text{gen}}(\sigma(\lambda))$ changes is determined by the quantum expansion Θ_s as

$$\delta S_{\text{gen}} \propto \Theta_s \delta \mathcal{A} \leq 0. \tag{3.48}$$

This implies that the contribution to $S_{\text{gen}}(\sigma(\lambda))$ from the inward flow of any infinitesimal patch is negative, and hence $S_{\text{gen}}(\sigma(\lambda))$ must decrease with λ.

The argument above relies on the flow equation. However, as shown in Section 3.5, it is possible that on coarse-graining, we obtain a new disconnected component of $\sigma_{\text{int}}(\lambda)$. While the appearance of such a component cannot be described by the flow equation, it comes with a negative contribution to the generalized entropy of the renormalized leaf. Thus, even on including this effect, we find that $S_{\text{gen}}(\sigma(\lambda))$ decreases with λ.

Containment of subregion flow

Consider the situation where we apply the holographic slice construction only to a finite subregion A of the leaf portion σ_{int}. This yields a sequence of renormalized leaves given by $\sigma(\lambda) = A(\lambda) \cup \overline{A}$. Here, $A(\lambda)$ represents a sequence of subregions that arise from the radial evolution of A.

Now, because of entanglement wedge nesting

$$\text{QEW}(\overline{A}) \subset \text{QEW}(\sigma(\lambda)) \tag{3.49}$$

for arbitrary λ, since $\overline{A} \subset \sigma(\lambda)$ for all λ. Here, $\text{QEW}(\overline{A})$ and $\text{QEW}(\sigma(\lambda))$ are determined by the corresponding minimal QESs. This implies that the boundary of $\text{QEW}(\overline{A})$ acts as an

extremal surface barrier for the flow of $A(\lambda)$. In particular, $A(\lambda)$ remains outside QEW($\overline{A}$) for all λ.

Incidentally, if there is another QES anchored to $\partial\overline{A}$ which lies outside QEW($\overline{A}$), then $A(\lambda)$ would not be able to go beyond this non-minimal extremal surface.

Remaining freedom

In general, the proof in Sec. 3.5 allows us to fix the direction of the flow at each point of $\sigma_{\text{int}}(\lambda)$ to be the vector s as discussed in Eq. (3.15). However, there is no canonical choice of normalization, reflecting the arbitrariness of choosing relative sizes of subregions for different points on $\sigma_{\text{int}}(\lambda)$. The ratio of these sizes must stay finite in the continuum limit, and yet it can still lead to inequivalent flow equations parameterized as

$$\frac{dx^\mu}{d\lambda} = \alpha(y^i, \lambda)(\Theta_k l^\mu + \Theta_l k^\mu), \tag{3.50}$$

where y^i represents the tangential coordinates on $\sigma_{\text{int}}(\lambda)$, and $\alpha(y^i, \lambda) > 0$. These flow equations in general result in different holographic slices, which are all gauge equivalent by the equations of motion. By choosing subregions of the same characteristic size at all p, we can fix the preferred normalization that leads to Eq. (3.16).

We note that this provides a natural gauge choice motivated by holography; the spacetime inside the holographic screen, which is now the Q-screen H', is parameterized by λ, y_i, and t, where t is a time parameter on the holographic screen giving a sequence of leaves at different times. (If disconnected components of $\sigma_{\text{int}}(\lambda)$ appear during the flow, then we must extend y_i to incorporate those components.)

An alternative choice for the normalization is to take λ to be the proper length along the trajectory $p(\lambda)$ of a point on $\sigma_{\text{int}}(\lambda)$. Here, the trajectory is defined such that if a point on $\sigma_{\text{int}}(\lambda + d\lambda)$ is located on the 2-dimensional surface orthogonal to $\sigma_{\text{int}}(\lambda)$ at $p(\lambda)$, then it is regarded as the "same" point as $p(\lambda)$, i.e. $p(\lambda + d\lambda)$. This provides another natural gauge choice motivated by holography.

End of the Flow

The quantum flow procedure described above provides a way to probe a spacetime inside the holographic screen by following the holographic slice inward. A key qualitative feature of the spacetime is given by how and where the holographic slice ends.

The holographic slice can end in one of the three possible ways:

(i) The slice ends at an empty surface. This can occur simply such that $\sigma_{\text{int}}(\lambda)$ keeps moving inward, and the slice is capped off at a point, as shown in Fig. 3.11. Alternatively, as discussed in Sec. 3.5, disconnected components of $\sigma_{\text{int}}(\lambda)$ may appear during the flow, which then grow outward and coalesce with the original component of $\sigma_{\text{int}}(\lambda)$ moving inward, ending up with an empty surface.

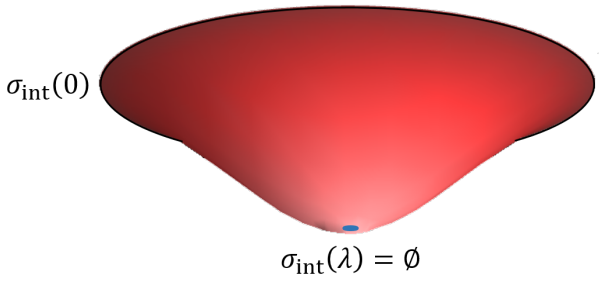

Figure 3.11: The holographic slice ending in an empty surface.

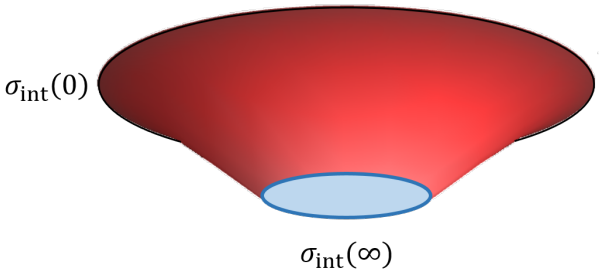

Figure 3.12: The holographic slice asymptoting to a quantum extremal surface.

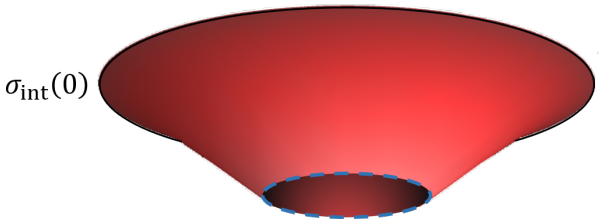

Figure 3.13: The holographic slice terminating abruptly.

(ii) The slice asymptotes to a QES as shown in Fig. 3.12. As the interior portion $\sigma_{\text{int}}(\lambda)$ of renormalized leaves approaches the QES, the flow slows down because $\Theta_k, \Theta_l \to 0$. Note that a QES homologous to the initial leaf portion $\sigma_{\text{int}}(0)$—even if it is non-minimal—acts as a barrier which cannot be crossed as we flow in.

(iii) The slice terminates abruptly as shown in Fig. 3.13. This occurs when the minimal QES associated with $\overline{A}$, the complement of an infinitesimal subregion A, becomes non-infinitesimal. At this point, we need to terminate the flow.

It is worth mentioning that while some of these cases have classical analogues, the second possibility of (i) and the case (iii) are exclusive to the quantum flow.

Examples

Various examples for the classical flow equation of Eq. (3.6) were discussed in Ref. [54]. In many situations, the minimal QES is a small perturbation to the classical HRT surface, and accordingly the quantum corrected flow equation in Eq. (3.16) results in a holographic slice that is perturbatively close to the classical holographic slice. There are, however, cases in which the two flows are significantly different. Here we illustrate an example of these: a black hole formed from collapse.

In the classical case, it was found that the holographic slice stays close to the horizon for a long time until it reaches the matter forming the black hole [54]. It is then capped off to form a complete Cauchy slice of the spacetime as seen in Figs. 5 and 6 of Ref. [54]. How is this modified at the quantum level?

Far from the black hole horizon, the flow is largely unaffected. It is, however, significantly modified once we approach the horizon. As the black hole evaporates, there are Hawking modes that escape to the region exterior to σ_{ext}, denoted R, leaving behind their interior partners entangled with them. As the leaf portion σ_{int} is moved inward by the flow, its classical area decreases but the entropy contribution from the Hawking partners increases. About a Planck distance inside the horizon, the two effects compete with each other, resulting in a QES where the flow ends. The mechanism by which the QES emerges here is identical to the one that appeared in a specific example in Ref. [97].[9] Thus, after including bulk quantum corrections, the holographic slice becomes a partial Cauchy slice of the spacetime that excludes a large portion of the interior.[10] The same feature can be found in the case of an AdS black hole, where one could allow the black hole to evaporate by coupling the CFT to a bath. Our coarse-graining procedure then leads to a flow that stops at the same QES as that found in Refs. [16, 17].

Another mechanism excising the black hole interior comes from the phenomenon discussed in Sec. 3.5. As the black hole evaporates, there are a large number of interior partners of Hawking radiation that accumulate behind the horizon, which eventually exceed the area of the horizon at the Page time. Hence the interior of such an old black hole would not be swept by renormalized leaves (even if the flow did not halt as described above).

The phenomenon that the holographic slice does not penetrate deep into the black hole horizon was already seen in the classical case. There is, however, an important difference in the quantum case. As shown in Figs. 3.14 and 3.15, holographic slices become partial Cauchy slices during the middle of the evolution of a black hole. (These can be contrasted with Figs. 5 and 6 of Ref. [54].) This implies, in particular, that with a given time parameterization on a boundary, e.g. on the holographic screen, the concept of black hole formation and evaporation can be rigorously defined through the behavior of the flow discussed earlier.

[9] Recently, Ref. [98] appeared which found such a non-trivial QES in cosmological spacetimes. The coarse-graining flow would end at the QES in these situations as well.

[10] This does not necessarily mean that the interior of the black hole is absent. It is possible that the semi-classical interior picture emerges through approximately state-independent operators acting on modes (the hard modes [99, 100]) whose characteristic frequencies are larger than the local Hawking temperature [101].

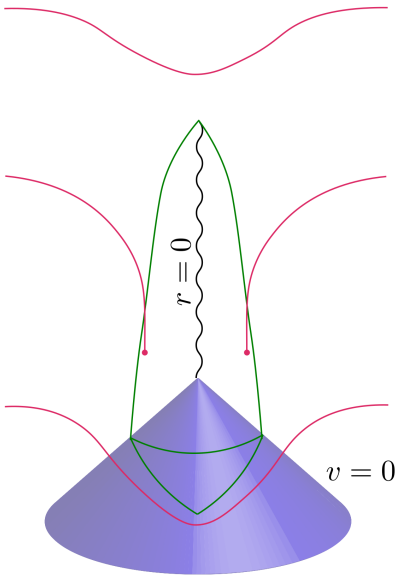

Figure 3.14: Eddington-Finkelstein diagram representing black hole formation and evaporation with quantum holographic slices depicted for three characteristic times.

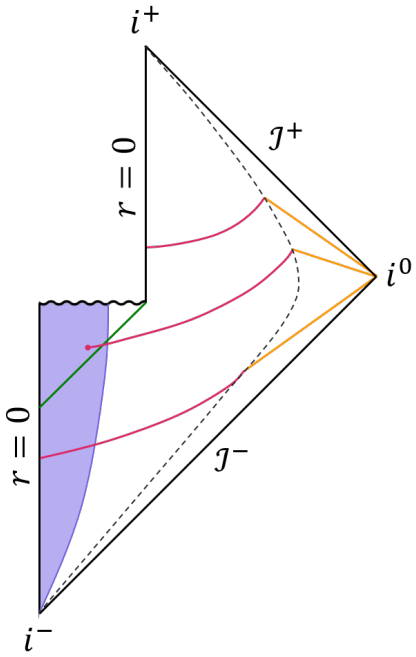

Figure 3.15: Penrose diagram version of Fig. 3.14. The region R outside σ_{ext} is depicted by orange lines.

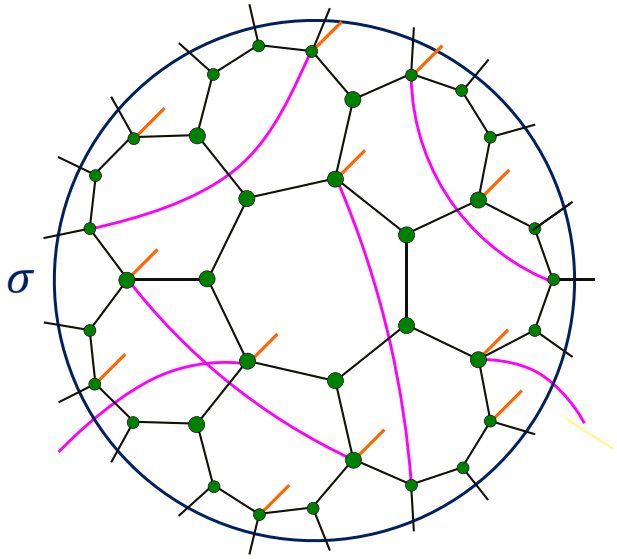

Figure 3.16: A TN representing a collection of states has dangling legs as well as nonuniversal tensors and nonlocal bonds.

3.7 Relation to Quantum Error Correction

In this section, we discuss the relation between our coarse-graining procedure and the picture that the holographic dictionary works as quantum error correction [3, 78, 79, 80], in which a small Hilbert space of semiclassical bulk states is mapped isometrically into a larger boundary Hilbert space. In our framework, this picture arises after considering a collection of states over which we want to build a low energy bulk description.

In the context of quantum error correction, one chooses the set of semiclassical bulk states that can be represented as a code subspace in the boundary theory. In a general time-dependent spacetime, however, there is no natural choice of code subspace fixed by the bulk effective theory. This is because degrees of freedom that appear natural on one time slice need not be in bijection with those that appear natural on a different time slice. For example, if a single heavy particle decays into a large number of radiation particles within the causal domain of σ_{int}, then we may naturally choose a code subspace associated with the degrees of freedom of the parent particle, e.g. its spin, or a larger subspace determined by the coarse-grained entropy of the final state radiation.

Our framework addresses this issue by providing a specific gauge choice given by the coarse-graining procedure. Suppose there are a set of states giving similar geometries on their holographic slices. Then, we can represent all these states approximately at once by a single TN, which has "dangling" legs so that different states in these legs correspond to different elements in the set; see Fig. 3.16. This is a choice of code subspace motivated by the coarse-graining procedure.

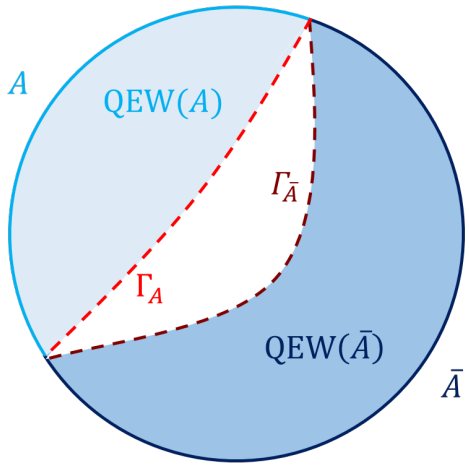

Figure 3.17: With the state in $\mathcal{H}_{\text{code}}$ being maximally mixed, the QESs Γ_A and $\Gamma_{\overline{A}}$ can differ.

The introduction of dangling legs amounts to dividing bulk degrees of freedom into two classes: those represented by a code subspace and the rest. Let us denote the associated Hilbert space factors by $\mathcal{H}_{\text{code}}$ and $\mathcal{H}_{\text{frozen}}$, respectively. States in $\mathcal{H}_{\text{code}}$ correspond to the bulk degrees of freedom that we aim to reconstruct, while $\mathcal{H}_{\text{frozen}}$ is viewed as "frozen." Namely, the degrees of freedom corresponding to $\mathcal{H}_{\text{frozen}}$ are treated essentially as part of the background, despite the fact that they are associated with quantum states in the conventional bulk effective field theory.

We can now define the coarse-graining in this setup, namely on a continuum analogue of a TN with dangling legs. Specifically, we take the maximally mixed state in $\mathcal{H}_{\text{code}}$, while picking a fixed state in $\mathcal{H}_{\text{frozen}}$ determined by the network structure, i.e. the background geometry. This can be thought of as considering a coarse-grained version of a generic state within the code subspace. Indeed, the maximally mixed state plays a crucial role in AdS/CFT, in which reconstruction of a certain operator in the maximally mixed state is sufficient for a given operator to be reconstructed on arbitrary states in the code subspace [102, 103].

The coarse-graining procedure then follows that in Secs. 3.4 and 3.5, but this time S_{bulk} receives contributions both from dangling legs, S_{code}, and nonlocal legs, S_{frozen}. Since the QESs for A and $\overline{A}$ need not agree (see Fig. 3.17), the region between the two surfaces—often termed the no-man's land—is partially entangled with both A and $\overline{A}$. Nevertheless, using Eq. (3.14) we can obtain a picture analogous to that in Secs. 3.4 and 3.5.

Once we perform the flow to obtain a renormalized leaf $\sigma(\lambda)$ appropriate to deal with the problem, e.g. by making $\sigma_{\text{int}}(\lambda)$ a surface surrounding the region we are interested in, then we can consider the set of all states in $\mathcal{H}_{\text{code}}$, rather than the maximally mixed state, to analyze the system in more detail. As in the corresponding TN case, we can then interpret such coarse-grained states in two ways.

One is to view a state in the set as defining an entangled state in the combined bulk-

boundary Hilbert space

$$|\psi\rangle \in \mathcal{H}_{\text{bulk}} \otimes \mathcal{H}_{\text{boundary}}, \tag{3.51}$$

where $\mathcal{H}_{\text{bulk}}$ represents the space of bulk states in the code subspace.

Another is to regard the set to give an isomorphic map between the bulk Hilbert space (i.e. the space of dangling legs) and a subspace of the much larger boundary Hilbert space:

$$\{|\psi\rangle\} : \mathcal{H}_{\text{bulk}} \leftrightarrow \mathcal{H}_{\text{code}} \subset \mathcal{H}_{\text{boundary}}. \tag{3.52}$$

Note that in the TN picture, $\mathcal{H}_{\text{boundary}}$ consists of both local and nonlocal bonds cut by the boundary surface obtained by the flow, as well as the part associated with σ_{ext}. This implies that the dimension of the boundary effective Hilbert space is given by

$$\ln |\mathcal{H}_{\text{boundary}}(\sigma(\lambda))| = \frac{\mathcal{A}(\sigma(\lambda))}{4G_N} + S_{\text{frozen}}(\Sigma(\lambda)). \tag{3.53}$$

This can be compared with Eq. (3.44).

In this way, holographic properties such as the HRT formula and entanglement wedge reconstruction can be naturally interpreted [78, 61]. The interpretation is consistent with the analysis in Ref. [102] that the region reconstructable by state-independent operators—termed the reconstruction wedge in Ref. [103]—can be computed by considering QEW(A) of the maximally mixed state in $\mathcal{H}_{\text{code}}$. In this picture, our coarse-graining procedure is interpreted to produce a sequence of holographic encoding maps parameterized by λ, each of which can be viewed as a holographic duality of the form in Eq. (3.52).

3.8 Discussion

In this chapter, we have generalized the holographic coarse-graining procedure described in Ref. [54] to include bulk quantum corrections. Interestingly, the generalization involves promoting classical expansions θ to quantum expansions Θ as has been found in many other examples [74, 73, 75, 76, 77]. We have demonstrated that the flow equation obtained in the bulk has all the properties consistent with an interpretation as a coarse-graining process in the holographic theory. Our procedure also gives a way in which the region exterior to the holographic screen is treated at the quantum level. It would be interesting to explicitly understand the detailed coarse-graining procedure from a boundary theory perspective.

Chapter 4

Holographic BCFT with a Defect on the End-of-the-World Brane

4.1 Introduction

AdS/BCFT [104, 105, 106] studies the gravity dual of boundary conformal field theory [107, 108]. The simplest, bottom-up model proposed for AdS/BCFT is a spacetime terminating at the End-of-the-World (EOW) brane [105, 106, 109]. This EOW brane is anchored to the BCFT boundary. This bottom-up model captures some qualitative aspects of stringy models for AdS/BCFT [110, 111, 112], and has served as a useful toy model for black hole evaporation [16, 17, 88, 89, 90, 115, 116, 117, 118, 113, 22, 114], interpreted as doubly-holographic brane-world models [119, 120, 121, 122]. On the other hand, this simplest model of AdS/BCFT is known to have several atypical features in the boundary operator spectrum amongst all holographic BCFTs, such as fine-tuned boundary operator spectrum [123] and the absence of interactions between distinct EOW branes. The latter, which is the main focus of this chapter, results in a fixed gap between the lowest eigenvalues of the BCFT with two distinct boundaries and the BCFT with identical boundaries [124].

We modify the conventional AdS/BCFT model by allowing the EOW branes with different tensions to be connected at defects. Geometries with intersecting EOW branes were first considered in [125]. In our model, we treat the defect explicitly by including an additional contribution to the action from the intersection. Clearly, this defect leads to an interaction between the EOW branes. We find that this interaction leads to several novel results:

- The defect modifies the lowest eigenvalue of the conventional AdS/BCFT model. In fact, the lowest eigenvalue in our refined model continuously interpolates between the identical boundary BCFT and the aforementioned spectral gap. We also include a bulk conical defect on the gravity side, which corresponds to a boundary operator [126, 127, 125, 128, 129].

- The bulk theory we propose can also be considered as a gravity dual of a BCFT

with corners [130, 131, 125]. In this duality, the corner on the boundary is in direct correspondence with the defect on the EOW branes.

- The holographic entanglement entropy in our model exhibits three different phases. This entanglement entropy can be seen as a toy model of a matter state prepared by cosmological spacetimes [132, 133]. Interestingly, we have a phase that breaks the time reflection symmetry, so the corresponding entanglement entropy is closely related to the pseudo entropy [134].
- The defect enables us to construct a wormhole saddle that connects multiple AdS boundaries, analogous to the replica wormhole with EOW branes considered in [89]. In our model, the wormhole saddle is allowed only when the BCFT is non-unitary, and this saddle is always subdominant compared to the factorized saddle without any wormholes.

Overview

In Sec. 4.2, we present our refined AdS/BCFT model and its connection to BCFT with a corner. In Sec. 4.3, we describe the bulk geometry that is dual to BCFT on a strip. In Sec. 4.3, we compute the Euclidean action for our geometry and use it to confirm that the BCFT has a richer spectrum in comparison with the conventional AdS/BCFT model. In Sec. 4.5, we compute the holographic entanglement entropy and describe its three phases. In Sec. 4.6, we construct wormhole geometries using our model. In Sec. 4.7, we conclude with discussions and future directions.

4.2 Gravity Dual

In this section, we describe our proposed AdS/BCFT model in which the EOW branes are connected at a defect. The geometry with such intersecting EOW branes was previously considered in [125], and we will give an explicit model with action which realizes such geometry. We use our proposal to find the bulk dual of a BCFT with a corner.

In the original AdS/BCFT proposal[105, 106], the holographic BCFT was dual to an asymptotically AdS spacetime M with an EOW brane Σ anchored to the BCFT boundary. This EOW brane might contain matter fields and have a non-trivial gravitational action. We take the bulk theory to be Einstein gravity

$$I_{\text{EH}} = -\frac{1}{16\pi G_N}\int_M \sqrt{g}\,(R-2\Lambda) - \frac{1}{8\pi G_N}\int_N \sqrt{h}K, \tag{4.1}$$

where N is the AdS boundary.

The simplest EOW brane action is given by the Gibbons-Hawking boundary term plus the tension term,

$$I_{\text{ETW}} = -\frac{1}{8\pi G_N}\int_\Sigma \sqrt{h}K + \frac{1}{8\pi G_N}\int_\Sigma \sqrt{h}T - \frac{1}{8\pi G_N}\int_{\Gamma_{\Sigma,N}} \sqrt{g_{\Gamma_{\Sigma,N}}}\left(\pi - \theta_{(\Sigma,N)}\right). \tag{4.2}$$

Here h_{ab} is the induced metric and K_{ab} is the extrinsic curvature defined using the outgoing normal vector. We also need to include the Hayward term for $\Gamma_{\Sigma,N}$, the corner between AdS boundary N and the EOW brane Σ, with internal angle $\theta_{(\Sigma,N)}$. This action leads to the equation of motion for the EOW brane

$$K_{ab} = (K - T)h_{ab}. \tag{4.3}$$

The boundary entropy S_B in 2d BCFT is defined in terms of the disk partition function via $Z_{\text{Disk}} = e^{S_B}$ [135], which counts the number of degrees of freedom on the boundary. The tension T of the EOW brane is related to the boundary entropy as

$$S_B = \frac{c}{6}\operatorname{arctanh}(\ell T), \tag{4.4}$$

where ℓ is the AdS radius [136]. In this simple model, there are no interactions and no intersections between EOW branes dual to distinct BCFT boundaries whereas for identical boundaries, the EOW branes can be smoothly connected. This simple interaction leads to a simple value for the lowest eigenvalue [124] that is highly non-generic, which we will discuss in Sec. 4.3.

The new ingredient introduced in here is such an interaction in the form of a defect that glues two distinct EOW branes. Since the dual spacetime terminates at some finite depth, the spectrum is no longer that simple, and indeed we have a new lowest eigenvalue as we show later. The simplest action for this defect is given by

$$I_{\text{defect}} = -\frac{1}{8\pi G_N}\int_{\Gamma_{(a,b)}} \sqrt{g_{\Gamma_{(a,b)}}}\left(\theta_{0:(a,b)} - \theta_{(a,b)}\right). \tag{4.5}$$

Here $\Gamma_{(a,b)}$ is the defect which glues two EOW branes Σ_a and Σ_b, and $\theta_{(a,b)}$ is the internal angle of M at $\Gamma_{(a,b)}$, see Fig. 4.1. Also, $\theta_{0:(a,b)} - \pi$ can be regarded as the tension of the defect, The action in (4.5) is called Hayward term [137] when $\theta_{0:(a,b)} = \pi$, and has been considered in different AdS/BCFT contexts in [109, 138, 139]. This Hayward term can be obtained by taking a singular limit of the Gibbons-Hawking-York term where the boundary has a sharp corner.

The total action is the sum of these three contributions,

$$I_{\text{total}} = I_{\text{EH}} + I_{\text{ETW}} + I_{\text{defect}}. \tag{4.6}$$

It is worth mentioning that this I_{total} has UV divergences coming from the region near the AdS boundary. To obtain a finite answer, these divergences need to be cured by introducing

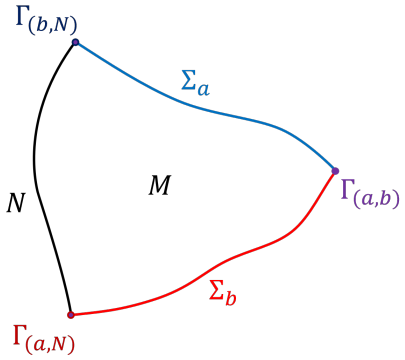

Figure 4.1: Sketch of our proposed gravity dual of BCFT. N is the AdS boundary where the BCFT lives. Σ_a and Σ_b are the EOW branes, and $\Gamma_{(a,b)}$ is the defect connecting them.

a short distance cutoff at the boundary and including appropriate counterterms to cancel the divergence.

The variation of I_{total} is

$$\begin{aligned}\delta I_{\text{total}} = &-\frac{1}{16\pi G_N}\int_M \sqrt{g}\left(R_{\mu\nu}-\frac{1}{2}Rg_{\mu\nu}+\Lambda g_{\mu\nu}\right)\delta g^{\mu\nu}\\ &-\sum_{i=a,b}\frac{1}{8\pi G_N}\int_{\Sigma_i}\sqrt{h}\left(K_{\alpha\beta}-Kh_{\alpha\beta}+T_i h_{\alpha\beta}\right)\delta h^{\alpha\beta}-\frac{1}{8\pi G_N}\int_N\sqrt{h}\left(K_{\alpha\beta}-Kh_{\alpha\beta}\right)\delta h^{\alpha\beta}\\ &-\frac{1}{8\pi G_N}\int_{\Gamma_{(a,b)}}\left(\theta_{0:(a,b)}-\theta_{(a,b)}\right)\delta\sqrt{g_{\Gamma_{(a,b)}}}-\sum_{i=a,b}\frac{1}{8\pi G_N}\int_{\Gamma_{(i,N)}}\left(\pi-\theta_{(i,N)}\right)\delta\sqrt{g_{\Gamma_{(i,N)}}}.\end{aligned}\tag{4.7}$$

In AdS/BCFT, the metric can fluctuate freely on Σ_i, but not at AdS boundary N, therefore

$$\begin{cases}\delta h^{\alpha\beta}_N = 0, & \delta h^{\alpha\beta}_{\Sigma_i} \text{ free},\\ \delta\sqrt{g_{\Gamma_{(i,N)}}} = 0, & \delta\sqrt{g_{\Gamma_{(a,b)}}} \text{ free}.\end{cases}\tag{4.8}$$

These boundary conditions at Σ_i and $\Gamma_{(a,b)}$ result in the following equations of motion

$$K_{\alpha\beta} = (K - T_i)h_{\alpha\beta},\tag{4.9}$$

$$\theta_{0:(a,b)} - \theta_{(a,b)} = 0.\tag{4.10}$$

These two equations determine the shapes of the EOW branes Σ_i and of the corner $\Gamma_{(a,b)}$. On the other hand, the above boundary conditions do not induce equations of motion at the AdS boundary and $\Gamma_{(a,N)}$ because of the Dirichlet boundary condition.

Gravity Dual of BCFT with a Corner

In this subsection, we examine the gravity dual of BCFT with a corner as a simple example. This dual is given by a vacuum AdS spacetime with two EOW branes glued at a defect.

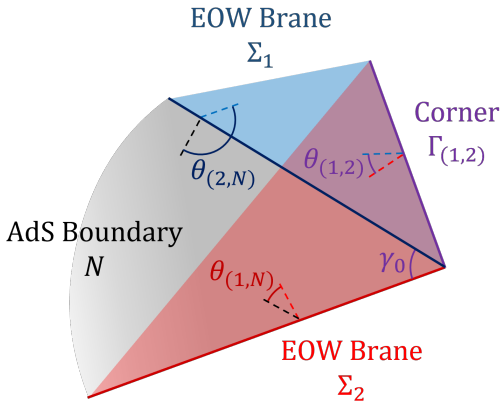

Figure 4.2: Two EOW branes embedded in Poincare AdS. They intersect in the bulk at an internal angle $\theta_{(1,2)}$ and on the boundary at an internal angle γ_0. The bulk region is dual to BCFT on the cornered region $N = D$.

Consider the Poincare background for vacuum AdS_3

$$ds^2 = \frac{\ell^2}{z^2}(dx^2 + dy^2 + dz^2) \tag{4.11}$$

with ℓ being the AdS length. We restrict to the region

$$D := \{u = re^{i\theta} \in \mathbb{C} | r \geq 0,\ 0 \leq \theta \leq \gamma_0\} \tag{4.12}$$

on the AdS boundary[1] with $u := x + iy$. Since this region has a corner at the origin, the bulk geometry is dual to BCFT with a corner. The bulk spacetime we consider is a spacetime bounded by two EOW branes anchored to ∂D. The equation of motion for the EOW brane fixes its shape to be a plane in (x, y, z) coordinates. Fig. 4.2 shows the bulk geometry with these two intersecting EOW branes. Since the bulk metric is the Poincare metric, the Fefferman-Graham expansion tells us that the stress tensor $\langle T_{uu} \rangle$ vanishes away from the boundaries.

Let us first assume that the two EOW branes have equal tensions, so the boundary entropies for the two boundaries are identical. The dimensionless tension $\mathcal{T}_a = \ell T_a$ of the EOW brane is related to the internal angle $\theta_{(a,N)}$ between the brane and the AdS boundary as

$$\mathcal{T}_a = -\cos\theta_{(a,N)}. \tag{4.13}$$

Note that the allowed values of the tension are given by $|\mathcal{T}| \leq 1$.

[1]The region D can be mapped to the upper half plane via a singular conformal transformation, and standard BCFT techniques can be applied [125]. See also [130].

The internal angle γ_0 at AdS boundary and the internal angle $\theta_{(1,2)}$ between EOW branes are related as

$$\gamma_0 = \begin{cases} \arccos\left(\frac{\cos\theta_{(1,2)}+\mathcal{T}^2}{1-\mathcal{T}^2}\right) & 2\arcsin|\mathcal{T}| < \theta_{(1,2)} < \pi \\ 2\pi - \arccos\left(\frac{\cos\theta_{(1,2)}+\mathcal{T}^2}{1-\mathcal{T}^2}\right) & \pi < \theta_{(1,2)} < 2\pi - 2\arcsin|\mathcal{T}| \end{cases}. \tag{4.14}$$

Since the configuration of the EOW brane is a plane in the (x, y, z) coordinates, $\theta_{(1,2)}$ is simply the angle of intersection of two planes.

For arbitrary tensions $\mathcal{T}_1$ and $\mathcal{T}_2$, we have

$$\gamma_0 = \begin{cases} \frac{1}{2}\arccos\left(\frac{\cos\theta_{(1,2)}+\mathcal{T}_1\mathcal{T}_2}{\sqrt{(1-\mathcal{T}_1^2)(1-\mathcal{T}_2^2)}}\right), \\ \qquad\qquad \arccos\left(\sqrt{(1-\mathcal{T}_1^2)(1-\mathcal{T}_2^2)} - \mathcal{T}_1\mathcal{T}_2\right) < \theta_{(1,2)} \text{ and} \\ \qquad\qquad \theta_{(1,2)} < \pi - \arccos\left(\sqrt{(1-\mathcal{T}_1^2)(1-\mathcal{T}_2^2)} + \mathcal{T}_1\mathcal{T}_2\right), \\ \pi - \frac{1}{2}\arccos\left(\frac{\cos\theta_{(1,2)}+\mathcal{T}_1\mathcal{T}_2}{\sqrt{(1-\mathcal{T}_1^2)(1-\mathcal{T}_2^2)}}\right), \\ \qquad\qquad \pi + \arccos\left(\sqrt{(1-\mathcal{T}_1^2)(1-\mathcal{T}_2^2)} + \mathcal{T}_1\mathcal{T}_2\right) < \theta_{(1,2)} \text{ and} \\ \qquad\qquad \theta_{(1,2)} < 2\pi - \arccos\left(\sqrt{(1-\mathcal{T}_1^2)(1-\mathcal{T}_2^2)} - \mathcal{T}_1\mathcal{T}_2\right). \end{cases} \tag{4.15}$$

In the following sections, we will use this geometry to construct the gravity dual of BCFT on a strip.

4.3 BCFT on a Strip

In this section, we construct the gravity dual of BCFT on an infinite Euclidean strip by using our refined model for AdS/BCFT. We suppose that conformal boundary conditions a and b have been imposed on the two boundaries of this strip.

Let us first review the conventional AdS/BCFT model which does not have any defects connecting the EOW branes. When the two boundary conditions are identical, the dual is given by thermal AdS with the EOW branes being connected without any defect (if the two boundaries are sufficiently close to each other) [105, 106, 124]. In this case, the lowest eigenvalue was found to be $E^{\mathrm{BCFT}}_{(a,b)} = -\frac{\pi c}{24\Delta x}$ where Δx is the width of the strip. This spectrum corresponds to the conformal dimension of the boundary condition changing operator being $h^{\mathrm{bcc}}_{(a,b)} = 0$.

When the boundary entropies of two boundary conditions are different, the dual geometry is given by two disconnected EOW branes in the Poincare background. As the result, the lowest eigenvalue for the BCFT was found to be $E^{\mathrm{BCFT}}_{(a,b)} = 0$, which corresponds to $h^{\mathrm{bcc}}_{(a,b)} = \frac{c}{24}$. These two results imply that there is no operator with conformal dimension between $h^{\mathrm{bcc}}_{(a,b)} = 0$ and $h^{\mathrm{bcc}}_{(a,b)} = \frac{c}{24}$ in the conventional AdS/BCFT model.

In the following subsections, we generalize this simple spectrum by introducing a defect that can connect the EOW branes, even if they have different tensions, or equivalently,

different boundary entropies. This will allow us to obtain any value for the lowest operator dimension between $h^{\rm bcc}_{(a,b)} = 0$ and $h^{\rm bcc}_{(a,b)} = \frac{c}{24}$.

Bulk Geometry

We are interested in constructing the gravity dual of an infinite Euclidean strip of width Δx. Let us start by considering the thermal AdS_3 geometry with two EOW branes connected through a defect. The metric of the thermal AdS_3 without any branes is

$$\mathrm{d}s^2 = \ell^2 \left(\frac{\mathrm{d}\tau^2}{z_0^2 \chi^2} + \frac{\mathrm{d}\chi^2}{h(\chi)\chi^2} + \frac{h(\chi)}{\chi^2} \mathrm{d}\phi^2 \right). \tag{4.16}$$

Here $h(\chi) = (1-\chi^2)$, with $0 < \chi \leq 1$. We denote the periodicity of the Euclidean time τ as $T^{-1}_{\rm BCFT} = 2\pi z_0 \chi_H$ which is assumed to be large compared to z_0 so that the thermal AdS saddle is dominant compared to Euclidean black hole. The ϕ coordinate has period 2π so that there is no conical defect at $\chi = 1$. Note that z_0 sets the length scale for the BCFT.

Let us first embed a single EOW brane without any defects in this geometry. Since the brane satisfies the equation of motion in (4.9), its profile is

$$\phi(\chi) = \phi(0) \pm \arctan \frac{\mathcal{T}\chi}{\sqrt{h(\chi) - \mathcal{T}^2}}, \tag{4.17}$$

in terms of the dimensionless tension $\mathcal{T}$. As explained in the next subsection, a bulk coordinate transformation can be used to show that this configuration is equivalent to EOW brane with tension $\mathcal{T}$ anchored to a line in Poincare AdS. The deepest point that the EOW brane reaches before turning back towards the AdS boundary is

$$\chi = \chi_0(\mathcal{T}) := \sqrt{1 - \mathcal{T}^2}. \tag{4.18}$$

Next we consider two EOW branes Σ_1 and Σ_2, with dimensionless tensions $\mathcal{T}_1$ and $\mathcal{T}_2$, respectively. We assume that these tensions satisfy $|\mathcal{T}_2| \leq |\mathcal{T}_1|$, without loss of generality. The branes are anchored to the AdS boundary at $\Gamma_{1,N} = \{\chi = 0,\, \phi = \pi - \alpha\}$ and $\Gamma_{2,N} = \{\chi = 0,\, \phi = \pi + \alpha\}$ respectively, with some $\alpha \in (0, \pi)$. As mentioned earlier, M denotes the bulk region between these branes. Its boundary ∂M consists of the two EOW branes Σ_1 and Σ_2, along with a region on the AdS boundary, $N = \{\chi = 0, \pi - \alpha \leq \phi \leq \pi + \alpha\}$. From the perspective of the AdS boundary, the angular size of N is $\Delta\phi = 2\alpha$. The width of the strip is $\Delta x = 2\alpha z_0$.

We want to calculate the angle $\theta_{(1,2)}$ at which the two EOW branes intersect in the bulk. Depending on the value of α, the bulk geometries are qualitatively different, so we need to treat the various cases separately.

As an illustration, let us consider the case where $\mathcal{T}_1, \mathcal{T}_2 > 0$ and α is small, in particular, $0 \leq \alpha \leq \frac{\pi}{4} + \frac{1}{2} \arctan \frac{\mathcal{T}_2 \sqrt{1-\mathcal{T}_1^2}}{\sqrt{\mathcal{T}_1^2 - \mathcal{T}_2^2}}$. We will state the results for the other cases momentarily. A

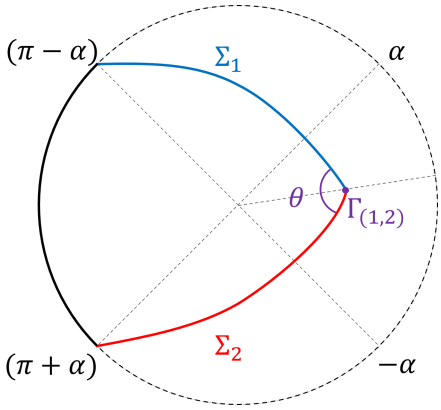

Figure 4.3: A constant τ slice of thermal AdS with two EOW branes, Σ_1 and Σ_2, meeting at the corner $\Gamma_{(1,2)}$.

constant τ slice of the bulk geometry, in this case, is shown in Fig. 4.3. The profiles of the EOW branes in the intersection region are

$$\phi_1(\chi) = -\alpha + \arctan\frac{\mathcal{T}_1\chi}{\sqrt{h(\chi)-\mathcal{T}_1^2}}, \qquad \phi_2(\chi) = \alpha - \arctan\frac{\mathcal{T}_2\chi}{\sqrt{h(\chi)-\mathcal{T}_2^2}}. \tag{4.19}$$

To obtain the intersection point χ_*, we set $\phi_1(\chi_*) = \phi_2(\chi_*)$ to get an equation for χ_*

$$\arctan\frac{\mathcal{T}_1\chi_*}{\sqrt{h(\chi_*)-\mathcal{T}_1^2}} + \arctan\frac{\mathcal{T}_2\chi_*}{\sqrt{h(\chi_*)-\mathcal{T}_2^2}} = 2\alpha. \tag{4.20}$$

This χ_* increases monotonically with α. The upper bound on α for this case is attained when χ_* equals the maximum value $\chi_0(\mathcal{T}_1) = \sqrt{1-\mathcal{T}_1^2}$ [2], and the explicit value is $\alpha = \frac{\pi}{4} + \frac{1}{2}\arctan\frac{\mathcal{T}_2\sqrt{1-\mathcal{T}_1^2}}{\sqrt{\mathcal{T}_1^2-\mathcal{T}_2^2}}$ as stated above. The angle of intersection between the two EOW branes is

$$\theta_{(1,2)} = \arccos\frac{\sqrt{(h(\chi_*)-\mathcal{T}_1^2)(h(\chi_*)-\mathcal{T}_1^2)}-\mathcal{T}_1\mathcal{T}_2}{h(\chi_*)}. \tag{4.21}$$

Now we state the result for general α. Assuming that the tensions satisfy the condition

[2]This maximal value corresponds to the deepest point on Σ_1 because we have assumed that $|\mathcal{T}_1| > |\mathcal{T}_2|$, which implies that $\chi_0(\mathcal{T}_1) < \chi_0(\mathcal{T}_2)$.

$|\mathcal{T}_2| \leq |\mathcal{T}_1|$, the equation to obtain the intersection point is

$$\begin{cases} \left| \arctan \frac{\mathcal{T}_1\chi_*}{\sqrt{h(\chi_*)-\mathcal{T}_1^2}} + \arctan \frac{\mathcal{T}_2\chi_*}{\sqrt{h(\chi_*)-\mathcal{T}_2^2}} \right| = 2\alpha, & 0 < \alpha < \frac{\pi}{4} + \frac{\mathrm{sgn}(\mathcal{T}_1)}{2} \arctan \frac{\mathcal{T}_2\sqrt{1-\mathcal{T}_1^2}}{\sqrt{\mathcal{T}_1^2-\mathcal{T}_2^2}}, \\ \left| \arctan \frac{\mathcal{T}_1\chi_*}{\sqrt{h(\chi_*)-\mathcal{T}_1^2}} - \arctan \frac{\mathcal{T}_2\chi_*}{\sqrt{h(\chi_*)-\mathcal{T}_2^2}} \right| = \pi - 2\alpha, & \frac{\pi}{4} + \frac{\mathrm{sgn}(\mathcal{T}_1)}{2} \arctan \frac{\mathcal{T}_2\sqrt{1-\mathcal{T}_1^2}}{\sqrt{\mathcal{T}_1^2-\mathcal{T}_2^2}} < \alpha < \frac{\pi}{2}, \\ \left| \arctan \frac{\mathcal{T}_1\chi_*}{\sqrt{h(\chi_*)-\mathcal{T}_1^2}} - \arctan \frac{\mathcal{T}_2\chi_*}{\sqrt{h(\chi_*)-\mathcal{T}_2^2}} \right| = 2\alpha - \pi, & \frac{\pi}{2} < \alpha < \frac{3\pi}{4} - \frac{\mathrm{sgn}(\mathcal{T}_1)}{2} \arctan \frac{\mathcal{T}_2\sqrt{1-\mathcal{T}_1^2}}{\sqrt{\mathcal{T}_1^2-\mathcal{T}_2^2}}, \\ \left| \arctan \frac{\mathcal{T}_1\chi_*}{\sqrt{h(\chi_*)-\mathcal{T}_1^2}} + \arctan \frac{\mathcal{T}_2\chi_*}{\sqrt{h(\chi_*)-\mathcal{T}_2^2}} \right| = 2\pi - 2\alpha, & \frac{3\pi}{4} - \frac{\mathrm{sgn}(\mathcal{T}_1)}{2} \arctan \frac{\mathcal{T}_2\sqrt{1-\mathcal{T}_1^2}}{\sqrt{\mathcal{T}_1^2-\mathcal{T}_2^2}} < \alpha < \pi, \end{cases} \tag{4.22}$$

and the angle of intersection is

$$\theta_{(1,2)} = \begin{cases} \arccos\left(\frac{\sqrt{(h(\chi_*)-\mathcal{T}_1^2)(h(\chi_*)-\mathcal{T}_2^2)}-\mathcal{T}_1\mathcal{T}_2}{h(\chi_*)} \right), & 0 < \alpha < \frac{\pi}{4} + \frac{\mathrm{sgn}(\mathcal{T}_1)}{2} \arctan \frac{\mathcal{T}_2\sqrt{1-\mathcal{T}_1^2}}{\sqrt{\mathcal{T}_1^2-\mathcal{T}_2^2}}, \\ \arccos\left(-\frac{\sqrt{(h(\chi_*)-\mathcal{T}_1^2)(h(\chi_*)-\mathcal{T}_2^2)}+\mathcal{T}_1\mathcal{T}_2}{h(\chi_*)} \right), & \frac{\pi}{4} + \frac{\mathrm{sgn}(\mathcal{T}_1)}{2} \arctan \frac{\mathcal{T}_2\sqrt{1-\mathcal{T}_1^2}}{\sqrt{\mathcal{T}_1^2-\mathcal{T}_2^2}} < \alpha < \frac{\pi}{2}, \\ 2\pi - \arccos\left(-\frac{\sqrt{(h(\chi_*)-\mathcal{T}_1^2)(h(\chi_*)-\mathcal{T}_2^2)}+\mathcal{T}_1\mathcal{T}_2}{h(\chi_*)} \right), & \frac{\pi}{2} < \alpha < \frac{3\pi}{4} - \frac{\mathrm{sgn}(\mathcal{T}_1)}{2} \arctan \frac{\mathcal{T}_2\sqrt{1-\mathcal{T}_1^2}}{\sqrt{\mathcal{T}_1^2-\mathcal{T}_2^2}}, \\ 2\pi - \arccos\left(\frac{\sqrt{(h(\chi_*)-\mathcal{T}_1^2)(h(\chi_*)-\mathcal{T}_2^2)}-\mathcal{T}_1\mathcal{T}_2}{h(\chi_*)} \right), & \frac{3\pi}{4} - \frac{\mathrm{sgn}(\mathcal{T}_1)}{2} \arctan \frac{\mathcal{T}_2\sqrt{1-\mathcal{T}_1^2}}{\sqrt{\mathcal{T}_1^2-\mathcal{T}_2^2}} < \alpha < \pi. \end{cases} \tag{4.23}$$

Here, $\mathrm{sgn}(x) := \frac{x}{|x|}$ is the sign function. Note that these results are valid even when one or both tensions are negative.

The equation of motion (4.10) fixes the angle of intersection to be $\theta_{(1,2)} = \theta_0$. This determines the value of α, and hence, the geometry in terms of θ_0 and the tensions of EOW branes. Indeed, substituting $\theta_{(1,2)} = \theta_0$ in (4.23), we get

$$\chi_* = \sqrt{1 - \frac{\mathcal{T}_1^2 + \mathcal{T}_2^2 + 2\mathcal{T}_1\mathcal{T}_2\cos\theta_0}{\sin^2\theta_0}}. \tag{4.24}$$

Also, the value of α that corresponds to this θ_0 is

$$\alpha_0 = \begin{cases} \frac{1}{2}\arccos\left(\frac{\cos\theta_0+\mathcal{T}_1\mathcal{T}_2}{\sqrt{(1-\mathcal{T}_1^2)(1-\mathcal{T}_2^2)}} \right), \\ \qquad\qquad \arccos\left(\sqrt{(1-\mathcal{T}_1^2)(1-\mathcal{T}_2^2)} - \mathcal{T}_1\mathcal{T}_2\right) < \theta_0 \text{ and} \\ \qquad\qquad \theta_0 < \pi - \arccos\left(\sqrt{(1-\mathcal{T}_1^2)(1-\mathcal{T}_2^2)} + \mathcal{T}_1\mathcal{T}_2\right), \\ \pi - \frac{1}{2}\arccos\left(\frac{\cos\theta_0+\mathcal{T}_1\mathcal{T}_2}{\sqrt{(1-\mathcal{T}_1^2)(1-\mathcal{T}_2^2)}} \right), \\ \qquad\qquad \pi + \arccos\left(\sqrt{(1-\mathcal{T}_1^2)(1-\mathcal{T}_2^2)} + \mathcal{T}_1\mathcal{T}_2\right) < \theta_0 \text{ and} \\ \qquad\qquad \theta_0 < 2\pi - \arccos\left(\sqrt{(1-\mathcal{T}_1^2)(1-\mathcal{T}_2^2)} - \mathcal{T}_1\mathcal{T}_2\right). \end{cases} \tag{4.25}$$

Note that (4.24) and (4.25) are symmetric in $\mathcal{T}_1$ and $\mathcal{T}_2$, therefore the formula applies even when $|\mathcal{T}_1| < |\mathcal{T}_2|$. Moreover, this result for α_0 is identical to (4.15) if we identify γ_0 with $2\alpha_0$.

In fact, the two bulk geometries can be identified by a bulk coordinate transformation which maps the infinite strip N to the cornered region D, as explained in the next subsection.

Let us now analyze the dependence of α_0 as we vary θ_0 for various values of the tensions. When the two tensions are equal $\mathcal{T}_1 = \mathcal{T}_2$, then θ_0 is a continuous function of α_0. In this case, (4.24) and (4.25) simplify to

$$\chi_* = \sqrt{1 - \frac{\mathcal{T}^2}{\sin^2(\theta_0/2)}}, \tag{4.26}$$

and

$$\alpha_0 = \begin{cases} \frac{1}{2}\arccos\left(\frac{\cos\theta_0+\mathcal{T}^2}{1-\mathcal{T}^2}\right), & 2\arcsin|\mathcal{T}| < \theta_0 \leq \pi, \\ \pi - \frac{1}{2}\arccos\left(\frac{\cos\theta_0+\mathcal{T}^2}{1-\mathcal{T}^2}\right), & \pi \leq \theta_0 < 2\pi - 2\arcsin|\mathcal{T}|. \end{cases} \tag{4.27}$$

If we also set $\theta_0 = \pi$, then we get $\alpha_0 = \frac{\pi}{2}$. The dual bulk geometry has a smooth EOW brane geometry without any defect, which is the same as the conventional AdS/BCFT model. Conversely, we find that $\theta_0 = \pi$ is possible only if $\mathcal{T}_1 = \mathcal{T}_2$.

When $\mathcal{T}_1 \neq \mathcal{T}_2$, the curve for θ_0 has a discontinuity at $\alpha_0 = \pi/2$. While all other values for α_0 are valid, $\alpha_0 = \pi/2$ is disallowed. This is because as we send θ_0 to its corresponding value, the defect approaches the boundary and one of the EOW branes disappears. For $\alpha_0 = \pi/2$, we only have one EOW brane and no defect, so this value needs to be excluded.

Conical defect in the bulk

So far, the geometries we have considered have a defect only on the EOW brane. We can construct more general geometries by including a bulk conical defect as well. First, we consider the metric (4.16), and embed the EOW branes whose profiles are given by (4.17) with internal angle $\theta_{(1,2)}$. A bulk conical defect located at $\chi = 1$ with a deficit angle of $\Delta\phi$ can be introduced by identifying $\phi = \phi_0$ and $\phi = \phi_0 + \Delta\phi$ in the geometry (4.16). Here, ϕ_0 is chosen such that the region given by $\phi \in [\phi_0, \phi_0 + \Delta\phi_0]$ is contained within the spacetime M which is bounded by EOW branes. This is possible if and only if

$$\mathcal{T}_1,\ \mathcal{T}_2 > 0, \qquad\qquad 2\alpha_0 \geq \Delta\phi. \tag{4.28}$$

The first condition $\mathcal{T}_1,\ \mathcal{T}_2 > 0$ is required for $\chi = 1$ to be contained in the geometry, and the second condition prevents self-intersection of the EOW branes [125]. For more recent analysis, see [126, 127, 128, 129, 140].

Extention of Boundary Conformal Transformation to Bulk

Let us examine the bulk coordinate transformation from the Poincare patch to another coordinate patch. This transformation is dual to the boundary conformal transformation from a plane to a 2d patch. In particular, we use this to procedure to find the map between vacuum AdS and thermal AdS.

The Poincare AdS_3 metric is

$$\mathrm{d}s^2 = \frac{\ell^2}{z^2}\left(-2\mathrm{d}v_+\mathrm{d}v_- + \mathrm{d}z^2\right). \tag{4.29}$$

Here we have used the light cone coordinate $v_\pm := \frac{1}{\sqrt{2}}(t \pm r)$ for the Minkowski space $\mathrm{d}s^2 = -2\mathrm{d}v_+\mathrm{d}v_- = -\mathrm{d}t^2 + \mathrm{d}r^2$ at the boundary of AdS.

Suppose we have a conformal transformation $v_\pm = f_\pm(u_\pm)$ that acts on the boundary. We can extend this to a bulk coordinate transformation via [141]

$$\begin{cases} v_\pm = f_\pm(u_\pm) + \frac{2\zeta^2 f'_\pm(u_\pm)^2 f''_\mp(u_\mp)}{8f'_+(u_+)f'_-(u_-) - \zeta^2 f''_+(u_+)f''_-(u_-)}, \\ z = \frac{8\zeta(f'_+(u_+)f'_-(u_-))^{3/2}}{8f'_+(u_+)f'_-(u_-) - \zeta^2 f''_+(u_+)f''_-(u_-)}. \end{cases} \tag{4.30}$$

where ζ is the new radial coordinate. This bulk transformation maps the Poincare AdS_3 metric to

$$\mathrm{d}s^2 = \ell^2\left(\frac{\mathrm{d}\zeta^2}{\zeta^2} + L_+\mathrm{d}u_+^2 + L_-\mathrm{d}u_-^2 - \left(\frac{2}{\zeta^2} + \frac{\zeta^2}{2}L_+L_-\right)\mathrm{d}u_+\mathrm{d}u_-\right). \tag{4.31}$$

Here $L_\pm$ are related to the Schwarzian of the conformal transformation and are given by

$$L_\pm := -\frac{1}{2}\{f_\pm(u_\pm), u_\pm\} = \frac{3f''^2_\pm - 2f'_\pm f'''_\pm}{4f'^2_\pm}. \tag{4.32}$$

Hence, the CFT stress tensor in the transformed coordinates is

$$T_{u_\pm u_\pm} = \frac{c}{12\pi}L_\pm, \qquad T_{u_+u_-} = 0. \tag{4.33}$$

The analytical continuation of $v_\pm$ to imaginary time is

$$v_\pm = \frac{t \pm r}{\sqrt{2}} \to \frac{-\mathrm{i}\tau \pm r}{\sqrt{2}}. \tag{4.34}$$

Similarly, for $\mathrm{d}s^2 = -2\mathrm{d}x_+\mathrm{d}x_- = -\mathrm{d}t_x^2 + z_0^2\mathrm{d}\phi^2$, we have

$$u_\pm = \frac{t_u \pm z_0\phi}{\sqrt{2}} \to \frac{-\mathrm{i}\tau_u \pm z_0\phi}{\sqrt{2}}. \tag{4.35}$$

In these complexified coordinates, the conformal transformation can be rewritten as $v = r + \mathrm{i}\tau = g(u),\ \bar{v} = r - \mathrm{i}\tau = \bar{g}(\bar{u})$ with $u := z_0\phi + \mathrm{i}\tau_u,\ \bar{u} := z_0\phi - \mathrm{i}\tau_u$. The metric is

$$\mathrm{d}s^2 = \ell^2\left(\frac{\mathrm{d}\zeta^2}{\zeta^2} + L\mathrm{d}u^2 + \bar{L}\mathrm{d}\bar{u}^2 + \left(\frac{1}{\zeta^2} + \zeta^2 L\bar{L}\right)\mathrm{d}u\mathrm{d}\bar{u}\right). \tag{4.36}$$

where we have defined

$$L := \frac{1}{2}\{g(u), u\} = -\frac{1}{4}\{f_-(u_-), u_-\}, \tag{4.37}$$

$$\bar{L} := -\frac{1}{2}\{\bar{g}(\bar{u}), \bar{u}\} = -\frac{1}{4}\{f_+(u_+), u_+\}. \tag{4.38}$$

Mapping a plane to a cylinder

We consider a conformal transformation from a cylinder to a plane,

$$v = z_0 e^{-\frac{\mathrm{i}}{z_0}u}, \qquad \bar{v} = z_0 e^{\frac{\mathrm{i}}{z_0}\bar{u}}. \tag{4.39}$$

Here we have defined the coordinates on the cylinder as

$$u := z_0\phi + \mathrm{i}\tau = -\sqrt{2}u_-, \quad \bar{u} := z_0\phi - \mathrm{i}\tau = \sqrt{2}u_+, \tag{4.40}$$

and the coordinates on the plane as

$$v := x - \mathrm{i}y = -\sqrt{2}v_-, \quad \bar{v} := x + \mathrm{i}y = \sqrt{2}v_+. \tag{4.41}$$

This conformal transformation can be also be expressed as $v_\pm = \pm\frac{z_0}{\sqrt{2}}e^{\frac{\mathrm{i}\sqrt{2}}{z_0}u_\pm}$.

Applying (4.30) to this conformal transformation, we obtain the bulk transformation between the Poincare metric, $\mathrm{d}s^2 = \frac{\ell^2}{s^2}(\mathrm{d}x^2 + \mathrm{d}y^2 + \mathrm{d}z^2)$, and thermal AdS, $\mathrm{d}s^2 = \ell^2\left(\frac{\mathrm{d}\tau^2}{z_0^2\chi^2} + \frac{\mathrm{d}\chi^2}{h(\chi)\chi^2} + \frac{h(\chi)\mathrm{d}\phi^2}{\chi^2}\right)$, to be

$$\begin{cases} v_\pm = \pm\frac{z_0}{\sqrt{2}}\sqrt{h(\chi)}e^{\mathrm{i}\sqrt{2}u_\pm/z_0}, \\ z = z_0 e^{i(u_+ + u_-)/(\sqrt{2}z_0)}\chi. \end{cases} \tag{4.42}$$

where we have related $\chi = \frac{4z_0\zeta}{\zeta^2 + 4z_0^2}$. This can also be expressed as

$$\begin{cases} x = z_0 e^{\tau/z_0}\sqrt{h(\chi)}\cos\phi, \\ y = z_0 e^{\tau/z_0}\sqrt{h(\chi)}\sin\phi, \\ z = z_0 e^{\tau/z_0}\chi, \end{cases} \tag{4.43}$$

For this transformation,

$$L_\pm = -\frac{1}{2z_0^2}, \tag{4.44}$$

so the stress tensor is given by

$$T_{\tau\tau} = -\frac{T_{\phi\phi}}{z_0^2} = \frac{c}{24\pi z_0^2}. \tag{4.45}$$

4.4 Euclidean Action and the BCFT Spectrum

In this section, we compute the Euclidean action for the bulk geometry dual to the strip. This action is directly related to the lowest eigenvalue of the BCFT.

First, consider the case with no conical defect in the bulk. After an explicit computation, we find that the total action given by (4.6) is

$$I_{\text{total}} = \frac{\ell\chi_H}{2G_N}\left[-\frac{\alpha_0}{\epsilon^2} + \frac{1}{2\epsilon}\sum_{a=1}^{2}\left(\frac{\mathcal{T}_a}{\sqrt{1-\mathcal{T}_a^2}} - \arccos\mathcal{T}_a\right)\right], \tag{4.46}$$

where we have introduced the short-distance cutoff ϵ at the AdS boundary to regulate the UV divergences.

To cancel these divergences, we need to include boundary counterterms. These counterterms must be covariant and local, and are chosen to cancel the divergences. In our case,

$$\begin{aligned} I_{\text{ct}} &= \frac{1}{8\pi G_N \ell}\int_N \sqrt{h_{\partial M}} + \sum_a \frac{\arccos\mathcal{T}_a}{8\pi G_N}\int_{\Gamma_{(a,N)}}\sqrt{g_{\Gamma_{(a,N)}}} \\ &= \frac{\ell\chi_H}{2G_N}\left[\alpha_0\left(\frac{1}{\epsilon^2}-\frac{1}{2}\right) - \frac{1}{2\epsilon}\sum_{a=1}^{2}\frac{\mathcal{T}_a}{\sqrt{1-\mathcal{T}_a^2}}\right] + \frac{\ell\chi_H}{4G_N\epsilon}\sum_{a=1}^{2}\arccos\mathcal{T}_a. \end{aligned} \tag{4.47}$$

On including these counterterms, we obtain the Euclidean action

$$I_E = -\frac{\ell\chi_H}{4G_N}\alpha_0 = -\frac{c}{6\pi\xi}\alpha_0^2. \tag{4.48}$$

Here we have defined the aspect ratio $\xi := \Delta x \cdot T_{\text{BCFT}}$ in order to have scale-invariant expressions. We have also used that the width of the strip is $\Delta x = 2\alpha_0 z_0$ and the central charge is $c = \frac{3\ell}{2G_N}$.

As an example, let us consider the case $\mathcal{T}_1 = \mathcal{T}_2$ and $\alpha_0 = \frac{\pi}{2}$, for which the EOW branes do not have a defect. Then the action is given by

$$I_E^{\text{con}} = -\frac{\pi c}{24\xi},$$

where the superscript denotes that this is the answer in the connected phase of the conventional AdS/BCFT model.

Let us generalize the above result to geometries with bulk conical defects, assuming $\mathcal{T}_1,\ \mathcal{T}_2 > 0$. The action can be obtained by subtracting off the contribution corresponding to the bulk portion that gets removed due to the conical defect. The result is

$$I_E = -\frac{\ell\chi_H}{4G_N}\left(\alpha_0 - \frac{\Delta\phi}{2}\right) = -\frac{c}{6\pi\xi}\left(\alpha_0 - \frac{\Delta\phi}{2}\right)^2. \tag{4.49}$$

Here we have used that the width of the strip is $\Delta x = (2\alpha_0 - \Delta\phi)z_0$.

Relation with the BCFT Spectrum

In this subsection, we examine the spectrum of the BCFT on a strip of width Δx. This BCFT is dual to the bulk geometry that is bounded by two EOW branes that are connected at a defect and it also has a conical defect in the bulk. For this purpose, we consider the partition function $Z^{\text{BCFT}}_{a,b}(T^{-1}_{\text{BCFT}}, \Delta x)$, where T^{-1}_{BCFT} is the periodicity in τ direction which we will take to be infinitely large. In this limit, we have

$$Z^{\text{BCFT}}_{a,b}(T^{-1}_{\text{BCFT}}, \Delta x) \xrightarrow[\Delta x \cdot T_{\text{BCFT}} \to 0]{} e^{-E^{\text{BCFT}}_{a,b} \cdot T^{-1}_{\text{BCFT}}}, \tag{4.50}$$

where $E^{\text{BCFT}}_{a,b}$ is the lowest eigenvalue of the BCFT Hamiltonian $H^{\text{BCFT}}_{a,b}$. In general, the corrections to the above equation are exponentially suppressed. Using this lowest eigenvalue, we can define the spectral gap as

$$\Delta E^{\text{BCFT}}_{a,b} := E^{\text{BCFT}}_{a,b} - \frac{1}{2}E^{\text{BCFT}}_{a,a} - \frac{1}{2}E^{\text{BCFT}}_{b,b}. \tag{4.51}$$

Suppose the EOW branes have dimensionless tensions $\mathcal{T}_1$ and $\mathcal{T}_2$. Since $Z \approx e^{-I_E}$ and using (4.49), the lowest eigenvalue is

$$E^{\text{BCFT}}_{a,b} = -\frac{c}{6\pi\Delta x}\left(\alpha_0 - \frac{\Delta\phi}{2}\right)^2. \tag{4.52}$$

The condition for the boundary changing operator to be the identity operator is

$$\alpha_0 - \frac{\Delta\phi}{2} = \frac{\pi}{2},$$

so the corresponding lowest eigenvalue is

$$E^{\text{BCFT}}_{a,b} = -\frac{\pi c}{24\Delta x}. \tag{4.53}$$

This situation includes the conventional model where the EOW branes are connected and have identical tensions, and there is no bulk conical defect. In particular, when the two boundary conditions are identical, we have $E^{\text{BCFT}}_{a,a} = -\frac{\pi c}{24\Delta x}$.

The lowest eigenvalue of any unitary BCFT must be higher than this value. Therefore, if we demand that the BCFT is unitary, the following condition needs to be satisfied

$$0 \le \alpha_0 - \frac{\Delta\phi}{2} \le \frac{\pi}{2}. \tag{4.54}$$

Therefore, for a fixed α_0, the spectrum obtained for an arbitrary $\Delta\phi$ subject to (4.54) satisfies

$$-\frac{\alpha_0^2 c}{6\pi\Delta x} \le E^{\text{BCFT}}_{a,b} \le 0. \tag{4.55}$$

We note that (4.55) generalizes the lowest eigenvalue dictated by the conventional AdS/BCFT model. In the conventional AdS/BCFT, neither intersections nor interactions between distinct EOW branes are allowed, so such EOW branes are disconnected. As the consequence, the lowest eigenvalue is given by

$$E_{a,b}^{\text{BCFT}} = 0. \tag{4.56}$$

The gravity dual that we have constructed using the defect on EOW branes generalizes this lowest eigenvalue to go below (4.56), for any choice of the two boundary entropies. Note that when two boundary conditions are identical, the lowest eigenvalue is given by the identity operator, so the dual geometry corresponds to $\theta_0 = \pi$ with $\Delta\phi = 0$ and $\alpha_0 = \pi/2$.

Finally, we note that $\alpha_0 = \pi/2$ is allowed only if $\mathcal{T}_1 = \mathcal{T}_2$, so there is no longer a defect on the EOW branes. This implies that we can attain the lowest eigenvalue (4.53) only when the boundary entropy of the two EOW branes are identical. In this case, the bulk conical defect can reproduce the spectrum

$$-\frac{\pi c}{24\Delta x} \leq E_{a,b}^{\text{BCFT}} \leq 0. \tag{4.57}$$

For $\mathcal{T}_1 \neq \mathcal{T}_2$, the corresponding α_0 can be made arbitrarily close to $\pi/2$ by tuning θ_0, but equality cannot be achieved.

To summarize, a key advantage of our model is that it has a rich spectrum even if two boundary entropies are distinct, as opposed to the conventional AdS/BCFT model which has fixed lowest eigenvalue (4.56).

CFT stress tensor for thermal AdS

The above results for the lowest eigenvalue can also be derived by analyzing the metric near the AdS boundary, without knowing the details of the bulk geometry. Rewriting the thermal AdS_3 metric in Fefferman-Graham coordinate, we have

$$\mathrm{d}s^2_{\text{FG}} = \frac{\ell^2}{r^2}\left(dr^2 + \frac{1+2r^2+r^4}{2z_0^2}\mathrm{d}\tau^2 + \frac{1-2r^2+r^4}{2}\mathrm{d}\phi^2\right), \tag{4.58}$$

with $\chi = \frac{2r}{1+r^2}$. Then the dual CFT stress tensor is given by [142]

$$\langle T_{\tau\tau}\rangle = -\langle T_{xx}\rangle = \frac{\ell}{16\pi G_N}\frac{1}{z_0^2} = \frac{c}{6\pi}\frac{\left(\alpha_0 - \frac{\Delta\phi}{2}\right)^2}{(\Delta x)^2}. \tag{4.59}$$

The lowest eigenvalue can be obtained by integrating the CFT stress tensor on the width of the strip,

$$E_{a,b}^{\text{BCFT}} = -\int_{-\Delta x/2}^{\Delta x/2}\mathrm{d}x\,\langle T_{\tau\tau}\rangle = -\frac{c}{6\pi\Delta x}\left(\alpha_0 - \frac{\Delta\phi}{2}\right)^2, \tag{4.60}$$

which matches our previous result.

Relation between bulk mass and the spectrum

In Euclidean global AdS_3, a massive particle at the center is described by the metric

$$\mathrm{d}s^2 = \left(\frac{r^2}{\ell^2} + 1 - \mu\right)^{-1} \mathrm{d}r^2 + \ell^2 \left(\frac{r^2}{\ell^2} + 1 - \mu\right) \mathrm{d}\tau^2 + r^2 \mathrm{d}\theta^2. \tag{4.61}$$

Here the mass parameter μ is related to the mass m through

$$\mu = 8G_N m \tag{4.62}$$

Also, θ is periodic with period 2π.

When $\mu < 1$, the massive particle corresponds to a conical defect with deficit angle $\Delta\theta = 2\pi\sqrt{1-\mu}$. When $\mu > 1$, this geometry is a Euclidean BTZ black hole. The relation between μ and the lowest energy eigenvalue can be obtained from (4.52). In particular, when the EOW brane has no defect i.e., $\alpha_0 = \pi/2$,

$$2\sqrt{1-\mu} - 1 = \sqrt{1 - \frac{24h^{\mathrm{bcc}}_{(a,b)}}{c}}, \tag{4.63}$$

where $h^{\mathrm{bcc}}_{(a,b)}$ is the chiral conformal dimension of the boundary condition changing operator. This relation perfectly matches the corresponding relation found in [126].

Spectral Gap in Liouville Theory

In this section, we show that Liouville theory with ZZ boundaries [143] gives a spectral gap $\Delta E^{\mathrm{BCFT}}_{a,b}$ which is similar to that of our gravity dual. We emphasize that this match is only a formal analogy because ZZ boundaries in Liouville theory have very different properties compared to the usual conformal boundaries of unitary BCFTs.

For comparison, the spectral gap for our gravity model without bulk conical defects is

$$\Delta E^{\mathrm{BCFT}}_{a,b} = \frac{\pi c}{24\Delta x}\left(1 - \frac{\alpha_0^2}{(\pi/2)^2}\right) \in \left[0, \frac{\pi c}{24\Delta x}\right]. \tag{4.64}$$

The central charge for the Liouville theory is $c = 1 + 6Q^2$ where $Q = b + b^{-1}$. The semiclassical limit $c \to \infty$ can be obtained by taking $b \to 0$. The degenerate representations appear at conformal dimensions

$$\Delta_{(m,n)} := \frac{Q^2}{4} - \frac{(m/b + nb)^2}{4} \tag{4.65}$$

and the corresponding degenerate characters are

$$\chi_{m,n}(\tau) = \frac{q^{-(m/b+nb)^2/4} - q^{-(m/b-nb)^2/4}}{\eta(\tau)}, \qquad q := e^{2\pi i\tau}, \tag{4.66}$$

where $n,\ m$ are positive integers. $\Delta_{(m,n)}$ are negative except for $\Delta_{(1,1)} = 0$. Therefore there is no direct connection between Liouville ZZ boundary states and our holographic construction. Nevertheless, when we restrict our attention to the spectral gap $\Delta E^{\rm BCFT}_{a,b}$, we can find an interesting formal match.

The inner product between two ZZ boundary states $|B_{(m,n)}\rangle$ is given by [143]

$$\langle B_{(m,n)}|e^{-\beta H/2}|B_{(m',n')}\rangle = \sum_{k=0}^{\min(m,m')-1}\sum_{l=0}^{\min(n,n')-1} \chi_{m+m'-2k-1,n+n'-2l-1}\left(\frac{\mathrm{i}}{\beta T_{\rm BCFT}}\right). \tag{4.67}$$

When we take the limit $\beta T_{\rm BCFT} \to 0$, the term with $k = l = 0$ dominates, so

$$\frac{\langle B_{(m,n)}|e^{-\Delta x H}|B_{(m',n')}\rangle}{\sqrt{\langle B_{(m,n)}|e^{-\Delta x H}|B_{(m,n)}\rangle\langle B_{(m',n')}|e^{-\Delta x H}|B_{(m',n')}\rangle}} \xrightarrow[\Delta x\cdot T_{\rm BCFT}\to 0]{} e^{-\Delta E^{\rm BCFT}_{(m,n),(m',n')}\cdot T^{-1}_{BCFT}}, \tag{4.68}$$

where

$$\Delta E^{\rm BCFT}_{(m,n),(m',n')} := \frac{\pi}{4\Delta x}\left((n-n')b + \frac{m-m'}{b}\right)^2. \tag{4.69}$$

We consider $b \ll 1$, which corresponds to the large c limit. Assuming that $m = m'$ and $|n - n'| \le 1/b^2 + 1$, the spectral gap ranges between

$$0 \le \Delta E^{\rm BCFT}_{(m,n),(m,n')} \le \frac{\pi(c-1)}{24\Delta x} \approx \frac{\pi c}{24\Delta x}. \tag{4.70}$$

This result matches the spectral gap in our AdS/BCFT model. However, we should reemphasize that match between Liouville theory with ZZ boundaries and our model is only formal which is clear from $\Delta_{(m,n)}$ being negative. Moreover, there is another peculiar feature about ZZ boundaries that distinguishes them from usual BCFT boundaries. Namely, we have

$$E^{\rm BCFT}_{(m,n),(m,n)} = \frac{\pi}{4\Delta x}\left((2n-1)b + \frac{2m-1}{b}\right)^2, \tag{4.71}$$

which is distinct from (4.53) although this amplitude is between identical states. This mismatch also disallows us from interpreting the Liouville theory with ZZ boundaries as the usual BCFT.

4.5 Entanglement Entropy and Entanglement Island

In this section, we study the holographic entanglement entropy in our model. We use the Ryu–Takayanagi (RT) prescription to compute this entanglement entropy. We restrict to the case with no bulk conical defect.

We start by considering a normalized boundary state for a conformal boundary condition B_a prepared on a circle with circumference $T^{-1}_{\rm BCFT}$,

$$|B_a(\Delta x/2)\rangle = \frac{e^{-\frac{1}{2}H_{\rm CFT}\Delta x}|B_a\rangle}{\sqrt{\langle B_a|e^{-H_{\rm CFT}\Delta x}|B_a\rangle}}. \tag{4.72}$$

This state is often used to model an initial state for a global quantum quench[144, 145].

In the following, we consider the entanglement entropy of a superposition state

$$|\Psi\rangle := \sum_a c_a |B_a(\Delta x/2)\rangle, \tag{4.73}$$

where the c_a's are complex coefficients. We restrict to the case where the boundary entropy S_{B_a} is equal to a fixed value S_B (or it is in a narrow window around S_B) for the boundary conditions B_a appearing in $|\Psi\rangle$. Let N_{S_B} be the number of such boundary states.

We assume that the inner products $\langle B_a(\Delta x/2)|B_b(\Delta x/2)\rangle$ have holographic duals with a defect connecting the EOW branes. For simplicity, we assume that $\theta_{(a,a)} = \pi$ and $\theta_{(a,b)} = \theta_0$ when $B_a \neq B_b$. Under these assumptions, the geometries with $\theta_{(a,b)} = \theta_0$ dominate the gravitational computation for $\langle B_a(\Delta x/2)|B_b(\Delta x/2)\rangle$ if

$$\sum_{a=1}^{N_{S_B}} |c_a|^2 \ll \left(\sum_{\substack{a,b=1 \\ a\neq b}}^{N_{S_B}} c_a^* c_b \right) \exp\left[-\frac{c}{6\pi\Delta x} \left(\frac{\pi^2}{4} - \alpha_0^2 \right) \right]. \tag{4.74}$$

If all the c_a's are approximately equal, then this condition can be satisfied only if $N_{S_B} \gg \exp\left[\frac{c}{6\pi\Delta x} \left(\frac{\pi^2}{4} - \alpha_0^2 \right) \right]$. Since the gravity dual for $\langle\Psi|\Psi\rangle$ is given by the geometry with $\theta_{(a,b)} = \theta_0$ in this case, the RT surfaces in this geometry compute the entanglement entropy of the state $|\Psi\rangle$.

One can also understand this RT surface in terms of the *pseudo entropy* [134]. The pseudo entropy is given by the von Neumann entropy $S_P(A) = -\operatorname{Tr}[X_A \log X_A]$ of a normalized transition matrix X_A. In our case, this transition matrix is

$$X_A := \frac{\operatorname{Tr}_A \left[|B_a(\Delta x/2)\rangle\langle B_b(\Delta x/2)| \right]}{\operatorname{Tr}_{AA^c} \left[|B_a(\Delta x/2)\rangle\langle B_b(\Delta x/2)| \right]}. \tag{4.75}$$

Three Phases of the RT Surface

In this subsection, we will use the RT surface prescription to compute the entanglement entropy for a subregion [144, 145] of the state $|\Psi\rangle$ or the pseudo entropy for X_A. We assume the tensions of the EOW branes are equal, $T_1 = T_2 = T$, and $\mathcal{T}$ is the corresponding dimensionless tension. Also, the internal angle at the defect is θ_0. We assume the bulk conical defect is absent for simplicity.

Recall that our BCFT is defined on the strip

$$N = \{(\tau,\, x = z_0\phi) \mid 0 \leq \tau \leq T_{\mathrm{BCFT}}^{-1},\ \pi - \alpha_0 \leq \phi \leq \pi + \alpha_0\}, \tag{4.76}$$

so the width of the strip is $\Delta x = 2z_0\alpha_0$. On this strip, we consider the subregion

$$A = \{(\tau,\, x = z_0(\pi - \sigma)) \mid 0 \leq \tau \leq |A|\}, \tag{4.77}$$

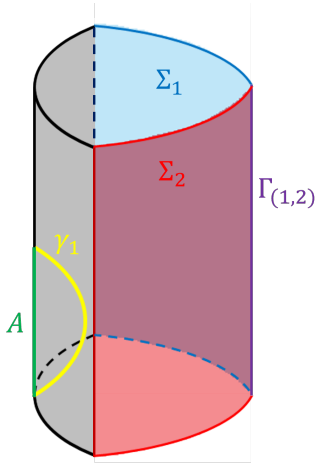

Figure 4.4: Thermal Phase of the RT surface for the boundary subregion A.

with a particular value of $\sigma \in [0, \alpha_0)$. Since τ is periodic with periodicity T_{BCFT}^{-1} and $|\Psi\rangle$ is a pure state, it is sufficient to consider the case $|A| < T_{\text{BCFT}}^{-1}/2$. There are three different phases of the RT surface described below.

Case 1: Thermal phase

In this case, the RT surface is a single connected surface. This surface is shown in Fig. 4.4 and we label it as γ_1. This phase is realized when the subregion A is sufficiently small. We will see that the entanglement entropy is extensive in this case.

The bulk geometry has reflection symmetry about the $\phi = \pi - \sigma$ plane, so the γ_1 lies on this plane. This surface is given by the geodesic

$$\sqrt{1-\chi^2} = \sqrt{1-\chi_0^2}\cosh\frac{\tau-\tau_0}{z_0} \tag{4.78}$$

with the parameters being

$$\tau_0 = \frac{|A|}{2}, \qquad \chi_0 = \tanh\frac{|A|}{2z_0}. \tag{4.79}$$

Note that $(\tau, \chi, \phi) = (\tau_0, \chi_0, \pi - \sigma)$ is the deepest point on this geodesic. If the maximum depth χ_0 is sufficiently large, γ_1 will be cut by the EOW branes in the negative tension case. Therefore, the thermal phase with $\mathcal{T} < 0$ exists only if $\mathcal{T} \geq -\frac{\tan(\alpha_0-\sigma)\,\mathrm{sech}(|A|/2z_0)}{\sqrt{\tan(\alpha_0-\sigma)^2+\tanh^2(|A|/2z_0)}}$.

The length of this RT surface is given by

$$\mathcal{A}(\gamma_1) = 2\int_{\epsilon}^{\chi_0} \mathrm{d}\chi \frac{\ell\chi_0}{\chi\sqrt{(1-\chi^2)(\chi_0^2-\chi^2)}} \tag{4.80}$$

$$= 2\ell \operatorname{arctanh}\sqrt{\frac{1-\epsilon^2/\chi_0^2}{1-\epsilon^2}} \tag{4.81}$$

$$\approx 2\ell\log\frac{2}{\epsilon} - \ell\log\frac{1-\chi_0^2}{\chi_0^2}. \tag{4.82}$$

Using the value of χ_0, the holographic entanglement entropy is

$$S(A) = \frac{\mathcal{A}(\gamma_1)}{4G_N} = \frac{c}{3}\log\frac{2}{\epsilon} + \frac{c}{3}\log\sinh(|A|/2z_0). \tag{4.83}$$

Since this result is independent of σ, analytically continuing it to real time does not give rise to any time dependence. For large $|A|$, this entropy demonstrates the volume law

$$S(A) \approx \frac{c}{3}\log\frac{2}{\epsilon} + \frac{c|A|}{6z_0} - \frac{c}{3}\log 2, \tag{4.84}$$

at an inverse effective temperature,

$$\beta_{|\Psi\rangle} = 2\pi z_0 = \frac{\pi}{2\alpha_0}(2\Delta x). \tag{4.85}$$

There is a prefactor $\frac{\pi}{2\alpha_0}$ here, which *lowers* the effective temperature for the same Δx for a given $\alpha_0 \leq \pi/2$ as compared to the conventional case for which $\alpha_0 = \pi/2$.

Case 2: Boundary phase.

In this phase, the RT surface has two disconnected pieces that end on the EOW branes. This surface is shown in Fig. 4.5 and we label it as γ_2. This phase is preferred over the thermal phase for sufficiently large $|A|$. We will see that the entanglement entropy is intensive in this case.

Each piece of γ_2 lies on a constant τ surface because of the τ reflection symmetry. These pieces are given by the geodesic

$$\sqrt{1-\chi^2}\cos(\phi - \pi + \sigma + \phi_0) = \cos\phi_0. \tag{4.86}$$

Here we have determined the parameter $\phi_0 = \alpha_0 - \sigma$ by requiring that the geodesic intersects the EOW brane orthogonally. The endpoints of γ_2, lying on the EOW brane Σ_1, are given by $\chi_{\text{ep}} = \sqrt{1-\mathcal{T}^2}\sin(\alpha_0 - \sigma)$.

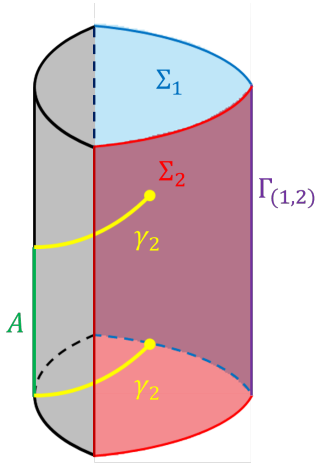

Figure 4.5: Boundary Phase of the RT surface for the boundary subregion A.

If $\alpha_0 \leq \pi/2$, or equivalently, $\theta_0 \leq \pi$, this geodesic exists for all values of σ. If $\alpha_0 \geq \pi/2$, the critical value corresponds to the endpoint lying on the defect. This is given by $\chi_{\text{ep}} = \chi_* = \sqrt{1 - \mathcal{T}^2 \csc^2(\frac{\theta_0}{2})}$, so the condition for the existence of this geodesic is

$$\alpha_0 - \sigma \leq \arccos \frac{\mathcal{T} \left|\cot(\frac{\theta_0}{2})\right|}{\sqrt{1-\mathcal{T}^2}}. \tag{4.87}$$

In particular, this surface exists for $\sigma = 0$ if and only if $\alpha_0 \leq \pi/2$.

To find the length of this RT surface, let us first specialize to $\sigma = 0$. For $\mathcal{T} > 0$

$$\mathcal{A}(\gamma_2) = 2\left(\int_{\epsilon}^{\sin\phi_0} \mathrm{d}\chi \frac{\ell \sin\phi_0}{\chi\sqrt{h(\chi) - \cos^2\phi_0}} + \int_{\chi_{\text{i}}}^{\sin\phi_0} \mathrm{d}\chi \frac{\ell \sin\phi_0}{\chi\sqrt{h(\chi) - \cos^2\phi_0}}\right) \tag{4.88}$$

$$\approx 2\ell \log \frac{2\sin\phi_0}{\epsilon} + 2\ell \operatorname{arctanh} \frac{\sqrt{h(\chi_{\text{i}}) - \cos^2\phi_0}}{\sin\phi_0} \tag{4.89}$$

$$= 2\ell \log \frac{2\sin(\alpha_0)}{\epsilon} + 2\ell \operatorname{arctanh}|\mathcal{T}|. \tag{4.90}$$

and for $\mathcal{T} < 0$,

$$\mathcal{A}(\gamma_2) = 2\int_{\epsilon}^{\chi_{\text{i}}} \mathrm{d}\chi \frac{\ell \sin\phi_0}{\chi\sqrt{h(\chi) - \cos^2\phi_0}} \tag{4.91}$$

$$\approx 2\ell \log \frac{2\sin\phi_0}{\epsilon} - 2\ell \operatorname{arctanh} \frac{\sqrt{h(\chi_{\text{i}}) - \cos^2\phi_0}}{\sin\phi_0} \tag{4.92}$$

$$= 2\ell \log \frac{2\sin(\alpha_0)}{\epsilon} - 2\ell \operatorname{arctanh}|\mathcal{T}|. \tag{4.93}$$

For non-zero σ, we just need to shift α_0 to $(\alpha_0 - \sigma)$ to adjust for the angular separation between A and Σ_1. The final result is

$$\mathcal{A}(\gamma_2) = 2\ell \log \frac{2}{\epsilon} + 2\ell \log \sin(\alpha_0 - \sigma) + 2\ell \operatorname{arctanh} \mathcal{T}, \tag{4.94}$$

so the holographic entanglement entropy is

$$S_A = \frac{\mathcal{A}(\gamma_2)}{4G_N} = \frac{c}{3} \log \frac{2}{\epsilon} + \frac{c}{3} \log \sin(\alpha_0 - \sigma) + 2S_B. \tag{4.95}$$

Here S_B is the boundary entropy

$$S_B = \frac{c}{6} \operatorname{arctanh} \mathcal{T}, \tag{4.96}$$

which can also be obtained using the disk partition function [106]. Note that there is an extremal but not minimal surface γ_2' ending on the other EOW brane Σ_2, i.e., the EOW brane anchored at $\phi = \pi + \alpha_0$. For this surface, we have

$$\frac{\mathcal{A}(\gamma_2')}{4G_N} = \frac{c}{3} \log \frac{2}{\epsilon} + \frac{c}{3} \log \sin(\alpha_0 + \sigma) + 2S_B. \tag{4.97}$$

The surface γ_2' exists when $\alpha_0 + \sigma \leq \arccos \frac{\mathcal{T}\left|\cot(\frac{\theta_0}{2})\right|}{\sqrt{1-\mathcal{T}^2}}$.

When we analytically continue this Euclidean entanglement entropy to real time, it is important to consider both $\mathcal{A}(\gamma_2)$ and $\mathcal{A}(\gamma_2')$, as well as cases where the two pieces of the RT surface ends on distinct EOW branes. To evaluate the entanglement entropy of the state $e^{-\mathrm{i}H^{\mathrm{CFT}}t}|\Psi\rangle$, we analytically continue $\frac{\mathcal{A}(\gamma_2)}{4G_N}$ and $\frac{\mathcal{A}(\gamma_2')}{4G_N}$ by taking $\sigma \to -\mathrm{i}\frac{t}{z_0}$. After this substitution, these two extremal areas are complex conjugates of the other, $\mathcal{A}(\gamma_2) = \overline{\mathcal{A}(\gamma_2')}$. The total areas in the other two cases are purely real and are equal to $\mathrm{Re}\,[\mathcal{A}(\gamma_2)] = \mathrm{Re}\,[\mathcal{A}(\gamma_2')]$. Therefore, the real time entanglement entropy is given by this real piece,

$$S_A = \mathrm{Re}\left[\frac{\mathcal{A}(\gamma_2)}{4G_N}\right] = \frac{c}{3} \log \frac{2}{\epsilon} + \frac{c}{6} \log \frac{\cosh(2t/z_0) - \cos(2\alpha_0)}{2} + 2S_B - \frac{c}{3} \log 2. \tag{4.98}$$

At late times $t \gg z_0$, this entanglement entropy is

$$S_A \approx \frac{c}{3} \log \frac{2}{\epsilon} + \frac{ct}{3z_0} + 2S_B. \tag{4.99}$$

Hence, at late times satisfying

$$t > \frac{|A|}{2} - \frac{6z_0 S_B}{c}, \tag{4.100}$$

the thermal phase will be favored over the boundary phase.

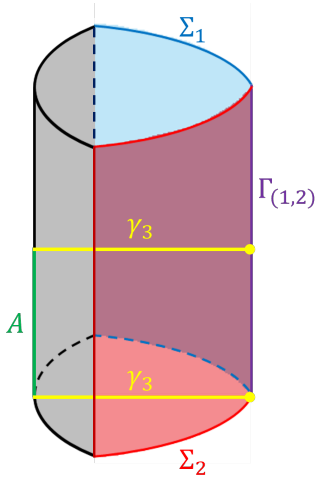

Figure 4.6: Defect Phase of the RT surface for the boundary subregion A.

Case 3: Defect phase.

In this phase, the RT surface has two disconnected pieces that end on the defect. This surface is shown in Fig. 4.6 and we label it as γ_3. As in the boundary phase, the entropy is intensive. This phase is always subdominant compared to the boundary entropy phase if the latter exists. Therefore, this phase is realized only when the subregion is sufficiently large and the boundary entropy phase is absent. For this reason, when $\alpha_0 \leq \pi/2$, this phase is irrelevant.

As earlier, each piece of γ_3 lies on a constant τ surface. These pieces are given by the geodesic

$$\sqrt{1-\chi^2}\cos(\phi-\pi+\sigma+\phi_0)=\cos\phi_0, \tag{4.101}$$

Here we have determined the parameter $\phi_0 = \arctan\frac{\sin(\theta_0/2)+\mathcal{T}\cos\sigma}{\mathcal{T}\sin\sigma}$ by requiring that the geodesic passes through the defect.

If $\mathcal{T} > 0$ this geodesic is guaranteed to exist. However, when $\mathcal{T} < 0$ this geodesic exists only if $\sigma \leq 2\arctan\left(\tan\left(\frac{\theta_0}{4}\right)\sqrt{\frac{\sin(\theta_0/2)+\mathcal{T}}{\sin(\theta_0/2)-\mathcal{T}}}\right)$. This implies that this phase always exists around $\sigma = 0$. The computation of the length of this RT surface is similar to previous case with $\sigma = 0$, and we get the final result

$$\frac{\mathcal{A}(\gamma_3)}{2R}=\log\frac{2}{\epsilon}+\frac{1}{2}\log\frac{(\sin(\frac{\theta_0}{2})+\mathcal{T}\cos\sigma)^2}{\sin^2(\frac{\theta_0}{2})-\mathcal{T}^2}. \tag{4.102}$$

The holographic entanglement entropy is

$$S_A=\frac{\mathcal{A}(\gamma_3)}{4G_N}=\frac{c}{3}\log\frac{2}{\epsilon}+\frac{c}{3}\log\frac{\sin(\theta_0/2)+\mathcal{T}\cos\sigma}{\sin(\theta_0/2)+\mathcal{T}}+2S_D. \tag{4.103}$$

Here we have defined

$$S_D := \frac{c}{12}\log\frac{\sin(\theta_0/2)+\mathcal{T}}{\sin(\theta_0/2)-\mathcal{T}}, \tag{4.104}$$

and we call it the defect entropy. This defect entropy can be considered as a generalization of the boundary entropy S_B and it reduces to S_B if we make the defect disappear by setting $\theta_0 = \pi$.

As mentioned earlier, the boundary phase is favored over this phase, $\mathcal{A}(\gamma_2) < \mathcal{A}(\gamma_3)$, if both phases exist. This is because γ_2 is minimal amongst all surfaces that end on the EOW brane.

The real time entanglement entropy is given by analytically continuing $\sigma \to -\mathrm{i}\frac{t}{z_0}$, so

$$S_A = \frac{c}{3}\log\frac{2}{\epsilon} + \frac{c}{3}\log\left(\frac{\mathcal{T}\cosh(t/z_0)+\sin(\theta_0/2)}{\mathcal{T}+\sin(\theta_0/2)}\right) + 2S_D. \tag{4.105}$$

Note that this result is manifestly real unlike case 2. At late times $t \gg z_0$, this entanglement entropy is

$$S_A \approx \frac{c}{3}\log\frac{2}{\epsilon} + \frac{ct}{3z_0} + 2S_D - \frac{c}{3}\log\frac{2\left(\mathcal{T}+\sin(\theta_0/2)\right)}{\mathcal{T}}. \tag{4.106}$$

It is also worth mentioning that the γ_3 is minimal but not extremal because of the singular nature of the defect. One can imagine a scenario when there is a matter theory on the EOW brane which smoothly interpolates between the two different tensions of the EOW branes, and the defect is realized as the sharp limit. In this case, the RT surface is extremal and the distinction between cases 2 and 3 disappears.

Interpretation as Entanglement Island

In this subsection, we explain and interpret the results in the previous section in terms of the island formula. We interpret the state $|\Psi\rangle$ as a field theoretic wavefunction being prepared by a matter field that lives on the EOW brane. In other words, the EOW brane is now the spacetime on which a quantum state $|\Psi\rangle$ is prepared [132, 133]. We are interested in the entanglement entropy of a subregion A of the state $|\Psi\rangle$. We assume that the matter theory is a holographic BCFT to simplify the analysis [146]. When the effective temperature of $|\Psi\rangle$ is sufficiently low, the EOW branes in the bulk are disconnected. When the temperature is sufficiently high, the EOW branes are connected via a defect, creating a closed universe that terminates at this defect.

The three phases of the RT surface in the previous section can be interpreted as the phases of the entanglement entropy of A [133]. When the subregion is sufficiently small, the entanglement entropy is given by the thermal answer from matter theory. This corresponds to case 1. When the subregion is large enough so that the naive thermal entropy is much larger than the boundary entropy, then an entanglement island is formed on the EOW brane (case 2) or on the defect (case 3).

In case 2, the two pieces of the RT surface can end on the same EOW brane or on different EOW branes. However, the "island" in the latter case cuts through the defect

on the EOW brane, so the corresponding entropy increases by the boundary entropy of the defect coming from the matter field on the EOW branes. Consequently, it can be argued that this configuration is subdominant when we are looking for the island. As the result, the island lies only on one of the two EOW branes. The bulk matter wavefunction on such an island is a transition matrix, so the matter part of the generalized entropy is given by the pseudo entropy. It is expected that there is a generalization of entanglement wedge reconstruction to such cases, although there are no quantum information theoretic foundations for this claim yet.

In case 3, the RT surface ends on the defect. This can be interpreted as an island lying exclusively on the defect. Therefore, a portion of the defect is included in the entanglement wedge of the subregion A.

4.6 Three-dimensional Wormhole Saddles

In this section, we construct a connected bulk geometry with multiple AdS boundaries using our model of EOW branes and defects. This geometry is similar to the replica wormhole in 2d gravity with EOW branes [89]. However, we will be interested in defects with $\theta_0 > \pi$, so these defects have negative energy.

One way to add such negative energy in the bulk is by adding non-local interaction between different boundaries [147], which can originate from integrating out "fast" degrees of freedom. Such non-local interaction between boundaries can make a non-traversable Einstein-Rosen bridge traversable, so that different boundaries can communicate with each other [147, 148]. We interpret our model in this section as a realization of such non-local interaction between BCFTs, and the non-unitarity of the BCFTs with $\theta_0 > \pi$ comes from such non-local interactions obtained by integrating out these fast degrees of freedom.

Let us consider two BCFTs that live on two different strips with widths Δx_1 and Δx_2 respectively. They have the same periodicity T_{BCFT}^{-1} in τ direction, so the aspect ratios are $\xi_1 = \Delta x_1 \cdot T_{\text{BCFT}}$ and $\xi_2 = \Delta x_2 \cdot T_{\text{BCFT}}$. Fig. 4.7 shows a constant τ slice for this setup.

We assume that the tensions satisfy $T_1 = T_3$ and $T_2 = T_4$ and that the angle of intersection between the Σ_1, Σ_3 EOW branes and the Σ_2, Σ_4 EOW branes is $\theta_0 > \pi$. This assumption is required to get connected geometries. it implies that $\alpha_0 > \frac{\pi}{2}$ and that the BCFTs are non-unitary.

The factorized geometry is shown in Fig. 4.8. The Euclidean action for this geometry is the sum of the two corresponding actions

$$I_E^{\text{f}} = -\frac{c}{6\pi}\frac{\alpha_0^2}{\xi_1} - \frac{c}{6\pi}\frac{\alpha_0^2}{\xi_2}. \tag{4.107}$$

where α_0 is given by (4.25).

The connected wormhole geometry is shown in Fig. 4.9. It is obtained by stitching together two geometries, each with a boundary angle $2\alpha_0$. The total boundary angle for this

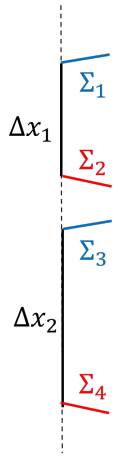

Figure 4.7: Constant τ slice for two BCFTs.

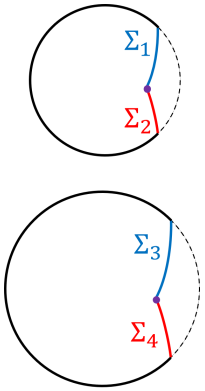

Figure 4.8: Constant τ slice of the factorized (disconnected) geometry.

wormhole geometry is $2\alpha_{\rm w} = (4\alpha_0 - 2\pi)$, where we have subtracted a 2π to account for the connection. The Euclidean action for the wormhole geometry is

$$I_E^{\rm w} = -\frac{c}{6\pi\xi_{\rm w}}\alpha_{\rm w}^2 = -\frac{c}{6\pi}\frac{(2\alpha_0 - \pi)^2}{\xi_1 + \xi_2}, \tag{4.108}$$

where $\xi_{\rm w} = \xi_1 + \xi_2$ is the total aspect ratio for the wormhole.

The factorized geometry strictly dominates over the wormhole geometry, since

$$I_E^{\rm f} = -\frac{c\alpha_0^2}{6\pi}\left(\frac{1}{\xi_1} + \frac{1}{\xi_2}\right) \leq -\frac{c\alpha_0^2}{6\pi}\frac{4}{\xi_1 + \xi_2} < -\frac{c(2\alpha_0^2 - \pi)^2}{6\pi}\frac{1}{\xi_1 + \xi_2} = I_E^{\rm w}. \tag{4.109}$$

Here we have used the arithmetic mean-harmonic mean inequality to establish the first inequality.

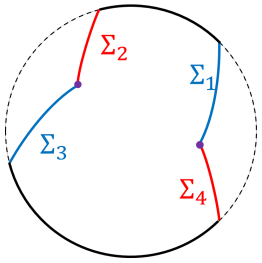

Figure 4.9: Constant τ slice of the wormhole (connected) geometry.

More generally, if we have n disconnected boundary regions with aspect ratios $\xi_i = \Delta x_i \cdot T_{\text{BCFT}}$, then the Euclidean actions for the factorized geometry is

$$I_E^{\text{f}} = -\frac{c}{6\pi} \sum_{i=1}^{n} \frac{\alpha_0^2}{\xi_i}, \tag{4.110}$$

and for the fully connected wormhole geometry is

$$I_E^{\text{w}} = -\frac{c}{6\pi} \frac{(n\alpha_0 - (n-1)\pi)^2}{\sum_{i=1}^{n} \xi_i}, \qquad . \tag{4.111}$$

This fully connected geometry exists only for $\alpha_0 \geq \frac{(n-1)\pi}{n}$. From these results, we can conclude that any wormhole geometry is subdominant compared to the corresponding factorized geometry, even though we have considered a non-unitary BCFT. Recall that without non-unitarity, it is not even possible to construct a connected saddle. Interestingly, in order to increase the number of boundary components, we need larger a α_0, which means that we need to make the BCFT "more" non-unitary.

4.7 Discussion

We have developed a generalization of the conventional AdS/BCFT model by including defects that connect EOW branes with different tensions. This construction enables us to study a BCFT whose lowest eigenvalue can be tuned arbitrarily close to that of the identity operator. This construction is particularly useful when the boundary entropies of the two boundaries are distinct, i.e. when the conventional model has a restricted lowest eigenvalue.

We conclude with some remarks and possible future directions. The construction in our model is based on 3d gravity, and we expect that the generalization to higher dimensions should be straightforward. Although we have calculated the real time entropy in section 4.5, we did not study the corresponding real time geometry. It would be interesting to develop this analytic continuation. It would also be interesting to generalize our defect on the EOW branes to a smooth configuration. We can imagine a model in which the tension of the

EOW brane is position dependent, and in particular, it interpolates smoothly between the two BCFT boundaries. Closely related models were studied in [149, 150]. We would like to understand the interpretation of the boundary entropy in this configuration, for which a specific example is given by the defect entropy in (4.103).

The connection between unitarity and connected geometries in Sec. 4.6 remains mysterious and interesting. We should emphasize that although the connected saddle exists in the non-unitary case, this saddle is always subleading compared to the disconnected saddle.

Chapter 5

The Multiverse in an Inverted Island

5.1 Introduction

In the last two decades or so, we have learned a lot about the origin of spacetime in quantum gravity. A key concept is holography [4, 5, 6, 81], which states that a fundamental description of quantum gravity resides in a spacetime, often non-gravitational, whose dimension is lower than that of the bulk spacetime. This concept has been successfully applied to understanding the dynamics of an evaporating black hole, in particular to address the information problem [1]; for recent reviews, see [151, 152, 153].

There are two distinct approaches to implementing the idea of holography. One is to start from global spacetime of general relativity and identify independent quantum degrees of freedom [16, 17, 88] using the quantum extremal surface (QES) prescription [9, 11, 12, 13]. When applying this prescription to a black hole, the existence of the interior is evident, whereas understanding unitary evolution requires non-perturbative gravitational effects [89, 90]. The other approach is to begin with a description that is manifestly unitary (if all the relevant physics is included in the infrared) and understand how the picture of global spacetime emerges [154, 155, 156, 99, 100, 157, 158]. Specifically, in this approach, the interior of an evaporating black hole arises as a collective phenomenon of soft (and radiation) modes [99, 100, 157, 159]. While the two approaches appear radically different at first sight, they are consistent with each other in the common regime of applicability.

In this chapter, we study the eternally inflating multiverse using the first approach which begins with global spacetime. A key assumption is that for a partial Cauchy surface R in a weakly gravitating region, we can use the QES prescription [13]. In particular, the von Neumann entropy of the microscopic degrees of freedom associated with the region R is given by the island formula [88]

$$S(\mathbf{R}) = \min_{I} \text{ ext } S_{\text{gen}}(I \cup R), \tag{5.1}$$

where I is a partial Cauchy surface spacelike separated from R.[1] Here, the boldface symbol

[1] In this chapter, I refers to a spacelike codimension-1 surface. Although it is more standard to refer to

$\mathbf{R}$ in the left-hand side is to emphasize that $S(\mathbf{R})$ is the microscopic von Neumann entropy of the fundamental degrees of freedom, while

$$S_{\rm gen}(X) = \frac{\mathcal{A}(\partial X)}{4G_N} + S_{\rm bulk}(X) \tag{5.2}$$

is the generalized entropy for partial Cauchy surface X calculated in bulk semiclassical theory, where $\mathcal{A}(\partial X)$ is the area of the boundary ∂X of X, and $S_{\rm bulk}(X)$ is the von Neumann entropy of the reduced density matrix of X calculated in the semiclassical theory.

In this work, we show that when R is a sufficiently large region on a late-time hypersurface in a bubble universe, an island I appears which encloses the bubble universe. Given that the semiclassical physics in I is fully reconstructed using the fundamental degrees of freedom in R, this implies that the full semiclassical physics of the multiverse needed to make cosmological predictions is encoded in the fundamental degrees of freedom of the region R, which has a finite volume!

While one might feel that this is too drastic a conclusion, in some respects it is not. Even for a black hole, the interior region described as an island I can have an ever-increasing spatial volume, which can even be infinite for an eternal black hole [160, 161]. However, in quantum gravity, the number of independent states associated with this region is bounded by the exponential of the entropy of the system. This is because exponentially small overlaps between semiclassically orthogonal states lead to a drastic reduction in the number of basis states [162, 163, 164, 165]. What happens in the multiverse is an "inside-out" version of the black hole case. As anticipated in [166, 167, 168], this allows us to address the cosmological measure problem [169, 170, 171, 172, 173] associated with the existence of an infinitely large spacetime at the semiclassical level.

Entanglement Castle

In the black hole case, the region R encloses I, so I looks geographically like an island. However, in our setup, I encloses R so it no longer appears as an island. Thus, we call I an inverted island.

The geography for a Cauchy surface Ξ containing R is depicted in Fig. 5.1.

It is usual to treat the regions R and I as "land" and everything else as "water." Following this convention, Ξ has a central land R surrounded by a moat $\overline{R \cup I_\Xi}$ which separates R from I_Ξ, where $I_\Xi = D(I) \cap \Xi$. To describe the multiverse at the semiclassical level, one only needs fundamental degrees of freedom associated with the complement of I_Ξ on Ξ, $\overline{I_\Xi} = R \cup (\overline{R \cup I_\Xi})$. This is the region corresponding to the castle—the multiverse lives in an entanglement castle.

the domain of dependence of I, $D(I)$, as the island, we also refer to I as an island in this chapter.

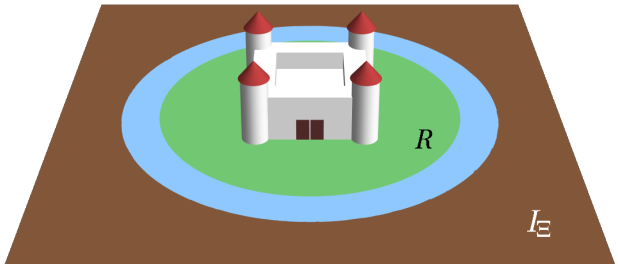

Figure 5.1: The multiverse as an entanglement castle. On a given Cauchy surface Ξ, the physics of the multiverse can be described by the fundamental degrees of freedom associated with the region $R \cup (\overline{R \cup I_\Xi})$, where $I_\Xi = D(I) \cap \Xi$ with I being the (inverted) island of a partial Cauchy surface R.

Relation to Other Works

Entanglement islands in cosmological spacetimes have been discussed in the context of toy models, e.g., models in which a nongravitational bath is entangled with a gravitational system as well as models in lower dimensional gravity [174, 178, 132, 98, 98, 19, 179, 180, 181, 175, 176, 177]. In this chapter, we study them in a realistic scenario of eternal inflation.

Several holographic descriptions of the multiverse have been proposed [182, 183, 184, 166, 167, 168, 185, 186, 51], mostly to address the measure problem. These correspond to the unitary description of a black hole, although the issue of unitarity at the fundamental level is not quite clear in cosmology.

Overview

In Section 5.2, we review the eternally inflating multiverse and describe some basic assumptions employed in our analysis. In Section 5.3, we discuss how bulk entanglement necessary for the emergence of an island can arise from accelerating domain walls, which are pervasive in the eternally inflating multiverse.

Section 5.4 is the main technical part of this chapter, in which we show that a sufficiently large region R in a bubble universe has an inverted island that surrounds R. Implications of this result for the multiverse are discussed in Section 5.5.

5.2 The Eternally Inflating Multiverse in Global Spacetime

In this chapter, we are concerned with eternally inflating cosmology. Eternal inflation occurs when the theory possesses a metastable vacuum which has a positive vacuum energy and

small decay rates to other vacua [187, 188]. If the universe sits in such a vacuum at some moment, there will always be some spacetime region that remains inflating for an arbitrarily long time.

This scenario of eternal inflation is naturally realized in the string landscape [189, 190, 191, 192]. In the string landscape, the number of local minima of the potential, i.e. false vacua, is enormous. Vacuum energies at these minima can be either positive or negative. Since exactly vanishing vacuum energy requires an infinite amount of fine-tuning, we expect that it is realized only in supersymmetric vacua.

Spacetime regions in different vacua are created by nucleation of bubbles, each of which can be viewed as a separate universe. We assume that bubble nucleation occurs through Coleman-De Luccia tunneling [193], although we expect that our results also apply to other vacuum transition mechanisms such as the thermal Hawking-Moss process [194, 195].

As explained in the introduction, we begin with the global spacetime picture, which is the infinitely large multiverse with a fractal structure generated by continually produced bubbles. We assume that the global quantum state on a Cauchy surface is pure. We are interested in studying the existence and location of the island corresponding to a partial Cauchy surface R in the global multiverse.

To address this problem, we focus on a particular bubble, which we call the central bubble. We assume that the central bubble is formed in a parent de Sitter (dS) bubble. After being nucleated, it undergoes collisions with other bubbles [188]. Let us follow a timelike geodesic to the future along (and outside) the bubble wall separating the central bubble from other bubbles. The last bubble that this geodesic encounters must be either an anti-de Sitter (AdS) bubble or a supersymmetric Minkowski bubble, or else the geodesic still has an infinite amount of time to encounter another bubble.

We assume that the last bubbles such geodesics encounter are all AdS bubbles and call them surrounding AdS bubbles. Since AdS bubbles generally end up with big crunch singularities [193], they are collapsing bubbles. Note that the choice of the central bubble was arbitrary, so all the bubbles have the feature of being surrounded by collapsing AdS bubbles. A typical example of the spacetime structure described here is illustrated in Fig. 5.2. (We have omitted an infinite number of bubbles that form a fractal structure in the asymptotic future infinity which are not relevant for the discussion here.)

We postulate that the cosmological history we study takes place in the semiclassical regime. This implies that the characteristic energy scale E of the potential is sufficiently smaller than the cutoff scale, and hence the Planck scale. On the other hand, in the string landscape we expect that this energy scale is not much smaller than the string scale, e.g., $E \sim O(10^{-5} - 10^{-1})/l_P$, where l_P is the Planck length. Note, however, that some of these bubbles could be associated with much smaller energy scales by selection effects. For instance, the bubble universe that we live in has a vacuum energy much smaller than the naive value of $O(E^4)$ [196, 197, 198].

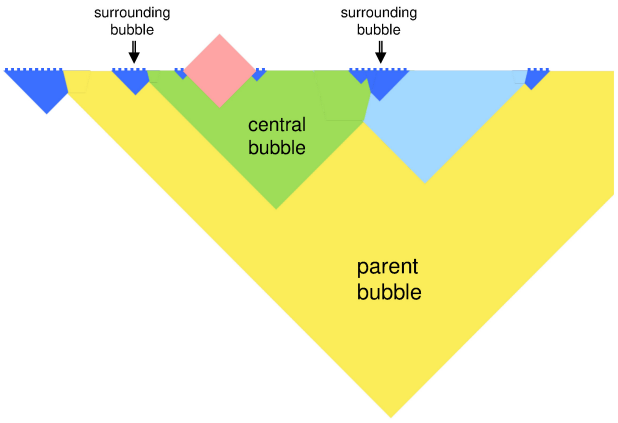

Figure 5.2: A sketch of the Penrose diagram of the multiverse. We focus on an arbitrarily chosen bubble, which we call the central bubble. The central bubble is nucleated in a parent dS bubble and is surrounded by collapsing AdS bubbles which collide with it at late times.

5.3 Bulk Entanglement from Accelerating Domain Walls

In this section, we discuss the possible origin of bulk entanglement $S_{\text{bulk}}()$ leading to an island in eternally inflating spacetime. As discussed in [98], an island cannot be created by $S_{\text{bulk}}()$ originating solely from entanglement between regular matter particles. In particular, the generation of $S_{\text{bulk}}()$ must involve spacetime (vacuum) degrees of freedom. Examples of such processes include Hawking radiation and reheating after inflation. Here we discuss another such process: $S_{\text{bulk}}()$ generated by Unruh radiation [199, 200] from accelerating domain walls.

Consider a domain wall in 4-dimensional flat spacetime which is extended in the x^2-x^3 directions and is accelerating in the x^1 direction. In an inertial reference frame, the domain wall appears to emit radiation. This occurs because the modes of a light quantum field colliding with the domain wall from behind are (partially) reflected by it, which converts these modes into semiclassical excitations on top of the vacuum; see blue arrows in Fig. 5.3. (For a review and recent analyses, see [201, 202, 203].)

An important point is that this process stretches the wavelength of reflected modes. In particular, radiation emitted later corresponds to a shorter wavelength mode at a fixed early time. We postulate that, as in the case of Hawking radiation [204] and the generation of fluctuations in cosmic inflation [205, 206, 207, 208], this picture can be extrapolated formally to an infinitely short distance, below the Planck length. This allows for converting an arbitrary amount of short distance vacuum entanglement to entanglement involving physical radiation. In particular, if we take a spatial region A that contains the radiation but not its partner modes, then we can obtain a large contribution to $S_{\text{bulk}}()$ from this process. This is illustrated in Fig. 5.3.

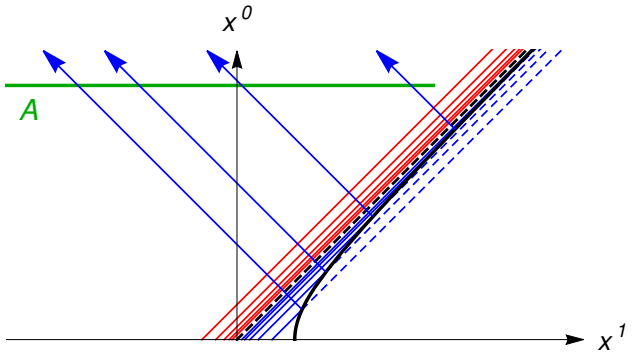

Figure 5.3: Generation of $S_{\rm bulk}()$ by an accelerating domain wall. The blue and red lines are entanglement partners of each other. This results in the region A, shown in green, to have a large $S_{\rm bulk}()$.

This mechanism of generating $S_{\rm bulk}()$ operates at any wall separating bubble universes. It converts entanglement in a semiclassical vacuum, which is assumed to take the flat space form at short distances [209], into that involving radiation emitted by the wall. There are two classes of walls relevant for our purpose.

The first is a bubble wall separating a nucleated bubble from the ambient bubble (parent dS bubble in our context). In this case, the bubble wall accelerates outward, so that the radiation lies inside the bubble. This radiation is homogeneous on a Friedmann-Robertson-Walker (FRW) equal-time slice and has coarse-grained entropy density

$$s \sim \left(\frac{\sqrt{-\kappa}}{2\pi a(t)}\right)^3, \tag{5.3}$$

where $a(t)$ is the scale factor at FRW time t, and $1/\sqrt{-\kappa}$ is the comoving curvature length scale at an early stage of the bubble universe, when $a(t) \approx \sqrt{-\kappa}\, t$.

The second is a domain wall separating two bubbles colliding with each other. A domain wall relevant for our discussion is that separating the central bubble and one of the surrounding AdS bubbles colliding with it. In this case, the domain wall accelerates outward in the AdS bubble [210, 211], so the mechanism described above applies to the AdS bubble; in Fig. 5.3 the regions left and right to the wall would correspond to the AdS and central bubbles, respectively. If the domain wall is also accelerating away from the central bubble, the radiation emitted into the central bubble also results in a large $S_{\rm bulk}()$, although this is not relevant for our setup.

5.4 Entanglement Island from Surrounding Collapsing Bubbles

In this section, we argue that a sufficiently large spacelike region R in the multiverse has an island I. We use the method of island finder [212] to demonstrate this. First, we locate a partial Cauchy surface I' that (i) is spacelike separated from R, (ii) provides a reduction of generalized entropy $S_{\rm gen}(I' \cup R) < S_{\rm gen}(R)$, and (iii) has the boundary $\partial I'$ that is quantum normal or quantum antinormal with respect to variations of the generalized entropy $S_{\rm gen}(I' \cup R)$. We will find such an I' which has a quantum antinormal boundary. We then argue that there is a partial Cauchy surface I_0 whose domain of dependence, $D(I_0)$, contains I' and whose boundary, ∂I_0, is quantum normal with respect to variations of $S_{\rm gen}(I_0 \cup R)$. Having such an I' and I_0 guarantees the existence of a non-empty island I.

We focus on $(3+1)$-dimensional spacetime throughout our analysis, although it can be generalized to other dimensions. In our analysis below, we assume that the central bubble is either a dS or Minkowski bubble, which simplifies the analysis [210, 211]. We believe that a similar conclusion holds for an AdS central bubble, but demonstrating this requires an extension of the analysis.

The argument in this section consists of several steps. First, we identify a two-dimensional quantum antinormal surface $\partial\Sigma'$ in a surrounding AdS bubble for a region R in the central bubble. Then, we gather a portion of $\partial\Sigma'$ in each surrounding bubble and sew them together to form a closed quantum antinormal surface $\partial I'$ which encloses R. Next, we argue that appending I' reduces the generalized entropy of R and hence it can serve as the I' of [212]. Then, we find I_0, establishing the existence of a non-empty QES for R. Finally, we include some discussion about the (inverted) island I.

While our argument applies more generally, in this section we consider a setup that involves only a central bubble and its surrounding AdS bubbles. We discuss more general cases in Section 5.5.

Quantum Antinormal Surface in a Colliding Collapsing Bubble

Let us consider the central bubble and only one of the surrounding AdS bubbles. These bubbles are separated by a domain wall. This system preserves invariance under an $SO(2,1)$ subgroup of $SO(3,1)$ symmetry of a single Coleman-De Luccia bubble. The spacetime is thus given by a warped product of a two-dimensional hyperboloid H_2 with a two-dimensional spacetime M_2. Consider a two-dimensional hyperbolic surface $\partial\Sigma'$ given by the $SO(2,1)$ orbit of a spacetime point as shown in Fig. 5.4. We denote the partial Cauchy surface which is bounded by $\partial\Sigma'$ and extending toward the AdS side by Σ'.

We focus on the region near the domain wall at late times. Given a $\partial\Sigma'$ in this region, let k^μ and l^μ be the future-directed null vectors orthogonal to $\partial\Sigma'$, pointing inward and outward relative to Σ', respectively, as depicted in Fig. 5.4. We normalize them such that $k \cdot l = -2$ and denote the corresponding classical and quantum expansions by $\theta_{k,l}$ and $\Theta_{k,l}$,

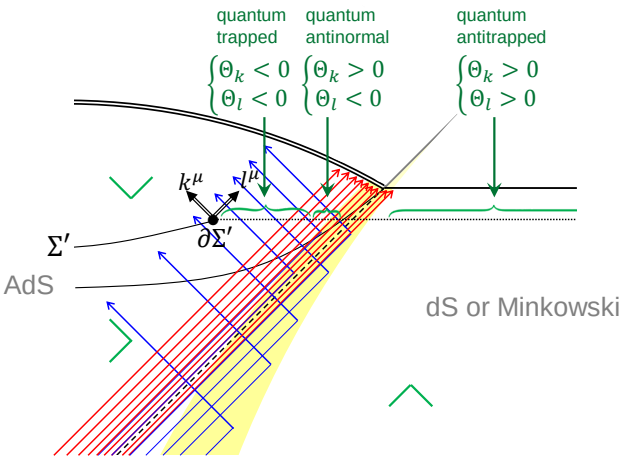

Figure 5.4: Penrose diagram showing the region near the domain wall (yellow strip) separating the central dS/Minkowski and surrounding AdS bubbles at late times. The transverse directions corresponding to the hyperboloid H_2 have been suppressed. $\partial\Sigma'$ is a boundary of a partial Cauchy surface Σ' and k^μ, l^μ are future-directed null vectors orthogonal to it. Blue and red arrows indicate Unruh radiation and their partner modes, respectively, and the double line at the top of the AdS bubble represents the big crunch singularity. The signs of classical expansions $\theta_{k,l}$ are shown in green following the Bousso wedge convention [213].

respectively. Here, $\Theta_{k,l}$ are given by the changes in the generalized entropy $S_{\rm gen}(\Sigma' \cup R)$ under infinitesimal null variations of $\partial\Sigma'$ [73].

Suppose that a surface $\partial\Sigma'$ in the AdS bubble is located near the big crunch singularity but sufficiently far from the domain wall. This surface is classically trapped ($\theta_k, \theta_l < 0$). When $\partial\Sigma'$ is moved toward the central bubble, first it becomes normal ($\theta_k < 0$, $\theta_l > 0$) and then antitrapped ($\theta_k, \theta_l > 0$) [210, 211]. What about the quantum expansions?

In general, $S_{\rm bulk}()$, and hence $S_{\rm gen}()$, can only be defined for a closed surface, and its change $\delta S_{\rm bulk}()$ under a small variation of the surface depends non-locally on the entire surface. In our setup, however, the only relevant contribution to $\delta S_{\rm bulk}(\Sigma' \cup R)$ comes from partner modes of the Unruh radiation emitted by the domain wall into the AdS bubble, and we can locally determine the signs of $\Theta_{k,l}$.[2]

Suppose we locally deform $\partial\Sigma'$ in the $\pm l$ direction. Then, $\delta S_{\rm bulk}()$ receives a contribution from reflected modes, depicted by blue arrows in Fig. 5.4. This contribution, however, is not strong enough to compete with the classical expansion, since the modes are spread out in the l direction.

To see this explicitly, let us assume that every radiation quantum carries $O(1)$ entropy, and that the rate of emission as viewed from the domain wall's frame is controlled by the

[2]The contribution from partner modes of Unruh radiation emitted into the central bubble is not relevant if R is sufficiently large, such that it intersects most of the radiation, since then the contribution has the same sign as the variation of the area $\mathcal{A}(\partial\Sigma')$.

Unruh temperature $T = a_w/2\pi$, where a_w is the acceleration of the domain wall. We then find that[3]

$$|\delta S_{\rm bulk}()| \sim \frac{a_w^3 \ell^6}{\lambda r^2 (t_\infty - x^-)^3} \delta r \, \Omega_{\rm H}, \tag{5.4}$$

where ℓ is the AdS radius in the bubble, (t, r) are the location of $\partial\Sigma'$ in the coordinates [210, 211]

$$ds^2 = -f(r)dt^2 + \frac{dr^2}{f(r)} + r^2 dH_2^2, \tag{5.5}$$

δr is the change of r when we deform $\partial\Sigma'$ in the l direction, and $\Omega_{\rm H}$ is the coordinate area of the portion of the hyperboloid for which we deform $\partial\Sigma'$. Also, λ is a parameter appearing in the trajectory of the domain wall

$$\begin{pmatrix} t \\ r \end{pmatrix} \simeq \begin{pmatrix} t_\infty - t_\infty e^{-\lambda(\tau-\tau_0)} \\ r_0 \, e^{\lambda(\tau-\tau_0)} \end{pmatrix}, \tag{5.6}$$

where τ is the proper time along the domain wall trajectory, with $r_0 = r(\tau = \tau_0)$ and $t_\infty = t(\tau = \infty)$, and we have introduced the null coordinates

$$x^\pm = t \pm \frac{\ell^2}{r}. \tag{5.7}$$

To derive the above expressions, we have assumed that $\lambda\ell \gtrsim 1$ and r is sufficiently larger than ℓ so that $f(r) \sim r^2/\ell^2$, which implies $t_\infty \sim \ell^2/r_0$ (also $t_\infty > \ell^2/r_0$).

The expression in Eq. (5.4) should be compared with the corresponding change in area,

$$\left| \frac{\delta \mathcal{A}}{4 l_P^2} \right| \sim \frac{1}{l_P^2} \, r \delta r \, \Omega_{\rm H}. \tag{5.8}$$

Assuming that the scalar potential responsible for the domain wall is characterized by a single energy scale E, we find $\ell \sim 1/E^2 l_P$ and $\lambda \sim a_w \sim E$,[4] so

$$\left| \frac{\delta S_{\rm bulk}()}{\delta \mathcal{A}/4 l_P^2} \right| \lesssim \frac{l_P}{\ell}, \tag{5.9}$$

where we have only considered $\partial\Sigma'$ satisfying $t < t_\infty$. We indeed find that the quantum effect, $\delta S_{\rm bulk}()$, is negligible compared to the classical contribution, $\delta\mathcal{A}/4l_P^2$, for ℓ sufficiently larger than l_P.

On the other hand, if we vary $\partial\Sigma'$ in the $\pm k$ direction, $\delta S_{\rm bulk}()$ receives a contribution from partner modes, depicted by red arrows in Fig. 5.4. If $\partial\Sigma'$ is far from the domain wall, this contribution is small, so that $\partial\Sigma'$ remains trapped at the quantum level: $\Theta_{k,l} < 0$.

[3] We thank Adam Levine for discussion on obtaining the quantum contributions.

[4] The second relationship holds for generic bubbles. For supersymmetric bubbles, we instead have $\lambda \sim a_w \sim 1/\ell$, but this does not affect our final conclusions.

However, if $\partial\Sigma'$ is moved toward the null surface to which the domain wall asymptotes, $x^+ = t_\infty$, the contribution becomes enhanced because the partner modes are squeezed there.

Specifically, the quantum effect can be estimated as

$$|\delta S_{\rm bulk}()| \sim \frac{a_w^3 \ell^6}{\lambda r^2 (x^+ - t_\infty)^3} \delta r \, \Omega_{\rm H}. \tag{5.10}$$

Here, we have assumed that the reflected modes, the partners of which $\partial\Sigma'$ crosses, all pass through Σ', which requires

$$t > t_\infty - \left(\frac{1-c}{1+c}\right)\frac{\ell^2}{r}, \tag{5.11}$$

where $c = (t_\infty - \ell^2/r_0)/(t_\infty + \ell^2/r_0)$ is a constant satisfying $0 < c < 1$. We thus find that the relevant ratio is given by

$$\left|\frac{\delta S_{\rm bulk}()}{\delta \mathcal{A}/4l_P^2}\right| \sim \frac{\ell^5 l_P}{r^3 (x^+ - t_\infty)^3}, \tag{5.12}$$

and the quantum effect can indeed compete with the classical contribution when $\partial\Sigma'$ approaches the null surface $x^+ = t_\infty$.[5]

Since the sign of $\delta S_{\rm bulk}()$ from this effect is such that $S_{\rm bulk}()$ gets reduced when $\partial\Sigma'$ is deformed in the $-k$ direction, Θ_k can become positive, making $\partial\Sigma'$ quantum antinormal:

$$\Theta_k > 0, \quad \Theta_l < 0. \tag{5.13}$$

We assume that this transition happens before $\partial\Sigma'$ changes from being classically trapped to normal.[6] This behavior of quantum expansions is depicted in Fig. 5.4.

Forming a Closed Quantum Antinormal Surface

In the previous subsection, we have shown that there is a quantum antinormal surface $\partial\Sigma'$ in the AdS bubble. If there were no other bubbles except for these two bubbles, then this surface would extend infinitely in H_2 and would have an infinite area.

However, this is not the case because the central bubble is surrounded by a multitude of AdS bubbles, as shown in Fig. 5.5. The surface $\partial\Sigma'$ corresponding to a particular AdS bubble is cut off by the domain walls resulting from collisions with the neighboring AdS bubbles. Thus, we are left with a finite portion of $\partial\Sigma'$. Such a finite-sized, quantum antinormal surface can be obtained in each AdS bubble, which we denote by σ_i' $(i = 1, 2, \cdots)$.

These surfaces σ_i' can be connected with appropriate smoothing in such a way that the resulting closed surface encloses the central bubble and is quantum antinormal everywhere. To see this, we note that we have some freedom in choosing the values of (t, r) for each σ_i'.

[5]For supersymmetric bubbles, the numerator becomes $\ell^4 l_P^2$. In this case, we need a more careful analysis to show that $\delta S_{\rm bulk}()$ can compete with $\delta\mathcal{A}/4l_P^2$.

[6]If this assumption does not hold, we still have an island as will be shown later.

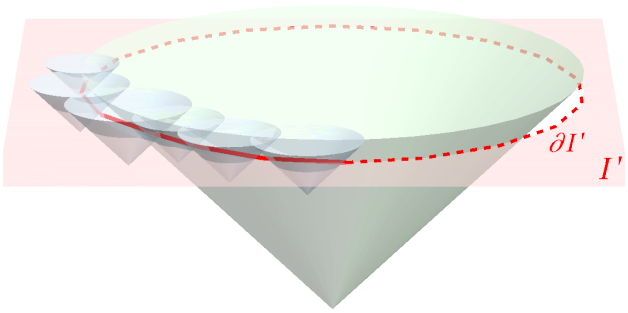

Figure 5.5: A sketch of the construction of closed codimension-2 surface $\partial I'$. The central bubble and some of the surrounding AdS bubbles are depicted as the green and blue cones, respectively. The region I' is defined as a partial Cauchy surface bounded by and outside $\partial I'$.

Using this freedom, we can make two adjacent σ_i''s intersect along a curve. The resulting "kink" can then be smoothed at a length scale smaller than that of bulk entanglement. This smoothing retains quantum antinormalcy, so we end up with a closed, quantum antinormal surface.

We label this closed surface as $\partial I'$, and the partial Cauchy surface bounded by $\partial I'$ and outside it as I'; see Fig. 5.5. Note that $\partial I'$ being quantum antinormal means that $\Theta_k > 0$ and $\Theta_l < 0$, where the quantum expansions are defined using $S_{\text{bulk}}(I' \cup R)$.

Reduction of the Generalized Entropy

We now move on to discuss the generalized entropy. For a sufficiently large R, we expect that the region I' reduces the generalized entropy of R in the sense that[7]

$$S_{\text{gen}}(I' \cup R) < S_{\text{gen}}(R). \tag{5.14}$$

To understand this, we first note that Unruh radiation from the bubble walls of the central and surrounding bubbles, as well as that from the domain walls separating the central and surrounding bubbles, contributes to entanglement between R and I'. Appending I' to R therefore reduces the $S_{\text{bulk}}()$ contribution to $S_{\text{gen}}()$.

To illustrate this, let us take R to be a spherically symmetric region in the central bubble. We assume that the distribution of AdS bubbles surrounding and colliding with the central bubble is statistically spherically symmetric. We then append I' to R and compare the decrease in $S_{\text{gen}}()$ due to the change of $S_{\text{bulk}}()$ with the increase in $S_{\text{gen}}()$ coming from $\mathcal{A}(\partial I')$.

[7]This implies that I' violates the Bekenstein bound [214, 215].

We do this comparison by focusing on an infinitesimal solid angle $\mathrm{d}\Omega_{\mathrm{S}}$ in the central bubble. Using Eq. (5.3), we can estimate the differential change in $S_{\mathrm{gen}}()$ due to Unruh radiation from the central bubble wall to be

$$\begin{aligned}\mathrm{d}S_{\mathrm{bulk}}() &\equiv \left[S_{\mathrm{bulk}}(I' \cup R) - S_{\mathrm{bulk}}(R)\right] \frac{\mathrm{d}\Omega_{\mathrm{S}}}{4\pi} \\ &\sim -\frac{1}{32\pi^3} \sinh\left(2\sqrt{-\kappa}\chi_*\right) \mathrm{d}\Omega_{\mathrm{S}}, \end{aligned} \tag{5.15}$$

where χ_* is the coordinate radius of R in the hyperbolic version of the FRW metric. Here, we have used the fact that the global state is pure, so that $S_{\mathrm{bulk}}(I' \cup R) = S_{\mathrm{bulk}}(\overline{I' \cup R})$. Moreover, we have assumed that $S_{\mathrm{bulk}}(\overline{I' \cup R})$ is sufficiently smaller than $S_{\mathrm{bulk}}(R)$ and have taken $\sqrt{-\kappa}\chi_* \gg 1$. These conditions can be satisfied if the bubble nucleation rates in the parent bubble are small, so that the collisions with AdS bubbles occur at large FRW radii in the central bubble.

The corresponding area element of $\partial I'$ is given by

$$\mathrm{d}\mathcal{A} \equiv \mathcal{A}(\partial I')\big|_{\mathrm{d}\Omega_{\mathrm{H}}} = r_{\sigma_i'}^2 \mathrm{d}\Omega_{\mathrm{H}}, \tag{5.16}$$

where $r_{\sigma_i'}$ is the location of σ_i' in coordinate r defined by Eq. (5.5), and $\mathrm{d}\Omega_{\mathrm{H}}$ is the hyperbolic solid angle. By matching the area element of the domain wall expressed in hyperbolic and FRW coordinates on the side of the central bubble, we find $\mathrm{d}\Omega_{\mathrm{S}} \sim \mathrm{d}\Omega_{\mathrm{H}}$. This leads to

$$\left|\frac{\mathrm{d}S_{\mathrm{bulk}}()}{\mathrm{d}\mathcal{A}/4l_P^2}\right| \sim \frac{l_P^2}{16\pi^3 r_{\sigma_i'}^2} e^{2\sqrt{-\kappa}\chi_*}. \tag{5.17}$$

(To do this properly, we need to regulate the solid angle Ω_{AdS} which an AdS bubble asymptotically occupies and take $\mathrm{d}\Omega_{\mathrm{S}}$ sufficiently small so that this area element fits within the corresponding domain wall. We can then take the limit $\Omega_{\mathrm{AdS}}, \mathrm{d}\Omega_{\mathrm{S}} \to 0$ afterward.)

The radius $r_{\sigma_i'}$ is microscopic and is controlled by l_P and ℓ_i, where ℓ_i is the AdS radius in the bubble in which σ_i' resides. When a surface $\partial\Sigma'$ is moved from an AdS bubble to the central bubble, the radius r grows and becomes macroscopic. However, this transition occurs mostly in the region where $\partial\Sigma'$ is classically normal, and since σ_i' resides on the AdS side of it, $r_{\sigma_i'}$ is small. In particular, from Eq. (5.12) we expect that $r_{\sigma_i'} \sim O(\ell_i)$.[8]

Therefore, we find that for a sufficiently large region R satisfying

$$\sqrt{-\kappa}\chi_* \gtrsim \log\left(\frac{4\pi^2 \mathrm{max}_i(r_{\sigma_i'})}{l_P}\right), \tag{5.18}$$

appending I' to R reduces $S_{\mathrm{gen}}()$, so Eq. (5.14) holds in this case.

[8]For supersymmetric bubbles, we must take $r_{\sigma_i'} \sim O(\ell_i^2/l_P)$.

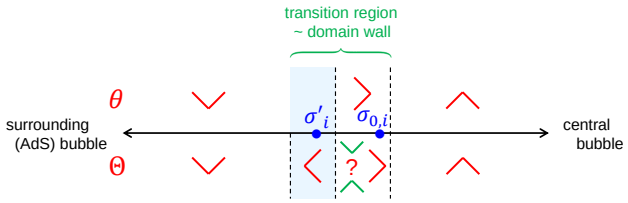

Figure 5.6: Variations of classical and quantum expansions, θ and Θ, when a two-dimensional surface $\partial\Sigma$ extending in the direction of hyperboloid H_2 is moved between the surrounding AdS and central bubbles. A finite area surface σ'_i ($\subset \partial\Sigma'$), which constitutes a portion of $\partial I'$, is taken in the regime where the surface is quantum antinormal. A surface $\sigma_{0,i}$ ($\subset \partial\Sigma_0$) which gives ∂I_0 after smoothing is in the quantum normal region.

Existence of a Quantum Extremal Surface

The existence of a surface $\partial I'$ satisfying Eqs. (5.13) and (5.14) is not sufficient to ensure that of a non-empty island I for R. The existence of an island, however, is ensured [212] if there is a partial Cauchy surface I_0 that (i) is spacelike separated from R, (ii) has the boundary ∂I_0 that is quantum normal with respect to $S_{\rm gen}(I_0 \cup R)$, and (iii) encloses I' in the sense that $I' \subset D(I_0)$.

To argue for the existence of such I_0, let us consider a codimension-2 surface $\partial\Sigma_0$ similar to $\partial\Sigma'$. Such a surface is specified by the coordinates (t, r) in Eq. (5.5). The analysis above then tells us that when $\partial\Sigma_0$ is moved from the near singularity region to the central bubble, it changes from being quantum trapped to quantum antinormal (as viewed from the side opposite to the central bubble, which we denote by Σ_0). This occurs before the classical expansions become normal. As we move the surface further, we expect that the quantum effect becomes subdominant at some point, making the signs of quantum expansions the same as those of classical expansions. In Fig. 5.6, we depict possible behaviors of quantum expansions in this region by green Bousso wedges which are consistent with the quantum focusing conjecture [73]. We can thus take $\partial\Sigma_0$ in the quantum normal region to construct the surface ∂I_0.

Like $\partial\Sigma'$, the surface $\partial\Sigma_0$ is truncated by AdS-AdS domain walls and becomes a finite surface σ_0. As earlier, we form a closed surface using these truncated surfaces $\sigma_{0,i}$ ($i = 1, 2, \cdots$) from each surrounding AdS bubble. By using the freedom of locating each surface, these pieces can be sewn together to form a closed surface enclosing the central bubble.

The resulting surface, however, has folds at the junctions between AdS bubbles, with angles opposite to those required for quantum normalcy. Nevertheless, the effect of these angles is suppressed by $O(\ell_i/r)$ compared to that of the expansions of $\sigma_{0,i}$'s in the interior of the AdS bubbles. Therefore, by locating $\sigma_{0,i}$'s at large r, we can smooth out the folds to form a closed surface that is classically normal and hence quantum normal.

This surface can play the role of ∂I_0:

$$\bigcup_i \sigma_{0,i} \xrightarrow[\text{smoothing}]{} \partial I_0, \tag{5.19}$$

where we define I_0 as a partial Cauchy surface bounded by and outside ∂I_0. It is easy to see that the smoothing can be done such that the resulting I_0 is spacelike separated from R and $I' \subset D(I_0)$. This guarantees the existence of an island for R.

We note that the existence of I_0 is sufficient by itself to ensure the existence of an island if R is very large, satisfying Eq. (5.18) with $\max_i(r_{\sigma_i'})$ replaced with the radius of I_0. Our argument involving I', however, indicates that the island exists for much smaller R.

Inverted Island and Entanglement Castle

Given that the collisions between the central and surrounding bubbles play an essential role in the existence of I' and I_0, we expect that ∂I is located in the region near the corresponding domain walls. In fact, it is reasonable to expect that the two possibilities for quantum expansions depicted in Fig. 5.6 are both realized, depending on the path along which a codimension-2 surface $\partial\Sigma$ is moved. The edge of island ∂I would then lie at the point where trajectories of $\partial\Sigma$ bifurcate to behave in these two different ways. The structure of the Bousso wedges around this location is indeed consistent with ∂I being a quantum maximin surface [59, 87].

Strictly speaking, this only implies that the surface ∂I is a QES. In order for this surface to be the boundary of an island, it must be the minimal QES. We assume that this is the case, which is true if R has only one nontrivial QES with $S_{\text{gen}}(I \cup R) < S_{\text{gen}}(R)$.

Since the topology of I is the same as that of I' or I_0, the island I for region R is an inverted island, and hence does not geographically look like an island. Let Ξ be a Cauchy surface containing R and $I_\Xi = D(I) \cap \Xi$ the section of the inverted island on this surface. Given the geography, we may refer to the region $\overline{I_\Xi}$, complement of I_Ξ on Ξ, as an entanglement lake. However, R occupies a significant portion of $\overline{I_\Xi}$, so (regarding R as a land as other authors do) the region $\overline{R \cup I_\Xi}$ which corresponds to water is more like a moat; see Fig. 5.1. In this sense, the region $\overline{I_\Xi}$ in the present context may be called an entanglement castle.

5.5 Cosmological Evolution

Consider a Cauchy surface Ξ in the global spacetime. The existence of a non-empty island I for a subregion R of Ξ implies that the information about the semiclassical state in $I_\Xi = D(I) \cap \Xi$ is encoded in the fundamental degrees of freedom associated with R. Therefore, physics at the semiclassical level can be fully described by the fundamental degrees of freedom associated with the partial Cauchy surface $\overline{I_\Xi} = \Xi \setminus I_\Xi$.

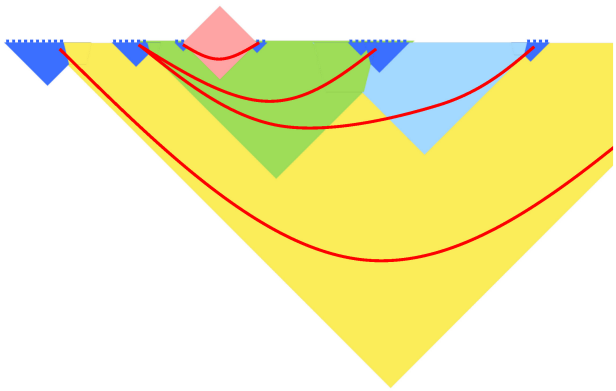

Figure 5.7: Several effective Cauchy surfaces for a given geometry are depicted by red lines. A microstate of the fundamental degrees of freedom on an effective Cauchy surface can describe the full semiclassical physics of the multiverse.

In the eternally inflating multiverse, an inverted island I appears for sufficiently large R. This implies that the semiclassical physics of the multiverse, which is all that we need to make cosmological predictions, is described by the fundamental degrees of freedom in a finite volume portion of a Cauchy slice that involves R. We call such a surface an effective Cauchy surface.

Here we make two general comments about effective Cauchy surfaces. First, the location of the island $D(I)$, or ∂I, depends on the Cauchy surface. For example, since R is spacelike separated from I, a Cauchy surface describing the state of the parent bubble cannot have ∂I around the central bubble as seen in the previous section. However, in this case there exists a region $R_{\rm p}$ in the parent bubble such that an island $I_{\rm p}$ appears around the parent bubble, so that the effective Cauchy surface is given by $\Xi \setminus (D(I_{\rm p}) \cap \Xi)$. In general, when we consider a Cauchy surface describing the state of an earlier bubble, the relevant island appears around that bubble.

Second, when two or more (non-surrounding) bubbles collide, we may want to consider Cauchy surfaces spanning all of these bubbles to describe the collision. In this case, we can choose a region $R_{\rm c}$ spanning the colliding bubbles such that the island $I_{\rm c}$ encloses all the colliding bubbles. This allows us to describe the bubble collision directly without relying on reconstruction from microscopic information in the fundamental degrees of freedom in R.

A sketch of the global multiverse illustrating the above points is given in Fig. 5.7, where possible effective Cauchy surfaces are depicted by red lines. For a given gauge choice, the state on an effective Cauchy surface Υ_1 can uniquely determine the state on an effective Cauchy surface Υ_2 that is in the future domain of dependence of Υ_1. In general, the final state of this time evolution is given by a superposition of states in different geometries $\mathcal{M}_i$:

$$|\Psi(\Upsilon_1)\rangle \xrightarrow[\text{evolution}]{\text{time}} \sum_{i\in\text{geometries}} c_i |\Psi(\Upsilon_{2,i})\rangle_{\mathcal{M}_i}. \tag{5.20}$$

Here, all $\mathcal{M}_i$'s share the surface Υ_1 and the state on it, and $\Upsilon_{2,i}$ is an effective Cauchy surface on the geometry $\mathcal{M}_i$ which is in the future domain of dependence of Υ_1.

It is worth noting that the evolution equation in Eq. (5.20) takes the form that once the knowledge of the current state, $|\Psi(\Upsilon_1)\rangle$, is given, we can predict its future, more precisely what an observer who is a part of the state can in principle see in their future. Note that the equation does not allow us to infer from $|\Psi(\Upsilon_1)\rangle$ the global state of the multiverse in the past. This structure is the same as time evolution of states in the Schrödinger picture of quantum mechanics.

Our approach solves the measure problem in the sense described above: once we are given the initial state on an effective Cauchy surface, we can in principle predict any future observations. The existence of the inverted island implies that the necessary information for this prediction, i.e. the physics of matter excitations over semiclassical spacetimes, is fully encoded in the microstate of the fundamental degrees of freedom associated with the effective Cauchy surface. As discussed in [100] for a dS spacetime, this information is expected to be encoded in quantum correlations between the matter and Unruh radiation degrees of freedom.

5.6 Discussion

We have shown that a Cauchy surface Ξ in an eternally inflating multiverse has an entanglement island for a sufficiently large subregion $R \subset \Xi$. The island I_Ξ on Ξ is, in fact, an inverted island surrounding the region R, implying that the semiclassical physics of the multiverse is fully described by the fundamental degrees of freedom associated with the finite region $\overline{I_\Xi}$, the complement of I_Ξ on Ξ. This provides a regularization of infinities which caused the cosmological measure problem.

As in the case of a black hole, the emergence of an island is related to the existence of a singularity in the global spacetime; in the multiverse, this role is played by the big crunch singularities in the collapsing AdS bubbles. This picture is consistent with the interpretation of singularities in [99, 100, 157]: their existence signals that a portion of the global spacetime is intrinsically semiclassical, arising only as an effective description of more fundamental degrees of freedom associated with other spacetime regions.

Our results strongly suggests the existence of a description of the multiverse on finite spatial regions. Proposals for such descriptions include [182, 183, 184] and [166, 168, 51] in which the fundamental degrees of freedom are associated with the spatial infinity of an asymptotic Minkowski bubble and the (stretched) cosmological horizon, respectively. It would be interesting to explore precise relations between these holographic descriptions and the description based on the global spacetime presented in this chapter.

Chapter 6

The Effect of Graybody Factors on Entanglement Islands

6.1 Introduction

Entanglement entropy for 2d free fermions

Entanglement entropy is an important quantity not just for finite or discrete quantum systems [216] but also for continuum quantum field theories and holography [217, 218]. In the continuum setting, however, entanglement entropies are notoriously hard to calculate and only few exact results exist. Lucky exceptions are provided by 2d conformal field theories [145] and the 2d free fermion [219, 220]. The 2d free fermion system is a particularly fruitful playground since not only the entanglement entropy, but exact expressions for the modular Hamilotonian of multicomponent regions can be computed [220, 221, 222]. In particular, the recent papers [221, 222] considered entanglement entropy and modular Hamiltonians for the 2d free fermion in the presence of a boundary or defect. In [222], the intervals that were considered were symmetric about a semitransparent defect that separates 2d flat space into two half-spaces.

We extend this repertoire of results by computing the entanglement entropy of 2d free fermions in the presence of a semitransparent defect, but allowing for the region under consideration to be asymmetric about the defect. Let (x^0, x^1) be flat coordinates on 2d Minkowski space, and let the defect be located at $x^1 = 0$. The t be the transmission coefficient through the defect, and let $r = 1 - t$ be the reflection coefficient. Let us focus on a single interval $[-L_-, L_+]$ that straddles the defect (and so L_- and L_+ are both positive real numbers). We are not able to compute the entanglement entropy of this interval in general, but we obtain results in three limits:

- When the defect is almost completely transmitting, so that r is small
- When the defect is almost completely reflecting, so that t is small

- When the interval is almost symmetric about the defect, so that $\gamma = \frac{L_- - L_+}{L_- + L_+}$ is small.

These results are presented in Sec. 6.3. In order to obtain these results, we have used the method of [219] and used the results in [223, 224, 225] for free fermion determinants in the presence of a boundary with non-translation invariant boundary conditions. This method can be used to obtain the entropies of any region, and most of our formal setup carries over to the more general case, but we focus on the particular application at hand to obtain explicit results.

Intuitively, the entropy should increase monotonically with the transmission coefficient t since the defect acts as a coupling between left and right, and hence the increasing coupling increases the entanglement entropy. Our results (6.109), (6.126) and (6.120) are consistent with this intuitive behavior.

Earlier results on von Neumann entropy in the presence of interfaces include [226, 227, 228]. See Sec. 3.2.1 of the review [145] for pointers to a few more results. See, for example, [136] for a study of the boundary entropy in holography.

Entanglement islands and graybody factors of black holes

Recent progress in the black hole information paradox has involved the semiclassical computation of the von Neumann entropy of Hawking radiation, reproducing the Page curve [16, 17]. The main player is the existence of a nontrivial Quantum Extremal Surface (QES) [13] at times larger than the Page time, whose generalized entropy tracks the shrinking area of the black hole horizon. The entanglement wedge of the Hawking radiation after the Page time contains a disconnected region deep in the gravitating spacetime, dubbed the entanglement island in [88].

Reference [229] exhibited the presence of entanglement islands in much simpler contexts that also play a role in avoiding an entropy paradox that exists in the eternal Schwarzschild geometry, due to Mathur [230]. By now, the presence of entanglement islands is well established in a wide variety of settings [231, 212, 98, 179, 181, 176, 97, 237, 238, 232, 233, 115, 117, 118, 113, 234, 235, 236, 21]. It has also been established that the nontrivial QES arises because spacetime wormholes dominate the computations of Rényi entropies [89, 90]. See the recent reviews [151, 153] for more on the black hole information problem and an overview of recent progress.

It is well-known that there are graybody factors in Hawking radiation [239]. It is hard to include graybody factors in the computations of the von Neumann entropy of bulk matter fields, and thus in the setups of [17, 229], which couple a flat space bath to AdS space, the interface is taken to be fully transparent. This is rightly so, since graybody factors are not expected to affect the qualitative features of the Page curve. Ref. [16] contained a qualitative discussion of graybody factors. The effect of graybody factors is also implicitly included in the higer-dimensional doubly-holographic setup of [231]. However, one would like to be more computationally explicit about graybody factors.

We take up this challenge in this chapter in what is perhaps the simplest example of an entanglement island: the static zero temperature setup in Sec. 2 of [229]. It was shown that when a zero-temperature AdS_2 black hole is coupled to flat, non-gravitating half-space via a fully transparent boundary, the QES of the boundary of AdS_2 does not lie at the Poincaré horizon, but lies at a finite value of the Poincaré radial coordinate. In other words, the entanglement wedge of the flat space region contains an entanglement island: the region between the Poincaré horizon and the QES.

In this work, instead of taking the AdS_2-flat space interface to be fully transparent, we take it to have a transmission coefficient t and a reflection coefficient $r = 1 - t$. This is a toy model for graybody effects in the atmosphere of a black hole. In the fully transparent case, reference [229] found a nontrivial QES and an entanglement wedge. In the fully reflecting case, the QES is at the Poincaré horizon: this is easy to see, since the AdS_2 and flat space regions are not coupled at all in this case, the entanglement wedge of the boundary of AdS_2 better be the entire Poincaré patch of AdS_2.

We take the bulk matter to be 2d free fermions, and use our results (6.109), (6.126) and (6.120) for the entanglement entropy of free fermions in the presence of a defect to see how the QES moves as we vary the reflection coefficient. What we find is that if we perturb away from fully transmitting case, the QES moves towards the Poincaré horizon from its location in [229]. If we perturb away from the fully reflecting case, the QES moves from the Poincaré horizon towards the boundary of AdS_2.

In brief, our results support the hypothesis that the location of QES behaves monotonically and smoothly interpolates between its locations at $t = 1$ (the fully transmitting case) and $t = 0$ (the fully reflecting case).

As future work, it would be interesting to extend our results to the islands in the eternal Schwarzschild geometry at finite temperature [229] and also the evaporating case [16, 17]. We suspect that the location of the QES behaves monotonically with the strength of graybody effects in all these cases.

Overview

In Secs. 6.2 and 6.3, we outline the computation of the entanglement entropy of free fermions in the presence of a semitransparent interface and present the results. In Sec. 6.4, we recap the zero temperature entanglement island of [229] and show that the entanglement island behaves monotonically with the strength of graybody effects.

6.2 Entanglement Entropy of Free Fermions with a Semitransparent Interface

The 2d massless Dirac fermion is a simple theory where one can explicitly compute not just the entanglement entropies of a region consisting of multiple intervals, but also the associated modular hamiltonians [219, 220, 222, 221].

To study the entanglement problem in the presence of a defect, we take the fermions to live on the line, with the defect placed at $x_1 = 0$. We denote the region $x^1 > 0$ by Ω^+ and the region $x^1 < 0$ by Ω^-. Fields living in the respective half-planes will carry a $+$ or $-$ superscript. The defect is only partially transparent, with a transmission coefficient t. We will be more precise in specifying the boundary conditions below.

We take the γ-matrices to be in the Weyl basis,

$$\gamma^0_{\text{Lor}} = \begin{pmatrix} 0 & -\mathrm{i} \\ -\mathrm{i} & 0 \end{pmatrix}, \quad \gamma^1 = \begin{pmatrix} 0 & \mathrm{i} \\ -\mathrm{i} & 0 \end{pmatrix}, \quad \gamma_* = \gamma^0_{\text{Lor}}\gamma^1 = \begin{pmatrix} -1 & 0 \\ 0 & 1 \end{pmatrix}. \tag{6.1}$$

Here γ_* denotes the chirality matrix and it is diagonal in the Weyl basis. The Dirac operator is

$$\mathrm{i}\gamma^\mu_{\text{Lor}}\partial_\mu = \begin{pmatrix} 0 & \partial_0 - \partial_1 \\ \partial_0 + \partial_1 & 0 \end{pmatrix}. \tag{6.2}$$

The two-component fermions are taken to have components

$$\psi = \begin{pmatrix} \psi_R \\ \psi_L \end{pmatrix}. \tag{6.3}$$

The equation of motion says that ψ_L is only a function of $x^0 + x^1$, which represents a left-moving wave, hence the subscript L for ψ_L; a similar logic applies for ψ_R.

From now on, we work in Euclidean signature using the convention $x_2 = \mathrm{i}x^0$. The ordering of the Euclidean coordinates will be (x_1, x_2). For future use, we also note that

$$\gamma^2 = \mathrm{i}\gamma^0_{\text{Lor}} = \begin{pmatrix} 0 & 1 \\ 1 & 0 \end{pmatrix}. \tag{6.4}$$

The boundary condition imposed at the defect is

$$\begin{pmatrix} \psi^+_R(0, x_2) \\ \psi^-_L(0, x_2) \end{pmatrix} = \mathcal{S} \begin{pmatrix} \psi^+_L(0, x_2) \\ \psi^-_R(0, x_2) \end{pmatrix}, \tag{6.5}$$

where $\mathcal{S}$ is the unitary scattering matrix

$$\mathcal{S} = \begin{pmatrix} c_1 & c_2 \\ c_3 & c_4 \end{pmatrix} = \begin{pmatrix} c_1 & -e^{\mathrm{i}\phi}c_3^* \\ c_3 & e^{\mathrm{i}\phi}c_1^* \end{pmatrix}. \tag{6.6}$$

These boundary conditions are energy conserving, and preserve one copy of Virasoro algebra after folding the plane along the defect. As can be seen in figure 6.1, the modes ψ^+_R and ψ^-_L are outgoing from the defect, whereas ψ^+_L and ψ^-_R are incoming. The quantity $t = |c_2|^2 = |c_3|^2$ is interpreted as a transmission coefficient, while $r = 1 - t = |c_1|^2 = |c_4|^2$ is interpreted as a reflection coefficient. The purely transmitting and the purely reflecting $\mathcal{S}$ matrices are

$$\mathcal{S}^{\text{t}} = \begin{pmatrix} 0 & 1 \\ 1 & 0 \end{pmatrix}, \quad \mathcal{S}^{\text{r}} = \begin{pmatrix} 1 & 0 \\ 0 & 1 \end{pmatrix}. \tag{6.7}$$

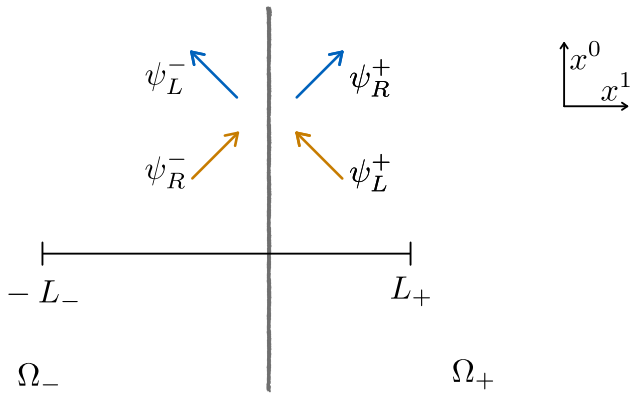

Figure 6.1: Setup for the fermion problem with a semitransparent interface.

It will be helpful to rewrite the boundary condition (6.5) as

$$\mathcal{B}\psi(0,x_2)=0, \tag{6.8}$$

where

$$\mathcal{B}=\begin{pmatrix} 1 & -c_1 & -c_2 & 0 \\ -c_1^* & 1 & 0 & -c_3^* \\ -c_2^* & 0 & 1 & -c_4^* \\ 0 & -c_3 & -c_4 & 1 \end{pmatrix}, \qquad \psi(0,x_2)=\begin{pmatrix} \psi_R^+(0,x_2) \\ \psi_L^+(0,x_2) \\ \psi_R^-(0,x_2) \\ \psi_L^-(0,x_2) \end{pmatrix}. \tag{6.9}$$

Note that $\mathcal{B}$ is a Hermitian matrix with rank two.

We consider the fermions to be in their ground state and focus on the reduced density matrix $\rho_{\mathcal{A}}$ of a given subset $\mathcal{A}\subset\mathbb{R}$. We specify $\mathcal{A}$ as a collection of disjoint intervals $[u_i,v_i]$ with $i\in\{1,\dots,p\}$. We will mostly be interested in the case of a single interval $[-L_-,L_+]$ that straddles the defect (both L_- and L_+ are positive real numbers). See figure 6.1 for the setup. We intend to compute the entanglement entropy $S(\mathcal{A})$ given by

$$S(\mathcal{A})=-\operatorname{Tr}(\rho_{\mathcal{A}}\log\rho_{\mathcal{A}})=\lim_{n\to1}S_n(\mathcal{A}), \tag{6.10}$$

where $S_n(\mathcal{A})$ is the Rényi entropy,

$$S_n(\mathcal{A})=\frac{1}{1-n}\log\operatorname{Tr}\left(\rho_{\mathcal{A}}^n\right). \tag{6.11}$$

Decoupling the replicas with gauge fields

We use the replica trick to compute $\operatorname{Tr}\left(\rho_{\mathcal{A}}^n\right)$. Our treatment closely follows [219]. The trace of $\rho_{\mathcal{A}}^n$ is given by the functional integral $Z[n]$ on the replica manifold,

$$\operatorname{Tr}\rho_{\mathcal{A}}^n=\frac{Z[n]}{Z[1]^n}, \tag{6.12}$$

where $Z[1]$ serves as a normalization factor that sets $\mathrm{Tr}\,\rho_{\mathcal{A}} = 1$.

When evaluating this trace for a fermionic field, we need to introduce a minus sign in the path integral boundary condition connecting the fields between the first and last replica copies [240]. Moreover, there is an additional factor of -1 for every copy because of non-trivial Lorentz rotation around the points u_i and v_i which is present in the Euclidean Hamiltonian when expressing $\mathrm{Tr}\,\rho_{\mathcal{A}}^n$ as a path integral [241]. Thus, we get an overall factor of $(-1)^{n+1}$ when connecting the fields along the first and last cuts.

Instead of dealing with the fields on the non-trivial replica manifold, we can work on a single plane by using the n-component field

$$\vec{\psi} = \begin{pmatrix} \psi_1(\mathbf{x}) \\ \vdots \\ \psi_n(\mathbf{x}) \end{pmatrix}, \tag{6.13}$$

where ψ_j is the fermion field on the j^{th} sheet of the replica manifold. The vector $\vec{\psi}$ is not single valued: If we go in a circuit around u_i, the vector $\vec{\psi}$ gets multiplied by the matrix

$$T = \begin{pmatrix} 0 & 1 & 0 & \cdots & 0 & 0 \\ 0 & 0 & 1 & \cdots & 0 & 0 \\ \vdots & \vdots & \vdots & \ddots & \vdots & \vdots \\ 0 & 0 & 0 & \cdots & 0 & 1 \\ (-1)^{n+1} & 0 & 0 & \cdots & 0 & 0 \end{pmatrix}, \tag{6.14}$$

whereas if we go in a circuit around v_i, it gets multiplied by T^{-1}.

We can diagonalize T by performing a unitary transformation. Note that the eigenvalues of T are $e^{2\pi \mathrm{i} k/n}$ with $k \in \{-\frac{n-1}{2}, -\frac{n-1}{2}+1, \ldots, \frac{n-1}{2}\}$. After this unitary transformation we end up with the decoupled fields ψ_k living on a single plane. The fields ψ_k are multivalued and get multiplied by $e^{2\pi \mathrm{i} k/n}$ when encircling u_i, and by $e^{-2\pi \mathrm{i} k/n}$ when encircling v_i. Note that this unitary transformation acts identically on the components of $\vec{\psi}$, so the boundary condition for ψ_k is still

$$\mathcal{B}\psi_k(0, x_2) = 0. \tag{6.15}$$

We can get rid of the multivaluedness of ψ_k by introducing an external gauge field $A_{k,\mu}(\mathbf{x})$. The gauge field is vortex-like near the end-points of the intervals:

$$\oint_{u_i} A_k = -\frac{2\pi k}{n}, \quad \oint_{v_i} A_k = \frac{2\pi k}{n}, \tag{6.16}$$

where the integrals are over closed contours encircling u_i or v_i. These holonomies are captured by the field strength

$$F_{k,12}(\mathbf{x}) = -\frac{2\pi k}{n} \sum_{i=1}^{p} \left(\delta^{(2)}(\mathbf{x} - \mathbf{u}_i) - \delta^{(2)}(\mathbf{x} - \mathbf{v}_i) \right). \tag{6.17}$$

where $\mathbf{u}_i = (u_i, 0)$ and $\mathbf{v}_i = (v_i, 0)$. Requiring that A_k^μ vanishes at infinity, we get the explicit formula

$$A_{k,\mu}(\mathbf{x}) = \frac{k}{n}\,\epsilon_{\mu\nu}\sum_{i=1}^{p}\left(\frac{(\mathbf{x}-\mathbf{u}_i)^\nu}{|\mathbf{x}-\mathbf{u}_i|^2} - \frac{(\mathbf{x}-\mathbf{v}_i)^\nu}{|\mathbf{x}-\mathbf{v}_i|^2}\right), \tag{6.18}$$

where we use the standard $\epsilon_{12} = -\epsilon_{21} = 1$.

In presence of the gauge field, the fermion action is

$$I_k[\psi_k, \overline{\psi}_k; A_k] = \int_{\Omega^+} \mathrm{d}^2x\, \overline{\psi}_k^+ \gamma^\mu \left(\partial_\mu + \mathrm{i}A_{k,\mu}\right)\psi_k^+ + \int_{\Omega^-} \mathrm{d}^2x\, \overline{\psi}_k^- \gamma^\mu \left(\partial_\mu + \mathrm{i}A_{k,\mu}\right)\psi_k^-. \tag{6.19}$$

The functional integral factorizes into

$$Z[n] = \prod_{k=-(n-1)/2}^{(n-1)/2} Z_k, \tag{6.20}$$

where Z_k is the functional integral over $\{\psi_k, \overline{\psi}_k\}$ with the background gauge field A_k given by (6.18) and with boundary conditions (6.15); the matrix $\mathcal{B}$ is given in (6.9).

Computing the functional integral Z_k

In this subsection, we outline the calculation of the functional integral

$$Z_k = \int D\overline{\psi}_k^{\pm} D\psi_k^{\pm} \exp\left(-\int_{\Omega^+} \mathrm{d}^2x\, \overline{\psi}_k^+ \left(\partial\!\!\!/ + \mathrm{i}A\!\!\!/_k\right)\psi_k^+ - \int_{\Omega^-} \mathrm{d}^2x\, \overline{\psi}_k^- \left(\partial\!\!\!/ + \mathrm{i}A\!\!\!/_k\right)\psi_k^-\right), \tag{6.21}$$

with the background gauge field A_k given by (6.18) and with boundary conditions (6.15); the matrix $\mathcal{B}$ is given in (6.9). An essential fact is that the chiral anomaly in two dimensions completely determines the dependence of the functional integral on the gauge field [242].[1]

A general gauge field in two dimensions can be expressed as a sum of a gradient and a curl

$$A_{k,\mu} = \partial_\mu \eta_k - \epsilon_{\mu\nu}\,\partial_\nu \Phi_k. \tag{6.22}$$

For the gauge field profile in (6.18), we can choose

$$\eta_k(\mathbf{x}) = 0, \quad \Phi_k(\mathbf{x}) = -\frac{k}{n}\sum_{i=1}^{p} \log\frac{|\mathbf{x}-\mathbf{u}_i|}{|\mathbf{x}-\mathbf{v}_i|}. \tag{6.23}$$

Note that $\Phi_k \sim \frac{1}{|\mathbf{x}|}$ as $|\mathbf{x}| \to \infty$.[2] Given a background gauge field of the form (6.22), we can decouple the fermions ψ_k^+ from the background gauge field A_k by a change of variables which is a combination of gauge and chiral transformations

$$\psi_k^+ = \exp\left(\mathrm{i}\eta_k + \gamma_* \Phi_k\right)\chi_k^+. \tag{6.24}$$

[1] An equivalent method is to bosonize the fermions.

[2] This decomposition of the gauge field as the sum of a gradient and a curl is not unique. In the purely reflecting case, we use a different decomposition which allows us to easily calculate the results in the purely reflecting case.

Essentially, we are changing variables from ψ_k^+ to χ_k^+ in the functional integral. The change in the fermionic measure under this transformation is nontrivial

$$D\overline{\psi}_k^+ D\psi_k^+ = J_k^+ \, D\overline{\chi}_k^+ D\chi_k^+, \tag{6.25}$$

where J_k^+ is the Jacobian of the transformation. For fermions living on the full line, the result for this Jacobian is well-known [242]. In case of manifolds with boundaries, we need to be careful about possible boundary contributions.

To separate the bulk and boundary contributions, we divide the positive real line into two intervals $(0, \epsilon^+)$ and (ϵ^+, ∞). For the interval (ϵ^+, ∞), we can obtain the bulk contribution using the result for closed manifolds [242],

$$\left(J_k^+\right)_{\text{bulk}} = \exp\left(-\frac{1}{2\pi}\int_{\Omega^+(\epsilon^+)} \mathrm{d}^2x \, \partial_\mu \Phi_k(\mathbf{x}) \partial^\mu \Phi_k(\mathbf{x})\right), \tag{6.26}$$

where $\Omega^+(\epsilon^+) = \{(x_1, x_2) : x_1 > \epsilon^+\}$. The boundary contribution is [225]

$$\left(J_k^+\right)_{\text{bdry}} = \exp\left(-\frac{1}{4\epsilon^+}\int_{\mathbb{R}} \mathrm{d}x_2 \, \Phi_k(0, x_2)\right). \tag{6.27}$$

A similar treatment can be done for the fermions on Ω_- to get the full Jacobian

$$J_k = \exp\left(-\frac{1}{2\pi}\int_{\Omega^+(\epsilon^+)\cup\Omega^-(\epsilon^-)} \mathrm{d}^2x \, \partial_\mu \Phi_k(\mathbf{x}) \partial^\mu \Phi_k(\mathbf{x}) - \left(\frac{1}{4\epsilon^+} + \frac{1}{4\epsilon^-}\right)\int_{\mathbb{R}} \mathrm{d}x_2 \, \Phi_k(0, x_2)\right), \tag{6.28}$$

with $\epsilon^- < 0$. Once we do the sum over k, the boundary terms will vanish (since Φ_k is linear in k) and henceforth they will be omitted.[3] Taking the limit $\epsilon^+, \epsilon^- \to 0$, we get

$$J_k = \exp\left(-\frac{1}{2\pi}\int_{\Omega} \mathrm{d}^2x \, \partial_\mu \Phi_k \, \partial^\mu \Phi_k\right). \tag{6.29}$$

This is the result for the Jacobian on the entire plane in [242].

The integral in (6.29) is easily evaluated by substituting Φ_k from (6.23), integrating by parts once and using the fact that $\nabla^2\Phi$ is a sum of delta functions. The result is

$$J_k = \exp\left(-\frac{2k^2}{n^2}\,\Xi(\{u_i\}, \{v_j\})\right), \tag{6.30}$$

where [219]

$$\Xi(\{u_i\}, \{v_j\}) := \sum_{i,j} \log|u_i - v_j| - \sum_{i<j} \log|u_i - u_j| - \sum_{i<j} \log|v_i - v_j| - p\log\varepsilon. \tag{6.31}$$

[3] We can also choose $\epsilon^+ = -\epsilon^-$, and then this term automatically vanishes.

Here, we have introduced the short-distance cutoff ε to split the coincidence points $|u_i - u_i|$, $|v_i - v_i| \to \varepsilon$, and the sum over i, j is over all the intervals comprising the region $\mathcal{A}$.

So far, we changed variables from ψ_k to χ_k (6.24) in the functional integral and obtained the Jacobian for this transformation. Since the Jacobian (6.30) is independent of χ_k, the functional integral can be expressed as

$$Z_k = J_k \tilde{Z}_k, \tag{6.32}$$

where $\tilde{Z}_k$ is the path integral over χ_k, now without any gauge fields

$$\tilde{Z}_k = \int D\overline{\chi}_k^{\pm} D\chi_k^{\pm} \exp\left(- \int_{\Omega^+} \mathrm{d}^2x \, \overline{\chi}_k^{+} \not{\partial} \chi_k^{+} - \int_{\Omega^-} \mathrm{d}^2x \, \overline{\chi}_k^{-} \not{\partial} \chi_k^{-} \right). \tag{6.33}$$

This integral gives a nontrivial contribution to the partition function (that depends on the interval endpoints u_i and v_i) because of the boundary conditions obeyed by χ_k. Using the definition of χ_k in (6.24) and the boundary condition (6.15) for ψ_k, we see that the boundary condition for χ_k is

$$\mathcal{B} \begin{pmatrix} e^{\gamma_* \Phi_k(0,x_2)} & 0 \\ 0 & e^{\gamma_* \Phi_k(0,x_2)} \end{pmatrix} \boldsymbol{\chi}_k(0, x_2) = 0, \tag{6.34}$$

where we have combined the two-component objects χ_k^+ and χ_k^- into a four component object $\boldsymbol{\chi}_k$ along the lines of the second relation in (6.9). We can rewrite this boundary condition as

$$\mathcal{B} \begin{pmatrix} e^{H_k(x_2)} & 0 & 0 & 0 \\ 0 & 1 & 0 & 0 \\ 0 & 0 & e^{H_k(x_2)} & 0 \\ 0 & 0 & 0 & 1 \end{pmatrix} \boldsymbol{\chi}_k(0, x_2) = 0, \quad \text{with } H_k(x_2) := -2\Phi_k(0, x_2). \tag{6.35}$$

6.3 Computing the Dirac Determinant on the Half-plane

In this section, we will compute the functional integral

$$\tilde{Z} = \int D\overline{\chi}^{\pm} D\chi^{\pm} \exp\left(- \int_{\Omega^+} \mathrm{d}^2x \, \overline{\chi}^{+} \not{\partial} \chi^{+} - \int_{\Omega^-} \mathrm{d}^2x \, \overline{\chi}^{-} \not{\partial} \chi^{-} \right). \tag{6.36}$$

where the fermionic fields satisfy the boundary conditions

$$\mathcal{B}\, e^{\mathcal{H}(x_2)} \, \chi(0, x_2) = 0, \tag{6.37}$$

with the matrices

$$\mathcal{B} = \begin{pmatrix} 1 & -c_1 & -c_2 & 0 \\ -c_1^* & 1 & 0 & -c_3^* \\ -c_2^* & 0 & 1 & -c_4^* \\ 0 & -c_3 & -c_4 & 1 \end{pmatrix}, \quad \mathcal{H}(x_2) = \begin{pmatrix} H(x_2) & 0 & 0 & 0 \\ 0 & 0 & 0 & 0 \\ 0 & 0 & H(x_2) & 0 \\ 0 & 0 & 0 & 0 \end{pmatrix}, \tag{6.38}$$

and the vector χ will be specified shortly. The matrix $\mathcal{B}$ has rank two.

The general computation can be done by using a theorem due to Forman [223], which was also used in [224, 225], in order to relate the fermion determinant with the position-dependent boundary condition (6.35) to the fermion determinant with the much simpler boundary condition $\mathcal{B}\chi_k(0, x_2) = 0$. In the process, one still needs to compute the trace of an infinite matrix, and we have been unable to solve this problem in general. We have however been able to obtain results in the three limits described in the introduction.

Purely Transmitting Case

In the purely transmitting case corresponding to $\mathcal{S}^{\rm t}$ in (6.7), the boundary condition in (6.35) is equivalent to $\mathcal{B}\chi_k(0, x_2) = 0$, so $\tilde{Z}_k = Z[1]$. Thus, the entropies come purely from the Jacobians J_k given in (6.30) [219]. The result for the von Neumann entropy is

$$S(\mathcal{A}) = \frac{1}{3}\,\Xi(\{u_i\}, \{v_j\}), \tag{6.39}$$

where Ξ was defined in (6.31). This is just the result of [219]. For a single interval $[-L_-, L_+]$, the answer has the familiar logarithmic expression dependence,

$$S([-L_-, L_+]) = \frac{1}{3}\log\frac{L_+ + L_-}{\varepsilon}. \tag{6.40}$$

Purely Reflecting Case

In the purely reflecting case corresponding to $\mathcal{S}^{\rm r}$ in (6.7), we can compute the functional integral by using a different decomposition for the gauge field in terms of η_k and Φ_k.

Instead of performing the gauge and chiral transformations given by (6.23), we now perform different transformations on the two half-planes. For later convenience, we take the Φ-functions for the two half-planes to satisfy $\Phi_k^{\pm}(0, y_2) = 0$. It is easy to obtain such a Φ_k using the method of images

$$\Phi_k^+(\mathbf{x}) = -\frac{k}{n}\sum_{i=1}^{p^+}\log\left(\frac{|\mathbf{x}-\mathbf{u}_i^+||\mathbf{x}-\overline{\mathbf{v}_i}^+|}{|\mathbf{x}-\mathbf{v}_i^+||\mathbf{x}-\overline{\mathbf{u}_i}^+|}\right), \tag{6.41}$$

with a similar expression for $\Phi_k^-(\mathbf{x})$. Here, $\mathcal{A}^+ = \bigcup_{i=1}^{p^+}[u_i^+, v_i^+]$ refers to the subset of $\mathcal{A}$ on the positive real axis and $\mathcal{A}^- = \bigcup_{i=1}^{p^-}[u_i^-, v_i^-]$ refers to the subset of $\mathcal{A}$ on the negative real axis. The η-functions can be obtained using (6.18) and (6.22),

$$\eta_k^+(\mathbf{x}) = -\frac{k}{n}\left[\sum_{i=1}^{p^+}\left(\arctan\frac{x_2}{x_1+u_i^+} - \arctan\frac{x_2}{x_1+v_i^+}\right) + \sum_{i=1}^{p^-}\left(\arctan\frac{x_2}{x_1-u_i^-} - \arctan\frac{x_2}{x_1-v_i^-}\right)\right], \tag{6.42}$$

with a similar expression for $\eta_k^-(\mathbf{x})$.

The Jacobian for the transformation (6.24) with this choice of Φ_k and η_k is

$$\log J_k^+ = -\frac{2k^2}{n^2}\,\xi\left(\{u_i^+\},\{v_j^+\}\right), \quad \log J_k^- = -\frac{2k^2}{n^2}\,\xi\left(\{u_i^-\},\{v_j^-\}\right), \tag{6.43}$$

where we have defined

$$\xi\left(\{u_i\},\{v_j\}\right) = \Xi\left(\{u_i\},\{v_j\}\right) - \frac{1}{2}\sum_{i,j}\log\left(\frac{|u_i+v_j||v_i+u_j|}{|u_i+u_j||v_i+v_j|}\right). \tag{6.44}$$

The quantity Ξ was defined in (6.31) [219]. The functional integral thus becomes $Z_k = J_k^+ J_k^- \tilde{\tilde{Z}}_k$, where

$$\tilde{\tilde{Z}}_k = \int D\overline{\zeta}_k^+ D\zeta_k^+ D\overline{\zeta}_k^- D\zeta_k^- \exp\left(-\int_{\Omega^+} \mathrm{d}^2x\,\overline{\zeta}_k^+ \not{\partial}\zeta_k^+ - \int_{\Omega^-} \mathrm{d}^2x\,\overline{\zeta}_k^- \not{\partial}\zeta_k^-\right). \tag{6.45}$$

Since $\Phi_k^\pm(0,x_2) = 0$, the boundary condition for the transformed fermionic field $\zeta_k = \exp(-\mathrm{i}\eta_k - \gamma_*\Phi_k)\psi_k$ is

$$\mathcal{B}\begin{pmatrix} e^{\mathrm{i}\tilde{H}_k(x_2)} & 0 & 0 & 0 \\ 0 & e^{\mathrm{i}\tilde{H}_k(x_2)} & 0 & 0 \\ 0 & 0 & 1 & 0 \\ 0 & 0 & 0 & 1 \end{pmatrix}\zeta_k(0,x_2) = 0, \quad \text{with } \tilde{H}_k(x_2) := \eta_k^+(0,x_2) - \eta_k^-(0,x_2). \tag{6.46}$$

In the purely reflecting case corresponding to $\mathcal{S}^{\mathrm{r}}$ in (6.7), the boundary condition in (6.46) is equivalent to $\mathcal{B}\zeta_k(0,x_2) = 0$, and so so $\tilde{\tilde{Z}}_k = Z[1]$. Thus, the entropy is

$$S(\mathcal{A}) = \frac{1}{3}\xi\left(\{u_i^+\},\{v_j^+\}\right) + \frac{1}{3}\xi\left(\{u_i^-\},\{v_j^-\}\right). \tag{6.47}$$

This expression agrees with the results in [221] and, as expected, breaks up into a sum of two terms that just depend on $\mathcal{A}_+$ and $\mathcal{A}_-$ respectively. For a single interval on one side of the boundary, one can check that the the reflecting answer reduces to the transmitting answer if the interval is far from the boundary.

For the interval $[-L_-, L_+]$, which is our case of interest, the entropy is

$$S([-L_-,L_+]) = \frac{1}{6}\log\frac{2L_-}{\varepsilon} + \frac{1}{6}\log\frac{2L_+}{\varepsilon}. \tag{6.48}$$

Notice that the entropy in the fully reflecting case is a sum of entropies on the left and right side of the defect, since the two half-planes are completely decoupled.

We now turn to our results for the entropy with nonzero reflection and transmission coefficients.

General Computation

Let us begin by folding the left half plane, Ω_-, to the right half-plane, Ω_+. This folding changes the coordinate $\mathbf{x} = (x_1, x_2) \in \Omega_-$ to $\overline{\mathbf{x}} := (-x_1, x_2) \in \Omega_+$, so we have the transformation for derivatives $(\partial_1, \partial_2) \to (\overline{\partial_1}, \overline{\partial_2}) = (-\partial_1, \partial_2)$ and for the fermionic fields $\chi_R^-(\mathbf{x}) \to \chi_L^-(\overline{\mathbf{x}})$, $\chi_L^-(\mathbf{x}) \to \chi_R^-(\overline{\mathbf{x}})$. In this folded geometry, the Dirac operator is $\mathrm{i}\not{\partial} \oplus \mathrm{i}\overline{\not{\partial}}$. In contrast to (6.9), after the folding, the fermion field has components in the following order:

$$\chi = \begin{pmatrix} \chi_R^+ \\ \chi_L^+ \\ \chi_L^- \\ \chi_R^- \end{pmatrix} \tag{6.49}$$

with all fields having a position argument belonging to the right half plane Ω_+.

We also remind the reader that for the application needed in the main text, $H_k(x_2) = -2\Phi_k(0, x_2)$ and $\Phi_k(\mathbf{x})$ is given in (6.23). The main tools needed to compute the partition function are described in references [223, 224, 225].

The fermion path integral (6.36) can be written as the functional determinant $\det(\mathrm{i}\not{\partial} \oplus \mathrm{i}\overline{\not{\partial}})$, subject to the boundary condition (6.37). To compute this determinant we will employ a theorem by Forman [223]. The idea is to consider a one-parameter family of boundary conditions labelled by τ such that $\tau = 0$ corresponds to the boundary condition $\mathcal{B}\chi(0, x_2) = 0$, and $\tau = 1$ corresponds to the boundary condition (6.37) that we are interested in. This gives rise to a family of functional determinants

$$\tilde{Z}(\tau) = \det(\mathrm{i}\not{\partial} \oplus \mathrm{i}\not{\partial})_{\mathcal{B}\mathcal{U}(\tau)}, \quad \mathcal{U}(\tau) := e^{\tau\, \mathcal{H}(x_2)}. \tag{6.50}$$

where the subscript labels the modified boundary condition $\mathcal{B}\mathcal{U}(\tau)\chi = \mathcal{B}e^{\tau \mathcal{H}(x_2)}\chi = 0$. Forman's theorem (theorem 2 of [223], see also [224]) states that[4]

$$\frac{\mathrm{d}}{\mathrm{d}\mu} \log \frac{\tilde{Z}(\tau + \mu)}{\tilde{Z}(\mu)} = \frac{\mathrm{d}}{\mathrm{d}\mu} \log \det \Phi_\mu(\tau). \tag{6.51}$$

We will explain the definition of the operator Φ below.

The Dirac operator $\mathrm{i}\not{\partial} \oplus \mathrm{i}\overline{\not{\partial}}$ is given in the Weyl basis ((6.1) and (6.4)) by

$$\mathrm{i}\not{\partial} \oplus \mathrm{i}\overline{\not{\partial}} = \begin{pmatrix} 0 & -\partial_1 + \mathrm{i}\partial_2 & 0 & 0 \\ \partial_1 + \mathrm{i}\partial_2 & 0 & 0 & 0 \\ 0 & 0 & 0 & \partial_1 + \mathrm{i}\partial_2 \\ 0 & 0 & -\partial_1 + \mathrm{i}\partial_2 & 0 \end{pmatrix}. \tag{6.52}$$

We will denote the elements of the kernel of this operator by χ and we take them to satisfy a fake boundary condition on the far-right side of the half-plane

$$\mathcal{B}\chi(L, x_2) = 0, \tag{6.53}$$

[4]Please note that the operator $\Phi_\mu(\tau)$ has nothing to do with the function $\Phi_k(\mathbf{x})$.

with $L \gg 1$. This boundary condition is arbitrary and is chosen for convenience, following [224]. Notice that we maintain translation symmetry along the line $x_1 = L$ in this fake problem (in contrast to the actual boundary condition (6.37) where the function $H(x_2)$ explicitly depends on x_2). We further compactify x_2 on a large circle of length T, and impose antiperiodic boundary conditions $\chi(x_1, -T/2) = -\chi(x_1, T/2)$. The elements of the kernel of (6.52) satisfying the boundary condition (6.53) and having definite Matsubara frequencies $w_n = (2n+1)\pi/T$ with $n \in \mathbb{Z}$ can be easily found

$$\chi_{An}(x_1, x_2) = \frac{e^{-\mathrm{i}w_n x_2}}{\sqrt{2\cosh(2w_n L)}} \begin{pmatrix} e^{-w_n(x_1-L)} \\ c_1^* e^{w_n(x_1-L)} \\ c_2^* e^{w_n(x_1-L)} \\ 0 \end{pmatrix}, \quad \chi_{Bn}(x_1, x_2) = \frac{e^{-\mathrm{i}w_n x_2}}{\sqrt{2\cosh(2w_n L)}} \begin{pmatrix} 0 \\ c_3^* e^{w_n(x_1-L)} \\ c_4^* e^{w_n(x_1-L)} \\ e^{-w_n(x_1-L)} \end{pmatrix}. \tag{6.54}$$

Note that $\{\chi_{An}, \chi_{Bn}\}$ satisfy the orthonormality condition $\frac{1}{T}\int_{-T/2}^{T/2} \mathrm{d}x_2\, \chi_I^\dagger(0, x_2)\, \chi_J(0, x_2) = \delta_{IJ}$, with $I \in \{A, B\} \times \mathbb{Z}$. The vectors in (6.54) when evaluated on the true boundary $x_1 = 0$ will not satisfy the boundary condition (6.37). Now we ask the question: By how much do $\chi_I(0, x_2)$ fail to satisfy the true boundary condition (6.37)? This will be proportional to $\mathcal{B}\mathcal{U}(\tau)\,\chi_I(0, x_2)$. We now pick a fixed basis of functions on the line $x_1 = 0$ that also satisfy $\mathcal{B}\widetilde{\chi} = 2\widetilde{\chi}$.[5] Explicitly, these are

$$\widetilde{\chi}_{An}(x_2) = \frac{e^{-\mathrm{i}w_n x_2}}{\sqrt{2}} \begin{pmatrix} 1 \\ -c_1^* \\ -c_2^* \\ 0 \end{pmatrix}, \qquad \widetilde{\chi}_{Bn}(x_2) = \frac{e^{-\mathrm{i}w_n x_2}}{\sqrt{2}} \begin{pmatrix} 0 \\ -c_3^* \\ -c_4^* \\ 1 \end{pmatrix}. \tag{6.55}$$

With the two sets of vectors defined in (6.54) and (6.55), the matrix $h(\tau)$ is defined to have matrix elements

$$h_{IJ}(\tau) := \frac{1}{T} \int_{-T/2}^{T/2} \mathrm{d}x_2\, \widetilde{\chi}_I^\dagger(x_2)\, \mathcal{B}\, e^{\tau \mathcal{H}(x_2)}\, \chi_J(0, x_2), \tag{6.56}$$

with $I, J \in \{A, B\} \times \mathbb{Z}$. The intuition is that the matrix h measures the failure of $\chi_J(x_1, x_2)$ to satisfy the correct boundary condition (6.37) for our problem. The quantity $\Phi_\mu(\tau)$ in (6.51) is defined via [223, 224, 225]

$$h(\mu + \tau) = \Phi_\mu(\tau)\, h(\mu)\,. \tag{6.57}$$

Our goal is to calculate $\tilde{Z}$ at $\tau = 1$. Let us take a τ derivative of Forman's result, (6.51),

$$\frac{\mathrm{d}}{\mathrm{d}\mu}\frac{\mathrm{d}}{\mathrm{d}\tau} \log \frac{\tilde{Z}(\mu + \tau)}{\tilde{Z}(\mu)} = \frac{\mathrm{d}}{\mathrm{d}\mu}\frac{\mathrm{d}}{\mathrm{d}\tau} \operatorname{Tr} \log \left(h(\mu + \tau) h^{-1}(\mu) \right). \tag{6.58}$$

[5] Since the vector $\mathcal{B}\mathcal{U}(\tau)\,\chi_I(0, x_2)$ is of the form $\mathcal{B}(\cdot)$, and $\mathcal{B}$ has eigenvalues 0 and 2, it lies in the subspace that has eigenvalue 2 under $\mathcal{B}$. Thus the inner product of $\mathcal{B}\mathcal{U}(\tau)\,\chi_I(0, x_2)$ and $\widetilde{\chi}_J$ measures the amount by which the boundary condition is violated.

On the LHS the τ derivative kills $\log \widetilde{Z}(\mu)$, whereas the RHS can be simplified by using $\frac{\mathrm{d}}{\mathrm{d}\tau} \operatorname{Tr} \log A(\tau) = \operatorname{Tr}(\dot{A}(\tau)\, A^{-1}(\tau))$ and cyclicity of the trace. So (6.58) simplifies to

$$\frac{\mathrm{d}^2}{\mathrm{d}\tau \mathrm{d}\mu} \tilde{Z}(\mu+\tau) = \frac{\mathrm{d}}{\mathrm{d}\mu} \operatorname{Tr}\left(\frac{\mathrm{d}h(\mu+\tau)}{d\tau} h^{-1}(\mu+\tau) \right). \tag{6.59}$$

Notice that the μ derivatives can now be traded for τ derivatives and, after setting $\mu = 0$, we end up with the differential equation

$$\frac{\mathrm{d}^2}{\mathrm{d}\tau^2} \log \tilde{Z}(\tau) = \frac{\mathrm{d}}{\mathrm{d}\tau} \operatorname{Tr}\left(\frac{\mathrm{d}h(\tau)}{\mathrm{d}\tau} h(\tau)^{-1} \right). \tag{6.60}$$

To solve for $\tilde{Z}(\tau)$, we integrate this twice and hence we need the value of $\tilde{Z}'(\tau = 0)$. We claim that $\tilde{Z}(\tau)$ is an even function of τ so $\tilde{Z}'(\tau = 0) = 0$. This is because the boundary condition for $\tilde{Z}(-\tau)$ is equivalent to

$$\mathcal{B} \begin{pmatrix} 1 & 0 & 0 & 0 \\ 0 & e^{\tau H(x_2)} & 0 & 0 \\ 0 & 0 & 1 & 0 \\ 0 & 0 & 0 & e^{\tau H(x_2)} \end{pmatrix} \chi(0, x_2) = 0, \tag{6.61}$$

upto an overall phase factor. This can be converted to the boundary condition for $\tilde{Z}(\tau)$ by interchanging the fermionic fields $\chi^+ \leftrightarrow \chi^-$. The action remains unchanged under this interchange, so $\tilde{Z}(-\tau) = \tilde{Z}(\tau)$. Hence we find,

$$\log\left(\frac{\tilde{Z}(1)}{\tilde{Z}(0)} \right) = \int_0^1 \mathrm{d}\tau \operatorname{Tr}\left(\frac{\mathrm{d}h(\tau)}{\mathrm{d}\tau} h(\tau)^{-1} \right). \tag{6.62}$$

Note that $\widetilde{Z}(\tau = 0) = Z[n = 1]$, with $Z[n]$ being the original path integral over the ψ variables in the main text. This is because when $n = 1$, the gauge field is zero, and so $Z[n = 1]$ and $\widetilde{Z}(\tau = 0)$ are both free fermion path integrals with the same boundary conditions.

So now our goal is to compute $\operatorname{Tr}(\frac{\mathrm{d}h}{\mathrm{d}\tau} h^{-1})$, and then do the integral on the right hand side of (6.62). A major difficulty is that h is an infinite matrix and its determinant or traces must be regularised. Our strategy is to find explicit expressions for the matrix elements of h, take the large L limit and then construct the inverse and compute $\operatorname{Tr}(\frac{\mathrm{d}h}{\mathrm{d}\tau} h^{-1})$. The final result is given in (6.98).

Computing the matrix elements of h is straightforward. In the large L limit, using (6.56),

we get for instance,

$$h_{Am,An}(\tau) = \frac{\sqrt{2}}{T}\int_{-T/2}^{T/2} \mathrm{d}x_2\; e^{\mathrm{i}(w_m-w_n)x_2}\begin{cases} e^{\alpha(x_2)} & \text{if } w_n>0 \\ -|c_1|^2-|c_3|^2 e^{\alpha(x_2)} & \text{if } w_n<0 \end{cases}, \tag{6.63}$$

$$h_{Am,Bn}(\tau) = \frac{\sqrt{2}}{T}\int_{-T/2}^{T/2} dx_2\; e^{i(w_m-w_n)x_2}\begin{cases} 0 & w_n>0 \\ c_1c_3^*\, e^{\alpha(x_2)} - c_1c_3^* & w_n<0 \end{cases}, \tag{6.64}$$

$$h_{Bm,An}(\tau) = \frac{\sqrt{2}}{T}\int_{-T/2}^{T/2} dx_2\; e^{i(w_m-w_n)x_2}\begin{cases} 0 & w_n>0 \\ c_1^*c_3\, e^{\alpha(x_2)} - c_1^*c_3 & w_n<0 \end{cases}, \tag{6.65}$$

$$h_{2Mm,2Mn}(\tau) = \frac{\sqrt{2}}{T}\int_{-T/2}^{T/2} dx_2\; e^{i(w_m-w_n)x_2}\begin{cases} 1 & w_n>0 \\ -|c_1|^2 e^{\alpha(x_2)} - |c_3|^2 & w_n<0 \end{cases}. \tag{6.66}$$

where, for brevity and following [225], we defined

$$\alpha(x_2) := \tau H(x_2). \tag{6.67}$$

Other similar calculations give us the matrix

$$h(\tau) = \sqrt{2}\begin{pmatrix} [e^\alpha]_{++} & -|c_3|^2[e^\alpha]_{+-} & 0 & c_1c_3^*[e^\alpha]_{+-} \\ [e^\alpha]_{-+} & -|c_3|^2[e^\alpha]_{--} - |c_1|^2\,\mathbb{1} & 0 & c_1c_3^*[e^\alpha]_{--} - c_1c_3^*\,\mathbb{1} \\ 0 & c_1^*c_3[e^\alpha]_{+-} & \mathbb{1} & -|c_1|^2[e^\alpha]_{+-} \\ 0 & c_1^*c_3[e^\alpha]_{--} - c_1^*c_3\,\mathbb{1} & 0 & -|c_1|^2[e^\alpha]_{--} - |c_3|^2\,\mathbb{1} \end{pmatrix}, \tag{6.68}$$

where the row and column indices are valued in $\{A,B\}\times\{+,-\} = \{A+, A-, B+, B-\}$ and each entry in (6.68) is itself an infinite matrix with rows and columns indexed by the *positive* integers. Essentially, because the positive and negative frequencies behave differently, as in (6.63), we need to treat them separately. Also, following [225], we have introduced a square-bracket notation for the matrix elements in the Matsubara basis

$$[f]_{m,n} = \frac{1}{T}\int_{-T/2}^{T/2} \mathrm{d}x_2\; e^{\mathrm{i}(w_m-w_n)x_2} f(x_2). \tag{6.69}$$

It is important to note that this is a Toeplitz matrix since $[f]_{m,n} = [f]_{m-n}$.

The derivative $\mathrm{d}h/\mathrm{d}\tau$ and the inverse h^{-1} can be obtained using the identities given in appendix B of [225]. The derivative can be obtained using

$$\frac{\mathrm{d}}{\mathrm{d}\tau}[e^\alpha]_{++} = \frac{1}{\tau}\left([\alpha]_{++}[e^\alpha]_{++} + [\alpha]_{+-}[e^\alpha]_{-+}\right), \tag{6.70}$$

$$\frac{\mathrm{d}}{\mathrm{d}\tau}[e^\alpha]_{+-} = \frac{1}{\tau}\left([\alpha]_{++}[e^\alpha]_{+-} + [\alpha]_{+-}[e^\alpha]_{--}\right), \tag{6.71}$$

$$\frac{\mathrm{d}}{\mathrm{d}\tau}[e^\alpha]_{-+} = \frac{1}{\tau}\left([\alpha]_{-+}[e^\alpha]_{++} + [\alpha]_{--}[e^\alpha]_{-+}\right), \tag{6.72}$$

$$\frac{\mathrm{d}}{\mathrm{d}\tau}[e^\alpha]_{--} = \frac{1}{\tau}\left([\alpha]_{-+}[e^\alpha]_{+-} + [\alpha]_{--}[e^\alpha]_{--}\right). \tag{6.73}$$

After a brute force explicit calculation, we find that the h^{-1} is composed of the block matrices

$$\sqrt{2}\,(h^{-1})_{A+,A+} = ([e^\alpha]_{++})^{-1}[M]_{++}, \tag{6.74}$$
$$\sqrt{2}\,(h^{-1})_{A+,A-} = -|c_3|^2([e^\alpha]_{++})^{-1}[M]_{++}[e^\alpha]_{+-}([e^\alpha]_{--})^{-1}, \tag{6.75}$$
$$\sqrt{2}\,(h^{-1})_{A+,B+} = 0, \tag{6.76}$$
$$\sqrt{2}\,(h^{-1})_{A+,B-} = c_1c_3^*([e^\alpha]_{++})^{-1}[M]_{++}[e^\alpha]_{+-}([e^\alpha]_{--})^{-1}, \tag{6.77}$$
$$\sqrt{2}\,(h^{-1})_{A-,A+} = \left(|c_1|^2\mathbb{1} + |c_3|^2([e^\alpha]_{--})^{-1}\right)[N]_{--}[e^\alpha]_{-+}([e^\alpha]_{++})^{-1}, \tag{6.78}$$
$$\sqrt{2}\,(h^{-1})_{A-,A-} = -\left(|c_1|^2\mathbb{1} + |c_3|^2([e^\alpha]_{--})^{-1}\right)[N]_{--}, \tag{6.79}$$
$$\sqrt{2}\,(h^{-1})_{A-,B+} = 0, \tag{6.80}$$
$$\sqrt{2}\,(h^{-1})_{A-,B-} = \frac{c_1}{c_3}\left(|c_1|^2\mathbb{1} + |c_3|^2([e^\alpha]_{--})^{-1}\right)[N]_{--} - \frac{c_1}{c_3}\mathbb{1}, \tag{6.81}$$
$$\sqrt{2}\,(h^{-1})_{B+,A+} = -c_1^*c_3[e^\alpha]_{+-}([e^\alpha]_{--})^{-1}[N]_{--}[e^\alpha]_{-+}([e^\alpha]_{++})^{-1}, \tag{6.82}$$
$$\sqrt{2}\,(h^{-1})_{B+,A-} = c_1^*c_3[e^\alpha]_{+-}([e^\alpha]_{--})^{-1}[N]_{--}, \tag{6.83}$$
$$\sqrt{2}\,(h^{-1})_{B+,B+} = \mathbb{1}, \tag{6.84}$$
$$\sqrt{2}\,(h^{-1})_{B+,B-} = -|c_1|^2[e^\alpha]_{+-}([e^\alpha]_{--})^{-1}[N]_{--}, \tag{6.85}$$
$$\sqrt{2}\,(h^{-1})_{B-,A+} = c_1^*c_3\left(\mathbb{1} - ([e^\alpha]_{--})^{-1}\right)[N]_{--}[e^\alpha]_{-+}([e^\alpha]_{++})^{-1}, \tag{6.86}$$
$$\sqrt{2}\,(h^{-1})_{B-,A-} = -c_1^*c_3\left(\mathbb{1} - ([e^\alpha]_{--})^{-1}\right)[N]_{--}, \tag{6.87}$$
$$\sqrt{2}\,(h^{-1})_{B-,B+} = 0, \tag{6.88}$$
$$\sqrt{2}\,(h^{-1})_{B-,B-} = -\mathbb{1} + |c_1|^2\left(\mathbb{1} - ([e^\alpha]_{--})^{-1}\right)[N]_{--}, \tag{6.89}$$

where we have defined

$$[M]_{++} := \left(\mathbb{1} - |c_3|^2[e^\alpha]_{+-}([e^\alpha]_{--})^{-1}[e^\alpha]_{-+}([e^\alpha]_{++})^{-1}\right)^{-1}, \tag{6.90}$$
$$[N]_{--} := \left(\mathbb{1} - |c_3|^2[e^\alpha]_{-+}([e^\alpha]_{++})^{-1}[e^\alpha]_{+-}([e^\alpha]_{--})^{-1}\right)^{-1}. \tag{6.91}$$

Using $\frac{\mathrm{d}h}{\mathrm{d}\tau}$ and h^{-1} so computed, we get

$$\begin{aligned}\tau\,\mathrm{Tr}\left(\frac{\mathrm{d}h}{\mathrm{d}\tau}h^{-1}\right) = {}& |c_1|^2\,\mathrm{Tr}\left([\alpha]_{-+}[e^\alpha]_{+-}([e^\alpha]_{--})^{-1}[N]_{--}\right) \\ & + |c_1|^2\,\mathrm{Tr}\left([\alpha]_{+-}[e^\alpha]_{-+}([e^\alpha]_{++})^{-1}[M]_{++}\right).\end{aligned} \tag{6.92}$$

We can simplify this further by using the following identities for quantities that appear in the definitions (6.90) and (6.91)

$$[e^\alpha]_{+-}\left([e^\alpha]_{--}\right)^{-1}[e^\alpha]_{-+}\left([e^\alpha]_{++}\right)^{-1} = \mathbb{1} - \left([e^{-\alpha}]_{++}\right)^{-1}\left([e^\alpha]_{++}\right)^{-1}, \tag{6.93}$$
$$[e^\alpha]_{-+}\left([e^\alpha]_{++}\right)^{-1}[e^\alpha]_{+-}\left([e^\alpha]_{--}\right)^{-1} = \mathbb{1} - \left([e^{-\alpha}]_{--}\right)^{-1}\left([e^\alpha]_{--}\right)^{-1}, \tag{6.94}$$

and perform a binomial series expansion, to get[6]

$$\begin{aligned}\tau \operatorname{Tr}\left(\frac{\mathrm{d}h}{\mathrm{d}\tau}h^{-1}\right) &= \sum_{p=0}^{\infty}(-1)^{p+1}|c_1/c_3|^{2p+2}\operatorname{Tr}\left([\alpha]_{-+}[e^{\alpha}]_{++}\left([e^{-\alpha}]_{++}[e^{\alpha}]_{++}\right)^p[e^{-\alpha}]_{+-}\right) \\ &+ \sum_{p=0}^{\infty}(-1)^{p+1}|c_1/c_3|^{2p+2}\operatorname{Tr}\left([\alpha]_{+-}[e^{\alpha}]_{--}\left([e^{-\alpha}]_{--}[e^{\alpha}]_{--}\right)^p[e^{-\alpha}]_{-+}\right) \qquad (6.95)\\ &= \tau\frac{\mathrm{d}}{\mathrm{d}\tau}\operatorname{Tr}\log\left(\mathbb{1}+|c_1/c_3|^2[e^{\alpha}]_{--}[e^{-\alpha}]_{--}\right) \qquad (6.96)\\ &= \tau\frac{\mathrm{d}}{\mathrm{d}\tau}\operatorname{Tr}\log\left(\mathbb{1}-|c_1|^2[e^{\alpha}]_{-+}[e^{-\alpha}]_{+-}\right). \qquad (6.97)\end{aligned}$$

Recalling that $r=|c_1|^2$ is the reflection coefficient and $\alpha(x_2)=\tau H(x_2)$, we get

$$\operatorname{Tr}\left(\frac{\mathrm{d}h}{\mathrm{d}\tau}h^{-1}\right) = -\frac{\mathrm{d}}{\mathrm{d}\tau}\sum_{m=1}^{\infty}\frac{r^m}{m}\operatorname{Tr}\left(\left([e^{\tau H(x_2)}]_{-+}[e^{-\tau H(x_2)}]_{+-}\right)^m\right). \qquad (6.98)$$

Substituting (6.98) into (6.62) and doing the τ integral, we get the result for the functional determinant

$$\log\left(\frac{\tilde{Z}(1)}{\tilde{Z}(0)}\right) = -\sum_{m=1}^{\infty}\frac{r^m}{m}\operatorname{Tr}\left(\left([e^{H}]_{-+}[e^{-H}]_{+-}\right)^m\right). \qquad (6.99)$$

Notice that the lower limit of the integral in (6.62) at $\tau=0$ does not contribute on the right hand side, because the indices of the matrices $[e^{\alpha}]_{-+}$ and $[e^{-\alpha}]_{+-}$ are purely off-diagonal and so $[1]_{+-}$ and $[1]_{-+}$ vanish.

We were unable to evaluate the expression on the right hand side of (6.99) in general. Thus, we will focus on computing the functional determinant $\tilde{Z}_k$ for the case needed in Sec. 6.4, which is a single interval $[-L_-,L_+]$ across the defect.

Perturbing away from the fully transmitting case

The goal of this subsection is to obtain the first order term in r in the von Neumann entropy of the interval $[-L_-,L_+]$, perturbing away from the fully transmitting case $r=0$.

The coefficient of the linear in r term in (6.99) is

$$\begin{aligned}\operatorname{Tr}\left([e^{H}]_{-+}[e^{-H}]_{+-}\right) &= \sum_{n\geq 0,l<0}\int\frac{\mathrm{d}y_1\mathrm{d}y_2}{T^2}e^{\frac{2\pi\mathrm{i}}{T}((y_1-y_2)(l-n))}e^{H(y_1)-H(y_2)} \qquad (6.100)\\ &= -\int_{\mathbb{R}^2}\frac{\mathrm{d}y_1\mathrm{d}y_2}{4\pi^2}\frac{e^{H(y_1)-H(y_2)}}{(y_1-y_2)^2}, \qquad (6.101)\end{aligned}$$

[6]One needs to use identities of the form $[e^{\alpha}]_{--}[e^{-\alpha}]_{--}+[e^{\alpha}]_{-+}[e^{-\alpha}]_{+-}=\mathbb{1}$, see appendix B of [225] for more on such relations.

where we have taken the $T \to \infty$ limit and the contours of integration for y_1 and y_2 are such that $\mathrm{Im}\,[y]_1 < 0$ and $\mathrm{Im}\,[y]_2 > 0$, so the geometric series in (6.100) converges. If we now expand in powers of H, we see that only terms at second order or higher will contribute, because for the constant and first order term, there is always one integral that vanishes after we close the contour in the respective half planes (the y_1 integral is closed in the lower half plane and the y_2 integral in the upper half plane).

Let us denote the $O(r)$ term in (6.99) by $f_k^{(1)}$ (with k being the replica index), then

$$f_k^{(1)} = r \int\limits_{\mathbb{R}^2} \frac{\mathrm{d}y_1 \mathrm{d}y_2}{4\pi^2 (y_1 - y_2)^2} \left(e^{H_k(y_1) - H_k(y_2)} - 1 - H_k(y_1) + H_k(y_2) \right). \tag{6.102}$$

To compute the entropy, we plug in the expression for H_k from (6.35) and (6.23), which we write as $H_k = -2\Phi_k = \frac{k}{n} \log \phi$, with

$$\phi(y) = \frac{y^2 + L_-^2}{y^2 + L_+^2}. \tag{6.103}$$

We now sum over k and take the $n = 1$ limit,

$$S^{(1)} = \lim_{n \to 1} \frac{1}{1-n} \sum_{k=-(n-1)/2}^{(n-1)/2} f_k^{(1)} = r \int\limits_{\mathbb{R}^2} \frac{\mathrm{d}y_1 \mathrm{d}y_2}{4\pi^2 (y_1 - y_2)^2} \left(1 - \frac{1}{2} \frac{\phi(y_1) + \phi(y_2)}{\phi(y_1) - \phi(y_2)} \log \left(\frac{\phi(y_1)}{\phi(y_2)} \right) \right). \tag{6.104}$$

Because of the logarithm in (6.104), we get branch cuts in the complex y_1 and y_2 planes. Let us assume, without loss of generality, that $L_- > L_+$. Since y_1 integration contour has a negative imaginary part, we deform the contour in the lower half plane and pick up a discontinuity from the branch cut that runs from $y_1 = -\mathrm{i}L_-$ to $y_2 = -\mathrm{i}L_+$. The discontinuity of the integrand of (6.104) is

$$-\frac{\mathrm{i}\pi}{L_-^2 - L_+^2} \frac{2y_1^2 y_2^2 + 2L_+^2 L_-^2 + (L_+^2 + L_-^2)(y_1^2 + y_2^2)}{4\pi^2 (y_1 - y_2)^2 (y_1^2 - y_2^2)}, \tag{6.105}$$

which when integrated over y_1 from $y_1 = -\mathrm{i}L_-$ to $y_1 = -\mathrm{i}L_+$ gives

$$\begin{aligned} -\frac{1}{16\pi (L_-^2 - L_+^2) y_2^3} \Bigg(& L_-^2 L_+^2 \pi^2 - 2L_- L_+ (L_- - L_+) y_2 + (L_-^2 + L_+^2) \pi y_2^2 - 2(L_- - L_+) y_2^3 \\ & + \pi y_2^4 + \mathrm{i}(L_-^2 + y_2^2)(L_+^2 + y_2^2) \log \left(\frac{(y_2 + \mathrm{i}L_+)(\mathrm{i}L_- - y_2)}{(y_2 - \mathrm{i}L_+)(\mathrm{i}L_- + y_2)} \right) \Bigg). \end{aligned} \tag{6.106}$$

Now, we need to do the y_2 integral, whose contour has a small positive imaginary part and can be deformed in the upper half-plane. The discontinuity comes from the logarithm in (6.106) and equals

$$-\frac{1}{8} \frac{(L_-^2 + y_2^2)(L_+^2 + y_2^2)}{(L_-^2 - L_+^2) y_2^3}. \tag{6.107}$$

Integrating this over y_2 from $y_2 = \mathrm{i}L_+$ to $y_2 = \mathrm{i}L_-$ gives

$$S^{(1)} = \frac{r}{8}\left(1 + \frac{L_-^2 + L_+^2}{L_-^2 - L_+^2}\log\frac{L_+}{L_-}\right). \tag{6.108}$$

Thus, to $O(r)$, the entropy is given by

$$S([-L_-, L_+]) = \frac{1}{3}\log\frac{L_+ + L_-}{\varepsilon} + \frac{r}{8}\left(1 + \frac{L_-^2 + L_+^2}{L_-^2 - L_+^2}\log\frac{L_+}{L_-}\right) + O(r^2)\,. \tag{6.109}$$

Higher order terms in the reflection coefficient can be computed in a similar way, but involve more integrals and a more complicated branch cut structure.

Perturbing in the asymmetry

In this subsection, we will perform a different approximation. While still working with a single interval $[-L_-, L_+]$ that straddles the defect, we will compute the functional integral $\tilde{Z}_k$ perturbatively in the asymmetry parameter

$$\gamma = \frac{L_- - L_+}{L_- + L_+} = \frac{L_- - L_+}{2L}, \tag{6.110}$$

where $2L = L_- + L_+$ is the length of the interval.

We start with the following series expansion for H_k,

$$H_k(y) = -2\Phi_k(0, y) = \frac{2k}{n}\sum_{j\in\text{odd}}\frac{(\mathrm{i}\gamma L)^j}{j}\left(\frac{1}{(y + \mathrm{i}L)^j} - \frac{1}{(y - \mathrm{i}L)^j}\right). \tag{6.111}$$

The advantage of this expansion is that at any finite order in γ, we have poles in the complex plane instead of branch cuts.

The $m = 1$ term of (6.99) is given by

$$\mathrm{Tr}\left([e^{H_k}]_{-+}[e^{-H_k}]_{+-}\right) = \frac{1}{T^2}\int_{-T/2}^{T/2}\mathrm{d}y_1\mathrm{d}y_2\,\frac{e^{H_k(y_1)-H_k(y_2)}}{\sin^2(\pi(y_2 - y_1)/T)}, \tag{6.112}$$

where $\mathrm{Im}\,[y]_1 < 0$ and $\mathrm{Im}\,[y]_2 > 0$ as mentioned earlier.

To evaluate these integrals, we will use the residue theorem. We close the contour for y_1 in the lower half-plane and for y_2 in the upper half-plane. This ensures that the only residues come from the pole at $y_1 = -\mathrm{i}L$ for the y_1 integral and the pole at $y_2 = \mathrm{i}L$ for the y_2 integral. We also get some contribution from integrals that were used to close the contours in the complex plane but these contributions vanish in the $T \to \infty$ limit.

In the limit $T \to \infty$, we have the leading order result in γ

$$\mathrm{Tr}\left([e^{H_k}]_{-+}[e^{-H_k}]_{+-}\right) = \frac{k^2}{n^2}\gamma^2\tau^2 + O(\gamma^4). \tag{6.113}$$

It is worth mentioning that the final answer must be even in γ. This is indeed the case for the above calculation.

In general, we want to compute $\mathrm{Tr}\left(\left([e^{H_k}]_{-+}[e^{-H_k}]_{+-}\right)^p\right)$. In the $T\to\infty$ limit, this is given by a contour integral

$$\mathrm{Tr}\left(\left([e^{H_k}]_{-+}[e^{-H_k}]_{+-}\right)^p\right)=\frac{(-1)^p}{\pi^{2p}}\int_{-\infty}^{\infty}\prod_{i=1}^{2p}\mathrm{d}y_i\frac{e^{H_k(y_1)-H_k(y_2)+\cdots+H_k(y_{2p-1})-H_k(y_{2p})}}{(y_2-y_1)\dots(y_{2p}-y_{2p-1})(y_1-y_{2p})},\quad(6.114)$$

where $\mathrm{Im}\,[y]_1,\mathrm{Im}\,[y]_3,\dots\mathrm{Im}\,[y]_{2p-1}<0$ and $\mathrm{Im}\,[y]_2,\mathrm{Im}\,[y]_4,\dots\mathrm{Im}\,[y]_{2p}>0$. We close the contours for $y_1,y_3,\dots y_{2p-1}$ in the lower half plane and the contours for $y_2,y_4,\dots y_{2p}$ in the upper half plane. This ensures that the contour does not enclose the poles coming from the $y_{i+1}-y_i$ terms in the denominator.

For H_k given in (6.111), each factor of γ corresponds to exactly one pole in the complex plane. Therefore, at order γ^j

$$\#(y_1)+\#(y_2)+\dots\#(y_{2p})=j,\quad(6.115)$$

where $\#(y_i)$ denotes the total number of poles (with multiplicity) for the y_i variable in the numerator $e^{H_k(y_1)-H_k(y_2)+\cdots+H_k(y_{2p-1})-H_k(y_{2p})}$. If $j<2p$, there is at least one variable that has no pole in the entire complex plane. If we do the contour integral over this variable first, the result is zero. Therefore, $\mathrm{Tr}(\left([e^{H_k}]_{-+}[e^{-H_k}]_{+-}\right)^p)$ only contributes non-trivially starting at $O(\gamma^{2p})$.

To summarize, the γ^j term in $\log\left(\tilde{Z}_k/Z[1]\right)$ vanishes if j is odd. If j is even, we get a non-zero contributions to the γ^j term from $\mathrm{Tr}(\left([e^{H_k}]_{-+}[e^{-H_k}]_{+-}\right)^p)$ only if $p=1,2,\dots j/2$. Using (6.113), we have the full result at order γ^2,

$$\log\frac{\tilde{Z}_k}{Z[1]}=-\gamma^2\frac{k^2}{n^2}r+O\left(\gamma^4\right),\quad(6.116)$$

so the Rényi entropy is

$$S_n\big([-L_-,L_+]\big)=\frac{n+1}{6n}\left[\log\frac{L_++L_-}{\varepsilon}-\frac{\gamma^2 r}{2}\right]+O\left(\gamma^4\right).\quad(6.117)$$

Similarly, we can determine the contribution at higher orders in γ,

$$\begin{aligned}\log\frac{\tilde{Z}_k}{Z[1]}=&r\frac{k^2}{n^2}\left(\gamma^2+\frac{\gamma^4}{2}+\frac{\gamma^6}{3}+\frac{\gamma^8}{4}\right)+rt\frac{k^4}{n^4}\left(\frac{\gamma^4}{2}+\frac{\gamma^6}{2}+\frac{65\gamma^8}{144}\right)\\&-rt(r-t)\frac{k^6}{n^6}\left(\frac{\gamma^6}{6}+\frac{\gamma^8}{4}\right)+rt\frac{k^6}{n^6}\frac{\gamma^8}{72}+rt(r-5t)(5r-t)\frac{k^8}{n^8}\frac{\gamma^8}{144}+O\left(\gamma^{10}\right),\end{aligned}\quad(6.118)$$

We can now easily do the sum over k to get the Rényi entropies and also take the $n \to 1$ limit to get the entanglement entropy.

$$\begin{aligned} S_n\big([-L_-, L_+]\big) =& \frac{n+1}{6n}\left[\log\frac{L_+ + L_-}{\varepsilon} + \frac{r}{2}\left(-\gamma^2 - \frac{\gamma^4}{2} - \frac{\gamma^6}{3} - \frac{\gamma^8}{4}\right)\right] \\ &+ \frac{(n+1)(7-3n^2)}{240n^3}\left[rt\left(\frac{\gamma^4}{2} + \frac{\gamma^6}{2} + \frac{65\gamma^8}{144}\right)\right] \\ &+ \frac{(n+1)(31-18n^2+3n^4)}{1344n^5}\left[rt(r-t)\left(\frac{\gamma^6}{6} + \frac{\gamma^8}{4}\right) - rt\frac{\gamma^8}{72}\right] \\ &+ \frac{(n+1)(381-239n^2+55n^4-5n^6)}{11520n^7}\left[rt(r-5t)(5r-t)\frac{\gamma^8}{144}\right] + O\left(\gamma^{10}\right), \end{aligned} \tag{6.119}$$

$$\begin{aligned} S\big([-L_-, L_+]\big) =& \frac{1}{3}\log\frac{L_+ + L_-}{\varepsilon} - \frac{r}{6}\left(\gamma^2 + \frac{\gamma^4}{2} + \frac{\gamma^6}{3} + \frac{\gamma^8}{4}\right) + \frac{rt}{30}\left(\frac{\gamma^4}{2} + \frac{\gamma^6}{2} + \frac{65\gamma^8}{144}\right) \\ &+ \frac{rt}{42}\left[(r-t)\left(\frac{\gamma^6}{6} + \frac{\gamma^8}{4}\right) - \frac{\gamma^8}{72}\right] + \frac{rt(r-5t)(5r-t)}{30}\left(\frac{\gamma^8}{144}\right) + O\left(\gamma^{10}\right). \end{aligned} \tag{6.120}$$

It is worth mentioning that the series multiplying r adds up to

$$-\frac{1}{6}\log(1-\gamma^2) = -\frac{1}{6}\log\frac{4L_-L_+}{(L_+ + L_-)^2}, \tag{6.121}$$

so these terms linearly interpolate between the purely transmitting limit, $r = 0$, and the purely reflecting limit, $r = 1$. All the other terms vanish at these two limits, and represent the deviation from this linear interpolation.

Perturbing away from the fully reflecting case

In this subsection, we will perform a third approximation to obtain the first order term in t, perturbing away from the fully reflecting case $t = 0$. . A calculation similar to those above gives us the result analogous to (6.99)

$$\log\frac{\tilde{\tilde{Z}}_k}{Z[1]} = -\sum_{p=1}^{\infty}\frac{t^p}{p}\,\mathrm{Tr}\left(\left([e^{\mathrm{i}\tilde{H}_k}]_{-+}[e^{-\mathrm{i}\tilde{H}_k}]_{+-}\right)^p\right). \tag{6.122}$$

Again, we restrict ourselves to computing the functional determinant $\tilde{\tilde{Z}}_k$ which corresponds to a single interval across the defect, $\mathcal{A} = [-L_-, L_+]$.

We can compute the $O(t)$ piece in the von Neumann entropy by perturbing away from the fully reflecting case. The result is

$$S^{(1)} = t\int_{\mathbb{R}^2}\frac{\mathrm{d}y_1\mathrm{d}y_2}{4\pi^2(y_1-y_2)^2}\left(1 - \frac{1}{2}\frac{\phi(y_1)+\phi(y_2)}{\phi(y_1)-\phi(y_2)}\log\left(\frac{\phi(y_1)}{\phi(y_2)}\right)\right). \tag{6.123}$$

where

$$\phi(x) = \frac{(x - \mathrm{i}L_-)(x + \mathrm{i}L_+)}{(x + \mathrm{i}L_-)(x - \mathrm{i}L_+)}. \tag{6.124}$$

Using a similar contour deformation argument as above, we find,

$$S^{(1)} = \frac{t}{8}\left(1 + \frac{L_-^2 - 6L_-L_+ + L_+^2}{2(L_- - L_+)\sqrt{L_-L_+}} \arctan\left(\frac{L_- - L_+}{2\sqrt{L_-L_+}}\right)\right). \tag{6.125}$$

The full answer for the entropy to order t^2 is then

$$S([-L_-, L_+]) = \frac{1}{6}\log\frac{4L_+L_-}{\varepsilon^2} + \frac{t}{8}\left(1 + \frac{L_-^2 - 6L_-L_+ + L_+^2}{2(L_- - L_+)\sqrt{L_-L_+}} \arctan\left(\frac{L_- - L_+}{2\sqrt{L_-L_+}}\right)\right) + O(t^2)\,. \tag{6.126}$$

We can also do a small γ expansion similar to the previous subsection. We just quote the final result

$$\begin{aligned} S\big([-L_-, L_+]\big) =& \frac{1}{6}\log\frac{4L_+L_-}{\varepsilon^2} + \frac{t}{6}\left(\gamma^2 + \frac{\gamma^4}{2} + \frac{\gamma^6}{3} + \frac{\gamma^8}{4}\right) + \frac{rt}{30}\left(\frac{\gamma^4}{2} + \frac{\gamma^6}{2} + \frac{65\gamma^8}{144}\right) \\ &+ \frac{rt}{42}\left[(r-t)\left(\frac{\gamma^6}{6} + \frac{\gamma^8}{4}\right) - \frac{\gamma^8}{72}\right] + \frac{rt(r-5t)(5r-t)}{30}\left(\frac{\gamma^8}{144}\right) + O\left(\gamma^{10}\right). \end{aligned} \tag{6.127}$$

This matches with (6.120) at the appropriate order in γ.

6.4 Entanglement Islands with Graybody Factors

In this section, we will apply our results for the von Neumann entropy to the zero temperature entanglement island calculations of [229]. The new component is the introduction of a reflection/transmission coefficient at the interface between AdS_2 and flat space. We will first quickly review the setup (see figure 6.2) and then show that the entanglement island behaves in a monotonic fashion as a function of the reflection/transmission coefficient.

The gravitational theory is taken to be AdS-JT gravity coupled to matter, whose action is given by [243]

$$I[g, \phi, \psi] = \phi_0 + \frac{1}{4\pi}\int \mathrm{d}^2x\,\sqrt{g}\,\phi\,(R+2) + I_{\mathrm{CFT}}[g, \psi], \tag{6.128}$$

where we have put $4G_N = 1$, the constant ϕ_0 gives the extremal entropy, and we have omitted the Gibbons-Hawking boundary term. The CFT matter action is given by I_{CFT} and we take the matter fields ψ to not couple to the dilaton. For the gravity variables, we put the usual boundary conditions $g_{uu}|_{\mathrm{bdy}} = 1/\varepsilon^2$ and $\phi|_{\mathrm{bdy}} = \phi_r/\varepsilon$.

Using coordinates (x^0, x^1) with $x^1 < 0$, the zero temperature solution of JT gravity is given by

$$\mathrm{d}s^2 = \frac{-(\mathrm{d}x^0)^2 + (\mathrm{d}x^1)^2}{(x^1)^2}, \quad \phi = \frac{\phi_r}{-x^1}. \tag{6.129}$$

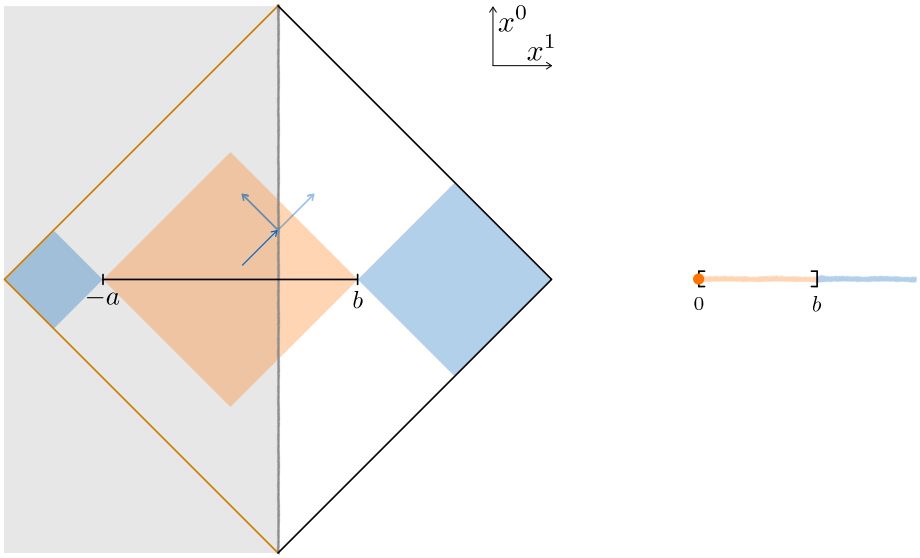

Figure 6.2: Setup for the QES calculation for a partially reflecting AdS_2 boundary is shown on the left. In the gray region, gravity is dynamical and we will consider the Poincaré patch with its horizon drawn in orange. This region is glued along the AdS_2 boundary to a flat space region on the right. The free fermion matter lives in both the AdS_2 and flat space regions, but there is partial reflection at the interface. A candidate entanglement wedge $[-a, b]$ is shaded orange and its complement is shaded blue. The dual SYK + wire system is shown on the right. The fundamental computation we are doing is of the entropy and the entanglement wedge of the interval $[\mathbf{0}, \mathbf{b}]$ in this non-gravitational description.

The JT boundary conditions imply that the AdS_2 boundary is at $x^1 = -\varepsilon$. We now couple the AdS_2 region to half of 2d flat-space, which is non-gravitating. The matter fields are taken to be free fermions and they propagate on both the AdS and the flat space regions, but we choose the boundary conditions for them so that they see a partially transmitting interface at $x_1 = -\varepsilon$, see equation (6.5). This is how our work differs from the previous papers [17, 229].

As emphasized in [229], one should think of the entropies as being fundamentally defined in a candidate dual description that does not involve gravity. This will look something like an SYK model coupled to a wire. The transmission coefficient encodes some property of the coupling between the SYK model and the wire, and the zero temperature equilibrium geometry corresponds to the ground state of the coupled Hamiltonian.

The goal is to compute the entanglement wedge of the region $[\mathbf{0}, \mathbf{b}]$ in the SYK+wire description. A candidate for a QES is the point $(x^0, x^1) = (0, -a)$ in the AdS_2 region (with $a > 0$). The entanglement wedge of $[\mathbf{0}, \mathbf{b}]$ will be the region $(-a_*, b)$ where a_* is the location of the QES. We need to compute the generalized entropy functional $S_{\text{gen}}()$ of a region $[-a, b]$ that is partially in the bath region and partially in the gravity region, see figure 6.2. For this,

we need the dilaton profile given in (6.129) and also an expression for the entropy of bulk matter fields in the semiclassical description, which were obtained in the previous section.

The generalized entropy of the interval $[-a, b]$ is given by

$$S_{\rm gen}(a) = \phi_0 + \frac{\phi_r}{a} + c\, S_{\text{Dirac, flat}}([-a, b]) - \frac{c}{6}\log a, \tag{6.130}$$

where the second term corresponds to the entropies we computed in Sec. 6.2 and the final term comes from the Weyl factor in the metric (6.129) at the left end-point of the interval $[-a, b]$. As already noted, the boundary conditions on the matter fields preserve one copy of the Virasoro algebra, so the Weyl factor term takes into account the fact that the interface is now between AdS space and flat space, rather than between two flat half-spaces. We have also taken c copies of the free Dirac fermion system, and as usual c is taken to be large so that the entropy coming from fluctuations in the gravity sector can be ignored. Let us define a quantity k with dimensions of length as

$$k := \frac{6\phi_r}{c}. \tag{6.131}$$

Extremizing $S_{\rm gen}(a)$ with respect to a gives us the location a_* of the QES. As before, we specialize to three cases:

- When the reflection coefficient r is small, we use (6.109) for $S_{\text{Dirac, flat}}$ and we get

$$a_*(r) = a_0 + r\frac{3a_0^2\left(a_0^4 - b^4 - 4a_0^2b^2\log(a_0/b)\right)}{4(a_0-b)^2\left((a_0+b)^2(a_0+2k) - 2a_0^3\right)} + O(r^2), \tag{6.132}$$

  where a_0 is the location of the island in the purely transmitting case [229],

$$a_0 = a_*(r=0) = \frac{1}{2}\left(b + k + \sqrt{b^2 + 6bk + k^2}\right). \tag{6.133}$$

  It is also instructive to look at the extreme limits for b in this expression.

$$a_\star = \frac{6\phi_r}{c} + r\,\frac{9\phi_r}{2c} + O(b, r^2) \qquad \text{(small } b\text{)}, \tag{6.134}$$

$$a_\star = \left(b + \frac{12\phi_r}{c}\right) + r\,\frac{12\phi_r}{c} + O(b^{-1}, r^2) \quad \text{(large } b\text{)}. \tag{6.135}$$

  We would like to argue that the second term in (6.132) in always positive, so that the QES moves from its location a_0 in the fully transmitting case towards the Poincaré horizon, where it lies in the fully reflecting case. It is easy to plot the second term of (6.132) as a function of b and k and check that it is positive, but we would like to give a more illuminating argument. First, note that $a_0 > b$, which as observed in [229] is a condition that is imposed by the Quantum Focusing Conjecture [73]. The function $S'_{\rm gen}(a)$ at full transmission is positive to the left of the QES, and negative to the right of the QES. As noted earlier, the correction term in (6.109) is negative definite and has a maximum value of 0 when $L_- = L_+$, or $a = b$ in the notation of this section. These facts dictate that the QES can only move leftwards from a_0.

- When the transmission coefficient t is small, we use (6.126) for $S_{\text{Dirac, flat}}$ and we get

$$a_*(r) = \left(\frac{1024\, bk^2}{9\pi^2}\right)^{\frac{1}{3}} t^{-\frac{2}{3}} + O(t^0). \tag{6.136}$$

  The QES goes to infinity as $t \to 0$. In the fully reflecting case, the QES is at the Poincaré horizon: the AdS_2 and flat space regions are not coupled at all in this case, and so the entanglement wedge of the boundary of AdS_2 better be the entire Poincaré patch of AdS_2.

  Note that since a_* is getting large, we might worry that the coefficient of the $O(t)$ term in the bulk entropy formula (6.126) is getting large. However, the overall size of the $O(t)$ term at the extremization point is seen to be $t^{\frac{2}{3}}$, which is small. In general, entropies cannot grow faster than linearly in the interval size, and so, if the expansion in t is well-behaved, we do not expect large powers of L_- to show up at higher orders in (6.126).

- Taking b to be very large, we expect, as in [229], that the quantity $\frac{a_*-b}{a_*+b}$ is small. Keeping terms up to order γ^2 in (6.120), we find

$$a_*(r) = b\left(1 + \frac{1}{1-r}\frac{2k}{b} + O\left(\frac{k^2}{b^2}\right)\right). \tag{6.137}$$

  This matches with the small r result (6.132) in the common domain of validity, but we should not trust the exact form of this answer in the $r \to 1$ limit, since γ is getting large in that limit.

6.5 Discussion

In summary, within the particular setup and the various limits that we have considered, we have shown that the location of the QES (and thus the size of the entanglement island) is a monotonic function of the transmission strength of the interface between the gravitating region and faraway flat space region. It would be interesting to extend our results to various other setups in which islands are known to exist, for instance in the $T > 0$ non-evaporating setup in [229]. It would also be nice to find way to incorporate explicitly-tunable greybody factors in the setup of double-holography [88], especially in higher dimensions [231]. Our prejudice is that such monotonicity should always hold. In the case of an evaporating black hole, specifically using the setup of [17], one should see the QES move from inside the horizon towards the horizon as one turns on graybody effects. This has to do with the fact that when the black hole is evaporating, the matter fields are taken to be in the Unruh state, and not the Hartle-Hawking state. That changes the formulas for the matter entanglement entropy. In this situation, if the interface is fully reflecting, the QES would be at the black hole

horizon. When we turn on a coupling between the AdS and the bath regions, thus making $r < 1$, the QES moves inwards, as discussed in [16, 17].

Independently of the motivation from black hole physics, it would also be valuable to go beyond the limits we have considered obtain exact results for the 2d free fermion von Neumann entropy and the modular Hamiltonian for a general set of intervals in the presence of a defect.

Part II

Top-down Approach

Chapter 7

Normalization of ZZ Instanton Amplitudes in Minimal String Theory

7.1 Introduction

The duality between minimal string theory and double-scaled matrix integrals [244] is the earliest known example of a duality between a gravitational and a non-gravitational system. The term minimal string theory refers to two-dimensional gravity coupled to $c < 1$ minimal models. These are non-critical string theories where the Liouville mode does not decouple. More precisely, the worldsheet theory consists of the (p', p) minimal model plus Liouville theory, with total central charge 26, together with the usual bc-ghosts. Here p' and p are relatively-prime positive integers, and we work with the convention that $p > p' \geq 2$. The models with $(2, p)$ matter are dual to matrix integrals over just one matrix. The $p \to \infty$ limit of the $(2, p)$ family is JT gravity [245], a subject which has been of much recent interest.

While the minimal string theories are toy models, one of the lessons from them that generalizes to even critical superstring theories is the existence of stronger-than-expected non-perturbative effects [246, 247]. Let g_s be the closed string coupling. Then the non-perturbative effects are of order $\exp(-Cg_s^{-1})$, rather than the $\exp(-Cg_s^{-2})$ expected from field theory. In the language of JT gravity, $g_s \propto e^{-S_0}$ where S_0 is the coefficient of the Euler characteristic term in the action. Given this identification, these effects are "doubly-nonperturbative" in the parameter S_0 [245].

These non-perturbative effects are known to arise from ZZ branes on the string theory side [143]. In the matrix integral, these effects correspond to one-eigenvalue instantons. A one-eigenvalue instanton refers to a subleading saddle point configuration in the matrix integral which differs from the leading saddle point by pulling one eigenvalue out of the droplet of eigenvalues and placing it at an extremum of the one-eigenvalue effective action [246, 248].

Let us consider the computation of the matrix integral $\mathfrak{Z}$ itself. Let T denote the action of the one-eigenvalue instanton or the "tension" of the ZZ brane, which is a positive quantity

of order g_s^{-1}. The quantity $\mathfrak{Z}$ admits an expansion of the form

$$\mathfrak{Z} = \mathfrak{Z}^{(0)} + \mathfrak{Z}^{(1)} + \ldots = \mathfrak{Z}^{(0)} \left(1 + \mathcal{N}\, e^{-T} + \ldots\right) . \tag{7.1}$$

Here $\mathfrak{Z}^{(0)}$ is the perturbative contribution to the matrix integral and $\mathfrak{Z}^{(1)}$ is the contribution to the matrix integral when one eigenvalue is in the classically forbidden region. One can also write (7.1) in terms of the free energy as $\log \mathfrak{Z} = \log \mathfrak{Z}^{(0)} + \mathcal{N}\, e^{-T} + \ldots$.

The object of interest to us in this chapter is the normalization constant $\mathcal{N}$. Roughly speaking, in string theory, $\mathcal{N}$ is the exponential of the worldsheet annulus with ZZ boundary conditions on both ends. This annulus amplitude has been computed using the worldsheet theory [249, 250] and is divergent. However, starting with [251, 252], many papers have computed a finite value for $\mathcal{N}$ using matrix integral technology [251, 252, 253, 254, 255, 256, 245], with ref. [256] containing the result for general (p', p).

This state of affairs is very reminiscent of the recent computations in the $c = 1$ system, where the annulus amplitude between ZZ branes is also divergent, while the matrix side of the duality provides a finite unambiguous answer [25]. It has been shown by one of us [257] that string field theory techniques allow us to compute $\mathcal{N}$ in this case and the result matches with the matrix computation.

The purpose of this note is to apply these string field theory tools to the $(2, p)$ minimal string theories and compute the value of $\mathcal{N}$ in these theories. We find perfect agreement with the matrix integral computations [251, 252, 253, 254, 255, 245]. We record the final result

$$\mathcal{N} = T^{-\frac{1}{2}}\, \frac{i}{\sqrt{32\pi}}\, \frac{\cot(\pi/p)}{\sqrt{p^2-4}} . \tag{7.2}$$

Let us make a few comments about the form of this answer. First, the combination $\mathcal{N} T^{\frac{1}{2}}$ is natural to consider since the dependence on g_s cancels out in this combination. This is important since it is impossible to fix the multiplicative constant between the genus counting parameters on the two sides of the duality, since we can always add the Euler characteristic term to the worldsheet action with an arbitrary coefficient. So, when trying to match precise numerical constants, one should compute quantities that are independent of g_s, like $\mathcal{N} T^{\frac{1}{2}}$ rather than $\mathcal{N}$ or T separately.[1] On the matrix integral side, the gaussian integral around the one-eigenvalue instanton gives a multiplicative factor in $\mathcal{N}$ that is proportional to $T^{-\frac{1}{2}}$. On the string theory side, this factor arises because the proper volume of the rigid $U(1)$ gauge group on the instanton is proportional to $T^{\frac{1}{2}}$ [257]. Division by this gauge group volume in the path integral produces the factor of $T^{-\frac{1}{2}}$. Second, the overall sign of the right hand side of (7.2) is ambiguous on both sides of the duality, as it depends on a two-fold choice of the contour of integration over one unstable mode. One should make this choice so that the result is the same for the matrix integral and the string theory. Third, the normalization

[1] Another quantity like this would be the ratio of the disk amplitude to the square-root of the sphere amplitude [258]. See also [259, 260].

constant $\mathcal{N}$ is purely imaginary and the instanton correction we are studying computes the leading imaginary part of the free energy. In this sense, this correction is similar to the case of "bounce" solutions in instanton physics [261] and the instanton correction is meaningful. Finally, note that the coefficient on the right hand side of (7.2) is finite in the JT gravity limit $p \to \infty$.

Overview

In Section 7.2, we present the computation of $\mathcal{N}$ in the double-scaled one-matrix integral, which is dual to the $(2, p)$ minimal string. The results of this section are not new, and we are including them to illustrate the relevant tools in the simpler setting of the one-matrix integral. In Section 7.3, we first present a general string field theory analysis of the divergences in the cylinder diagram with both boundaries lying on a D-instanton. We then apply these tools to the $(2, p)$ minimal string and obtain a finite answer that agrees with the matrix integral result. In Section 7.4, we make a few remarks about the extension of these results to the more general (p', p) minimal string.

7.2 Matrix Integral Computation

In this section, we will compute the normalization constant $\mathcal{N}$ for the one-matrix integrals that are dual to the $(2, p)$ minimal string. The results in this section are not new and can be found in many papers, including [245, 251, 252, 253, 254, 255, 256, 262]. We choose to follow the streamlined presentation given in the recent work [245].

We start by explaining the setup. The starting point is an integral over all $L \times L$ hermitian matrices

$$\mathfrak{Z} = \int \mathrm{d}H \, e^{-L \operatorname{Tr} V(H)} \, . \tag{7.3}$$

Here V is a potential which can be taken to be an even polynomial of degree $p + 1$. The matrix integral $\mathfrak{Z}$ is a function of the coefficients in this polynomial. In the large L limit, we can talk about a smooth density of eigenvalues and it is supported on a finite interval on the real axis. The double-scaling limit refers to a procedure where, in addition to taking $L \to \infty$, we zoom in near the left edge of the spectrum and tune the coefficients of the potential such that the dominant double-line Feynman diagrams in the perturbation expansion of (7.3) resemble continuum surfaces [244] . In this limit, the density of states is non-normalizable and is supported on the entire positive real axis.

We focus on the so-called "conformal background" [263], where the leading density of

states in the double-scaling limit reads[2]

$$\langle \rho(E) \rangle^{(0)} = \frac{e^{S_0}}{\pi} \sinh\left(p \operatorname{arcsinh} \sqrt{\frac{E}{2\kappa}} \right) \Theta(E) \,. \tag{7.4}$$

Here $\Theta(E)$ denotes the Heaviside theta function. This is the density of states that is dual to standard Liouville theory with only the cosmological constant term in the action turned on. See, for example, [258] for an explicit family of potentials that lead to the density of states (7.4) in the double scaling limit. Here, e^{S_0} is the genus counting parameter after taking the double-scaling limit and κ is an arbitrary energy scale.

Using the relationship between the form of the density of states and the spectral curve, we conclude that the spectral curve is given by [264, 250]

$$y(z) = \sin\left(p \arcsin \frac{z}{\sqrt{2\kappa}} \right) = (-1)^{\frac{p-1}{2}} T_p\left(\frac{z}{\sqrt{2\kappa}} \right) , \tag{7.5}$$

where T_p denotes the p-th Chebyshev-T polynomial. One way to see this is to note that the leading density of states $\langle \rho(E) \rangle^{(0)}$ is determined from the spectral curve as $\langle \rho(E) \rangle^{(0)} = -i\pi^{-1} e^{S_0} y(i\sqrt{E})$ for $E > 0$. It is also a standard result in one-matrix integrals that the derivative $V'_{\text{eff}}(E)$ of the one-eigenvalue effective potential $V_{\text{eff}}(E)$, that includes contributions from both the potential V that appears in (7.3) and the Vandermonde determinant, is proportional to $y(\sqrt{-E})$ in the forbidden region $E < 0$ (see, for example, [245] for a recent exposition). The precise relationship is

$$V'_{\text{eff}}(E) = e^{S_0} \left(-2y\left(\sqrt{-E} \right) \right) \qquad (\text{for } E < 0) \,. \tag{7.6}$$

Integrating this using (7.5) and taking $V_{\text{eff}}(E = 0) = 0$ we get, for $E < 0$ that

$$V_{\text{eff}}(E) = -2\, e^{S_0}\, \kappa \left[\frac{1}{p+2} \sin\left((p+2) \arcsin \sqrt{\frac{-E}{2\kappa}} \right) - \frac{1}{p-2} \sin\left((p-2) \arcsin \sqrt{\frac{-E}{2\kappa}} \right) \right] \tag{7.7}$$

$$= 2\, e^{S_0}\, \kappa\, (-1)^{\frac{p-1}{2}} \left[\frac{1}{p+2} T_{p+2}\left(\sqrt{\frac{-E}{2\kappa}} \right) - \frac{1}{p-2} T_{p-2}\left(\sqrt{\frac{-E}{2\kappa}} \right) \right] . \tag{7.8}$$

Let us now look at the extrema of the one-eigenvalue effective action. From (7.6) and (7.5), we see that as we move towards negative energies starting at $E = 0$, the first zero of $V'_{\text{eff}}(E)$ occurs at

$$E^\star = -2\kappa \sin^2 \frac{\pi}{p} \,. \tag{7.9}$$

[2]To get to the density of states in JT gravity, we need to take $\kappa \sim p^2$ as $p \to \infty$ [245].

We record the values of $V_{\text{eff}}(E^\star)$ and $V''_{\text{eff}}(E^\star)$, which are obtained from (7.7) and (7.6) using (7.5):

$$V_{\text{eff}}(E^\star) = e^{S_0}\kappa\,\frac{4p\sin(2\pi/p)}{p^2-4}\,, \tag{7.10}$$

$$V''_{\text{eff}}(E^\star) = -e^{S_0}\kappa^{-1}\frac{p}{\sin(2\pi/p)}\,. \tag{7.11}$$

Now we organize various contributions to the integral (7.3) depending on how many eigenvalues are in the classically allowed region $E > 0$ and how many are in the classically forbidden region $E < 0$. The leading contribution $\mathfrak{Z}^{(0)}$ comes from the integration region where all eigenvalues are in the classically allowed region. The next important contribution $\mathfrak{Z}^{(1)}$ comes from the integration region when only one eigenvalue is in the forbidden region. Next, we borrow a couple of results from [245, 252, 253, 255], which in the notations of [245] are as follows:

$$\frac{\mathfrak{Z}^{(1)}}{\mathfrak{Z}^{(0)}} = \int_F \mathrm{d}E\,\langle\rho(E)\rangle\,, \tag{7.12}$$

$$\langle\rho(E)\rangle = \frac{1}{-8\pi E}\exp(-V_{\text{eff}}(E)) \quad \text{for } E<0\,. \tag{7.13}$$

Here the subscript F on the integral denotes integration over the classically forbidden region $E < 0$. The formula (7.13) captures the small amount of quantum mechanical leakage of eigenvalues into the classically forbidden region.[3]

We now plug in (7.13) into (7.12) and use the saddle point approximation about $E^\star$ to compute the integral (along a contour to be specified momentarily):

$$\frac{\mathfrak{Z}^{(1)}}{\mathfrak{Z}^{(0)}} = \frac{1}{-8\pi E^\star}\exp\left(-V_{\text{eff}}(E^\star)\right)\int \mathrm{d}E\,\exp\left[\frac{1}{2}\left|V''_{\text{eff}}(E^\star)\right|(E-E^\star)^2\right] \tag{7.14}$$

$$= \frac{1}{-8\pi E^\star}\exp\left(-V_{\text{eff}}(E^\star)\right)\times\frac{\mathrm{i}}{2}\sqrt{\frac{2\pi}{|V''_{\text{eff}}(E^\star)|}}\,. \tag{7.15}$$

It is important to note from (7.11) that $V''_{\text{eff}}(E^\star) < 0$ and thus the steepest descent contour is parallel to the imaginary-E axis. Furthermore, we only integrate over half of the steepest descent contour, since, in the perturbative region $E \gg \kappa$, the defining contour must lie along the real axis [245]. Figure 7.1 shows this contour. On the string theory side, this "unstable mode" is the open string tachyon and one has a similar contour of integration over the tachyon mode [257].[4] These facts give us the factor of $i/2$ in the gaussian integral.[5]

[3] As commented upon in [245], the expression for V_{eff} in (7.8) is negative for certain intervals on the negative real axis. However, in the regime $E \in [E^\star, 0]$, with $E^\star$ as in (7.9), this issue does not arise, and this interval is all that we will need. See the discussion of the integration contour below.

[4] In fact, such a contour is common in decay rate computations using bounce solutions. See, for example, [261].

[5] Since we are only interested in computing the imaginary part, we don't need to worry about the part of the contour along the real axis, which contributes something real.

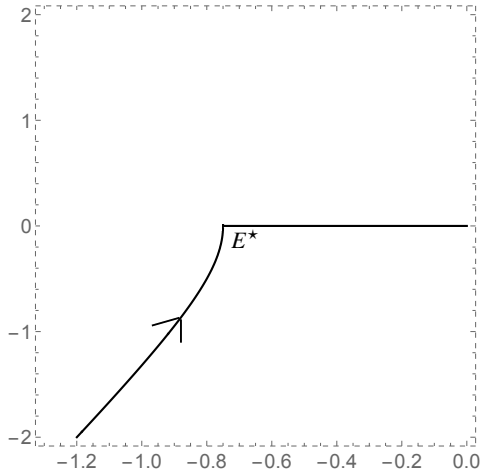

Figure 7.1: The contour of integration for the eigenvalues showing that we only need to include "half" of the steepest descent contour for the instanton saddle point. We have shown the numbers for the case $p = 3$ with $\kappa = \frac{1}{2}$ but it is qualitatively similar for all p. In string theory, the integration contour for the open string tachyon also looks like this.

Comparing (7.15) to (7.1) and using equations (7.9), (7.10) and (7.11), we get

$$T = V_{\rm eff}(E^\star) = e^{S_0}\kappa\,\frac{4p\sin(2\pi/p)}{p^2-4}\,, \tag{7.16}$$

$$\mathcal{N} = e^{-\frac{S_0}{2}}\kappa^{-\frac{1}{2}}\,\frac{\mathrm{i}}{16\sqrt{\pi}}\,\sqrt{\frac{\cos(\pi/p)}{p\sin^3(\pi/p)}}\,. \tag{7.17}$$

As explained in the introduction, it is natural to factor out $T^{-\frac{1}{2}}$ from the expression for $\mathcal{N}$, and so we write the above result as

$$\mathcal{N} = T^{-\frac{1}{2}}\,\frac{\mathrm{i}}{\sqrt{32\pi}}\,\frac{\cot(\pi/p)}{\sqrt{p^2-4}}\,. \tag{7.18}$$

Refs. [251, 252, 253, 254] contain this result for $p = 3$, while the result for general p can be found in [255].[6] Ref. [245] was interested in the limit $p \to \infty$.

We would like to explain one subtlety in the above analysis. One can explicitly check that the effective potential given in equation (7.8) has $(p-1)/2$ extrema on the negative-E axis. Roughly half of them are maxima and half are minima. The extremum at $E^\star$ in (7.9) is the one closest to the origin and is a local maximum. However, even among the local

[6]Note that some of these references are computing an integral over the full steepest contour through the saddle point, and others are including contributions from both ends of the eigenvalue cut, and thus the pre-factors quoted there are a multiple of the value in (7.18).

maxima, this is not the one with the smallest value of the effective potential, in general. This raises the question of why we have chosen the saddle point $E^\star$ in (7.9) as the relevant saddle. The point is that we want the perturbation series of the matrix integral to match with the vacuum string perturbation theory, and so we should not allow the integration contour for the matrix eigenvalues to pass through regions on the real axis with $V_{\rm eff} < 0$, since these regions will give real contributions to the matrix integral that are much larger than the terms in perturbation theory around the saddle point (7.4). This can be avoided by turning the integration contour along the steepest descent contour once it reaches E^*.

7.3 String Theory Computation

In this section we shall describe the string theory computation of the leading imaginary part of the partition function, arising from a single ZZ-instanton contribution.

The string theory that is dual to the double-scaled one-matrix integral described in Section 7.2 is Liouville theory coupled to the $(2, p)$ minimal model and the bc-ghost system. The b parameter that appears in the Liouville lagrangian is determined by p and is such that the total central charge of Liouville, the matter CFT and ghosts adds up to zero. One finds $b = \sqrt{2/p}$.

The cylinder diagram and its divergences

We shall begin by describing some general issues that arise in the analysis of the cylinder diagram with boundaries lying on a D-instanton (whose analog in non-critical string theory is the ZZ instanton). We can express the cylinder partition function in the open string channel as:

$$A = \int_0^\infty \frac{\mathrm{d}t}{2t} F(t)\,, \tag{7.19}$$

where $F(t)$ has the structure

$$F(t) = \sum_b e^{-2\pi h_b t} - \sum_f e^{-2\pi \hat{h}_f t}\,, \tag{7.20}$$

with h_b and $\hat{h}_f$ being the L_0 eigenvalues of the bosonic and fermionic states of the open string with any ghost number and subject to the Siegel gauge condition. A state $|\chi\rangle$ is said to satisfy the Siegel gauge condition if

$$b_0|\chi\rangle = 0 \quad \text{(Siegel gauge condition)}. \tag{7.21}$$

The states are taken to be fermionic if they carry even ghost number and bosonic if they carry odd ghost number – this is the correct assignment of statistics when we regard the coefficients of these states as modes of the open string field on the D-instanton. The Siegel gauge condition (7.21) is needed, since without this condition there will be an equal number

of bosonic and fermionic states related by the action of the ghost zero modes b_0 or c_0, and the partition function will vanish. The way this gets implemented in the worldsheet computation is via the insertion of b_0c_0 to soak up the ghost zero modes on the cylinder [265].

In theories of interest to us, the integral (7.19) has no divergence in the $t \to 0$ limit, indicating that the (regulated) number of fermionic and bosonic states are equal. In the hypothetical situation where h_b and $\hat{h}_f$ are all positive, there are no divergences in the $t \to \infty$ limit either, and A is given by

$$A = \frac{1}{2} \ln \frac{\prod_f \hat{h}_f}{\prod_b h_b} \,. \tag{7.22}$$

For positive $h_b, \hat{h}_f$ this can be used to express the normalization factor $\mathcal{N}$ accompanying the instanton amplitude as an integral,

$$\begin{aligned} \mathcal{N} = e^A &= \left(\frac{\prod_f \hat{h}_f}{\prod_b h_b} \right)^{\frac{1}{2}} = \frac{\prod'_f \hat{h}_f}{\prod_b h_b^{1/2}} \\ &= \int \prod_b \frac{\mathrm{d}\phi_b}{\sqrt{2\pi}} {\prod_f}' \mathrm{d}p_f \mathrm{d}q_f \, \exp\left[-\frac{1}{2} \sum_b h_b \phi_b^2 - {\sum_f}' \hat{h}_f p_f q_f \right] , \end{aligned} \tag{7.23}$$

where ϕ_b are grassmann even variables and p_f, q_f are grassmann odd variables. The prime on the summation and the product symbols indicate that, since $\hat{h}_f$'s occur in pairs,[7] we let the sum and product over f run over half the number of original variables, and for each f introduce a pair of grassmann odd variables p_f, q_f. The final expression in (7.23) may be regarded as the path integral over open string fields in Siegel gauge, with the understanding that open string fields live on the zero dimensional worldvolume of the D-instanton and therefore are just ordinary variables. Our conventions for the open string field action are described at the end of this section.

As long as h_b and $\hat{h}_f$ are positive, (7.19), (7.22) and (7.23) are all well defined and are identically equal. However in most situations, some of the h_b's are negative or zero, and some of the $\hat{h}_f$'s may vanish. In that case (7.19) and (7.22) are ill-defined. The final expression in (7.23) is also ill-defined but we can try to make sense of this using insights from string field theory. We shall now describe this procedure.

First we note that, for $h_b, h_f > 0$, we can pick any non-negative integer n and write

[7] This can be seen as follows. For any choice of basis states $\{|a\rangle\}$ for Siegel gauge states with a fixed L_0 eigenvalue, $\langle a|c_0|b\rangle$ gives a non-degenerate inner product matrix. Since this inner product pairs states of ghost number n and $(2-n)$, we see that for every n other than $n = 1$, the L_0 eigenvalues occur in pairs in sectors with ghost numbers n and $(2-n)$. Since fermions arise from even ghost number sector, the $\hat{h}_f$'s always occur in pairs.

State	L_0 eigenvalue	Ghost number	In Siegel gauge?	Field name	Grassmann parity of field
$c_1\|0\rangle$	-1	1	Yes	ϕ_1	even
$c_0c_1\|0\rangle$	-1	2	No	-	odd
$\|0\rangle$	0	0	Yes	p_1	odd
$c_0\|0\rangle$	0	1	No	ψ	even
$c_1c_{-1}\|0\rangle$	0	2	Yes	q_1	odd
$c_0c_1c_{-1}\|0\rangle$	0	3	No	-	even

Table 7.1: A list of states that are relevant for the discussion of divergences in the cylinder diagram. We have ordered the states first by their L_0 eigenvalues and then by their ghost numbers. A state and the corresponding field appear multiplied together in the expansion of the open string field as $|\Psi\rangle = \phi_1 c_1|0\rangle + \ldots$.

hybrid expressions for A and $\mathcal{N}$ as

$$\begin{aligned} A &= \int_0^\infty \frac{\mathrm{d}t}{2t}\left[F(t) - \sum_{b=1}^{2n} e^{-2\pi t h_b} + \sum_{f=1}^{2n} e^{-2\pi t \hat{h}_f}\right] + \int_0^\infty \frac{\mathrm{d}t}{2t}\left[\sum_{b=1}^{2n} e^{-2\pi t h_b} - \sum_{f=1}^{2n} e^{-2\pi t \hat{h}_f}\right] \\ &= \int_0^\infty \frac{\mathrm{d}t}{2t}\left[F(t) - \sum_{b=1}^{2n} e^{-2\pi t h_b} + \sum_{f=1}^{2n} e^{-2\pi t \hat{h}_f}\right] + \frac{1}{2}\log\left[\frac{\prod_{f=1}^{2n}\hat{h}_f}{\prod_{b=1}^{2n} h_b}\right], \end{aligned} \tag{7.24}$$

$$\begin{aligned} \mathcal{N} = e^A = \exp&\left[\int_0^\infty \frac{\mathrm{d}t}{2t}\left[F(t) - \sum_{b=1}^{2n} e^{-2\pi t h_b} + \sum_{f=1}^{2n} e^{-2\pi t \hat{h}_f}\right]\right] \\ &\times \int \prod_{b=1}^{2n} \frac{\mathrm{d}\phi_b}{\sqrt{2\pi}} \prod_{f=1}^{n} dp_f dq_f \exp\left[-\frac{1}{2}\sum_{b=1}^{2n} h_b \phi_b^2 - \sum_{f=1}^{n} \hat{h}_f p_f q_f\right]. \end{aligned} \tag{7.25}$$

Now, when some of the h_b's or $\hat{h}_f$'s are negative or zero, we shall choose n to be such that for $b, f > 2n$ all the h_b's and $\hat{h}_f$'s are positive. Then the term in the first line of (7.25) is finite since we have subtracted the 'bad' contributions involving $h_b, \hat{h}_f \le 0$ terms from $F(t)$. Furthermore, since the subtraction term vanishes as $t \to 0$, the integral is free of divergences from the $t \to 0$ end as well. Thus, we are left with the goal of making sense of the integral over the modes ϕ_b for $b \le 2n$ and p_f, q_f for $f \le n$.

For the D-instantons that we shall discuss, the bad modes consist of one bosonic mode – the tachyon mode ϕ_1 corresponding to the state $c_1|0\rangle$ with $h_b = -1$, and a pair of fermionic modes p_1, q_1 corresponding to the states $i|0\rangle$ and $ic_1c_{-1}|0\rangle$ with $\hat{h}_f = 0$. The coefficients i in these states have been chosen to ensure that the modes multiplying these states are real. Since there is only one bad bosonic mode and two bad fermionic modes, we can choose $n = 1$

in (7.25). See Table 7.1 for a list of the states that are relevant for the discussion and their basic properties.

First we shall discuss the integration over the bosonic modes ϕ_1 and ϕ_2. Since $h_2 > 0$, the integration over ϕ_2 gives a standard gaussian integral. The integration over ϕ_1 is problematic since the exponent takes the form $\exp(\phi_1^2/2)$. We shall carry out this integral by regarding this as a contour integral in the complex ϕ_1 plane as follows[257]. Since the vacuum without any D-instanton is represented by a particular solution of the open string field theory corresponding to some positive value β of ϕ_1, the integration contour must pass through β. For this reason we take the integration contour to lie along the positive real axis for $\mathrm{Re}\,[(]\,\phi_1) > 0$. However once we reach $\phi_1 = 0$, we take the contour to be along (half of) the steepest descent contour – either from $-\mathrm{i}\infty$ to 0, or from $\mathrm{i}\infty$ to 0. The integration along the real axis is real and can be regarded as the perturbative contribution since the contour passes through the perturbative vacuum. The leading imaginary part comes from the part of the contour from $\pm\mathrm{i}\infty$ to 0. These two choices differ by a sign – an ambiguity that is also present in the matrix model. Choosing the contour to be from $-\mathrm{i}\infty$ to 0 for definiteness, we can write (the leading imaginary part of) the bosonic part of the integral as:

$$\int_{-\mathrm{i}\infty}^{0} \frac{\mathrm{d}\phi_1}{\sqrt{2\pi}} e^{\phi_1^2/2} \int_{-\infty}^{\infty} \frac{\mathrm{d}\phi_2}{\sqrt{2\pi}} e^{-h_2\phi_2^2/2} = \frac{\mathrm{i}}{2} h_2^{-1/2}\,. \tag{7.26}$$

Next we turn to integration over the fermion zero modes p_1, q_1. We can get physical insight into the origin of these modes if, instead of a D-instanton, we consider a Dp-brane extending along some directions in space-time in any bosonic string theory. In that case the gauge field $a_\mu(k)$ living on the brane appears in the expansion of the open string field as a term proportional to $\int \mathrm{d}^{p+1}k\, a_\mu(k)\alpha_{-1}^\mu c_1|k\rangle$ where α_n^μ are the oscillators associated with the scalars X^μ describing coordinates tangential to the brane and $|k\rangle = e^{ik\cdot X(0)}|0\rangle$ are momentum carrying states. In string field theory, gauge transformations appear as BRST exact states $Q_B|\Lambda\rangle$ (plus higher order terms), and $|\Lambda\rangle$ is referred to as the "gauge transformation parameter". For instance, usual spacetime gauge transformations of the gauge field $\delta a_\mu(k) \propto ik_\mu\theta(k)$ appear via the term $i\int \mathrm{d}^{p+1}k\,\theta(k)|k\rangle$ in $|\Lambda\rangle$. Note that this term in $|\Lambda\rangle$ has ghost number zero. Then the linearized gauge transformation $Q_B|\Lambda\rangle$ produces a term proportional to $\mathrm{i}\int \mathrm{d}^{p+1}k\,\theta(k)k_\mu\alpha_{-1}^\mu c_1|k\rangle$. Comparing to the state representing the gauge field, we see that this generates the usual gauge transformation law $\delta a_\mu(k) \propto \mathrm{i}\,k_\mu\theta(k)$.

The gauge transformation $Q_B|\Lambda\rangle$ also produces a state proportional to $\mathrm{i}\int \mathrm{d}^{p+1}k\,\theta(k)k^2 \times c_0|k\rangle$. This translates to a transformation $\delta\psi(k) \propto k^2\theta(k)$ where $\psi(k)$ is the field multiplying the state $ic_0|k\rangle$. The Siegel gauge choice corresponds to setting $\psi(k) = 0$. This produces a Jacobian proportional to k^2, which is represented by a pair of Fadeev-Popov ghosts $p_1(k)$, $q_1(k)$ multiplying the states $ic_1c_{-1}|k\rangle$ and $i|k\rangle$. Since these states have conformal weight $\hat{h}_1 = k^2$, integration over p_1 and q_1 will precisely produce the required Fadeev-Popov determinant k^2, for $k \neq 0$.

Now, the issue is that, on a D-instanton we have $k = 0$. Thus, neither the "gauge field" nor the field ψ multiplying $ic_0|0\rangle$ transforms, showing that the Siegel gauge choice breaks

down. This is a reflection of the fact that the usual local U(1) symmetry on the Dp-brane becomes a rigid symmetry on the D-instanton. The remedy is to go back to the "original" form of the path integral where we carry out integration over all the "classical" modes of the theory and explicitly divide by the volume of the gauge group. In string field theory language, fields that multiply states of ghost number one are referred to as classical since the physical open string states belong to this sector. Concretely, among the states in table 7.1, this means that instead of integrating over $\{\phi_1, p_1, q_1\}$, we integrate over $\{\phi_1, \psi\}$ and divide by the volume of gauge group. The precise normalization of the integration measure can be fixed by carefully following the line of argument described above and gives the replacement rule[257]:

$$\int \mathrm{d}p_1 \mathrm{d}q_1 \quad \longrightarrow \quad \frac{\int \mathrm{d}\psi\, e^{-\psi^2}}{\int \mathrm{d}\theta} = \frac{\sqrt{\pi}}{\int \mathrm{d}\theta}\,. \tag{7.27}$$

The $-\psi^2$ in the exponent is the result of evaluating the open string field theory action for the out-of-Siegel-gauge grassmann-even mode ψ,[8] . The quantity θ can be related to the rigid U(1) symmetry paramater $\tilde{\theta}$, under which an open string with one end on the instanton picks up a phase $e^{i\tilde{\theta}}$, by comparing the string field theory gauge transformation to the rigid U(1) transformation. For canonically normalized fields and gauge transformation parameters, the transformation law of a charged field Φ is proportional to $ig_o\,\theta\,\Phi$, as in conventional quantum field theories. Here g_o is defined to be the coefficient of the cubic term in the open string field theory action, with conventions as described at the end of this section. This should be equated to the transformation law $\delta\Phi = \mathrm{i}\,\tilde{\theta}\,\Phi$ under infinitesimal rigid U(1) transformation. A detailed calculation of the constant appearing in the string field theory gauge transformation law leads to $\theta = \tilde{\theta}/g_o$[257]. On the other hand, the open string coupling g_o is related to the instanton action T via $g_o = (2\pi^2 T)^{-\frac{1}{2}}$.[9] Therefore we have

$$\int \mathrm{d}\theta = g_o^{-1} \int \mathrm{d}\tilde{\theta} = 2\pi g_o^{-1} = 2^{\frac{3}{2}}\pi^2 T^{\frac{1}{2}}\,, \tag{7.28}$$

since $\tilde{\theta}$ has period 2π.

Substituting (7.26), (7.27) and (7.28) into (7.25) we get:

$$\mathcal{N} = \exp\left[\int_0^\infty \frac{\mathrm{d}t}{2t}\left[F(t) - \left(e^{2\pi t} + e^{-2\pi h t} - 2\right)\right]\right] \times \mathrm{i}\,2^{-\frac{5}{2}}\pi^{-\frac{3}{2}}\,h^{-\frac{1}{2}}\,T^{-\frac{1}{2}}, \tag{7.29}$$

where $h = h_2$. One can easily check that the expression is independent of h by taking derivative with respect to h. Therefore we do not need to choose $h = h_2$, any choice of $h > 0$ will give the same result.

[8] The generalization of this term to a Dp-brane would be $-\int \mathrm{d}^{p+1}x\,(\psi + \gamma\,\partial_\mu a^\mu)^2$, where the constant γ is chosen such that the combination $\psi + \gamma\,\partial_\mu a^\mu$ is gauge invariant.

[9] There are many ways to derive this result, but the one that holds universally is from the observation that the tachyon vacuum solution in open string field theory has action $T - (2\pi^2 g_o^2)^{-1}$ [266, 267]. Since this describes the vacuum, we must equate this to zero, leading to $T = (2\pi^2 g_o^2)^{-1}$.

Specialization to minimal string theory

We shall now use (7.29) to compute the normalization of the instanton amplitude in the $(2,p)$ minimal string theory. The form of the integrand $F(t)$ for the cylinder diagram in minimal string theory is well-known [249]. Since we are studying the cylinder diagram, we need to specify boundary conditions for the worldsheet fields. For the Liouville CFT, we pick the "$(m,n)=(1,1)$" ZZ boundary condition [143], as this is the one that corresponds to the saddle point $E^\star$ in equation (7.9) in the matrix integral [250, 259]. For the matter CFT, we pick the Cardy state on both ends so that the open string channel only contains the identity character [268].[10]

Let t be the modulus of the cylinder that corresponds to time in the open string channel and let $q=e^{-2\pi t}$. The partition function of Liouville theory on the cylinder with $(m,n)=(1,1)$ ZZ boundary conditions on both ends is [143]

$$Z_{\text{Liouville}}(t) = \left(q^{-1}-1\right) q^{-\frac{1}{4}(b^{-1}-b)^2}\,\eta(it)^{-1} = \left(q^{-1}-1\right) q^{-\frac{(p-2)^2}{8p}}\,\eta(it)^{-1}\,. \tag{7.30}$$

The partition function of the matter CFT with the given boundary conditions equals the identity character in the minimal models, which is given by [269, 270]

$$Z_{\text{matter}}(t) = \eta(it)^{-1}\sum_{k=-\infty}^{\infty}\left(q^{\frac{(4pk+p-2)^2}{8p}} - q^{\frac{(4pk+p+2)^2}{8p}}\right)\,. \tag{7.31}$$

Multiplying the contribution $\eta(it)^2$ from the ghosts (see, for example, [265]), we find

$$F(t) = \left(e^{2\pi t}-1\right)\sum_{k=-\infty}^{\infty}\left(e^{-2\pi t k(2pk+p-2)} - e^{-2\pi t(pk+1)(2k+1)}\right)\,. \tag{7.32}$$

It is important to note that the leading terms in $F(t)$ as $t\to\infty$ are the ones with $k=0$:

$$F(t) = \left(e^{2\pi t}-1\right)\left(1-e^{-2\pi t}+O(e^{-4\pi t})\right) = e^{2\pi t}-2+O(e^{-2\pi t})\,. \tag{7.33}$$

As discussed earlier, the $e^{2\pi t}$ term arises from the open string tachyon, while the -2 arises from the two ghost zero modes.[11]

If we substitute (7.32) into (7.29) and choose $h=1$, we can see that the $k=0$ term in the sum exactly cancels the subtraction term $(e^{2\pi t}+e^{-2\pi t}-2)$. The rest of the terms may be analyzed using the general result:

$$\int_0^\infty \frac{\mathrm{d}t}{2t}\left(e^{-2\pi h_1 t}-e^{-2\pi h_2 t}\right) = \frac{1}{2}\ln\frac{h_2}{h_1}\,. \tag{7.34}$$

[10]For the $(2,p)$ minimal string, there are $(p-1)/2$ possible ZZ brane boundary conditions [264]. By comparing the relative tensions of these branes (given in, for example, [250]), to the relative heights of the extrema of the matrix effective potential (7.8), one can establish that it is the $(m,n)=(1,1)$ ZZ brane, with identity character from the matter CFT, that corresponds to the matrix saddle point at $E^\star$ in (7.9) with $V_{\text{eff}}(E^\star)$ as in (7.16).

[11]In the $c=1$ case, we have $F(t)=e^{2\pi t}-1$ exactly. The change of coefficient in the $L_0=0$ sector comes from an additional bosonic zero mode that corresponds to time translations of the D-instanton [25, 257].

Using this we can rewrite (7.29) as

$$\begin{aligned}\mathcal{N} &= \mathrm{i}\, 2^{-\frac{5}{2}}\pi^{-\frac{3}{2}}T^{-\frac{1}{2}} \prod_{\substack{k=-\infty\\ k\neq 0}}^{\infty}\left[\frac{(pk+1)(2k+1)-1}{k(2pk+p-2)-1}\,\frac{k(2pk+p-2)}{(pk+1)(2k+1)}\right]^{\frac{1}{2}} \\ &= \mathrm{i}\, 2^{-\frac{5}{2}}\pi^{-\frac{3}{2}}T^{-\frac{1}{2}}\left[\prod_{\substack{k=-\infty\\ k\neq 0}}^{\infty}\frac{1-\frac{4}{p^2(2k+1)^2}}{1-\frac{1}{p^2k^2}}\right]^{\frac{1}{2}}.\end{aligned} \tag{7.35}$$

We now use

$$\sin\pi x = \pi x\prod_{k=1}^{\infty}\left(1-\frac{x^2}{k^2}\right), \quad \cos\pi x = \frac{\sin 2\pi x}{2\sin\pi x} = \prod_{k=1}^{\infty}\left(1-\frac{4x^2}{(2k-1)^2}\right) \tag{7.36}$$

to write

$$\cot\frac{\pi}{p} = \frac{p}{\pi}\prod_{k=1}^{\infty}\frac{1-\frac{4}{p^2(2k-1)^2}}{1-\frac{1}{p^2k^2}}\,. \tag{7.37}$$

Using this it is easy to see that product over terms in (7.35) for $k<0$ produces $\frac{\pi}{p}\cot\frac{\pi}{p}$. For positive k, (7.35) is missing the $1-4/p^2$ term from the cosine infinite product in (7.36). Thus the infinite product term in (7.35) produces

$$\frac{\pi}{p}\cot\frac{\pi}{p}\times\frac{1}{1-\frac{4}{p^2}}\times\frac{\pi}{p}\cot\frac{\pi}{p} = \frac{\pi^2}{p^2-4}\cot^2\frac{\pi}{p}\,. \tag{7.38}$$

Using this result in (7.35) yields

$$\mathcal{N} = T^{-\frac{1}{2}}\,\frac{\mathrm{i}}{\sqrt{32\pi}}\,\frac{\cot(\pi/p)}{\sqrt{p^2-4}}\,, \tag{7.39}$$

in perfect agreement with the matrix integral result (7.18).

Conventions for the open string field theory action

Let us denote by $|\Psi\rangle$ the open string field which takes the form

$$|\Psi\rangle = \phi_1 c_1|0\rangle + \mathrm{i}\psi c_0|0\rangle + \ldots \tag{7.40}$$

The vacuum state is normalized so that

$$\langle 0|c_{-1}c_0c_1|0\rangle = 1\,. \tag{7.41}$$

Our starting point is the path integral over fields with ghost number one, divided by the volume of the gauge group. In the string field theory literature, the fields with ghost number

one are known as "classical" fields since the physical open string states belong to this sector. We take the weight in the path integral to be $\exp(-S)$ with the quadratic part of the action being

$$S = \frac{1}{2}\langle\Psi|Q_B|\Psi\rangle\,. \tag{7.42}$$

The BRST charge Q_B is given by

$$Q_B = \oint \frac{\mathrm{d}z}{2\pi\mathrm{i}}\,(c\,T_m + :b\,c\,\partial c:)\,, \tag{7.43}$$

where T_m is the matter stress tensor. There is also a cubic term in the action[271]. See for example, [266] for a detailed form of this coupling. If we normalize the string field so that the kinetic term is independent of the coupling as in (7.42), then the cubic term has an explicit factor of the open string coupling g_o.

From the above equations, one can see, for example, that the contribution of the tachyon field ϕ_1 to the quadratic action is

$$S \supset \frac{1}{2}\langle 0|\phi_1 c_{-1}\,Q_B\,\phi_1 c_1|0\rangle = -\frac{1}{2}\phi_1^2\,, \tag{7.44}$$

and thus the weight in the path integral is $\exp(\phi_1^2/2)$. The action for ψ is similarly seen to be ψ^2.

7.4 Generalization to (p', p) Models

A more general class of minimal string models is Liouville theory coupled to the (p', p) minimal model and the bc-ghost system. Here p and p' are relatively-prime integers with $p > p' \geq 2$. The b parameter of Liouville theory is determined by the requirement that the total central charge vanishes; the result is $b = \sqrt{p'/p}$.

The Liouville sector admits ZZ boundary conditions labeled by two integers (m, n) [143]. We leave a general analysis to future work, but for illustration purposes, we note here that the computation in Section 7.3 can be extended to the (p', p) minimal string with the same boundary conditions. That is, we pick the $(m, n) = (1, 1)$ ZZ state for Liouville, and for the matter CFT, we pick the Cardy state on both ends so that the open string channel only contains the identity character [268]. This gives the partition functions [143, 269, 270]

$$Z_{\text{Liouville}}(t) = \left(q^{-1} - 1\right) q^{-\frac{(p-p')^2}{4pp'}}\,\eta(it)^{-1}\,, \tag{7.45}$$

$$Z_{\text{matter}}(t) = \eta(it)^{-1} \sum_{k=-\infty}^{\infty} \left(q^{\frac{(2pp'k+p-p')^2}{4pp'}} - q^{\frac{(2pp'k+p+p')^2}{4pp'}} \right)\,. \tag{7.46}$$

Combining the Liouville, matter and ghost contributions to $F(t)$, using (7.29), and following the same steps as earlier, we get

$$\begin{aligned}
\mathcal{N} &= \mathrm{i}\, 2^{-\frac{5}{2}}\pi^{-\frac{3}{2}}T^{-\frac{1}{2}} \prod_{\substack{k=-\infty\\ k\neq 0}}^{\infty} \left[\frac{(pk+1)(p'k+1)-1}{k(pp'k+p-p')-1}\,\frac{k(pp'k+p-p')}{(pk+1)(p'k+1)}\right]^{1/2} \\
&= \mathrm{i}\, 2^{-\frac{5}{2}}\pi^{-\frac{3}{2}}T^{-\frac{1}{2}} \prod_{k=1}^{\infty}\left[\left(1-\frac{1}{k^2}\left(\frac{1}{p}-\frac{1}{p'}\right)^2\right)\left(1-\frac{1}{k^2}\left(\frac{1}{p}+\frac{1}{p'}\right)^2\right)\right. \\
&\qquad\qquad \left.\times\left(1-\frac{1}{k^2p^2}\right)^{-2}\left(1-\frac{1}{k^2p'^2}\right)^{-2}\right]^{\frac{1}{2}} \qquad (7.47)\\
&= T^{-\frac{1}{2}}\,\frac{i}{\sqrt{32\pi}}\left[\frac{\sin\left(\frac{\pi}{p}+\frac{\pi}{p'}\right)\sin\left(\frac{\pi}{p'}-\frac{\pi}{p}\right)}{\sin^2(\pi/p)\sin^2(\pi/p')\,(p^2-p'^2)}\right]^{\frac{1}{2}} \\
&= T^{-\frac{1}{2}}\,\frac{i}{\sqrt{32\pi}}\sqrt{\frac{\cot^2(\pi/p)-\cot^2(\pi/p')}{p^2-p'^2}}\,.
\end{aligned}$$

This agrees with (7.39) when $p'=2$.

For $p>p'\geq 3$, these string theories are dual to the double-scaled limit of a two-matrix integral [272, 273]. The two-matrix integral is more complicated, so we won't go into the full analysis of the eigenvalue instanton in this case [260, 256], and just note that the result (7.47) agrees with the $m=n=1$ expression given in [256].[12] We leave a fuller investigation of the two-matrix case to future work.

[12]In carrying out this comparison, following the comment in footnote 6, we have divided the result of [256] by two. However, since the saddle point corresponding to $m=n=1$ is not the dominant saddle point in general, we need to carefully analyze the full integration contour to figure out how the steepest descent contour fits in. Since this issue exists both in the matrix model and in string theory, we expect any additional factor to affect both sides in the same way. Hence it should not affect the comparison.

Chapter 8

Multi-instantons in Minimal String Theory and in Matrix Integrals

8.1 Introduction

Minimal string theories are toy models of string theory where the worldsheet CFT consists of a minimal model, the Liouville field and the bc ghosts [244, 274]. These theories admit a dual description in terms of double-scaled matrix integrals [244]. An insight from these toy models that generalizes to even critical superstring theory is the existence of "D-instanton" effects, which are nonperturbative effects of order $\exp(-A\, g_s^{-1})$ [246, 248, 247] for some constant A, rather than $\exp(-A\, g_s^{-2})$ that might be expected from field theory considerations. Here g_s is the closed string coupling. In minimal string theory, these objects were later identified as ZZ branes [143]. From the perspective of the matrix integral, these nonperturbative effects correspond to one-eigenvalue instantons [246].

Motivated by the study of instanton effects in the $c = 1$ string theory [25, 275, 257, 276], as well as critical (superstring) theories [277, 278, 279, 280, 281], in our previous work [23] we used tools from string field theory to compute the normalization constant that multiplies these instanton contributions to various physical quantities. In particular, the genus expansion of the free energy F reads

$$F = \sum_{g=0}^{\infty} F_g\, g_s^{-2+2g} + \mathcal{N} \exp\left(-A\, g_s^{-1}\right) + \dots \tag{8.1}$$

and we are interested in computing the constant $\mathcal{N}$. We have indicated the perturbative contribution and one particular instanton contribution. The dots indicate other nonperturbative corrections. Physically, Ag_s^{-1} is the tension of the ZZ brane and $\mathcal{N}$ is the exponential of the annulus diagram. The annulus diagram between two ZZ branes is known [143, 249, 250], but, unfortunately, is ill-defined when the two boundaries of the annulus lie on the same ZZ brane. The dual matrix integral, on the other hand, predicts a finite value for $\mathcal{N}$ [248, 252, 255, 253, 254, 256, 282, 283, 245]. In [23], we resolved this tension by noting that

the exponentiated ZZ annulus is, in fact, finite. This is done by identifying the source of the divergence as a pair of Majorana zero modes, which are zero modes because Siegel gauge breaks down in the presence of D-instantons [257]. In particular, this happens because the usual $U(1)$ gauge symmetry on the worldvolume of D-branes is a rigid $U(1)$ symmetry in the case of D-instantons. Reverting back to a non gauge-fixed form of the path integral then yields meaningful results which agree with the matrix integral [257, 23].

Since the perturbation series given in (8.1) is not Borel summable, the significance of non-perturbative instanton corrections is not a priori clear. In [23] we addressed this issue by noting that while the coefficients F_g are all real, the normalization constant $\mathbb{N}$ is purely imaginary. Therefore instanton corrections give the leading imaginary contribution to the free energy, and this can be reliably computed using D-instanton physics. In this chapter, we shall take a somewhat different point of view that was already present in the early papers on this subject, for example in [252]. In the matrix model, once we express the integral over matrices as integration over eigenvalues, the effective potential of the eigenvalues develops various saddle points. We can then choose to integrate all the eigenvalues over the Lefschetz thimble (generalization of steepest descent contour for multi-dimensional integrals [284, 285, 286]) of the perturbative saddle point, or we can choose to integrate all but a finite number of eigenvalues along the Lefschetz thimble of the perturbative saddle point and distribute the integration over the rest of the eigenvalues along the Lefschetz thimbles of various non-perturbative saddle points. This gives a definition of the general multi-instanton contribution to the matrix model partition function. Eventually, the complete non-perturbative result is obtained by expressing the actual integration contour as sum over the Lefschetz thimbles of different saddle points with appropriate weights, but this involves a separate analysis. From this view point, the analysis of [23] involved the contribution from the integration contour where all but one of the eigenvalues are integrated over the Lefschetz thimble of the perturbative saddle point and one of the eigenvalues is integrated over the Lefschetz thimble of a non-perturbative saddle point. One minor difference between these two perspectives is that in the analysis of [23], since we focused on the full integration contour that happened to contain only half of the Lefschetz thimble of the non-perturbative saddle point, the instanton contribution had an extra factor of half that will be absent in the new perspective.

We believe that a similar perspective should also exist in string (field) theory, but since at present we do not have an independent non-perturbative definition of string theory, we cannot give a fully rigorous description of what the D-instanton contributions represent. Nevertheless, we can offer the following limited perspective. Formally, D-branes with different boundary conditions, as well as the perturbative vacuum, are expected to be different classical solutions in a parent open string field theory that can be the open string field theory on a particular D-brane configuration [266, 287, 267, 288].[1] We can then regard the contribution from a given set of D-instantons as the result of path integral in the open (+ closed)

[1]In the critical superstring theory, the role of the parent theory could be played by the open string field theory on a set of unstable space-filling D-branes or brane-anti-brane systems. Various D-branes, including D-instantons, as well as the perturbative vacuum, can be regarded as classical solutions in this theory [289, 290, 291].

string field theory along the Lefschetz thimble of one of these saddle points. Irrespective of the details, the conformal field theory approach gives a systematic procedure for computing the contribution due to the D-instantons, and this is what is needed for comparison with the matrix integral results.

In this article, we continue our analysis of such nonperturbative effects in the partition function of both the matrix integral and the minimal string theory, and extend our results to include a general configuration of instantons. By a general configuration, we mean that we can have ℓ_1 instantons of one type, ℓ_2 instantons of another type, and so on. We present both the string theory and the matrix integral computations for completeness, although various special cases of the matrix integral computation have been discussed earlier. For a single instanton in the one-matrix integral, the matrix integral computation has been considered by many authors [248, 252, 255, 253, 254, 282, 245]. For a single instanton in the two-matrix model, see [256, 260]. For ℓ identical instantons in the one-matrix model, see [283, 292]. We review and extend these results to a general configuration of instantons in the two-matrix integral.

We find perfect agreement between the string theory result and the matrix model result. The structure of the results, equation (8.31) in the string theory case and equation (8.137) in the matrix integral case, are identical. Further, the quantities appearing in these formulas also match precisely.

To prevent the reader from getting lost in the technical details, we end this introduction by highlighting the key qualitative ideas in our computation.

- When we place ℓ eigenvalues at an extremum of the one-eigenvalue effective potential, the result does not vanish despite the presence of the Vandermonde determinant. This is because we need to do an $\ell \times \ell$ Gaussian matrix integral exactly.

- In the matrix computation of the normalization constant for the two-matrix integral, we need to take into account a slight subtlety that the expansion of $\log Z$ contains terms that are proportional to $N \log N$ [256].

- We compute the matrix integral results before taking the double-scaling limit, for which we need to take into account some $1/N$ corrections in the one-eigenvalue effective potential and the perturbative free energy [282].

- On the string theory side, the cylinder between identical ZZ branes requires a string field theory analysis to get a finite meaningful answer [257, 23]. Instead of using Siegel gauge, one needs to do the path integral over the fields with ghost number one, and explicitly divide by the volume of the gauge group. The rigid gauge group on the worldvolume of ℓ ZZ branes is $U(\ell)$ and we need to carefully compute the proper volume of this group [293].

- In the presence of non-identical instantons, the result depends on the cylinder connecting two different ZZ branes. This cylinder is finite [249, 250] and we do not need to

resort to any string field theory analysis. For the sake of completeness, we re-derive these results from a different perspective.

Overview

Section 8.2 discusses the string theory computation of the multi-instanton contribution to the partition function in (p', p) minimal string theory. Section 8.3 discusses the computation in one-matrix integrals that are dual to $(2, p)$ minimal string theory. Section 8.4 discusses the same computation in two-matrix integrals that are dual to general (p', p) minimal string theory. The appendices contain various technical details of the computations as well as some background material.

8.2 String Theory Computation

The worldsheet CFT for the minimal string theory of interest consists of the (p', p) minimal model serving the role of a matter sector, the Liouville field and the bc-ghosts [274]. Here p' and p are two relatively prime integers with $p' < p$. The central charge of the minimal model and Liouville sectors is

$$c_{\text{matter}} = 1 - \frac{6(p-p')^2}{pp'}\,, \quad c_{\text{Liouville}} = 1 + \frac{6(p+p')^2}{pp'}\,. \tag{8.2}$$

The b parameter of Liouville theory is given by $b = \sqrt{p'/p}$.

Minimal string theory contains ZZ-branes [143] which are akin to D-instantons. These branes have the ZZ boundary conditions [143] for the Liouville sector and Cardy boundary conditions [268] for the minimal model. They give rise to nonperturbative effects proportional to $\exp(-Ag_s^{-1})$, realizing the fact that closed string worldsheets can develop boundaries nonperturbatively [247]. There are some BRST equivalences between these boundary conditions, and an independent set of boundary conditions can be obtained by restricting to the (m, n) ZZ boundary condition for the Liouville field [143] and the most basic Cardy state for the minimal model (the one that only contains the identity character in the open string channel) [260, 264]. The integers m, n are restricted to the range $1 \le m \le p'-1$, $1 \le n \le p-1$ with further identification under $(m, n) \to (p'-m, p-n)$.

In general, minimal string theory is dual to the double-scaling limit of a two-matrix integral [272, 273]. When $p' = 2$, one of the matrix potentials is Gaussian and the matrix integral can be reduced to a one-matrix integral.

Cylinder with identical boundary conditions

We begin by quoting our result from [23] about the exponential of the ZZ annulus with $(1, 1)$ boundary conditions on both ends. This requires un-gauge fixing back out from Siegel gauge and using a form of the string field theory path integral with an explicit division by the

volume of the rigid gauge group on the worldvolume of the ZZ instanton. The result takes the form:

$$\mathcal{N}_{1,1} = (T_{1,1})^{-\frac{1}{2}} \frac{\mathrm{i}}{\sqrt{8\pi}} \left(\frac{\cot^2(\pi/p) - \cot^2(\pi/p')}{p^2 - p'^2} \right)^{\frac{1}{2}} . \tag{8.3}$$

As remarked in Section 8.1, compared to [23], we have integrated over the full steepest descent contour, rather than only half of it.

The annulus diagram between two identical ZZ branes, both labelled by (m, n), is given by [143]

$$Z^{\text{Liouville}}_{m,n}(t) = \sum_{k=1}^{m} \sum_{l=1}^{n} \chi_{2k-1,2l-1}(t) , \quad \text{with} \tag{8.4}$$

$$\chi_{k,l}(t) = \eta(\mathrm{i}t)^{-1} \left(q^{-kl} - 1\right) q^{-(kp-lp')^2/4pp'}, \qquad q := e^{-2\pi t} . \tag{8.5}$$

The contribution from the minimal model Cardy state is [268, 270]

$$Z^{\text{matter}}_{1,1}(t) = \eta(it)^{-1} \sum_{j=-\infty}^{\infty} \left(q^{\frac{(2pp'j+p-p')^2}{4pp'}} - q^{\frac{(2pp'j+p+p')^2}{4pp'}} \right) , \tag{8.6}$$

and the contribution from the ghosts is $\eta(\mathrm{i}t)^2$ [265]. The net result is a contribution $\sum_{k=1}^{m} \sum_{\ell=1}^{n} F_{2k-1,2l-1}(t)$ with

$$F_{k,l}(t) := \left(q^{-kl} - 1\right) q^{-(kp-lp')^2/4pp'} \sum_{j=-\infty}^{\infty} \left[q^{(2pp'j+p-p')^2/4pp'} - q^{(2pp'j+p+p')^2/4pp'} \right] . \tag{8.7}$$

The exponentiated annulus thus becomes a product

$$\mathcal{N}_{m,n} = \exp\left[\sum_{k=1}^{m} \sum_{l=1}^{n} \int_0^\infty \frac{\mathrm{d}t}{2t} F_{2k-1,2l-1}(t) \right] = \prod_{k=1}^{m} \prod_{l=1}^{n} \mathcal{M}_{2k-1,2l-1} \tag{8.8}$$

where we have defined

$$\mathcal{M}_{k,l} := \exp\left[\int_0^\infty \frac{\mathrm{d}t}{2t} F_{k,l}(t) \right] . \tag{8.9}$$

Note that $F_{1,1}$ has a small q expansion that reads $q^{-1} - 2 + O(q)$, which causes $\mathcal{M}_{1,1}$ to be ill-defined. There are two issues: The tachyon gives the q^{-1} and the two fermionic zero modes give the -2. These need to be dealt with using insights from string field theory, as was explained in detail for the case of minimal string theory in [23].

The main identity that we need to compute $\mathcal{M}_{2k-1,2l-1}$ is

$$\int_0^\infty \frac{\mathrm{d}t}{2t} \left(e^{-2\pi h_1 t} - e^{-2\pi h_2 t} \right) = \frac{1}{2} \log \frac{h_2}{h_1} . \tag{8.10}$$

This identity is valid for $h_1, h_2 > 0$. If either h_1 or h_2 is negative, we can use the right hand side to compute the analytic continuation of the left hand side. The use of analytic continuation may be justified by noting that in string field theory the steepest descent contour for a mode with negative h runs along the imaginary axis instead of the real axis.

When $(k,l) \neq (1,1)$, we can use the analytically continued version of (8.10) to perform the integral over t, which gives us[2]

$$\begin{aligned}
\mathcal{M}_{k,l} =& \prod_{j\in\mathbb{Z}} \left[\left\{ \frac{(2pp'j+p+p')^2-(kp+lp')^2}{(2pp'j+p+p')^2-(kp-lp')^2} \right\} \left\{ \frac{(2pp'j+p-p')^2-(kp-lp')^2}{(2pp'j+p-p')^2-(kp+lp')^2} \right\} \right]^{\frac{1}{2}} \\
=& \prod_{j\in\mathbb{Z}} \left[\frac{(2pp'j+(k+1)p+(l+1)p')(2pp'j-(k-1)p-(l-1)p')}{(2pp'j+(k+1)p-(l-1)p')(2pp'j-(k-1)p+(l+1)p')} \right. \\
& \qquad \left. \times \frac{(2pp'j+(k+1)p-(l+1)p')(2pp'j-(k-1)p+(l-1)p')}{(2pp'j+(k+1)p+(l-1)p')(2pp'j-(k-1)p-(l+1)p')} \right]^{\frac{1}{2}} \\
=& \prod_{j\in\mathbb{Z}} \left[\frac{(j+\frac{k+1}{2p'}+\frac{l+1}{2p})(j-\frac{k-1}{2p'}-\frac{l-1}{2p})(j+\frac{k+1}{2p'}-\frac{l+1}{2p})(j-\frac{k-1}{2p'}+\frac{l-1}{2p})}{(j+\frac{k+1}{2p'}-\frac{l-1}{2p})(j-\frac{k-1}{2p'}+\frac{l+1}{2p})(j+\frac{k+1}{2p'}+\frac{l-1}{2p})(j-\frac{k-1}{2p'}-\frac{l+1}{2p})} \right]^{\frac{1}{2}} \\
=& \prod_{j\in\mathbb{Z}} \left[\frac{(j+\frac{l+1}{2p}+\frac{k+1}{2p'})(j+\frac{l-1}{2p}+\frac{k-1}{2p'})(j+\frac{l+1}{2p}-\frac{k+1}{2p'})(j+\frac{l-1}{2p}-\frac{k-1}{2p'})}{(j+\frac{l-1}{2p}-\frac{k+1}{2p'})(j+\frac{l+1}{2p}-\frac{k-1}{2p'})(j+\frac{l-1}{2p}+\frac{k+1}{2p'})(j+\frac{l+1}{2p}+\frac{k-1}{2p'})} \right]^{\frac{1}{2}} .
\end{aligned} \tag{8.11}$$

In the last step we have made a $j \to -j$ transformation in the second and third factors in the numerator, and in the first and fourth factors in the denominator. Now we can use the infinite product identity

$$\prod_{j\in\mathbb{Z}} \frac{j+a}{j+b} = \frac{a}{b} \prod_{j\in\mathbb{Z}^*} \frac{1+\frac{a}{j}}{1+\frac{b}{j}} = \frac{a}{b} \prod_{j\in\mathbb{Z}^+} \frac{1-\frac{a^2}{j^2}}{1-\frac{b^2}{j^2}} = \frac{\sin(\pi a)}{\sin(\pi b)} \tag{8.12}$$

to get

$$\begin{aligned}
\mathcal{M}_{k,l} =& \left[\frac{\sin(\pi(\frac{l+1}{2p}+\frac{k+1}{2p'}))\sin(\pi(\frac{l-1}{2p}+\frac{k-1}{2p'}))\sin(\pi(\frac{l+1}{2p}-\frac{k+1}{2p'}))\sin(\pi(\frac{l-1}{2p}-\frac{k-1}{2p'}))}{\sin(\pi(\frac{l-1}{2p}-\frac{k+1}{2p'}))\sin(\pi(\frac{l+1}{2p}-\frac{k-1}{2p'}))\sin(\pi(\frac{l-1}{2p}+\frac{k+1}{2p'}))\sin(\pi(\frac{l+1}{2p}+\frac{k-1}{2p'}))} \right]^{\frac{1}{2}} \\
=& \left[\frac{\left(\sin^2(\frac{\pi(l+1)}{2p})-\sin^2(\frac{\pi(k+1)}{2p'})\right)\left(\sin^2(\frac{\pi(l-1)}{2p})-\sin^2(\frac{\pi(k-1)}{2p'})\right)}{\left(\sin^2(\frac{\pi(l-1)}{2p})-\sin^2(\frac{\pi(k+1)}{2p'})\right)\left(\sin^2(\frac{\pi(l+1)}{2p})-\sin^2(\frac{\pi(k-1)}{2p'})\right)} \right]^{\frac{1}{2}} .
\end{aligned} \tag{8.13}$$

[2]As discussed at the end of this section, for special values of (p',p) we get some vanishing exponents of q even for $(k,\ell) \neq (1,1)$. For now we shall ignore this problem and simply use the fact that the problematic terms cancel pairwise. However we should keep in mind that for these special values of (p',p), our string theory results remain somewhat formal.

Armed with this formula for $\mathcal{M}_{k,l}$, we can see that the product formula for $\mathcal{N}_{m,n}$ in equation (8.8) telescopes. We first do the product over all values of $(2k-1, 2l-1)$ except $(1,l)$.

$$\begin{aligned}
\mathcal{N}_{m,n} &= \left(\prod_{l=1}^{n}\mathcal{M}_{1,2l-1}\right)\prod_{k=2}^{m}\prod_{l=1}^{n}\mathcal{M}_{2k-1,2l-1} \\
&= \left(\prod_{l=1}^{n}\mathcal{M}_{1,2l-1}\right)\prod_{k=2}^{m}\prod_{l=1}^{n}\left[\frac{\left(\sin^2(\frac{\pi l}{p})-\sin^2(\frac{\pi k}{p'})\right)\left(\sin^2(\frac{\pi(l-1)}{p})-\sin^2(\frac{\pi(k-1)}{p'})\right)}{\left(\sin^2(\frac{\pi(l-1)}{p})-\sin^2(\frac{\pi k}{p'})\right)\left(\sin^2(\frac{\pi l}{p})-\sin^2(\frac{\pi(k-1)}{p'})\right)}\right]^{\frac{1}{2}} \\
&= \left(\prod_{l=1}^{n}\mathcal{M}_{1,2l-1}\right)\left[\frac{\left(\sin^2(\frac{\pi n}{p})-\sin^2(\frac{\pi m}{p'})\right)\left(\sin^2(\frac{\pi}{p'})\right)}{\left(\sin^2(\frac{\pi m}{p'})\right)\left(\sin^2(\frac{\pi n}{p})-\sin^2(\frac{\pi}{p'})\right)}\right]^{\frac{1}{2}} \\
&= \left(\prod_{l=1}^{n}\mathcal{M}_{1,2l-1}\right)\left[\frac{\cot^2(\frac{\pi n}{p})-\cot^2(\frac{\pi m}{p'})}{\cot^2(\frac{\pi n}{p})-\cot^2(\frac{\pi}{p'})}\right]^{\frac{1}{2}}.
\end{aligned} \tag{8.14}$$

Now we compute the remaining product over l, but leaving out $\mathcal{M}_{1,1}$.

$$\begin{aligned}
\prod_{l=1}^{n}\mathcal{M}_{1,2l-1} &= \mathcal{M}_{1,1}\prod_{l=2}^{n}\left[\frac{\left(\sin^2(\frac{\pi}{p'})-\sin^2(\frac{\pi l}{p})\right)\left(\sin^2(\frac{\pi(l-1)}{p})\right)}{\left(\sin^2(\frac{\pi l}{p})\right)\left(\sin^2(\frac{\pi}{p'})-\sin^2(\frac{\pi(l-1)}{p})\right)}\right]^{\frac{1}{2}} \\
&= \mathcal{M}_{1,1}\prod_{l=2}^{n}\left[\frac{\cot^2(\frac{\pi}{p'})-\cot^2(\frac{\pi l}{p})}{\cot^2(\frac{\pi}{p'})-\cot^2(\frac{\pi(l-1)}{p})}\right]^{\frac{1}{2}} = \mathcal{M}_{1,1}\left[\frac{\cot^2(\frac{\pi}{p'})-\cot^2(\frac{\pi n}{p})}{\cot^2(\frac{\pi}{p'})-\cot^2(\frac{\pi}{p})}\right]^{\frac{1}{2}}.
\end{aligned} \tag{8.15}$$

Combining (8.14) and (8.15), we get

$$\mathcal{N}_{m,n} = \mathcal{M}_{1,1}\left[\frac{\cot^2(\frac{\pi m}{p'})-\cot^2(\frac{\pi n}{p})}{\cot^2(\frac{\pi}{p'})-\cot^2(\frac{\pi}{p})}\right]^{\frac{1}{2}}. \tag{8.16}$$

Now, we need to treat $\mathcal{M}_{1,1}$ using string field theory. Each brane, labeled by the integers (m,n), has a worldvolume theory. There is an action for this theory, which is the standard cubic action of open string field theory [271]. The overall coefficient in front of this action is $\left(g_o^{(m,n)}\right)^{-2}$, and the tension of the brane is related to this coupling via [266]

$$T_{m,n} = \frac{1}{2\pi^2}\left(g_o^{(m,n)}\right)^{-2}. \tag{8.17}$$

Minimal string theories are known to have branes with negative tension. We expect that the relation (8.17) will continue to hold in that case as well if we demand that the universal

'tachyon condensation' on those branes continue to give the perturbative vacuum as usual. Note that for negative tension branes the universal tachyon has positive mass-squared and 'tachyon condensation' actually raises the tension instead of lowering it.

We will not repeat the steps of the string field theory analysis, but the main insight is that the two zero modes arise due to the failure of Siegel gauge, which, in turn, is related to the fact that the usual gauge symmetry on a D-brane worldvolume is a rigid symmetry in the case of D-instantons. So we need to work with the string field theory path integral over fields with ghost number one, and explicitly divide by the volume of the rigid symmetry group. The proper volume of that group equals $2\pi/g_o^{(m,n)} = 2\sqrt{2}\pi^2 T_{m,n}^{-1/2}$ [257]. Following these steps gives us the result identical to (8.3), except for the replacement of $T_{1,1}$ by $T_{m,n}$:

$$\mathcal{M}_{1,1} = (T_{m,n})^{-\frac{1}{2}} \ \frac{\mathrm{i}}{\sqrt{8\pi}} \left(\frac{\cot^2(\pi/p) - \cot^2(\pi/p')}{p^2 - p'^2} \right)^{\frac{1}{2}} . \tag{8.18}$$

Equation (8.16) now gives

$$\mathcal{N}_{m,n} = (T_{m,n})^{-\frac{1}{2}} \ \frac{\mathrm{i}}{\sqrt{8\pi}} \left(\frac{\cot^2(\pi n/p) - \cot^2(\pi m/p')}{p^2 - p'^2} \right)^{\frac{1}{2}} . \tag{8.19}$$

Cylinder with non-identical boundary conditions

Let us extend the result to the annulus diagram with the one boundary lying on an (m, n) ZZ brane and the other on an (m', n') ZZ brane. In some sense, this computation is easier since the worldsheet computation yields a finite answer, and there is no need to resort to string field theory. This computation has already been done [249, 250], but we reproduce the result here using a different method.

The Liouville contribution is [143]

$$Z^{\text{Liouville}}_{(m,n)(m',n')}(t) = \sum_{k=|m-m'|+1,2}^{m+m'-1} \ \sum_{l=|n-n'|+1,2}^{n+n'-1} \chi_{k,l}(t) \, , \tag{8.20}$$

where the 2 in the subscript of the summation sign indicates that we sum over every other value of the indices k and l. The normalization constant is given by

$$C_{(m,n),(m',n')} = \exp\left[\int_0^\infty \frac{\mathrm{d}t}{t} \, Z^{\text{Liouville}}_{(m,n)(m',n')}(t) \, Z^{\text{Matter}}_{(1,1)}(t) \, \eta(\mathrm{i}t)^2 \right] . \tag{8.21}$$

Note that the measure for the t-integral is now $\frac{\mathrm{d}t}{t}$ as opposed to $\frac{\mathrm{d}t}{2t}$ because the two sides of the annulus are distinct. If $(m, n) \neq (m', n')$, this can be written as a product of the contributions $\mathcal{M}_{k,l}$ given in (8.13) which telescopes

$$
\begin{aligned}
C_{(m,n),(m',n')} &= \prod_{k=|m-m'|+1,2}^{m+m'-1} \prod_{l=|n-n'|+1,2}^{n+n'-1} (\mathcal{M}_{k,l})^2 \\
&= \prod_{k=|m-m'|+1,2}^{m+m'-1} \prod_{l=|n-n'|+1,2}^{n+n'-1} \frac{\left(\sin^2(\frac{\pi(l+1)}{2p}) - \sin^2(\frac{\pi(k+1)}{2p'})\right)}{\left(\sin^2(\frac{\pi(l-1)}{2p}) - \sin^2(\frac{\pi(k+1)}{2p'})\right)} \\
&\qquad \times \frac{\left(\sin^2(\frac{\pi(l-1)}{2p}) - \sin^2(\frac{\pi(k-1)}{2p'})\right)}{\left(\sin^2(\frac{\pi(l+1)}{2p}) - \sin^2(\frac{\pi(k-1)}{2p'})\right)} \\
&= \frac{\left(\sin^2(\frac{\pi(n+n')}{2p}) - \sin^2(\frac{\pi(m+m')}{2p'})\right)\left(\sin^2(\frac{\pi|n-n'|}{2p}) - \sin^2(\frac{\pi|m-m'|}{2p'})\right)}{\left(\sin^2(\frac{\pi|n-n'|}{2p}) - \sin^2(\frac{\pi(m+m')}{2p'})\right)\left(\sin^2(\frac{\pi(n+n')}{2p}) - \sin^2(\frac{\pi|m-m'|}{2p'})\right)}.
\end{aligned}
\tag{8.22}
$$

This agrees with the result of [250] for the annulus between two different ZZ branes after using some trigonometric identities. An important point is that the annulus between two different ZZ branes is finite and completely well-defined. As we will see, this is the case for matrix integrals as well.

General multi-instanton contribution to the partition function

We shall now determine the ratio of the contribution to the partition function from ℓ ZZ branes of type (m,n) to the perturbative contribution to the partition function in the (p',p) minimal string theory. The $\ell = 1$ case has already been discussed in [23], and our goal will be to express the result for general ℓ in terms of quantities that already appear in the result for $\ell = 1$. For this let us express the result for $\ell = 1$ as

$$
\frac{Z^{(1)}}{Z^{(0)}} = \exp\left[-T_{m,n}\right]\, \widetilde{B}_{m,n}\, \frac{g_o^{(m,n)}}{2\pi}\,, \tag{8.23}
$$

where, from (8.17) and (8.19), we have

$$
\widetilde{B}_{m,n} = \frac{2\pi}{g_o^{(m,n)}} \mathbb{N}_{m,n} = \mathrm{i}\,\pi^{3/2}\, \left(\frac{\cot^2(\pi n/p) - \cot^2(\pi m/p')}{p^2 - p'^2}\right)^{\frac{1}{2}}. \tag{8.24}
$$

An important point to recall is that in (8.23) the $g_o^{(m,n)}/(2\pi)$ term comes from division by the volume of the $U(1)$ gauge group and the $\widetilde{B}_{m,n}$ factor comes from integration over the tachyon, all the massive modes and the out-of-Siegel-gauge mode.

For ℓ instantons, the action is $\ell\, T_{m,n}$. Furthermore, the open string spectrum gets repeated ℓ^2 times. So the contribution from massive states, tachyon as well as the out-of-Siegel-gauge mode gets repeated ℓ^2 times. This produces a net factor:

$$
\exp\left[-\ell\, T_{m,n}\right]\, \left(\widetilde{B}_{m,n}\right)^{\ell^2}\,. \tag{8.25}
$$

The slightly non-trivial part of the calculation is division by the volume of the gauge group. For this we follow the logic of [293]. We denote by θ^a the string field theory gauge transformation parameters and by $\tilde{\theta}^a$ the $U(\ell)$ gauge transformation parameters on the D-instanton worldvolume. Then we have the relation [293]

$$\theta^a = \tilde{\theta}^a / g_o^{(m,n)} \,. \tag{8.26}$$

Now, using (8.26) we see that division by the gauge group volume generates a factor of

$$(g_o^{(m,n)})^{\ell^2} / V_{U(\ell)} \,, \tag{8.27}$$

where $V_{U(\ell)}$ denotes the volume of the group $U(\ell)$ as measured by the parameters $\tilde{\theta}^a$. The volume $V_{U(\ell)}$ in this normalization was found in [293]. The result is[3]

$$V_{U(\ell)} = \frac{(2\pi)^{\frac{1}{2}(\ell^2+\ell)}}{G_2(\ell+1)} \,, \tag{8.28}$$

where $G_2(\ell+1) = \prod_{i=1}^{\ell-1} i!$ is the Barnes-G double gamma function. In particular, in the normalization convention for $\tilde{\theta}^a$ in which (8.26) is valid, the volume of the $U(1)^\ell$ diagonal subgroup of $U(\ell)$ is $(2\pi)^\ell$. In Section 8.3 we have computed the volume of $U(\ell)$ using the same normalization and reproduced the result in (8.28).

Multiplying (8.25) by (8.27) and using (8.28), we get the net normalization factor:

$$\frac{Z^{(\ell)}}{Z^{(0)}} = \exp\left[-\ell\, T_{m,n}\right] \, (B_{m,n})^{\ell^2} \, \frac{G_2(\ell+1)}{(2\pi)^{\frac{1}{2}(\ell^2+\ell)}} \,, \tag{8.29}$$

$$B_{m,n} := \widetilde{B}_{m,n}\, g_o^{(m,n)} = 2\pi\, \mathbb{N}_{m,n} = (T_{m,n})^{-\frac{1}{2}} \, \mathrm{i} \sqrt{\frac{\pi}{2}} \left(\frac{\cot^2(\pi n/p) - \cot^2(\pi m/p')}{p^2 - p'^2} \right)^{\frac{1}{2}} \,. \tag{8.30}$$

We shall see in Sections 8.3 and 8.4 that this result agrees with the matrix model result for ℓ-instantons. For $\ell = 1$ and $(m,n) = (1,1)$ this agreement was observed in [23].

One can now easily generalize the result to the case where we have ℓ_α instantons of type α, where α takes values over different pairs (m,n). The result is:

$$\frac{Z^{\{\ell_\alpha\}}}{Z^{(0)}} = \prod_\alpha \left\{ \exp\left[-\ell_\alpha T_\alpha\right] \, (B_\alpha)^{\ell_\alpha^2} \, \frac{G_2(\ell_\alpha+1)}{(2\pi)^{\frac{1}{2}(\ell_\alpha^2+\ell_\alpha)}} \right\} \prod_{\alpha,\beta:\alpha<\beta} (C_{\alpha,\beta})^{\ell_\alpha \ell_\beta} \,, \tag{8.31}$$

where B_α is as in (8.30) and $C_{\alpha,\beta}$, given in (8.22), accounts for the contribution from the exponential of the annulus amplitude with one boundary on the instanton of type α and the other boundary on the instanton of type β. The exponent $\ell_\alpha \ell_\beta$ represents the trace over the Chan-Paton factors on the two boundaries.

[3]The relation between θ^a and $\tilde{\theta}^a$ in [293] had an extra factor of 2 compared to (8.26), but this can be traced to an extra factor of 2 in the definition of the SFT gauge transformation parameters and in fact cancels against a factor of 2 coming from the out-of-Siegel-gauge mode integral. So as far as the volume of $U(\ell)$ is concerned, there is no difference and we can directly take the result of [293].

Integer dimensions in the open string spectrum

Our analysis in the following sections will show that the string theory results for the instanton partition function agree perfectly with the matrix model results. However we shall now argue that for some class of instantons this agreement is somewhat formal.

For (m,n) type ZZ branes, the spectrum of open strings is built by the action of ghost oscillators and matter and Liouville Virasoro generators on Liouville $\times$ matter primaries $\times$ ghost vacuum $c_1|0\rangle$ of dimension:

$$\begin{aligned} h_{k\ell} &= -\frac{1}{4pp'}\{(2m-2k-1)p+(2n-2\ell-1)p'\}^2+\frac{1}{4pp'}(p-p')^2, \\ &0\le k\le m-1, \quad 0\le \ell\le n-1\,. \end{aligned} \tag{8.32}$$

If $h_{k\ell}$ is a negative integer for any k,ℓ, then by acting with ghost oscillators and matter Virasoro generators we shall produce zero modes. This means that in (8.7), the power series expansion in q will have some constant terms. This in turn will produce logarithmic divergence in the integration over t. The finiteness of the final result (8.13) shows that the net coefficient of the logarithmically divergent term vanishes, but in the spirit of string field theory the correct procedure is to interpret the divergences caused by individual terms as arising from integration over zero modes and to carry out the integration over these zero modes carefully. Since our analysis ignores this subtlety, our results remain somewhat formal. We shall now determine under what condition we get such additional zero modes.

The expression for $h_{k,\ell}$ may be written as

$$\begin{aligned} h_{k,\ell} &= -\frac{1}{4pp'}\left[(2m-2k-2)p+(2n-2\ell)p'\right]\left[(2m-2k)p+(2n-2\ell-2)p'\right] \\ &= -\frac{1}{pp'}[ap+(b+1)p'][(a+1)p+bp'] \\ &= -ab-(a+1)(b+1)-a(a+1)\frac{p}{p'}-b(b+1)\frac{p'}{p}\,, \quad \text{with} \\ a &:= m-k-1, \quad b:=n-\ell-1, \quad 0\le a\le m-1, \quad 0\le b\le n-1\,. \end{aligned} \tag{8.33}$$

Since p,p' are relatively prime, in order that $h_{k,\ell}$ is a negative integer, we must have

$$p' \mid a(a+1), \qquad p\mid b(b+1)\,. \tag{8.34}$$

A simple solution is $a=b=0$ with $h_{k,\ell}=-1$. This corresponds to the product of the identity fields from the matter and Liouville sector and the ghost vacuum $c_1|0\rangle$. The zero modes produced from this sector correspond to ghost zero modes associated with the breakdown of the Siegel gauge. These have already been taken into account in our analysis. But there are other solutions. Here are some examples:

$$\begin{aligned} p'=2, \quad p=15, \quad a=0, \quad b=5, \\ p'=6, \quad p=55, \quad a=2, \quad b=10, \\ p'=6, \quad p=35, \quad a=2, \quad b=14\,. \end{aligned} \tag{8.35}$$

For such pairs (p', p), the string theory results remain formal for (m, n) type ZZ instantons with $m \geq a + 1$, $n \geq b + 1$.

8.3 One-matrix integrals

The one-matrix integral (in the double-scaling limit) is dual to the $(2, p)$ family of minimal string theories, where $p \geq 3$ is an odd integer. The computation of the normalization constant for the case of ℓ identical instantons in the one-matrix integral was done in [283] using a degeneration limit of the two-cut solution to the matrix integral. We will present a simpler approach that is similar to [254, 282]. We follow the conventions of [294, 282] and we refer to them for more details, whose notations we also use.

The quantity of interest is the integral over $N \times N$ Hermitian matrices M:

$$Z(N,t) := \frac{1}{V_{U(N)}} \int \mathrm{d}M \exp\left[-\frac{N}{t}\operatorname{Tr} V(M)\right] \tag{8.36}$$

$$= \frac{1}{N!} \int \prod_{i=1}^{N} \frac{\mathrm{d}x_i}{2\pi} \prod_{i,j=1:i<j}^{N} (x_i - x_j)^2 \exp\left[-\frac{N}{t}\sum_{i=1}^{N} V(x_i)\right] . \tag{8.37}$$

As usual, the large-N limit is taken keeping the 't Hooft coupling t fixed.[4] The measure $\mathrm{d}M$ is defined as the volume measure that is induced by the metric $\mathrm{d}s^2 = \operatorname{Tr}(\mathrm{d}M^2)$ on the space of Hermitian matrices. We diagonalize $M = U\mathrm{diag}(x_i)U^\dagger$ and change variables to the eigenvalues x_i and U. Here $V_{U(N)}$ denotes the volume of the $U(N)$ group, with a local measure that is induced on the space of U's by the above change of variables. The factor $(N!\,(2\pi)^N)^{-1}$ on the right hand side denotes the volume of $U(1)^N \times S_N$ which corresponds to rotating the phase of each column of U and the permutations of the eigenvalues. This subgroup is left "unfixed" when we change variables from M to the x_i's and U. Also note that even though we have chosen a convenient normalization of $Z(N,t)$ in (8.36), this choice will not affect our final result since we shall be computing the ratio of two different contributions to $Z(N,t)$.

The large-N limit

We consider the aforementioned integrals over an $N \times N$ hermitian matrix M. We take the potential to be an even polynomial, for simplicity. The planar free energy F_0 is defined as

$$F_0(t) := \lim_{N\to\infty} \frac{1}{N^2}\, t^2 \log Z(N,t)\,. \tag{8.38}$$

[4] Hopefully, there is no confusion between using the same letter t for the 't Hooft coupling in the matrix integral and the open string modulus in string theory.

We work with the one-cut solution in which the resolvent takes the form

$$\omega_0(x) := \lim_{N\to\infty} \frac{1}{N} \left\langle \mathrm{Tr}\, \frac{1}{x-M} \right\rangle = \int_{-b}^{b} \mathrm{d}y\, \frac{\rho(y)}{x-y}\,, \tag{8.39}$$

The support of the eigenvalue density $\rho(y)$ is on the interval $[-b,b]$. One can show that [282]

$$2t\,\omega_0(x) = V'(x) - M(x)\sqrt{x^2-b^2}\,, \tag{8.40}$$

where, if $V(x)$ is a polynomial of degree $d+1$, then $M(x)$ is a polynomial of degree $d-1$. It will be understood that $\sqrt{x^2-b^2} \simeq x$ for large $|x|$ on the physical sheet. Both $M(x)$ and b can be determined using the fact that $\omega_0(x) = 1/x + O(x^0)$ as $x\to\infty$ on the physical sheet; they depend on t. An important relation that will be useful for us is [294]

$$\frac{\partial}{\partial t}(t\omega_0(x)) = \frac{1}{\sqrt{x^2-b^2}}\,. \tag{8.41}$$

The *holomorphic* effective potential is defined via [282]

$$V_{\text{eff}}(x) := V(x) - 2t\int_{-b}^{b} \mathrm{d}y\,\rho(y)\,\log(y-x) = V(x) - 2t\int_{-\Lambda}^{x} \mathrm{d}x'\,\omega_0(x') - 2t\log\Lambda\,, \tag{8.42}$$

where the limit $\Lambda\to\infty$ is understood in the last expression. Since we shall define the double-scaling limit by zooming in near the region $x\simeq -b$, we have defined $V_{\text{eff}}(x)$ such that it is real on the negative x-axis. A consequence of the large-N saddle point equation is that the *real part* of the effective potential is constant on the interval $[-b,b]$. Using (8.41) we get the derivative of the derivative of the effective potential with respect to t:

$$\partial_t V_{\text{eff}}(x) = -2\int_{-\Lambda}^{x} \mathrm{d}x'\,\frac{1}{\sqrt{x'^2-b^2}} - 2\log\Lambda = -2\log\left(\frac{-x-\sqrt{x^2-b^2}}{2}\right)\,. \tag{8.43}$$

It follows from (8.39) that the imaginary part of ω_0 in the interval $[-b,b]$ is given by $\pi\rho(x)$. On the other hand we see from (8.40) that the imaginary part of $2t\omega_0$ in the same interval is given by $M(x)\sqrt{b^2-x^2}$. This gives

$$\rho(x) = \frac{1}{2\pi t} M(x)\sqrt{b^2-x^2}\;\Theta(b-|x|)\,. \tag{8.44}$$

From (8.42) and (8.40) we also have

$$V'_{\text{eff}}(x) = V'(x) - 2t\omega_0(x) = M(x)\sqrt{x^2-b^2}. \tag{8.45}$$

Next, we collect the following results for the planar free energy and its t-derivatives [282, 295]

$$F_0(t) = -\frac{t}{2}\int_{-b}^{b} \mathrm{d}x\,\rho(x)V(x) - \frac{t}{2}V_{\text{eff}}(-b)\,, \tag{8.46}$$

$$\partial_t F_0(t) = -V_{\text{eff}}(-b)\,, \tag{8.47}$$

$$\partial_t^2 F_0(t) = 2\log\frac{b}{2}\,. \tag{8.48}$$

To derive (8.46), we need to use the fact that the real part of $V_{\rm eff}$ is constant on the cut, and so $V(x) - 2t\int \mathrm{d}y\,\rho(y)\log|x-y| = V_{\rm eff}(-b)$ for $x \in [-b,b]$. Using this to simplify the Coulomb-repulsion term in the on-shell action for the defining integral (8.37), we get

$$\begin{aligned}\frac{1}{t^2}F_0(t) &= -\frac{1}{t}\int_{-b}^{b}\mathrm{d}x\rho(x)V(x) + \int_{-b}^{b}\int_{-b}^{b}\mathrm{d}x\mathrm{d}y\,\rho(x)\rho(y)\log|x-y| \\ &= -\frac{1}{2t}\int_{-b}^{b}\mathrm{d}x\rho(x)V(x) - \frac{1}{2t}V_{\rm eff}(-b)\,,\end{aligned} \tag{8.49}$$

as desired. To derive (8.47), we use the relation $\partial_t \log Z = \frac{N^2}{t^2}\int_{-b}^{b}\mathrm{d}x\,\rho(x)V(x)$ which follows directly by taking a t-derivative in the definition (8.37). Using the large-N approximation $\log Z = N^2F_0/t^2$ and (8.46), we get (8.47). To derive (8.48), we take a t-derivative in (8.47) and use (8.43), together with the fact that $V'_{\rm eff}(-b) = 0$ so that $\partial_t b$ does not contribute.

We also need the connected correlator of two resolvent operators [296, 297] (see, for example, [245], for a recent exposition)

$$R_{0,2}(x_1,x_2) := \left\langle \mathrm{Tr}\,\frac{1}{x_1-M}\,\mathrm{Tr}\,\frac{1}{x_2-M}\right\rangle_{\rm c} = \frac{1}{2(x_1-x_2)^2}\left(\frac{x_1x_2-b^2}{\sqrt{x_1^2-b^2}\sqrt{x_2^2-b^2}}-1\right). \tag{8.50}$$

We integrate this twice to get the connected correlator that we need

$$A_{0,2}(x_1,x_2) := \langle \mathrm{Tr}\log(x_1-M)\,\mathrm{Tr}\log(x_2-M)\rangle_{\rm c}\,. \tag{8.51}$$

We first integrate over x_2 and get

$$\int_{-\infty}^{x_2}\mathrm{d}x_2'\,R_{0,2}(x_1,x_2') = \left(\frac{1}{2(x_2-x_1)} - \frac{1}{2(x_2-x_1)}\sqrt{\frac{x_2^2-b^2}{x_1^2-b^2}}\right) + \frac{1}{2\sqrt{x_1^2-b^2}}\,. \tag{8.52}$$

At large x_1, this expression behaves as x_1^{-2} so we should not have any problems integrating it. The final answer is

$$A_{0,2}(x_1,x_2) = -\frac{1}{2}\log\left[\frac{2(x_1x_2-b^2+\sqrt{x_1^2-b^2}\sqrt{x_2^2-b^2})}{(x_1+\sqrt{x_1^2-b^2})(x_2+\sqrt{x_2^2-b^2})}\right]. \tag{8.53}$$

Eventually, we will need the following combination, which we get using (8.43), (8.48) and (8.53)

$$\exp\left(\partial_t^2F_0 + \partial_tV_{\rm eff}(x_1) + \partial_tV_{\rm eff}(x_2) + 4A_{0,2}(x_1,x_2)\right) = \left(\frac{b}{x_1x_2-b^2+\sqrt{x_1^2-b^2}\sqrt{x_2^2-b^2}}\right)^2. \tag{8.54}$$

A more geometrical perspective

We will now recast some of the above formulas in terms of a more formal perspective, using the language of algebraic curves. This will help us in understanding the generalization to the two-matrix case. We follow the notations of [298].

The starting point is to define a function $Y(x)$ via

$$Y(x) := V'(x) - \frac{2t}{N} \left\langle \mathrm{Tr}\, \frac{1}{x - M} \right\rangle . \tag{8.55}$$

Using (8.42), we note that $Y(x) = V'_{\mathrm{eff}}(x)$. We can use a Schwinger-Dyson equation in the defining matrix integral to show that $Y(x)$ satisfies a polynomial equation

$$Y(x)^2 = V'(x)^2 - 4tP(x)\,, \quad \text{where} \tag{8.56}$$

$$P(x) := \frac{1}{N} \left\langle \mathrm{Tr} \left(\frac{V'(x) - V'(M)}{x - M} \right) \right\rangle . \tag{8.57}$$

Let us define the spectral curve Σ as

$$\Sigma := \{(u, v) \in \mathbb{C}^2 \mid v^2 - V'(u)^2 + 4tP(u) = 0\} . \tag{8.58}$$

We can restate the Schwinger-Dyson equation as the statement that the point $(x, Y(x))$ lies on Σ, with $Y(x)$ defined in (8.55).

If $V(x)$ is a polynomial of degree $d+1$, then $P(x)$ is a polynomial of degree $d-1$, which makes the right hand side of (8.56) a polynomial of degree $2d$. Note, in particular that if $V(x) = x^2/2$, then $P(x) = 1$. If we do not insist on using an even polynomial, then we can take $d = p - 1$ in order to describe the $(2, p)$ minimal string. The "one-cut assumption" can be rephrased as the condition that $d-1$ of the roots of the polynomial $V'(x)^2 - 4tP(x)$ have multiplicity two, so that $V'(x)^2 - 4tP(x) = M(x)^2(x-a)(x-b)$. The roots of $M(x)$, which are $d-1$ in number, are precisely the locations of the one-eigenvalue instantons.[5] Note also that, in the immediate neighborhood of a one-eigenvalue instanton, the equation defining the spectral curve looks like $y^2 - c\,(x - x_*)^2 = 0$ (for some constant c), clearly exhibiting the "double-point" singularity [264].

If all the roots of $V'(x)^2 - 4tP(x)$ were distinct, the spectral curve Σ would have genus $d-1$, and we would have an eigenvalue density supported on d distinct arcs in the complex-x plane. In the one-cut solution, $d-1$ of these arcs have length zero, giving us $d-1$ distinct one-eigenvalue instantons, as also argued in the previous paragraph.

Let us now specialize to the one-cut case. The curve defined by (8.56) admits a uniformization parameter z with the projection to the x-coordinate given by

$$x = \frac{a+b}{2} + \gamma \left(z + z^{-1} \right) , \quad \gamma := \frac{b-a}{4} . \tag{8.59}$$

[5] Not all of these one-eigenvalue instantons survive in the double-scaling limit. To get the conformal background of $(2, p)$ minimal string theory, we can take a polynomial of degree $d + 1 = p$, or we could also take an even polynomial of degree $d + 1 = p + 1$. In either case, only $(p-1)/2$ of the $d-1$ one-eigenvalue instantons will survive in the double-scaling limit.

The special property of the above map is that the cut end-points $x = a$ and $x = b$ get mapped to $z = -1$ and $z = 1$. These are also the points where $\mathrm{d}x/\mathrm{d}z = 0$. We need two copies or sheets of the x-plane to cover the z-plane, the "physical sheet" is the one whose z-image contains $z = \infty$, the second sheet is the one whose z-image contains $z = 0$. The boundary dividing the z-image of these two sheets is the unit circle in the complex-z plane.

Further specializing to an even potential, so that $b = -a > 0$ and $b = 2\gamma$, we see that, on the physical sheet we have

$$x = \gamma\left(z + z^{-1}\right) , \quad \sqrt{x^2 - 4\gamma^2} = \gamma\left(z - z^{-1}\right) . \tag{8.60}$$

Thus, we see that many of the formulas in the previous section would be somewhat simpler when written in terms of z. For instance, we can rewrite (8.43), (8.53) and (8.54) as

$$\partial_t V_{\text{eff}} = -2\log(-\gamma z) , \tag{8.61}$$

$$A_{0,2}(x_1, x_2) = -\log\frac{x_1 - x_2}{\gamma z_1 - \gamma z_2} = \log\frac{z_1 z_2}{z_1 z_2 - 1} , \tag{8.62}$$

$$\exp\left(\partial_t^2 F_0 + \partial_t V_{\text{eff}}(x_1) + \partial_t V_{\text{eff}}(x_2) + 4A_{0,2}(x_1, x_2)\right) = \left(\frac{z_1 z_2}{\gamma(z_1 z_2 - 1)^2}\right)^2 . \tag{8.63}$$

Gaussian matrix integral

The Gaussian matrix integral corresponds to the potential $V(x) = \frac{x^2}{2}$, and it is given by [294]

$$Z_G(\ell) := \frac{1}{\ell!}\int \prod_{i=1}^{\ell}\frac{\mathrm{d}x_i}{2\pi}\,\Delta(x)^2\,\exp\left(-\frac{N}{t}\sum_{i=1}^{\ell}\frac{x_i^2}{2}\right) = \frac{G_2(\ell+1)}{(2\pi)^{\ell/2}}\,\left(\frac{t}{N}\right)^{\ell^2/2} . \tag{8.64}$$

Here G_2 denotes the Barnes-G double gamma function. This equation is exact, and, in particular, is true even if ℓ is of order N. This can be derived using the fact that Hermite polynomials are orthogonal with respect to the Gaussian measure [294]. We note that the asymptotic expansion of $Z_G(N)$ reads [294]

$$\log Z_G(N) = N^2\left(\frac{1}{2}\log t - \frac{3}{4}\right) + O(\log N) . \tag{8.65}$$

We identify the first term as $N^2 F_{0,G}(t)/t^2$. In particular, note that terms of order $N\log N$ or N are absent. This will no longer be the case in the two-matrix integral. The above expression implies the following result that we need for our calculations

$$\log\frac{Z_G(N-\ell, t - t\ell/N)}{Z_G(N,t)} = \frac{N^2}{t^2}\left(F_{0,G}(t - t\ell/N) - F_{0,G}(t)\right) + O\left(\frac{1}{N}\right) . \tag{8.66}$$

We can use the result (8.64) and the equality between the two integrals (8.36) and (8.37) to check the expression (8.28) for the volume of the group $U(\ell)$. The gaussian integral over

the matrix in (8.36) can be done in a trivial fashion by doing ℓ^2 separate gaussian integrals over the individual matrix elements of M. The upshot is that

$$Z_G(\ell) = \frac{1}{V_{U(\ell)}} \left(\frac{2\pi t}{N}\right)^{\ell^2/2} . \tag{8.67}$$

Equating the right hand side of this equation to (8.64), we get

$$V_{U(\ell)} = \frac{(2\pi)^{\frac{1}{2}(\ell^2+\ell)}}{G_2(\ell+1)} . \tag{8.68}$$

Matrix integral dual to $(2,p)$ minimal string theory

Next we consider a more general class of matrix integrals where the potential is an even polynomial, with degree $p+1$,

$$V(x) = \frac{x^2}{2} + \sum_{k=1}^{(p-1)/2} \frac{g_{2k+2}}{2k+2} x^{2k+2} . \tag{8.69}$$

We focus on the case where the perturbative contribution to the free energy comes from the so-called one-cut saddle point. The one-cut saddle point is the one where the eigenvalues of the matrix are distributed on a single interval $[-b, b]$. The cut end-point b depends on t and on all the coefficients g_{2k+2} appearing in the potential.

It is expected that $\log Z(N,t)$ has an asymptotic expansion in powers of N^{-2} [295, 299, 244]:

$$\log Z(N,t) \stackrel{?}{=} \sum_{g=0}^{\infty} \left(\frac{N}{t}\right)^{2-2g} F_g(t) . \tag{8.70}$$

This is almost correct. However, a more precise statement is that, in order to get this asymptotic series, one needs to divide by the Gaussian matrix integral (the matrix integral with all the coefficients g_{2k+2} set to zero), see the rigorous mathematical treatment in [300].

$$\log \frac{Z(N,t)}{Z_G(N,t)} = \sum_{g=0}^{\infty} \left(\frac{N}{t}\right)^{2-2g} (F_g(t) - F_{g,G}(t)) . \tag{8.71}$$

The subtlety has to do with the fact that the $\log Z_G$ contains terms proportional to $\log N$ (see equation (8.65)), and every matrix integral contains these same terms. An intuitive reason for this is that if we compute the integral via perturbation theory in the couplings g_{2k+2}, we get the Gaussian matrix integral as an overall factor [295].

More rigorously, consider a general potential $V(M)$ of the form given in (8.69). Here $F_0(t)$ differs from the result for quadratic potential, but the logarithmic terms remain unchanged. One way to see this is as follows. Introducing the function $r(\xi)$ satisfying the

"string equation" [299, 294, 244]

$$t\,\xi = r(\xi) + \sum_{k=1}^{(p-1)/2} g_{2k+2} \binom{2k+1}{k+1} r(\xi)^{k+1}\,, \tag{8.72}$$

the planar part of the free energy can be written as

$$F_0(t) = t^2 \int_0^1 \mathrm{d}\xi\,(1-\xi)\log r(\xi)\,. \tag{8.73}$$

This integral is obtained as a continuum approximation to a discrete sum [299, 294, 244], with errors potentially given by the Euler-Maclaurin formula. Note that $r(\xi) \approx t\xi$ as $\xi \to 0$. The relation $r(\xi) = t\xi$ would be exact for the Gaussian matrix integral. The integrand in (8.73) thus behaves as $\log \xi$ near the lower limit $\xi = 0$. It is for this reason that the combination

$$F_0(t) - F_{0,G}(t) = t^2 \int_0^1 \mathrm{d}\xi\,(1-\xi)\log \frac{r(\xi)}{t\xi} \tag{8.74}$$

is better behaved and $\log \frac{Z(N,t)}{Z_G(N,t)}$ has a good asymptotic expansion without logarithmic terms [299, 294, 300].

We intend to go beyond the perturbative expansion (8.70) and include effects from one-eigenvalue instantons [246, 248]. A single eigenvalue in the matrix integral (8.37) at position x_i feels an effective potential

$$V(x_i) - \frac{2t}{N} \sum_{j:j\neq i} \log|x_i - x_j|\,. \tag{8.75}$$

In the large-N limit, it is useful to introduce a *holomorphic* effective potential defined as [282]

$$V_{\text{eff}}(x,t) := V(x) - 2t \int_{-b}^{b} \mathrm{d}y\,\rho(y)\log(y-x)\,, \tag{8.76}$$

where $\rho(y)$ is the eigenvalue density normalized according to $\int_{-b}^{b} \mathrm{d}y\,\rho(y) = 1$. The actual potential felt by an eigenvalue is the *real part* of the holomorphic effective potential. For a review of some basic properties of the effective potential and more features of the large-N one-cut saddle point. Here, we just mention the following important relations [294], reviewed in (8.44), (8.45),

$$V'_{\text{eff}}(x) = M(x)\sqrt{x^2 - b^2}\,, \tag{8.77}$$

$$\rho(x) = \frac{1}{2\pi t} M(x)\sqrt{b^2 - x^2}\;\Theta(b - |x|)\,, \tag{8.78}$$

where $\Theta(x)$ is the Heaviside step function and $M(x)$ is a polynomial determined from the potential by the requirement that the resolvent $\omega_0(x) = \frac{1}{2t}(V'(x) - M(x)\sqrt{x^2 - b^2})$ behaves as $1/x$ as $x \to \infty$ on the physical x-sheet.

The one-eigenvalue instantons correspond to the extrema of $V_{\text{eff}}(x)$ with x being outside the interval $[-b, b]$. Once we have identified these extrema $\{x_\alpha\}$, we can define a general ℓ-instanton partition function $Z^{\{\ell_\alpha\}}(N, t)$ as follows. Let $\{\ell_\alpha\}$ be a finite sequence of non-negative integers (all being $O(N^0)$, not all zero) satisfying $\sum_\alpha \ell_\alpha = \ell$. Then $Z^{\{\ell_\alpha\}}(N, t)$ is defined as the contribution to the integral (8.37) where a number ℓ_α of eigenvalues are integrated along the steepest descent contour of the particular extremum x_α and $(N-\ell)$ of the eigenvalues are integrated along the interval $[-b, b]$ corresponding to the perturbative regime. The quantity $Z^{(0)}$ denotes the contribution to the matrix integral where the integration range of each eigenvalue extends over the perturbatively allowed region $[-b, b]$. Once we have chosen a particular integration contour for the x_i's in (8.37), we can express this contour as a weighted sum of the steepest descent contours. Accordingly, the partition function is given by a weighted sum of the $Z^{\{\ell_\alpha\}}$'s.

Unlike [257, 23, 245], in this chapter we will not be careful about the defining contour for the eigenvalues for the full partition function, and what linear combination of the steepest descent contours is homologous to the defining contour. In particular, the question of the existence of the double-scaling limit, at finite values of the double-scaled coupling constant, is beyond the scope of this work. Hence, we will simply compute $Z^{\{\ell_\alpha\}}$ by integrating the eigenvalues along the *full* steepest descent contours.

Identical instantons

We will consider the most general instanton configuration in the next subsection, but for now we consider ℓ identical instantons. To be more precise, we integrate ℓ eigenvalues along the steepest descent contour corresponding to the extremum $x^\star$ of the one-eigenvalue effective potential, and we want to compute the ratio $\frac{Z^{(\ell)}(N,t)}{Z^{(0)}(N,t)}$.

The definition of $V_{\text{eff}}(x, t)$ given in (8.76) was in the strict large-N limit. Since we want to compute the answer including the one-loop correction, we need to carefully keep track of $1/N$ corrections. For this we need to take into account the fact that the original cut now only contains $N - \ell$ eigenvalues. Since the overall coefficient in front of the potential remains N/t, if we want to interpret the second term in (8.76) as an expectation value in the matrix model, this integral over $N - \ell$ eigenvalues must be evaluated at a shifted value of the 't Hooft coupling, namely $t' = t - t\ell/N$. This is so that N/t can be rewritten as $(N - \ell)/t'$.

An important remark is that we need to properly treat the Vandermonde repulsion between the ℓ eigenvalues. If $\ell > 1$ and we naively substitute $x^\star$ for each of the ℓ eigenvalues, the result will vanish. This means that there is an $\ell \times \ell$ Gaussian matrix integral that we need to compute exactly.

Separating out ℓ eigenvalues to be placed near $x^\star$ in the integral (8.37), we get the

expression

$$Z^{(\ell)}(N,t) = \frac{1}{N!}\binom{N}{\ell}\int_{\mathcal{C}_0}\prod_{i=1}^{N-\ell}\frac{\mathrm{d}x_i}{2\pi}\prod_{\substack{i,j=1\\ i<j}}^{N-\ell}(x_i-x_j)^2\exp\left[-\frac{N}{t}\sum_{i=1}^{N-\ell}V(x_i)\right]$$
$$\times\int_{\mathcal{C}_1}\prod_{i=N-\ell+1}^{N}\frac{\mathrm{d}x_i}{2\pi}\prod_{\substack{i,j=N-\ell+1\\ i<j}}^{N}(x_i-x_j)^2\exp\Big[-\frac{N}{t}\sum_{i=N-\ell+1}^{N}V_{\text{eff}}(x_i,t-t\ell/N) \quad (8.79)$$
$$+2\sum_{i=N-\ell+1}^{N}\sum_{j=N-\ell+1}^{N}A_{0,2}(x_i,x_j,t-t\ell/N)+\cdots\Big]$$

where

$$V_{\text{eff}}(x,t-t\ell/N)) = V(x) - \frac{2t}{N}\left\langle\sum_{j=1}^{N-\ell}\ln(x-x_j)\right\rangle, \quad (8.80)$$

$$A_{0,2}(x,x',t-t\ell/N) = \sum_{i=1}^{N-\ell}\sum_{j=1}^{N-\ell}\left\langle\ln(x-x_i)\ln(x'-x_j)\right\rangle_c. \quad (8.81)$$

We used the fact that $\langle e^X\rangle = e^{\langle X\rangle+\frac{1}{2}\langle X^2\rangle_c+\cdots}$. Here $\mathcal{C}_0$ is the perturbatively allowed range for the eigenvalues and $\mathcal{C}_1$ is the steepest descent contour of the effective potential around the non-perturbative saddle point. In the large-N limit with t fixed, the quantities V_{eff} and $A_{0,2}$ are of order unity with corrections of order $1/N^2$. The quantity $A_{0,2}$ denotes the *connected* two-point function of the Vandermonde potential exerted by the $N-\ell$ eigenvalues. It contributes at the same order as the one-loop Gaussian integral around the non-perturbative saddle point.

Recall that $x^\star$ denote the location of an extremum of $V_{\text{eff}}(x,t)$ and let us denote the derivative with respect to x with a prime.[6] We now approximate the term $V_{\text{eff}}(x_i,t-\ell t/N)$ appearing in (8.79) as follows

$$V_{\text{eff}}(x_i,t-\ell t/N) \approx V_{\text{eff}}(x^\star,t) + \frac{1}{2}V''_{\text{eff}}(x^\star,t)\,(x_i-x^\star)^2 - \frac{\ell t}{N}\,\partial_t V_{\text{eff}}(x^\star,t)\,. \quad (8.82)$$

Since we are interested in the answer up to one-loop order, we need to keep the last term [282]. We also replaced x_i with $x^\star$ in this last term, since we will be evaluating the x_i integral by saddle point. As far as the term $A_{0,2}(x,x',t-t\ell/N)$ is concerned, we can replace it with $A_{0,2}(x^\star,x^\star,t)$.

[6]The quantity $x^\star$ depends on t and so the shift in the argument $t\to t-\ell t/N$ causes a shift of order $1/N$ in the value of $x^\star$. However the effect of this is suppressed by inverse powers of $1/N$ compared to the terms we keep. Hence we shall ignore this effect.

Using these ingredients, we get

$$Z^{(\ell)}(N,t) = Z^{(0)}(N-\ell, t-t\ell/N)\, \exp\left[-\frac{N}{t}\ell\, V_{\rm eff}(x^\star,t) + \ell^2 \partial_t V_{\rm eff}(x^\star,t) + 2\ell^2 A_{0,2}(x^\star,x^\star,t)\right] \times \frac{1}{\ell!}\int_{\mathcal{C}_1} \prod_{i=N-\ell+1}^{N} \frac{{\rm d}x_i}{2\pi} \prod_{\substack{i<j \\ i,j=N-\ell+1}}^{N} (x_i-x_j)^2 \exp\left[-\frac{N}{t} V''_{\rm eff}(x^\star,t) \sum_{i=N-\ell+1}^{N} \frac{1}{2}(x_i-x^\star)^2\right]. \tag{8.83}$$

We now recognize the second line as a Gaussian matrix integral over $\ell \times \ell$ matrices, so we can use (8.64). Writing $Z^{(0)}(N-\ell, t-t\ell/N) \approx \exp\left(\frac{N^2}{t^2} F_0(t-t\ell/N)\right)$ and Taylor expanding $F_0(t-t\ell/N)$ to second order we get[7]

$$\frac{Z^{(\ell)}(N,t)}{Z^{(0)}(N,t)} = \exp\left[-\frac{N}{t}\ell\,\mathcal{A}\right]\, \mathcal{B}^{\ell^2}\, \frac{G_2(\ell+1)}{(2\pi)^{\frac{1}{2}(\ell^2+\ell)}}\,, \tag{8.84}$$

where we have defined

$$\mathcal{A} := V_{\rm eff}(x^\star,t) + \partial_t F_0(t)\,, \tag{8.85}$$

$$\mathcal{B} := \exp\left[\frac{1}{2}\partial_t^2 F_0(t) + \partial_t V_{\rm eff}(x^\star,t) + 2A_{0,2}(x^\star,x^\star,t)\right]\left(\frac{2\pi t}{N V''_{\rm eff}(x^\star)}\right)^{\frac{1}{2}}\,, \tag{8.86}$$

and $G_2(\ell+1) = \prod_{i=1}^{\ell} i^{\ell-i}$ is the Barnes-G double gamma function. The quantity $N\mathcal{A}/t$ is interpreted as the tension of a single instanton. The exponential expression appearing in the quantity $\mathcal{B}$ turns out to have a simple formula in terms of the perturbative one-cut saddle point, see (8.54). As described in (8.47), the quantity $\partial_t F_0(t)$ is equal to minus the real part of the effective potential on the cut. This implies that

$$\mathcal{A} = \int_{-b}^{x^\star} {\rm d}x\, V'_{\rm eff}(x)\,. \tag{8.87}$$

We shall see that the quantities $N\mathcal{A}/t$ and $\mathcal{B}$ stay finite in the double-scaling limit.

General multi-instanton configuration

Suppose we integrate ℓ_1 of the eigenvalues along the steepest descent contour of the extremum $x_1^\star$ (of the one-eigenvalue effective potential), ℓ_2 of the eigenvalues along the steepest descent contour of the extremum $x_2^\star$, and so on. Let $\ell = \sum_\alpha \ell_\alpha$ denote the total number of eigenvalues

[7] As discussed below (8.71), $\log Z^{(0)}(N,t)$ has logarithmic terms that invalidate the expansion in power series in N^{-2}. However these logarithmic terms are the same as those that appear in the gaussian matrix integral $Z_G(N,t)$. We show in (8.66) that the effect of the logarithmic terms drops out in the ratio $\frac{Z_G(N-\ell,t-t\ell/N)}{Z_G(N,t)}$, and hence it also drops out in the ratio $\frac{Z^{(0)}(N-\ell,t-t\ell/N)}{Z^{(0)}(N,t)}$.

that have been pulled out of the original cut, which now contains $N-\ell$ eigenvalues. First of all, we get a factor like the one on the right hand side of (8.84) for each α. Besides this, we get four new types of contributions involving each pair (α,β) for $\alpha\neq\beta$:

- The term $\ell^2\,\partial_t^2 F_0$ now contains terms proportional to $\ell_\alpha\ell_\beta\,\partial_t^2 F_0$.
- There will be a contribution proportional to $\ell_\alpha\ell_\beta\,A_{0,2}(x^\star_\alpha,x^\star_\beta,t)$ with $A_{0,2}$ given by the connected correlator (8.81) of the Vandermonde potential exerted by the $N-\ell$ eigenvalues in the cut $[-b,b]$.
- For each $x^\star_\alpha$, the last term of (8.82) is still proportional to ℓ. Therefore, in (8.83) it generates a term proportional to $\ell\,\ell_\alpha\,\partial_t V_{\rm eff}(x^\star_\alpha,t)$. After writing $\ell=\sum_\beta\ell_\beta$ this leads to terms of the form $\ell_\alpha\ell_\beta\,\partial_t V_{\rm eff}(x^\star_\alpha,t)$.
- There are an $\ell_\alpha\ell_\beta$ number of factors of $(x^\star_\alpha-x^\star_\beta)^2$ in the Vandermonde determinant.

Keeping these four things in mind and repeating the steps in the previous subsection, we get

$$\frac{Z^{\{\ell_\alpha\}}(N,t)}{Z^{(0)}(N,t)}=\exp\left[-\frac{N}{t}\sum_\alpha\ell_\alpha\mathcal{A}_\alpha\right]\prod_\alpha\left\{(\mathcal{B}_\alpha)^{\ell_\alpha^2}\,\frac{G_2(\ell_\alpha+1)}{(2\pi)^{\frac{1}{2}(\ell_\alpha^2+\ell_\alpha)}}\right\}\prod_{\alpha<\beta}(C_{\alpha,\beta})^{\ell_\alpha\ell_\beta}\,, \tag{8.88}$$

where

$$\mathcal{A}_\alpha:=V_{\rm eff}(x^\star_\alpha,t)+\partial_t F_0(t)=\int_{-b}^{x^\star_\alpha}\mathrm{d}x\,V'_{\rm eff}(x)\,, \tag{8.89}$$

$$\mathcal{B}_\alpha:=\exp\left[\frac{1}{2}\partial_t^2F_0(t)+\partial_tV_{\rm eff}(x^\star_\alpha,t)+2A_{0,2}(x^\star_\alpha,x^\star_\alpha,t)\right]\left(\frac{2\pi t}{NV''_{\rm eff}(x^\star_\alpha)}\right)^{\frac{1}{2}}\,, \tag{8.90}$$

$$\mathcal{C}_{\alpha,\beta}:=(x^\star_\alpha-x^\star_\beta)^2\,\exp\left[\partial_t^2F_0(t)+\partial_tV_{\rm eff}(x^\star_\alpha,t)+\partial_tV_{\rm eff}(x^\star_\beta,t)+4A_{0,2}(x^\star_\alpha,x^\star_\beta,t)\right]\,. \tag{8.91}$$

The quantities $\mathcal{A}_\alpha$ and $\mathcal{B}_\alpha$ are the same as in (8.85) and (8.86) with $x^\star$ replaced by $x^\star_\alpha$, but we have reproduced them here for completeness.

The quantities $\mathcal{B}_\alpha$ and $\mathcal{C}_{\alpha,\beta}$ turn out to have a simple formula in terms of the perturbative one-cut saddle point, even outside of the double-scaling limit [254, 282]. Using (8.54) we get,

$$\mathcal{B}_\alpha=\frac{b}{2((x^\star_\alpha)^2-b^2)}\left(\frac{2\pi t}{NV''_{\rm eff}(x^\star_\alpha)}\right)^{\frac{1}{2}}\,, \tag{8.92}$$

$$\mathcal{C}_{\alpha,\beta}=(x^\star_\alpha-x^\star_\beta)^2\left(\frac{b}{x^\star_\alpha x^\star_\beta-b^2+\sqrt{(x^\star_\alpha)^2-b^2}\sqrt{(x^\star_\beta)^2-b^2}}\right)^2\,. \tag{8.93}$$

The double-scaling limit

The double-scaling limit refers to a procedure where we tune the parameters of the potential and simultaneously zoom in near an edge of the eigenvalue spectrum, say the left one, such that the Feynman diagrams dominating the partition sum resemble continuum surfaces [244]. We define the energy variable E via $x = -b + \varepsilon E$, and also introduce the variable z via $E = -z^2$. The double-scaling limit is taken by sending ε to zero and N to infinity keeping the combination [8]

$$e^{S_0} := N\varepsilon^{\frac{p}{2}+1} \tag{8.94}$$

fixed. At the same time, we tune the coefficients of the polynomial potential V in a suitably analytic fashion such that $N\rho(x)\,\mathrm{d}x$ approaches $e^{S_0}\,\mathrm{d}E$ times a finite function of E in this limit. This function of E is supported on the entire positive real axis. There is some freedom in this process. We want to focus on the so-called "conformal background" [263] of minimal string theory, where only the cosmological constant operator is turned on. In this case the density of states $\rho(E)$ takes the form:[9]

$$\rho(E) = \varepsilon^{\frac{p}{2}+1}\,\frac{1}{\pi}\,\sinh\left(p\,\operatorname{arcsinh}\sqrt{E}\right) + O\left(\varepsilon^{\frac{p}{2}+2}\right)\,. \tag{8.95}$$

In this limit, e^{-S_0} becomes the genus expansion parameter and the perturbative contribution to the partition function has an expansion in even powers of e^{-S_0}. The precise relation between e^{-S_0} and the string coupling g_s may be found by comparing the matrix model results with the string theory results. From now on, we shall use E instead of x as the argument of V_{eff} and ρ, and by an abuse of notation, we will denote derivatives with respect to E also by a prime.

From (8.77) and (8.78) we see that the analytic continuation of $2\pi i t\rho(E)$ from the interval $[-b, b]$ on the real line to the complex plane gives $V'_{\text{eff}}(E)$. Using the form of $\rho(E)$ given in (8.95) we get the effective potential

$$V_{\text{eff}}(E) = -t\,\varepsilon^{\frac{p}{2}+1}\,\left[\frac{1}{p+2}\sin\left((p+2)\arcsin\sqrt{-E}\right) - \frac{1}{p-2}\sin\left((p-2)\arcsin\sqrt{-E}\right)\right]\,. \tag{8.96}$$

We have chosen the additive constant in the potential such that V_{eff} vanishes at $E = 0$. Note that $V_{\text{eff}}(E)$ introduced here differs from that of [23] by an overall normalization factor. See figure 8.1 for a plot of $V_{\text{eff}}(E)$ for the case $p = 7$.

[8] In the z coordinate introduced in (8.60), the double-scaling limit is defined by zooming in near $x = -2\gamma$ or $z = -1$. Using the relation $x = -2\gamma + \gamma(z+1)^2 + \ldots$ in the neighborhood of $z = -1$, and $x = -2\gamma + \varepsilon E$, we see that in this limit $z \simeq -1 + \sqrt{-\varepsilon E/\gamma}$.

[9] See, for example, [245] for a recent discussion on this and [258] for explicit potentials that lead to the above density of states in the double-scaling limit. Compared to the conventions of [23], we have set the constant κ appearing there to be $\kappa = 1/2$.

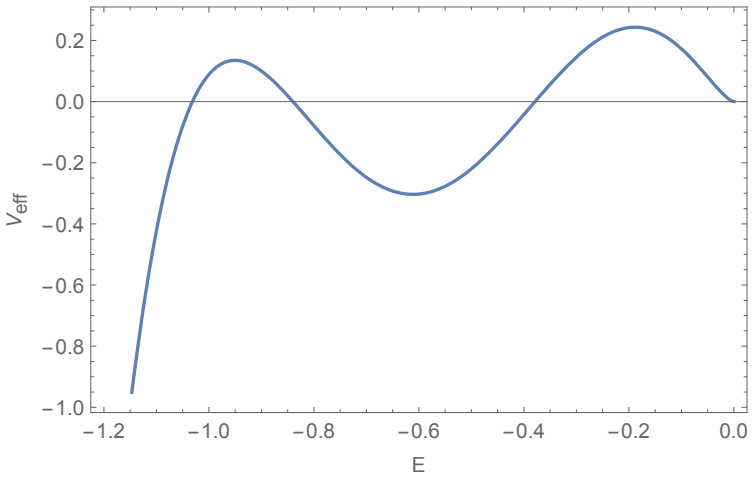

Figure 8.1: A plot of $V_{\rm eff}(E)\,\varepsilon^{-1-\frac{p}{2}}$ in equation (8.96) for the case $p=7$. We have set $t=1$. In general there are $\frac{p-1}{2}$ extrema in the forbidden region, given by (8.97). These extrema are in a one-to-one correspondence with the $(1,n)$ ZZ branes in the $(2,p)$ minimal string theory. The extremum closest to $E=0$ is always a maximum and corresponds to the simplest $(1,1)$ ZZ brane.

Since the zeros of $V'_{\rm eff}(E)$ on the negative real axis give the locations of the instanton, we conclude that the instantons are located at

$$E_n^\star = -\left(\sin\frac{n\pi}{p}\right)^2\,, \quad n\in\left\{1,\ldots,\frac{p-1}{2}\right\}\,. \tag{8.97}$$

The index n is the same as the one that appears in the label $(1,n)$ for the ZZ branes in the $(2,p)$ minimal string (see more on this below). From (8.97) and (8.96) we conclude that

$$V_{\rm eff}(E_n^\star) = (-1)^{n+1}\,t\,\varepsilon^{\frac{p}{2}+1}\,\frac{2p\sin(2\pi n/p)}{p^2-4}\,, \tag{8.98}$$

$$V''_{\rm eff}(E_n^\star) = (-1)^{n}\,t\,\varepsilon^{\frac{p}{2}+1}\,\frac{2p}{\sin(2\pi n/p)}\,. \tag{8.99}$$

It follows from (8.88), (8.89) and the relation $V_{\rm eff}(0)=0$, that the tension T_α of the α-th ZZ brane is given by,

$$T_\alpha = \frac{N}{t}\mathcal{A}_\alpha = \frac{N}{t}V_{\rm eff}(E_\alpha^\star) = (-1)^{n+1}\,e^{S_0}\,\frac{2p\sin(2\pi n/p)}{p^2-4} \quad \text{for } \alpha=(1,n)\,. \tag{8.100}$$

Since the right hand side does not involve N or ε, this has finite double-scaling limit. In order to compare this with the string theory result, we need to find the explicit relation between e^{S_0} and g_s via perturbative computation. We shall not attempt to do this here.

Instead we shall follow [23] and express our result for the other quantities in terms of the tension of the instanton given in (8.100).

Next, we need to work out the quantities $\mathcal{B}_\alpha$ and $\mathcal{C}_{\alpha,\beta}$ in the double-scaling limit. The expression for $\mathcal{B}_\alpha$ before taking this limit is given in (8.92). In the double-scaling limit, the first factor in (8.92) equals $\frac{1}{-4\varepsilon E}$. This ε in the denominator combines with the $\partial_x^2 V_{\rm eff}$ appearing in (8.92) to convert the ∂_x^2 into an ∂_E^2. Thus, the combination $\frac{1}{\varepsilon^2}\frac{t}{N\,\partial_x^2 V_{\rm eff}(x^\star)}$ equals $\frac{t}{N\partial_E^2 V_{\rm eff}(E^\star)}$. This gives

$$\mathcal{B}_\alpha = \frac{1}{-4E_\alpha^\star}\left(\frac{2\pi t}{NV''_{\rm eff}(E_\alpha^\star)}\right)^{\frac{1}{2}} = \frac{1}{4\sin^2(n\pi/p)}\left(\frac{(-1)^n\,\pi\,\sin(2\pi n/p)}{e^{S_0}p}\right)^{1/2} \quad \text{for } \alpha=(1,n). \tag{8.101}$$

There are no subtleties in taking the double-scaling limit for $\mathcal{C}_{\alpha,\beta}$, since the expression given in (8.93) remains finite in this limit. The final result takes the form:

$$\mathcal{C}_{\alpha,\beta} = \left(\frac{\sqrt{-E_\alpha^\star}-\sqrt{-E_\beta^\star}}{\sqrt{-E_\alpha^\star}+\sqrt{-E_\beta^\star}}\right)^2 \quad \Rightarrow \quad \mathcal{C}_{(1,n),(1,n')} = \left(\frac{\sin\frac{n\pi}{p}-\sin\frac{n'\pi}{p}}{\sin\frac{n\pi}{p}+\sin\frac{n'\pi}{p}}\right)^2 . \tag{8.102}$$

To compare these with the string theory results, we note that (8.88) has the same structure as (8.31) with B_α replaced by $\mathcal{B}_\alpha$ and $C_{\alpha,\beta}$ replaced by $\mathcal{C}_{\alpha,\beta}$. Therefore we need to compare B_α with $\mathcal{B}_\alpha$ and $C_{\alpha,\beta}$ with $\mathcal{C}_{\alpha,\beta}$. First, we see from (8.22) with $p'=2$, $m=m'=1$ that,

$$C_{(1,n),(1,n')} = \frac{\cos^2\left(\frac{\pi(n+n')}{2p}\right)\,\sin^2\left(\frac{\pi|n-n'|}{2p}\right)}{\cos^2\left(\frac{\pi|n-n'|}{2p}\right)\,\sin^2\left(\frac{\pi(n+n')}{2p}\right)} = \mathcal{C}_{(1,n),(1,n')}. \tag{8.103}$$

Next, using (8.100), we can express (8.101) as

$$\mathcal{B}_{1,n} = (T_{1,n})^{-\frac{1}{2}}\;\mathrm{i}\sqrt{\frac{\pi}{2}}\frac{\cot(\pi n/p)}{\sqrt{p^2-4}}\,. \tag{8.104}$$

On the other hand, from (8.30) with $p'=2$, $m=1$, we get

$$B_{1,n} = (T_{1,n})^{-\frac{1}{2}}\;\mathrm{i}\sqrt{\frac{\pi}{2}}\left(\frac{\cot^2(\pi n/p)}{p^2-4}\right)^{\frac{1}{2}}\,. \tag{8.105}$$

Therefore, we see that there is perfect agreement between the result in $(2,p)$ minimal string theory and the double-scaled one-matrix model.

We remind the reader that the result presented here for $\mathcal{B}T^{\frac{1}{2}}$ is twice that quoted in our previous work [23], which only dealt with the case $n=1$. This is because we are integrating over the full steepest descent contour of the saddle point, and we are not worrying about what linear combination of the steepest descent contours is homologous to the defining contour.

Let us remark that we can perform a consistency check of (8.100) by comparing the dependence on n to that obtained from the string theory computation. In string theory, the

tension of the ZZ branes can be obtained, up to an overall proportionality constant, using the formulas for the boundary state wavefunction $\Psi_{1,n}(P)$ [143]. Indeed, the entire dependence on n is given by a multiplicative factor $\sinh(2\pi nbP)$ (see equation (5.15) of [143]). Here P represents the Liouville momentum, which labels the exponential Liouville operators $e^{2\alpha\phi}$ with $\alpha = (b+b^{-1})/2 + \mathrm{i}P$. Therefore we set P to $-\mathrm{i}(b-b^{-1})/2$ in order to get the one-point function of the cosmological constant operator $e^{2b\phi}$ [259, 250]. Since $\langle e^{2b\phi}\rangle = \partial_\mu Z_{\text{disk}}$ and Z_{disk} is proportional to the tension of the ZZ brane, we see that $T_{1,n} \propto \sinh(2\pi nbP)$ with $P = -\mathrm{i}(b-b^{-1})/2$. Using the fact that $b = \sqrt{2/p}$, we get $T_{1,n} \propto (-1)^{n-1}\sin(2\pi n/p)$. This reproduces the n-dependence of the matrix integral formula (8.100).

8.4 Two-matrix integrals

The general (p', p) minimal string theory is dual to a matrix integral over two matrices [272, 273]. Denoting the matrices by M_1 and M_2, the action is $\frac{N}{t}\operatorname{Tr}(V_1(M_1) + V_2(M_2) - M_1M_2)$. Here M_1 and M_2 are Hermitian matrices, both of size $N \times N$. Using the Harishchandra-Itzykson-Zuber formula [301, 302, 303], it is possible to reduce this integral, up to an overall constant, to the following integral over the eigenvalues

$$Z(N,t) := \frac{1}{N!}\int \prod_{i=1}^{N} \frac{\mathrm{d}x_i \mathrm{d}y_i}{2\pi} \Delta(x)\Delta(y) \exp\left[-\frac{N}{t}\sum_{i=1}^{N}(V_1(x_i) + V_2(y_i) - x_iy_i)\right]. \tag{8.106}$$

Here, the x_i are the eigenvalues of M_1 and y_i are the eigenvalues of M_2. Note that there is only one power of the Vandermonde determinant for each set of eigenvalues.

The two-matrix Gaussian integral is given by [304]

$$Z_{G,2}(\ell) := \frac{1}{\ell!}\int \prod_{i=1}^{\ell} \frac{\mathrm{d}x_i \mathrm{d}y_i}{2\pi}\, \Delta(x)\Delta(y)\, \exp\left(-\frac{N}{t}\sum_{i=1}^{\ell}\left(\frac{c_1x_i^2}{2} + \frac{c_2y_i^2}{2} - c_3x_iy_i\right)\right) \tag{8.107}$$

$$= G_2(\ell+1)\left(\frac{t}{N}\right)^{\frac{1}{2}(\ell^2+\ell)} (c_1c_2 - c_3^2)^{-\frac{1}{2}\ell^2} c_3^{\frac{1}{2}(\ell^2-\ell)}. \tag{8.108}$$

The lemma in the appendix of [304] allows us to reduce this integral to the one-matrix Gaussian integral. Alternatively, one can derive it using two-matrix orthogonal polynomial technology; the orthogonal polynomials are still the Hermite polynomials. Again, this expression is exact and can be used for ℓ of order N. The asymptotic expansion of $Z_{G,2}(N)$ reads

$$\log Z_{G,2}(N) = N^2\left(\frac{1}{2}\log t - \frac{1}{2}\log\frac{c_1c_2 - c_3^2}{c_3} - \frac{3}{4}\right) - \frac{1}{2}N\log N + \frac{1}{2}N\log\frac{2\pi t}{c_3} + O(\log N). \tag{8.109}$$

We identify the first term on the right hand side as $N^2 F_{0,G}(t)/t^2$. Note the presence of terms of order $N \log N$ and N. Using the above expression we see that

$$\log \frac{Z_{G,2}(N-\ell, t-t\ell/N)}{Z_{G,2}(N,t)} = \frac{N^2}{t^2}\left(F_{0,G}(t-t\ell/N) - F_{0,G}(t)\right) - \frac{\ell}{2}\log\frac{2\pi t}{c_3 N} + O\left(\frac{1}{N}\right). \tag{8.110}$$

Comparing this to (8.66), we see the presence of an extra logarithmic term [256], which will be important in our analysis.

Now let us consider more general class of matrix integrals obtained by varying. While doing this, we choose to keep the coefficients of the quadratic terms fixed. For much the same reasons as discussed in Section 8.3, we obtain a nice asymptotic expansion in powers of $1/N^2$ after dividing by the Gaussian matrix integral

$$\log \frac{Z(N,t)}{Z_G(N,t)} = \sum_{g=0}^{\infty} N^{2-2g}(F_g(t) - F_{g,G}(t)). \tag{8.111}$$

We are interested in corrections to $\log Z$ that are of order e^{-N}. A single instanton would correspond to placing one pair (x_i, y_i) at an extremum of the effective potential that this pair feels. Explicitly, from (8.106), this effective potential is

$$V_{\text{eff}}(x_i, y_i) := V_1(x_i) - \frac{t}{N}\sum_{j:j\neq i}\log(x_i - x_j) + V_2(y_i) - \frac{t}{N}\sum_{j:j\neq i}\log(y_i - y_j) - x_i y_i. \tag{8.112}$$

Reference [256] obtained the normalization constant for a single instanton in the two-matrix integral. We shall now generalize this to the case of multiple instantons, possibly of different types. Our results at the intermediate stages will differ from that of [256] since we express our results in terms of correlation functions in the theory with N eigenvalues while [256] expresses the results in terms of correlation functions in the theory with $(N-1)$ eigenvalues [282].

The large-N limit

Recall that, we have defined the two-matrix integral via

$$Z(N,t) := \frac{1}{N!}\int \prod_{i=1}^{N}\frac{\mathrm{d}x_i \mathrm{d}y_i}{2\pi}\Delta(x)\Delta(y)\exp\left[-\frac{N}{t}\sum_{i=1}^{N}(V_1(x_i) + V_2(y_i) - x_i y_i)\right]. \tag{8.113}$$

Up to an overall normalization, this integral is proportional to

$$Z(N,t) \propto \int \mathrm{d}M_1 \mathrm{d}M_2 \exp\left[-\frac{N}{t}\operatorname{Tr}\left(V_1(M_1) + V_2(M_2) - M_1 M_2\right)\right], \tag{8.114}$$

via the Harishchandra-Itzykson-Zuber formula [301, 302, 303]. In order to get to the (p', p) minimal string, we can take V_1 to be a polynomial of degree p and V_2 to be a polynomial of degree p' [273]. To get back the one-matrix case, one can set $p' = 2$ and integrate out the matrix M_2.

We define two functions $Y(x)$ and $X(y)$ as follows [305]

$$Y(x) := V_1'(x) - \frac{t}{N}\left\langle \mathrm{Tr}\,\frac{1}{x - M_1}\right\rangle , \tag{8.115}$$

$$X(y) := V_2'(y) - \frac{t}{N}\left\langle \mathrm{Tr}\,\frac{1}{y - M_2}\right\rangle . \tag{8.116}$$

Note that in terms of $V_{1,\mathrm{eff}}(x)$ and $V_{2,\mathrm{eff}}(y)$ defined in (8.124) and (8.125), we have

$$V_{1,\mathrm{eff}}'(x) = Y(x), \qquad V_{2,\mathrm{eff}}'(y) = X(y)\,. \tag{8.117}$$

We have suppressed the dependence on t, with the understanding that both sides will have the same dependence on t. Let us define the spectral curve Σ via

$$\Sigma := \{(u, v) \in \mathbb{C}^2 \,|\, (V_1'(u) - v)(V_2'(v) - u) - P(u, v) + t = 0\}\,, \quad \text{where} \tag{8.118}$$

$$P(u, v) := \frac{t}{N}\left\langle \mathrm{Tr}\left(\frac{V_1'(u) - V_1'(M_1)}{u - M_1}\frac{V_2'(v) - V_2'(M_2)}{v - M_2}\right)\right\rangle . \tag{8.119}$$

It can be shown, via Schwinger-Dyson equations, that *both* the points $(x, Y(x))$ and $(X(y), y)$ lie on the spectral curve Σ [305]. Generically, we can use either x or y as the local coordinate on Σ. The projection to x ceases to be a good coordinate when $\mathrm{d}Y(x)/\mathrm{d}x = \infty$. Typically, this will happen when $Y(x)$ has a square root behavior near some x. A similar remark holds for projection to y.

Like in the one-matrix case, we work with the case when Σ has genus zero (apart from the singular points to be discussed below). Denoting the uniformization parameter by $z \in \mathbb{C} \cup \{\infty\}$, we can coordinatize Σ as [305, 306]

$$(\mathcal{X}(z), \mathcal{Y}(z)) \in \Sigma\,, \tag{8.120}$$

$$\mathcal{X}(z) = \gamma z + \sum_{k=0}^{p'-1} \alpha_k\, z^{-k}\,, \quad \mathcal{Y}(z) = \gamma z^{-1} + \sum_{k=0}^{p-1} \beta_k\, z^k\,. \tag{8.121}$$

This means that for given x, we can find a z such that $x = \mathcal{X}(z)$, $Y(x) = \mathcal{Y}(z)$, and for given y, we can find a z' such that $X(y) = \mathcal{X}(z')$, $y = \mathcal{Y}(z')$. The map $\mathcal{X} : z \mapsto x$ is, generically, a p'-to-1 map except at p' values of z where $\mathrm{d}\mathcal{X}(z)/\mathrm{d}z = 0$. This means that we need p' number of x-sheets to cover the z-plane, or, equivalently, to cover Σ. The "physical" x-sheet contains the point $z = \infty$, near which the resolvent $\frac{1}{N}\langle \mathrm{Tr}\,\frac{1}{x - M_1}\rangle$ behaves as $\frac{1}{x}$. The boundary of the physical x-sheet on Σ is where the eigenvalues of M_1 are distributed. Of course, analogous comments apply to the map $\mathcal{Y}(z) : z \mapsto y$, with p' replaced by p. The

important distinction is that the physical y-sheet contains the point $z = 0$, near which the resolvent $\frac{1}{N}\langle \mathrm{Tr}\, \frac{1}{y-M_2}\rangle$ behaves as $\frac{1}{y}$.

If $y = Y(x)$, then $(x, y) \in \Sigma$. On the other hand, $(X(y), y)$ is also on Σ. However it does not follow from this that $x = X(y)$, since in general (x, y) and $(X(y), y)$ belong to different Riemann sheets. Exceptions are the "one-eigenvalue instantons" since it follows from (8.129) and (8.117) that they are located at the points $(x^\star, y^\star)$ satisfying

$$x^\star = X(y^\star), \quad y^\star = Y(x^\star)\,. \tag{8.122}$$

It then follows that if $\mathcal{X}(z^\star) = x^\star$, then $\mathcal{Y}(z^\star) = Y(x^\star) = y^\star$. These represent ZZ branes in minimal string theory after taking the double-scaling limit [264]. However, in the neighborhood of $(x^\star, y^\star)$ the points $(x, Y(x))$ and $(X(y), y)$ belong to different branches and there will exist *two distinct values* of z, call them $z^{\star(1)}$ and $z^{\star(2)}$, such that

$$(x^\star, y^\star) = (\mathcal{X}(z^{\star(1)})\,, \mathcal{Y}(z^{\star(1)})) = (\mathcal{X}(z^{\star(2)})\,, \mathcal{Y}(z^{\star(2)}))\,. \tag{8.123}$$

In the neighborhood of these points the equation defining Σ looks like $\alpha(x-x^\star)^2-\beta(y-y^\star)^2 = 0$ and the surface is singular.[10]

Identical instantons

In this section, we shall analyze the contribution due to ℓ instantons of the same type. The main idea is similar to that in Section 8.3. We pull out ℓ pairs (x_i, y_i) and place them at one particular extremum of $V_{\text{eff}}(x_i, y_i)$. Let us denote this extremum by $(x^\star, y^\star)$.

We define the following quantities

$$V_{1,\text{eff}}(x, t - t\ell/N)) = V_1(x) - \frac{t}{N}\left\langle \sum_{j=1}^{N-\ell} \ln(x - x_j) \right\rangle\,, \tag{8.124}$$

$$V_{2,\text{eff}}(y, t - t\ell/N)) = V_2(y) - \frac{t}{N}\left\langle \sum_{j=1}^{N-\ell} \ln(y - y_j) \right\rangle\,, \tag{8.125}$$

[10] As a simple example, consider the "figure-8" curve defined by $x^4 = x^2 - y^2$, embedded in $\mathbb{R}^2$ and parametrized as $(x, y) = (\sin t, \sin t \cos t)$. The point $(0, 0)$ is a double point, and corresponds to both $t = 0$ and $t = \pi$. In the discussion of the one-matrix case, the two values of the uniformizing coordinate at the instanton locations are related as $z^{\star(2)} = 1/z^{\star(1)}$.

and also the connected correlators of the Vandermonde potentials

$$A^{(1)}_{0,2}(x,x',t-t\ell/N)=\sum_{i=1}^{N-\ell}\sum_{j=1}^{N-\ell}\left\langle \ln(x-x_i)\ln(x'-x_j)\right\rangle_c\,, \tag{8.126}$$

$$A^{(2)}_{0,2}(y,y',t-t\ell/N)=\sum_{i=1}^{N-\ell}\sum_{j=1}^{N-\ell}\left\langle \ln(y-y_i)\ln(y'-y_j)\right\rangle_c\,, \tag{8.127}$$

$$A^{(3)}_{0,2}(x,y,t-t\ell/N)=\sum_{i=1}^{N-\ell}\sum_{j=1}^{N-\ell}\left\langle \ln(x-x_i)\ln(y-y_j)\right\rangle_c\,. \tag{8.128}$$

It follows from (8.112)-(8.125) that $(x^\star,y^\star)$ are determined from the equations

$$V'_{1,\text{eff}}(x^\star,t)=y^\star,\qquad V'_{2,\text{eff}}(y^\star,t)=x^\star\,, \tag{8.129}$$

up to corrections that do not affect the result to the order of $1/N$ expansion that we are interested in.

Qualitatively, we have the same terms as in the one-matrix case: since there are $N-\ell$ pairs of eigenvalues that are integrated on the perturbative contour, and the coefficient N/t does not change, the 't Hooft coupling is shifted to $t-\ell t/N$. This contributes t-derivatives of F_0, $V_{1,\text{eff}}$ and $V_{2,\text{eff}}$. We also get the connected correlators of the Vandermonde potentials. There is an $\ell\times\ell$ two-matrix Gaussian integral that one needs to do exactly. So we have

$$\begin{aligned}
Z^{(\ell)}(N,t)=\frac{1}{N!}\binom{N}{\ell}\int_{\mathcal{C}_0}\prod_{i=1}^{N-\ell}\frac{\mathrm{d}x_i\mathrm{d}y_i}{2\pi}\prod_{\substack{i<j\\ i,j=1}}^{N-\ell}(x_i-x_j)(y_i-y_j)\\
\exp\left[-\frac{N}{t}\sum_{i=1}^{N-\ell}\{V_1(x_i)+V_2(y_i)-x_iy_i\}\right]\\
\times\int_{\mathcal{C}_1}\prod_{i=N-\ell+1}^{N}\frac{\mathrm{d}x_i\mathrm{d}y_i}{2\pi}\prod_{\substack{i<j\\ i,j=N-\ell+1}}^{N}(x_i-x_j)(y_i-y_j)\\
\exp\Bigg[-\frac{N}{t}\sum_{i=N-\ell+1}^{N}\{V_{1,\text{eff}}(x_i,t-t\ell/N)+V_{2,\text{eff}}(y_i,t-t\ell/N)-x_iy_i\}\\
+\frac{1}{2}\sum_{i,j=N-\ell+1}^{N}\{A^{(1)}_{0,2}(x_i,x_j,t)+A^{(2)}_{0,2}(y_i,y_j,t)+2A^{(3)}_{0,2}(x_i,y_j,t)\}+\cdots\Bigg]\,.
\end{aligned} \tag{8.130}$$

Here $\mathcal{C}_0$ is the perturbatively allowed range for the eigenvalues and $\mathcal{C}_1$ is the Lefschetz thimble of the effective potential around the non-perturbative saddle point. Just as in the one-matrix case (8.82), we need to Taylor expand $V_{1,\text{eff}}(x_i,t-t\ell/N)$ and $V_{2,\text{eff}}(y_i,t-t\ell/N)$ to first order in ℓ/N, while the shift in t can be ignored in the connected correlators; indeed we have already

replaced $t - t\ell/N$ with t for these terms. Also, we need to Taylor expand $V_{1,\text{eff}}(x_i, t - t\ell/N)$ and $V_{2,\text{eff}}(y_i, t - t\ell/N)$ to second order in $x_i - x^\star$ and $y_i - y^\star$, while we can replace x_i and y_i by their saddle point values in the connected correlators. The integral over $\mathcal{C}_1$ now forms a two-matrix Gaussian integral that is given in (8.108). Thus, we get

$$\begin{aligned} Z^{(\ell)}(N,t) = Z^{(0)}(N-\ell, t - t\ell/N) \\ \times \exp\left[\frac{\ell^2}{2}\left(A^{(1)}_{0,2}(x^\star,x^\star,t) + A^{(2)}_{0,2}(y^\star,y^\star,t) + 2A^{(3)}_{0,2}(x^\star,y^\star,t)\right)\right] \\ \times \exp\left[\ell^2\left(\partial_t V_{1,\text{eff}}(x^\star,t) + \partial_t V_{2,\text{eff}}(y^\star,t)\right)\right] \times \exp\left[-\frac{N}{t}\,\ell\, V_{\text{eff}}(x^\star,y^\star)\right] \\ \times G_2(\ell+1)\left(\frac{t}{N}\right)^{\frac{1}{2}(\ell^2+\ell)} \left(V''_{1,\text{eff}}(x^\star,t)V''_{2,\text{eff}}(y^\star,t) - 1\right)^{-\ell^2/2} . \end{aligned} \tag{8.131}$$

Now we would like to compute the ratio $\frac{Z^{(\ell)}(N,t)}{Z^{(0)}(N,t)}$. From the above equation we see that this involves the ratio $\frac{Z^{(0)}(N-\ell,t-t\ell/N)}{Z^{(0)}(N,t)}$. The main novelty as compared to the one-matrix case is that we need to worry about the division by the Gaussian matrix integral. As we remarked in (8.111), it is $\frac{Z^{(0)}(N,t)}{Z_{G,2}(N,t)}$ that has a nice asymptotic expansion, and from (8.110) we see that

$$\log\frac{Z_{G,2}(N-\ell,t-t\ell/N)}{Z_{G,2}(N,t)} = \frac{N^2}{t^2}\left(F_{0,G}(t-t\ell/N) - F_{0,G}(t)\right) - \frac{\ell}{2}\log\frac{2\pi t}{N} + O\left(\frac{1}{N}\right) . \tag{8.132}$$

We want to emphasize the term $-\frac{\ell}{2}\log\frac{2\pi t}{N}$ in this equation, which is novel in the two-matrix case.[11] This means that in the large-N limit we should write

$$\frac{Z^{(0)}(N-\ell,t-t\ell/N)}{Z^{(0)}(N,t)} = \exp\left[\frac{N^2}{t^2}\left(-\frac{\ell t}{N}\partial_t F_0(t) + \frac{1}{2}\frac{\ell^2 t^2}{N^2}\partial_t^2 F_0(t)\right)\right]\left(\frac{N}{2\pi t}\right)^{\frac{\ell}{2}} . \tag{8.133}$$

The multiplicative power of $N^{\ell/2}$ is important since it combines with $N^{-\frac{1}{2}(\ell^2+\ell)}$ in (8.131) to give $N^{-\ell^2/2}$. It is important to get this power, otherwise the answer would not agree with the string theory result.

Thus, the final result is

$$\frac{Z^{(\ell)}(N,t)}{Z^{(0)}(N,t)} = \exp\left[-\frac{N}{t}\,\ell\,\mathcal{A}\right]\mathcal{B}^{\ell^2}\,\frac{G_2(\ell+1)}{(2\pi)^{\frac{1}{2}(\ell^2+\ell)}} \tag{8.134}$$

[11] We can see from (8.66) that the correction is order $1/N$ in the one-matrix case, and hence not important to the order that we are working at. This was discussed in footnote 7.

with the quantities $\mathcal{A}$ and $\mathcal{B}$ defined as

$$\mathcal{A} := V_{\text{eff}}(x^\star, y^\star) + \partial_t F_0(t)\,, \tag{8.135}$$

$$\begin{aligned}\mathcal{B} := \left(\frac{2\pi t}{N}\,\frac{1}{V''_{1,\text{eff}}(x^\star,t)V''_{2,\text{eff}}(y^\star,t)-1}\right)^{\frac{1}{2}} \exp\Bigg[&\frac{1}{2}\partial_t^2 F_0(t) + \partial_t V_{1,\text{eff}}(x^\star,t)\\ &+\partial_t V_{2,\text{eff}}(y^\star,t) + \frac{1}{2}A^{(1)}_{0,2}(x^\star,x^\star,t) + \frac{1}{2}A^{(2)}_{0,2}(y^\star,y^\star,t) + A^{(3)}_{0,2}(x^\star,y^\star,t)\Bigg]\,.\end{aligned} \tag{8.136}$$

These quantities are similar to (8.85) and (8.86) in the one-matrix case. They represent the on-shell action and the total one-loop contribution about the instanton configuration. Furthermore, we shall see later that $N\mathcal{A}/t$ and $\mathcal{B}$ are finite in the double-scaling limit, representing the tension of the ZZ brane and the exponential of the annulus between a ZZ brane and itself.

General multi-instanton configuration

We now follow the logic of one-matrix case and generalize to an arbitrary configuration of instantons. Let us integrate an ℓ_1 number of (x, y) pairs along the Lefschetz thimble of the saddle point $(x_1^\star, y_1^\star)$, an ℓ_2 number of (x, y) pairs along the Laefscetz thimble of the saddle point $(x_2^\star, y_2^\star)$, and so on. Let $\ell = \sum_\alpha \ell_\alpha$ be the total number of instantons. For each α we shall get a factor of the form (8.134). Besides this, there are four types of contributions that give rise to a multiplicative factor $\mathcal{C}_{\alpha,\beta}^{\ell_\alpha \ell_\beta}$. They are similar to the ones we enumerated in one-matrix case, except that we have more functions to keep track of. Also, the Vandermonde contribution is now a power of $(x_\alpha^\star - x_\beta^\star)(y_\alpha^\star - y_\beta^\star)$.

After a straightforward, though perhaps slightly tedious calculation, we arrive at the result

$$\frac{Z^{(\ell_1,\ell_2,\ldots)}(N,t)}{Z^{(0)}(N,t)} = \exp\left[-\frac{N}{t}\sum_\alpha \ell_\alpha \mathcal{A}_\alpha\right] \prod_\alpha \left\{(\mathcal{B}_\alpha)^{\ell_\alpha^2}\,\frac{G_2(\ell_\alpha+1)}{(2\pi)^{\frac{1}{2}(\ell_\alpha^2+\ell_\alpha)}}\right\} \prod_{\alpha<\beta} \mathcal{C}_{\alpha,\beta}^{\ell_\alpha\ell_\beta}\,, \tag{8.137}$$

with the definitions

$$\mathcal{A}_\alpha := V_{\text{eff}}(x_\alpha^\star, y_\alpha^\star) + \partial_t F_0(t)\,, \tag{8.138}$$

$$\begin{aligned}\mathcal{B}_\alpha := \left(\frac{2\pi t}{N}\,\frac{1}{V''_{1,\text{eff}}(x_\alpha^\star)V''_{2,\text{eff}}(y_\alpha^\star)-1}\right)^{\frac{1}{2}} \exp\Bigg[&\frac{1}{2}\partial_t^2 F_0(t) + \partial_t V_{1,\text{eff}}(x_\alpha^\star) + \partial_t V_{2,\text{eff}}(y_\alpha^\star) +\\ &+ \frac{1}{2}A^{(1)}_{0,2}(x_\alpha^\star,x_\alpha^\star) + \frac{1}{2}A^{(2)}_{0,2}(y_\alpha^\star,y_\alpha^\star) + A^{(3)}_{0,2}(x_\alpha^\star,y_\alpha^\star)\Bigg]\,,\end{aligned} \tag{8.139}$$

$$\begin{aligned}\mathcal{C}_{\alpha,\beta} := (x_\alpha^\star - x_\beta^\star)(y_\alpha^\star - y_\beta^\star)\exp\Big[&\partial_t^2 F_0(t) + \partial_t V_{1,\text{eff}}(x_\alpha^\star) + \partial_t V_{2,\text{eff}}(y_\alpha^\star) + \partial_t V_{1,\text{eff}}(x_\beta^\star)\\ &+\partial_t V_{2,\text{eff}}(y_\beta^\star) + A^{(1)}_{0,2}(x_\alpha^\star,x_\beta^\star) + A^{(2)}_{0,2}(y_\alpha^\star,y_\beta^\star) + A^{(3)}_{0,2}(x_\alpha^\star,y_\beta^\star) + A^{(3)}_{0,2}(x_\beta^\star,y_\alpha^\star)\Big]\,.\end{aligned} \tag{8.140}$$

The quantities $\mathcal{A}_\alpha$ and $\mathcal{B}_\alpha$ are the same as what we derived in the previous section, but we have included them in this result for the sake of convenience. Comparing (8.137) with (8.29) we see that the matrix model results agree with the string theory results provided we identify T_α with $N\mathcal{A}_\alpha/t$, B_α with $\mathcal{B}_\alpha$ and $C_{\alpha,\beta}$ with $\mathcal{C}_{\alpha,\beta}$. We shall verify these in the next subsection.

Now we come to the calculation of the objects that we need, namely those that appear in the formulas (8.138), (8.139) and (8.140). Using the expressions in [306], it was shown in [256] that

$$\mathcal{A}_\alpha = V_{\text{eff}}(x^\star, y^\star) + \partial_t F_0 = \int_{z^{\star(2)}}^{z^{\star(1)}} \mathrm{d}z\, \mathcal{Y}(z)\, \frac{\mathrm{d}\mathcal{X}(z)}{\mathrm{d}z}\,. \tag{8.141}$$

It was shown in [306] that

$$\partial_t^2 F_0 = 2\log\gamma\,, \tag{8.142}$$

which is directly analogous to the equation (8.48) in the one-matrix case. Further, we have the following equality of one-forms [306]

$$\partial_t Y(x)|_{x=\mathcal{X}(z)}\ \mathrm{d}\mathcal{X}(z) = -\,\partial_t X(y)|_{y=\mathcal{Y}(z)}\ \mathrm{d}\mathcal{Y}(z) = -\frac{\mathrm{d}z}{z} \tag{8.143}$$

In the one-matrix case, the analog of this equation would be (8.41). To get an expression for the t-derivatives of the effective potentials, note that the definition (8.124) implies that

$$V_{1,\text{eff}}(x) = \int_{\Lambda_x}^{x} \mathrm{d}x'\, Y(x') + \left(V_1(\Lambda_x) - t\log\Lambda_x\right)\,, \tag{8.144}$$

where the limit $\Lambda_x \to \infty$ on the physical x-sheet is understood. Using (8.143) we see that if we introduce the variable z' via $x' = \mathcal{X}(z')$ then,

$$\partial_t V_{1,\text{eff}}(x) = -\int_{\Lambda_x}^{x} \mathrm{d}x'\, \frac{1}{z'}\,\frac{\mathrm{d}z'}{\mathrm{d}x'} - \log\Lambda_x = -\int_{\Lambda_x/\gamma}^{z} \frac{\mathrm{d}z'}{z'} - \log\Lambda_x = -\log(z\gamma)\,, \tag{8.145}$$

where we used the fact that $x \approx \gamma z$ near $x = \infty$ on the physical x-sheet, see (8.121). This equation is the direct analog of (8.61) in the two-matrix case. Similarly, we have

$$\partial_t V_{2,\text{eff}}(y) = \int_{\Lambda_y}^{y} \mathrm{d}y'\, \frac{1}{z'}\,\frac{\mathrm{d}z'}{\mathrm{d}y'} - \log\Lambda_y = \int_{\gamma/\Lambda_y}^{z} \frac{\mathrm{d}z'}{z'} - \log\Lambda_y = -\log(\gamma/z)\,, \tag{8.146}$$

where we used the fact that $y \approx \gamma/z$ near $y = \infty$ on the physical y-sheet, see (8.121). Finally, the connected two-point correlators of the Vandermonde potential, defined in (8.126), (8.127) and (8.128) are given by [273, 256]

$$A^{(1)}_{0,2}(x_1, x_2) = -\log\frac{\mathcal{X}(z_1) - \mathcal{X}(z_2)}{\gamma z_1 - \gamma z_2}, \qquad \text{for } x_1 = \mathcal{X}(z_1),\ \ x_2 = \mathcal{X}(z_2)\,, \tag{8.147}$$

$$A^{(2)}_{0,2}(y_1, y_2) = -\log\frac{\mathcal{Y}(z_1) - \mathcal{Y}(z_2)}{\gamma/z_1 - \gamma/z_2}, \qquad \text{for } y_1 = \mathcal{Y}(z_1),\ \ y_2 = \mathcal{Y}(z_2)\,, \tag{8.148}$$

$$A^{(3)}_{0,2}(x_1, y_2) = -\log\left(1 - \frac{z_2}{z_1}\right), \qquad \text{for } x_1 = \mathcal{X}(z_1),\ \ y_2 = \mathcal{Y}(z_2)\,. \tag{8.149}$$

These formulas generalize (8.62) to the two-matrix case. From now on we shall drop the $\star$'s and add a subscript α to a variable to denote its value at the α-th saddle point.

Using these formulas, let us compute the quantity $\mathcal{C}_{\alpha,\beta}$ defined in (8.140) that appears in the general multi-instanton contribution to the partition function:

$$\begin{aligned}\log \mathcal{C}_{\alpha,\beta} = \log[(x_\alpha - x_\beta)(y_\alpha - y_\beta)] + 2\log\gamma - \log(z_\alpha^{(1)}\gamma) - \log(z_\beta^{(1)}\gamma) \\ - \log(\gamma/z_\alpha^{(2)}) - \log(\gamma/z_\beta^{(2)}) - \log\frac{x_\alpha - x_\beta}{\gamma z_\alpha^{(1)} - \gamma z_\beta^{(1)}} \\ - \log\frac{y_\alpha - y_\beta}{\gamma/z_\alpha^{(2)} - \gamma/z_\beta^{(2)}} - \log\left(1 - \frac{z_\beta^{(2)}}{z_\alpha^{(1)}}\right) - \log\left(1 - \frac{z_\alpha^{(2)}}{z_\beta^{(1)}}\right) . \quad (8.150)\end{aligned}$$

In writing these formulas, we have to pick the branch $z_\alpha^{(1)}$ for x_α and the branch $z_\alpha^{(2)}$ for y_α. We now see that the $\log\gamma$ terms cancel and the contribution $\log[(x_\alpha - x_\beta)(y_\alpha - y_\beta)]$ from the Vandermonde factors also cancels with the corresponding factors from $A_{0,2}^{(1)}$ and $A_{0,2}^{(2)}$. Simplifying a bit, we find[12]

$$\log \mathcal{C}_{\alpha,\beta} = \log\frac{z_\alpha^{(1)} - z_\beta^{(1)}}{z_\alpha^{(1)} - z_\beta^{(2)}}\frac{z_\alpha^{(2)} - z_\beta^{(2)}}{z_\alpha^{(2)} - z_\beta^{(1)}} . \quad (8.151)$$

Now let us come to the computation of $\mathcal{B}_\alpha$ defined in (8.139). Again, we have to pick the branch $z_\alpha^{(1)}$ for x_α and the branch $z_\alpha^{(2)}$ for y_α. We first simplify the exponential piece appearing in (8.139):

$$\begin{aligned}\frac{1}{2}\partial_t^2 F_0 + \partial_t V_{1,\text{eff}} + \partial_t V_{2,\text{eff}} + \frac{1}{2}A_{0,2}^{(1)} + \frac{1}{2}A_{0,2}^{(2)} + A_{0,2}^{(3)} \\ = \log\gamma - \log(\gamma z_\alpha^{(1)}) - \log(\gamma/z_\alpha^{(2)}) - \frac{1}{2}\log\left(\frac{1}{\gamma}\frac{\mathrm{d}\mathcal{X}}{\mathrm{d}z}(z_\alpha^{(1)})\right) \\ - \frac{1}{2}\log\left(-\frac{1}{\gamma}(z_\alpha^{(2)})^2\frac{\mathrm{d}\mathcal{Y}}{\mathrm{d}z}(z_\alpha^{(2)})\right) - \log\left(1 - \frac{z_\alpha^{(2)}}{z_\alpha^{(1)}}\right) . \quad (8.152)\end{aligned}$$

We see again that the $\log\gamma$ cancels out and the expression simplifies to

$$\begin{aligned}\exp\left[\frac{1}{2}\partial_t^2 F_0 + \partial_t V_{1,\text{eff}} + \partial_t V_{2,\text{eff}} + \frac{1}{2}A_{0,2}^{(1)} + \frac{1}{2}A_{0,2}^{(2)} + A_{0,2}^{(3)}\right] \\ = \frac{1}{z_\alpha^{(1)} - z_\alpha^{(2)}}\left(-\frac{\mathrm{d}\mathcal{X}}{\mathrm{d}z}(z_\alpha^{(1)})\frac{\mathrm{d}\mathcal{Y}}{\mathrm{d}z}(z_\alpha^{(2)})\right)^{-\frac{1}{2}} . \quad (8.153)\end{aligned}$$

[12] As a consistency check, we can see that this expression is consistent with the one-matrix results where $z_\alpha^{(2)} = 1/z_\alpha^{(1)}$. To see this, we multiply (8.63) with the contribution from the Vandermonde $(x_\alpha - x_\beta)^2$ and use $x_\alpha = \gamma(z_\alpha + 1/z_\alpha)$ and the corresponding relation for x_β. This gives $\mathcal{C}_{\alpha,\beta} = \frac{z_\alpha - z_\beta}{z_\alpha - 1/z_\beta}\frac{1/z_\alpha - 1/z_\beta}{1/z_\alpha - z_\beta}$ in agreement with (8.151).

The prefactor term in (8.139) combines nicely with the second term in the above equation. To see this note that $V''_{1,\text{eff}}(x) = \frac{\mathrm{d}Y}{\mathrm{d}x}$ and $V''_{2,\text{eff}}(y) = \frac{\mathrm{d}X}{\mathrm{d}y}$. Thus, we get

$$\mathcal{B}_\alpha = \sqrt{\frac{2\pi t}{N}} \frac{1}{z_\alpha^{(1)} - z_\alpha^{(2)}} \left(\frac{\mathrm{d}\mathcal{X}}{\mathrm{d}z}(z_\alpha^{(1)}) \frac{\mathrm{d}\mathcal{Y}}{\mathrm{d}z}(z_\alpha^{(2)}) - \frac{\mathrm{d}\mathcal{X}}{\mathrm{d}z}(z_\alpha^{(2)}) \frac{\mathrm{d}\mathcal{Y}}{\mathrm{d}z}(z_\alpha^{(1)}) \right)^{-\frac{1}{2}} . \tag{8.154}$$

The double-scaling limit

Finally we discuss the double-scaling limit. The double-scaling limit is defined by zooming in near a point on Σ that corresponds to an end point of the distribution of the eigenvalues of M_1 (the symmetry between M_1 and M_2 is broken by which potential has a higher degree). This is a point that lies on the boundary of the z-image of the physical x-sheet. We appropriately choose the parameters in the potentials V_1 and V_2 and introduce new variables x, y, z and new functions $\widetilde{X}$, $\widetilde{Y}$, $\widetilde{\mathcal{X}}$ and $\widetilde{\mathcal{Y}}$ as,

$$\begin{aligned} x = c_x + d_x \varepsilon^{\frac{p'}{2}}\, \tilde{x}, \qquad & y = c_y + d_y \varepsilon^{\frac{p}{2}}\, \tilde{y}, \qquad z = c_z + d_z \varepsilon^{\frac{1}{2}} \tilde{z}\,, \\ X(y) = c_x + d_x \varepsilon^{\frac{p'}{2}}\, \widetilde{X}(\tilde{y})\,, \qquad & Y(x) = c_y + d_y \varepsilon^{\frac{p}{2}}\, \widetilde{Y}(\tilde{x}), \\ \mathcal{X}(z) = c_x + d_x \varepsilon^{\frac{p'}{2}}\, \widetilde{\mathcal{X}}(\tilde{z})\,, \qquad & \mathcal{Y}(z) = c_y + d_y \varepsilon^{\frac{p}{2}}\, \widetilde{\mathcal{Y}}(\tilde{z})\,, \end{aligned} \tag{8.155}$$

for appropriate constants $c_x, c_y, c_z, d_x, d_y, d_z$. We now take the limit $N \to \infty$, $\varepsilon \to 0$, while keeping fixed the combination

$$e^{S_0} := \frac{N}{t}\, d_x d_y\, \varepsilon^{\frac{p}{2} + \frac{p'}{2}}\,. \tag{8.156}$$

The analog of the conformal background for the one matrix case is a special choice of the parameters of the potential V_1, V_2 and the parameters $c_x, c_y, c_z, d_x, d_y, d_z$ such that [264, 250]

$$\widetilde{\mathcal{X}}(\tilde{z}) = T_{p'}(\tilde{z}), \qquad \widetilde{\mathcal{Y}}(\tilde{z}) = T_p(\tilde{z})\,. \tag{8.157}$$

Here T_p denotes the Chebyshev polynomial of the first kind which is defined by the relation $\cos p\theta = T_p(\cos\theta)$. Equation (8.157) also implicitly defines the functions $\widetilde{X}$ and $\widetilde{Y}$ after eliminating $\tilde{z}$. In the new variables the spectral curve of the conformal background of the (p', p) minimal string is the following curve [264]

$$\Sigma = \{(\tilde{x}, \tilde{y}) \in \mathbb{C}^2 \,|\, T_p(\tilde{x}) - T_{p'}(\tilde{y}) = 0\}\,, \tag{8.158}$$

with $\tilde{z}$ being the uniformization parameter of this surface. This follows as

$$T_p\left(\mathcal{X}(\tilde{z})\right) = T_p\left(T_{p'}(\tilde{z})\right) = T_{pp'}(\tilde{z}) = T_{p'}\left(T_p(\tilde{z})\right) = T_{p'}\left(\mathcal{Y}(\tilde{z})\right)\,. \tag{8.159}$$

The relations (8.122), (8.123) defining the instanton locations now take the form:

$$\tilde{x}^\star = \widetilde{X}(y^\star), \quad \tilde{y}^\star = \widetilde{Y}(x^\star)\,, \tag{8.160}$$

$$(\tilde{x}^\star, \tilde{y}^\star) = (\,\widetilde{\mathcal{X}}(\tilde{z}^{\star(1)})\,, \widetilde{\mathcal{Y}}(\tilde{z}^{\star(1)})\,) = (\,\widetilde{\mathcal{X}}(\tilde{z}^{\star(2)})\,,\, \widetilde{\mathcal{Y}}(\tilde{z}^{\star(2)})\,)\,. \tag{8.161}$$

These represent locations of the instantons which are also the singular points of Σ. Explicitly, there are $(p'-1)(p-1)/2$ singular points on Σ given by

$$(\tilde{x}_{m,n}, \tilde{y}_{m,n}) = \left((-1)^m \cos\frac{\pi n p'}{p}\,,\, (-1)^n \cos\frac{\pi m p}{p'}\right)\,, \quad \text{with} \tag{8.162}$$

$$m \in \{1, \ldots, p'-1\}\,, \quad n \in \{1, \ldots, p-1\}\,, \tag{8.163}$$

and subject to the identification $(m,n) \equiv (p'-m, p-n)$ since these two labels give the same point on the curve Σ. We have omitted the stars from the notation to reduce the clutter; the subscripts m,n make it clear that these values refer to the singular points. Each of these singular points corresponds to two distinct values of the uniformizing coordinate z. Explicitly, these are

$$\tilde{z}^{(1)}_{m,n} = \cos\left(\frac{\pi m}{p'} + \frac{\pi n}{p}\right)\,, \quad \tilde{z}^{(2)}_{m,n} = \cos\left(\frac{\pi m}{p'} - \frac{\pi n}{p}\right)\,. \tag{8.164}$$

From the analysis given above, we cannot determine which of the two values $\cos(\frac{\pi m}{p'} \pm \frac{\pi n}{p})$ corresponds to $\tilde{z}^{(1)}_{m,n}$ and which to $\tilde{z}^{(2)}_{m,n}$. However, exchanging them changes the signs of $T_\alpha = N\mathcal{A}_\alpha/t$ and $(\mathcal{B}_\alpha)^2$ computed from (8.141) and (8.154), respectively, and leaves $\mathcal{C}_{\alpha,\beta}$ computed from (8.151) unchanged. Since we only compare the combinations $\mathcal{B}_\alpha T_\alpha^{1/2}$ and $\mathcal{C}_{\alpha,\beta}$ with the string theory results, this ambiguity does not affect our analysis. Ref. [256] resolves this ambiguity using a physical input.

Let us now compute the on-shell action of the instanton labeled by (m,n). Using (8.155) and (8.156), we can recast (8.141) as

$$\frac{N}{t}\mathcal{A}_{m,n} = e^{S_0} \int_{\tilde{z}^{(2)}_{m,n}}^{\tilde{z}^{(1)}_{m,n}} \mathrm{d}\tilde{z}\, \widetilde{\mathcal{Y}}(\tilde{z})\, \frac{\mathrm{d}\widetilde{\mathcal{X}}(\tilde{z})}{\mathrm{d}\tilde{z}}\,. \tag{8.165}$$

In particular since $\widetilde{\mathcal{X}}(\tilde{z}^{(1)}_{m,n}) = \widetilde{\mathcal{X}}(\tilde{z}^{(2)}_{m,n}) = \tilde{x}_{m,n}$, the constant terms c_x and c_y in (8.155) drop out of this equation. To evaluate this, we first compute the indefinite integral of $T_p(\tilde{z})\frac{\mathrm{d}}{\mathrm{d}\tilde{z}}T_{p'}(\tilde{z})$:

$$\int^{\tilde{z}} \mathrm{d}u\, T_p(u)\frac{\mathrm{d}}{\mathrm{d}u}T_{p'}(u) = \frac{p'}{2}\left(\frac{1}{p+p'}\,T_{p+p'}(\tilde{z}) - \frac{1}{p-p'}\,T_{p-p'}(\tilde{z})\right) + C\,, \tag{8.166}$$

where C is the constant of integration. Taking the difference between this indefinite integral expression evaluated at the two values of $\tilde{z}$ in (8.164), we get

$$T_{m,n} := \frac{N}{t}\,\mathcal{A}_{m,n} = e^{S_0}\,(-1)^{m+n}\frac{2pp'}{p'^2-p^2}\,\sin\frac{\pi m p}{p'}\,\sin\frac{\pi n p'}{p}\,. \tag{8.167}$$

We now take the double-scaling limit in the formula (8.154) for $\mathcal{B}_\alpha$. The result is

$$\begin{aligned}\mathcal{B}_{m,n} &= e^{-S_0/2}\,\frac{\sqrt{2\pi}}{\tilde{z}_\alpha^{(1)}-\tilde{z}_\alpha^{(2)}}\left(\frac{\mathrm{d}\widetilde{\mathcal{X}}}{\mathrm{d}\tilde{z}}(\tilde{z}_\alpha^{(1)})\frac{\mathrm{d}\widetilde{\mathcal{Y}}}{\mathrm{d}\tilde{z}}(\tilde{z}_\alpha^{(2)})-\frac{\mathrm{d}\widetilde{\mathcal{X}}}{\mathrm{d}\tilde{z}}(\tilde{z}_\alpha^{(2)})\frac{\mathrm{d}\widetilde{\mathcal{Y}}}{\mathrm{d}\tilde{z}}(\tilde{z}_\alpha^{(1)})\right)^{-\frac{1}{2}}\\ &= e^{-S_0/2}\,\frac{\sqrt{2\pi}}{2\sin\frac{\pi m}{p'}\sin\frac{\pi n}{p}}\left(\frac{2p'p\,(-1)^{m+n}\sin\frac{\pi mp}{p'}\sin\frac{\pi np'}{p}}{\sin^2\frac{\pi m}{p'}-\sin^2\frac{\pi n}{p}}\right)^{-\frac{1}{2}}\,.\end{aligned} \tag{8.168}$$

Using (8.167), we see that

$$\mathcal{B}_{m,n} = (T_{m,n})^{-\frac{1}{2}}\;\mathrm{i}\sqrt{\frac{\pi}{2}}\left(\frac{\cot^2(\pi n/p)-\cot^2(\pi m/p')}{p^2-p'^2}\right)^{\frac{1}{2}}\,, \tag{8.169}$$

agreeing precisely with the string theory result (8.30). Note that the overall sign of $\mathcal{B}_{m,n}$ can be changed by changing the orientation of the steepest descent integration contour in the complex eigenvalue plane. This sign is not significant since the string theory computation also has a similar ambiguity.

Finally, we discuss the double-scaling limit of $\mathcal{C}_{\alpha,\beta}$. Since z just undergoes a shift and rescaling by $\varepsilon^{\frac{1}{2}}$, we get from (8.151) that

$$\mathcal{C}_{\alpha,\beta} = \frac{\tilde{z}_\alpha^{(1)}-\tilde{z}_\beta^{(1)}}{\tilde{z}_\alpha^{(1)}-\tilde{z}_\beta^{(2)}}\times\frac{\tilde{z}_\alpha^{(2)}-\tilde{z}_\beta^{(2)}}{\tilde{z}_\alpha^{(2)}-\tilde{z}_\beta^{(1)}}\,, \tag{8.170}$$

with $\tilde{z}_\alpha$ given in (8.164). This yields

$$\mathcal{C}_{(m,n)(m',n')} = \frac{\cos\left(\frac{\pi m}{p'}+\frac{\pi n}{p}\right)-\cos\left(\frac{\pi m'}{p'}+\frac{\pi n'}{p}\right)}{\cos\left(\frac{\pi m}{p'}+\frac{\pi n}{p}\right)-\cos\left(\frac{\pi m'}{p'}-\frac{\pi n'}{p}\right)}\times\frac{\cos\left(\frac{\pi m}{p'}-\frac{\pi n}{p}\right)-\cos\left(\frac{\pi m'}{p'}-\frac{\pi n'}{p}\right)}{\cos\left(\frac{\pi m}{p'}-\frac{\pi n}{p}\right)-\cos\left(\frac{\pi m'}{p'}+\frac{\pi n'}{p}\right)}\,. \tag{8.171}$$

After some simplification using basic trigonometric identities, we see that this agrees with the string theory result (8.22).

Finally, let us make a remark about the ratio of the tensions of the various ZZ branes. From (8.167) we see that the matrix integral predicts that

$$\frac{T_{m,n}}{T_{1,1}} = (-1)^{m+n}\,\frac{\sin\frac{\pi mp}{p'}\sin\frac{\pi np'}{p}}{\sin\frac{\pi p}{p'}\sin\frac{\pi p'}{p}}\,. \tag{8.172}$$

Similar to the remarks in Section 8.3, this agrees with the results from the the string theory side [143, 259, 250]. The boundary state wavefunction $\Psi_{m,n}(P) \propto \sinh(2\pi mPb^{-1})\times\sinh(2\pi nPb)$ which for $P=-\mathrm{i}(b-b^{-1})/2$ equals $(-1)^{m+n}\sin\frac{\pi mp}{p'}\sin\frac{\pi np'}{p}$.

Chapter 9

The ZZ Annulus One-point Function in Non-critical String Theory

9.1 Introduction

The study of non-perturbative effects due to ZZ instantons [143] in two-dimensional string theory by Balthazar, Rodriguez, and Yin [25] has motivated a string field theory analysis of IR divergences in instanton amplitudes. The agreement between the string field theory analyses and the predictions from the dual matrix quantum mechanics is impressive [26, 307, 257]. The string field theory analysis of instanton amplitudes has been extended to other non-critical string models [23, 24, 276, 308, 309] where the computations agree precisely with the predictions from the dual matrix models. It has also been extended to critical superstrings [281, 277, 293, 278, 279] where the D-instanton effects match precisely with the predictions from superstring dualities. In [280], worldsheet computations of instanton effects were performed in Calabi-Yau orientifold compactifications, which is a new result and was not previously known from a dual description.

Among all these successes, there is one particular observable that stands out and does not match with the dual prediction. This is the annulus one-point amplitude in the original $c = 1$ string theory computation of [25], which is relevant for computing the first subleading-in-g_s correction to the D-instanton induced n-point amplitude of closed-string operators. This amplitude receives divergent contributions from integration over the worldsheet moduli near the boundaries of moduli space. This leads to an additive ambiguous term in the amplitude. Extracting the finite part of the worldsheet amplitude via numerical integration over the moduli space, and comparing this with the amplitude from the dual matrix quantum mechanics leads to a prediction for the ambiguous piece of the worldsheet amplitude [25, 310]. In [307], a string field theory analysis was performed to determine the ambiguous piece, but the result was found to not match with [25, 310], leading to a puzzle.

In the present work, we resolve this mismatch. We first simplify the model by working with the $c < 1$ non-critical string, and we study the integrated correlation functions of the

cosmological constant operator. The first simplification is that one does not have to worry about the translation zero mode of the $c = 1$ scalar. Second, the one-point annulus amplitude of the cosmological operator has a simple form that can be obtained by differentiating the partition function with respect to the world-sheet cosmological constant μ. Third, because of the Liouville equation of motion, the cosmological operator is a total derivative and the moduli space integral reduces to just boundary contributions, obviating the need for numerical integration over the moduli space. In trying to compute the one-point annulus amplitude in this simpler model, we were able to identify a subtle issue in the computation in appendix D of [307], which analyzed the disk amplitude with one closed string puncture and three open string punctures. This was needed for finding the relation between the string field theory gauge transformation parameter and the rigid $U(1)$ transformation parameter under which an open string with one end on the instanton picks up a phase.

Let us briefly explain the subtlety. The disk amplitude with one closed string puncture and three open string punctures has a two-dimensional moduli space. String field theory instructs us to integrate a two-form on a subset S of this moduli space that excludes certain regions around the boundaries. The two-form turns out to be exact. Let's denote it by $\mathrm{d}J$, so that the moduli-space integral reduces to the integral of J over the boundary ∂S of S. It so happens that in appendix D of [307], when we go once around ∂S, the open string punctures do not return to their original position, but to a configuration related to the initial one by the one-parameter subgroup of $\mathrm{PSL}(2,\mathbb{R})$ that keeps the point $z = \mathrm{i}$ in the upper half plane fixed. In such a situation, one must make sure that the contraction of J with the tangent vector along the orbits of this $\mathrm{PSL}(2,\mathbb{R})$ transformation is zero, something that was not true for the J chosen in [307]. It turns that one can add an exact one-form to J so that it satisfies the desired property. (Alternatively, one can reduce the orbits under discussion to points by fixing the location of one of the punctures and work directly with the two-dimensional moduli space.) After this fix, the mismatch goes away and one-finds agreement with predictions from the dual matrix models both in the $c < 1$ and the $c = 1$ case.

Now we present the main result of this work. Let $V = e^{2b\phi}$ denote the bulk cosmological constant vertex operator in minimal string theory. The integrated correlation functions of V can be obtained by taking μ-derivatives of the partition function. Let g_s^{-1} be the tension of the ZZ brane. Further, let $g_s f$ denote the disk two-point of V, divided by the square of the disk one-point function of V, and let $g_s g$ denote the annulus one-point of V, divided by the disk one-point function of V. By taking μ-derivatives of the partition function and setting $\mu = \frac{1}{\pi}$, one finds

$$f = \frac{2b}{Q} - 1\,, \quad g = \frac{1}{2}\,. \tag{9.1}$$

Our goal will be to reproduce both of these results via explicit integrals over the relevant moduli spaces, using string field theory to regulate divergences from the boundaries.

Overview

The rest of the paper is devoted to setting up the problem in the $c < 1$ case and explaining the above remarks in more detail. In Section 9.2, we briefly review the $c < 1$ non-critical string theory, and also certain conventions for the Liouville and ghost CFTs and for string amplitudes that will be important for us. In Section 9.3, we provide the general analysis that leads to a concrete prediction for the disk two-point function and the annulus one-point function of the cosmological constant operator, leading to the predictions (9.1). The key point is that the correlation functions of the cosmological constant operator can be related to μ-derivatives of the partition function. In Section 9.4, we compute the disk two-point function of the cosmological constant operator by integrating over the one-dimensional moduli space, which matches with the prediction (9.1). The disk two-point function contributes at the same order as the annulus one-point function, and was already found to match the matrix quantum mechanics result in the $c = 1$ case [25, 310, 307]. Finally, in Section 9.5, we compute the annulus one-point function exploiting the total derivative nature of the cosmological constant operator to integrate over the two-dimensional moduli space. The analysis of Section 9.4 and Section 9.5 requires computing string field theory Feynman diagrams to get finite results. Since the analysis of [307] was quite lengthy overall, we will not repeat all the computational details of the various contributions and instead emphasize the conceptual points that are different in our analysis. The appendices contain details of various overall normalizations of string amplitudes that are important for our work.

9.2 Setup and conventions

Conventions for string amplitudes

We will follow the conventions of [277]. One important convention is that the integrated closed string vertex operators are integrated with the measure $\frac{\mathrm{d}x\,\mathrm{d}y}{\pi}$. For the upper half plane geometry, the open string punctures are integrated along the real axis with measure $\mathrm{d}x$.

We take the three-point function of the c-ghost in the upper half plane to be

$$\langle c(z_1)c(z_2)c(z_3)\rangle_{\mathrm{UHP}} = -(z_1 - z_2)(z_2 - z_3)(z_1 - z_3)\,. \tag{9.2}$$

This normalization, with the string field theory path integral being weighted as

$\exp[\frac{1}{2}\langle\Psi|Q_B|\Psi\rangle]$, gives rise to the path integral weight $\exp[-\frac{1}{2}h_b\phi_b^2]$ for a Siegel-gauge bosonic field ϕ_b with $L_0 = h_b$.[1] For example, in the case of the the tachyon $\phi_1 c_1|0\rangle$, the action evaluates to $\frac{1}{2}\phi_1^2\,\langle 0|c_{-1}\,c_0 L_0\,c_1|0\rangle = \frac{1}{2}\phi_1^2$, which is the correct result since $h_b = -1$ for the tachyon. For later use, we also need the out-of-Siegel gauge field ψ that appears in the

[1] In our convention where the path integral is weighted by exponential of the action, an n-point interaction term in the action gives a contribution to the n-point amplitude without any extra minus sign or factor of i.

string field as

$$\Psi = \phi_1 c_1|0\rangle + \mathrm{i}\psi c_0|0\rangle + \dots \tag{9.3}$$

The path integral weight of ψ is $\exp(-\psi^2)$, so that the propagator of ψ equals $\frac{1}{2}$.

We define g_s so that nonperturbative contributions to string amplitudes carry an overall factor of $\exp(-g_s^{-1})$. In other words, the action of the instanton is $-g_s^{-1}$.

In the conventions of [277], the one point function of a closed string vertex operator ψ_c on the upper half plane is given by

$$A_{\text{disk}}(\psi_c) = \frac{1}{4g_s}\left\langle (\partial c - \overline{\partial}\overline{c})\psi_c \right\rangle_{\text{UHP}} . \tag{9.4}$$

The upper half plane amplitude for n closed string punctures and m open string punctures, with one closed puncture and one open string puncture fixed is

$$A_{\text{disk}}(\psi_c^n \psi_o^m) = \frac{\mathrm{i}\pi}{g_s}\int \langle \psi_c^n \psi_o^m \rangle_{\text{UHP}} . \tag{9.5}$$

The factor of i was explained in appendix A of [278]. In this paper, we will instead be interested in the case where the $\mathrm{PSL}(2,\mathbb{R})$ symmetry is fixed by fixing the position of one closed string puncture at $z = \mathrm{i}$ and fixing the x-coordinate of another closed string puncture to zero. This is analyzed in the next subsection.

Fixing $\mathrm{PSL}(2,\mathbb{R})$ with two closed string punctures

We want to study the integration measure for the upper half plane amplitude $A(\psi_c^n \psi_o^m)$ when all the open string punctures are integrated, one closed string puncture is fixed at i, and another closed string puncture is fixed at $\mathrm{i}y$.

The only non-trivial part is the overall normalization since the y dependence of the measure is captured by the correlation function where appropriate ghost factors are included in the definition of the unintegrated vertex operators. We start with the original configuration with one open string vertex operator fixed at the origin and one closed string vertex operator fixed at $z = \mathrm{i}$. For convenience, let us consider the case where we have only one open string vertex operator and two closed string vertex operators. We take the unintegrated form of the closed and open string vertex operators to be $\psi_c = c\overline{c}V_c$ and $\psi_o = cV_o$, respectively. (Here V_c is a dimension $(1,1)$ bulk operator, and V_o is a dimension 1 boundary operator in the worldsheet theory.) Let the integrated closed string vertex operator be at $z = x + \mathrm{i}y$. In this case the integrand is

$$\frac{\mathrm{d}x\mathrm{d}y}{\pi}\,\frac{\mathrm{i}\pi}{g_s}\,\langle \psi_c(\mathrm{i}) V_c(z)\psi_o(0)\rangle . \tag{9.6}$$

Now we shall make a $\mathrm{PSL}(2,\mathbb{R})$ transformation

$$z' = \frac{z-a}{1+az} . \tag{9.7}$$

Denoting $z' = x' + \mathrm{i}y'$, we adjust a so that x' vanishes. This will move the open string at the origin to $x'' = -a$. The new configuration is labelled by x'' and y' and our goal will be to rewrite the original measure as

$$C\, g_s^{-1}\, \mathrm{d}x'' \mathrm{d}y' \langle \psi_c(\mathrm{i})(c+\bar{c}) V_c(\mathrm{i}y') V_o(x'')\rangle \,. \tag{9.8}$$

It is the constant C that we want to determine. This can be done by taking (x, y) to be close to the origin so that $x' = 0$ can be achieved by an infinitesimal transformation with $a = x$. This gives $x'' = -a = -x$ and $y' = y$. Therefore we have $\mathrm{d}x\mathrm{d}y = \mathrm{d}x''\mathrm{d}y'$, and both x' and x'' are integrated from $-\infty$ to $+\infty$. Using (9.2), the ghost correlator in (9.6) is

$$\langle c\bar{c}(\mathrm{i})c(0)\rangle = -2\,\mathrm{i}\,, \tag{9.9}$$

while that in (9.8) is

$$\langle c\bar{c}(\mathrm{i})(c(\mathrm{i}y') + \bar{c}(\mathrm{i}y'))\rangle \approx -4\,\mathrm{i} \quad \text{for } y' \approx 0\,. \tag{9.10}$$

Equality of (9.6) and (9.8) now gives

$$C = \frac{\mathrm{i}}{2}\,. \tag{9.11}$$

Even though we have derived this in the special case of only two closed strings and one open string, we can now generalize this to give the amplitude of n closed strings and m open strings, keeping fixed one closed string vertex operator at $z = \mathrm{i}$ and integrating another closed string vertex operator along the imaginary axis with measure $\mathrm{d}y$ from $y = 0$ to $y = 1$:

$$A_{\mathrm{disk}}(\psi_c^n \psi_o^m) = \frac{\mathrm{i}}{2g_s} \int \langle \psi_c^n \psi_o^m \rangle_{\mathrm{UHP}}\,. \tag{9.12}$$

The important point about (9.12) is the precise overall numerical factor.

Minimal string theory and Liouville CFT

The term minimal string theory refers to a worldsheet model where the matter sector consists of the (p', p) minimal model [244, 274]. Here p' and p are two relatively prime integers and our convention is that $p' < p$. The minimal model is a CFT with central charge $c = 1 - \frac{6(p-p')^2}{pp'}$. The conformal mode of the metric does not decouple and gives rise to the Liouville CFT with central charge $26 - c$. Together with the bc-ghosts we have an anomaly free worldsheet theory. These theories have a dual description via an integral over two Hermitian matrices in the double-scaling limit [272, 273]. When $p' = 2$, the integral over one of the matrices is purely Gaussian and it can be integrated out giving rise to a one-matrix integral.

The path integral of Liouville field theory on a two-dimensional Euclidean manifold with metric g is given by [143]

$$\int [D\phi] \exp\left[-\int \mathrm{d}x\, \mathrm{d}y\, \sqrt{g}\, \left(\frac{1}{4\pi}\, g^{\mu\nu} \partial_\mu \phi \partial_\nu \phi + \frac{1}{4\pi} Q R \phi + \mu\, e^{2b\phi} \right) \right] , \quad \text{where} \tag{9.13}$$

$$Q = \frac{1}{b} + b\,, \quad b = \sqrt{\frac{p'}{p}}\,. \tag{9.14}$$

We will be interested in the correlation function of the marginal operator $V := e^{2b\phi}$. Fixing the background metric to be flat, one sees that the equation of motion of the Liouville field is

$$\frac{1}{4\pi}(\partial_x^2 + \partial_y^2)\phi = \mu\, b\, e^{2b\phi}\,. \tag{9.15}$$

So we see that the operator $e^{2b\phi}$ is a total derivative. While this derivation holds in the semi-classical limit $b \to 0$, the result holds even for finite b [311]. In fact, this equation of motion is only the first in an infinite series of "higher" equations of motion in Liouville theory [311]. These equations of motion have been previously used to compute integrated correlation functions in minimal string theory on the sphere topology [312, 313, 314, 315]. It will be useful for us to introduce a rescaled cosmological constant

$$\widetilde{\mu} := \pi\mu \tag{9.16}$$

so that the interaction term in the Liouville action takes the form $\int \frac{\mathrm{d}x\mathrm{d}y}{\pi}\,\widetilde{\mu}\, e^{2b\phi}$. This will be useful, since we will be integrating closed string punctures with the measure $\frac{\mathrm{d}x\mathrm{d}y}{\pi}$, as in [277]. With the definition of $\widetilde{\mu}$ and changing to complex coordinates $z = x + \mathrm{i}y$, we rewrite (9.15) as

$$V = e^{2b\phi} = \frac{1}{\widetilde{\mu}\, b}\,\partial\overline{\partial}\phi\,. \tag{9.17}$$

Another fact that we will need is the following. Because of the term in the action proportional to $QR\phi$, the operators $\partial\phi$ and $\overline{\partial}\phi$ are not conformal primaries but transform as

$$\partial\phi(z,\overline{z}) \to \frac{Q}{2}\frac{f''(z)}{f'(z)} + f'(z)\,\partial\phi(f(z),\overline{f(z)})\,, \tag{9.18}$$

with a similar relation for $\overline{\partial}\phi$. We will also need the following OPE between the operators $\partial\phi$ and V

$$\partial\phi(z,\overline{z})V(\mathrm{i}) = -\frac{b}{z-\mathrm{i}}\,V(\mathrm{i}) + \dots\,. \tag{9.19}$$

Instanton effects in minimal string theory are represented by open string worldsheets with ZZ boundary conditions, which are labeled by a pair of integers [143]. In this paper we will only work with one ZZ brane of the simplest $(1,1)$ type. The boundary state for the matter sector will be taken to be the Cardy state that contains only the identity operator in the open string channel [268, 108]. Denoting by $2\pi t$ the Euclidean time in the open string channel and letting

$$v := e^{-2\pi t}\,, \tag{9.20}$$

the annulus partition function of the minimal string with the desired boundary conditions is given by [143, 269, 249]

$$C_2 := \int_0^\infty \frac{\mathrm{d}t}{2t}\, Z(v)\,, \quad \text{with} \tag{9.21}$$

$$Z(v) = (v^{-1}-1)\, v^{-(p-p')^2/4pp'} \sum_{j=-\infty}^{\infty} [v^{(2pp'j+p-p')^2/4pp'} - v^{(2pp'j+p+p')^2/4pp'}] \tag{9.22}$$

$$= v^{-1} - 2 + O(v)\,. \tag{9.23}$$

In the last line we have displayed the terms that give rise to divergent contributions from the $t = \infty$ end of the integral. The v^{-1} term arises from the open string tachyon that multiplies the state $c_1|0\rangle$ with $L_0 = -1$, and the -2 arises from two Grassmann-odd modes p_1 and q_1 that multiply the states $|0\rangle$ and $c_{-1}c_1|0\rangle$ with $L_0 = 0$. One of the insights of [26] was that p_1 and q_1 are ghost zero modes that arise because of the breakdown of Siegel gauge. This is related to the fact that the worldvolume of a D-instanton is zero dimensional. One needs to instead integrate over the ghost-number one field ψ that multiplies the state $c_0|0\rangle$ and divide by the volume of the "gauge group" of the worldvolume theory of the D-instanton, which is finite:

$$\int \mathrm{d}p_1 \mathrm{d}q_1 \quad \to \quad \frac{\int \mathrm{d}\psi \exp(-\psi^2)}{\int \mathrm{d}\theta}\,. \tag{9.24}$$

In particular, the open string field ψ can run in internal propagators; such contributions to string amplitudes are not captured by the worldsheet analysis and need to be explicitly added [307].

Let us now discuss the bulk-boundary OPE with ZZ boundary conditions. Working with the upper half plane coordinate system, this takes the form [143]

$$\partial\phi(z,\overline{z}) = -\frac{Q}{z-\overline{z}} + O(z-\overline{z}) \tag{9.25}$$

$$\overline{\partial}\phi(z,\overline{z}) = +\frac{Q}{z-\overline{z}} + O(z-\overline{z})\,. \tag{9.26}$$

The coefficient of the leading term is fixed by using the equation of motion (9.17) and the fact that the one-point function of $V(z,\overline{z})$ is given by $\frac{Q}{\widetilde{\mu}b}\frac{1}{|z-\overline{z}|^2}$ [143]. Setting $\widetilde{\mu} = 1$, note in particular that

$$\langle V(\mathrm{i})\rangle_{\mathrm{UHP}} = \frac{Q}{4b}. \tag{9.27}$$

That the expression for the one-point function of $V(z,\overline{z})$ resembles the metric of hyperbolic space $\mathbb{H}^2$ (represented using the upper half plane) and with the correct radius of curvature in the semi-classical limit is tied to the fact that physically the ZZ boundary conditions

represent the Liouville field theory placed on the pseudosphere. Note also that there are no $O((z-\overline{z})^0)$ terms in (9.25) and (9.26) since the boundary theory in the Liouville sector does not have any state of conformal weight 1 (the only boundary operator is the identity, so that the L_{-1} descendant is null). Finally, we note that (9.18), (9.25), (9.26) and the scale invariance of the upper half plane imply that

$$\langle \partial\phi(z,\overline{z})\rangle_{\rm UHP} = -\frac{Q}{z-\overline{z}}\,, \quad \langle \overline{\partial}\phi(z,\overline{z})\rangle_{\rm UHP} = \frac{Q}{z-\overline{z}}\,. \tag{9.28}$$

9.3 General predictions for the disk two-point function and the annulus one-point function

In perturbation theory, the string partition function is given by a sum over closed string worldsheets, organized by genus. This series is asymptotic and contains non-perturbative corrections due to instanton effects [246, 316, 252], which, in the case of critical strings can be thought as being due to worldsheets with Dirichlet boundaries in all target space directions [317]. In the context of minimal strings, the relevant boundary conditions are of the ZZ type [143], which are analogous to Dirichlet boundary conditions in the critical string. As already mentioned, throughout this paper we will focus on a single ZZ brane of the simplest $(1,1)$ type, and also the simplest Cardy state for the matter sector.

The string partition function including the one-instanton contribution is given by

$$\mathcal{Z}(\vec{t},g_s) = \mathcal{Z}^{(0)}(\vec{t},g_s) + \mathcal{Z}^{(1)}(\vec{t},g_s) + \dots\,, \tag{9.29}$$

$$\mathcal{Z}^{(1)}(\vec{t},g_s) = \mathcal{Z}^{(0)}(\vec{t},g_s)\exp\left[g_s^{-1}A(\vec{t}) + \frac{1}{2}\log g_s + B(\vec{t}) + C(\vec{t})g_s + \cdots\right]\,, \tag{9.30}$$

where g_s is the closed string coupling, $\vec{t}$ are the set of parameters that label the various possible deformations of minimal string theory or the dual double-scaled matrix model, and $\mathcal{Z}^{(0)}(\vec{t},g_s)$ is the perturbative contribution to the partition function. The dots in (9.29) denote contributions from multi-instantons, which we do not study in this paper.[2] The point $\vec{t}=\vec{0}$ represents the conformal background, with only the worldsheet cosmological constant switched on [263]. The coefficient $\frac{1}{2}$ multiplying the $\log g_s$ term is special to the $c<1$ minimal string [23].

Taking derivatives of $\mathcal{Z}^{(1)}(\vec{t},g_s)$ with respect to the t_i's, we can get the one-instanton contribution to the n-point function. The full diagrammatics of the one-instanton contribution was discussed in section 2 of [318]. In taking the derivatives, there will be terms in which one or more derivatives hit the $\mathcal{Z}^{(0)}(\vec{t},g_s)$ factor in (9.30). Such terms will produce closed-string worldsheet components without boundaries and will not be the subject of interest in our

[2] Even though the g_s dependence of $\mathcal{Z}(\vec{t},g_s)$ can be determined from its $\vec{t}$ dependence, we regard g_s as an independent variable.

work, so we shall not write them. So we have

$$\frac{1}{\mathcal{Z}^{(0)}}\frac{\partial^n \mathcal{Z}^{(1)}}{\partial t_{i_1}\cdots\partial t_{i_n}}\bigg|_{\vec{t}=0} \supset e^{g_s^{-1}A(\vec{0})+\frac{1}{2}\log g_s+B(\vec{0})}\, g_s^{-n}\left\{\prod_{\alpha=1}^{n}\frac{\partial A}{\partial t_{i_\alpha}}\right\} \times\left[1+g_s\sum_{\substack{\beta,\gamma=1\\ \beta<\gamma}}^{n}\frac{\partial^2 A}{\partial t_{i_\beta}\partial_{t_{i_\gamma}}}\Big/\left(\frac{\partial A}{\partial t_{i_\beta}}\frac{\partial A}{\partial t_{i_\gamma}}\right)+g_s\sum_{\beta=1}^{n}\frac{\partial B}{\partial t_{i_\beta}}\Big/\frac{\partial A}{\partial t_{i_\beta}}+g_s\,C+O(g_s^2)\right]. \tag{9.31}$$

It is understood that all quantities on the right hand side are evaluated at $\vec{t}=\vec{0}$, and we have only displayed those terms on the right hand side in which all the derivatives act on the explicit exponential factor in (9.30).

We now compare various terms in (9.31) with the expected string amplitudes. The quantity $g_s^{-1}A(\vec{0})$ is the instanton action and $\exp[\frac{1}{2}\log g_s + B(\vec{0})]$ is the exponential of the annulus partition function studied in [23].

Ignoring all contributions with vertex operators inserted on closed-string worldsheets, since they represent terms where some of the derivatives act on the $\mathcal{Z}^{(0)}$ factor in (9.30), the leading term for the n-point correlation function comes from the product of n disk one-point functions (times the exponentials of the instanton action and the cylinder partition function that accompany all correlation functions).[3] This takes the form

$$e^{g_s^{-1}A(\vec{0})+\frac{1}{2}\log g_s+B(\vec{0})}\, g_s^{-n}\prod_{\alpha=1}^{n}h_{i_\alpha}\,, \tag{9.32}$$

where $g_s^{-1}h_i$ has the interpretation of the disk one-point function of the vertex operator associated with the t_i deformation.[4] This matches the leading term in (9.31) if we identify

$$h_i=\frac{\partial A}{\partial t_i}\,. \tag{9.33}$$

For a given instanton, we choose to pick t_{i_α}'s on the left hand side of (9.31) such that the disk one-point function of the operator associated with the t_{i_α} deformation does not vanish.

At the next order, again ignoring terms with vertex operators inserted on closed-string worldsheets, we expect three types of contributions:[5]

- Product of $(n-2)$ disk one-point functions and a disk two-point function. If we denote by $g_s f_{ij}$ the ratio of the disk two-point function of operators associated with the t_i, t_j

[3] In non-critical string theory, one- and two-point functions on the sphere are non-zero, so contributions that are more important than this contribution exist.

[4] We normalize the closed string vertex operators in such a way that they do not carry any factor proportional to g_s.

[5] So we are not studying contributions from, for instance, a three-punctured sphere times $(n-3)$ one-punctured disks, and the one-punctured torus times $(n-1)$ one-punctured disks.

deformations to the product of the disk one-point functions of the same operators, then this contribution takes the form:

$$e^{g_s^{-1}A(\vec{0})+\frac{1}{2}\log g_s+B(\vec{0})}\, g_s^{-(n-1)} \left\{\prod_{\alpha=1}^{n}\frac{\partial A}{\partial t_{i_\alpha}}\right\} \sum_{\substack{\beta,\gamma=1\\ \beta<\gamma}}^{n} f_{i_\beta i_\gamma}\,. \tag{9.34}$$

- Product of $(n-1)$ disk one-point functions and an annulus one-point function. If we denote by $g_s\, g_i$ the ratio of the annulus one-point function and the disk one-point function of the vertex operator associated with the t_i deformation, then this contribution takes the form:

$$e^{g_s^{-1}A(\vec{0})+\frac{1}{2}\log g_s+B(\vec{0})}\, g_s^{-(n-1)} \left\{\prod_{\alpha=1}^{n}\frac{\partial A}{\partial t_{i_\alpha}}\right\} \sum_{\beta=1}^{n} g_{i_\beta}\,. \tag{9.35}$$

- Product of n disk one-point functions with the $O(g_s)$ corrections to the instanton action coming from the three-holed sphere and the handle-disk. If we denote by $g_s\widetilde{C}$ this $O(g_s)$ correction to the instanton action, this contribution takes the form

$$e^{g_s^{-1}A(\vec{0})+\frac{1}{2}\log g_s+B(\vec{0})}\, g_s^{-(n-1)} \left\{\prod_{\alpha=1}^{n}\frac{\partial A}{\partial t_{i_\alpha}}\right\} \widetilde{C}\,. \tag{9.36}$$

Comparing these three contributions to the three $O(g_s)$ terms inside the square brackets in (9.31), we arrive at the prediction:

$$f_{ij} = \frac{\partial^2 A}{\partial t_i \partial t_j}\Big/\left(\frac{\partial A}{\partial t_i}\frac{\partial A}{\partial t_j}\right), \qquad g_i = \frac{\partial B}{\partial t_i}\Big/\frac{\partial A}{\partial t_i}, \qquad \widetilde{C} = C\,. \tag{9.37}$$

So far our analysis involved a general n-point function, but now we specialize to the main case of interest in our work. Consider a special case where all t_i's appearing in (9.31) correspond to deformations of the cosmological constant $\widetilde{\mu}$ from its background value, which we shall take to be 1. The Liouville action (9.13) tells us that taking a $\widetilde{\mu}$ derivative brings down an insertion of $-\int \frac{\mathrm{d}x\mathrm{d}y}{\pi}\, e^{2b\phi}$ on the worldsheet. Thus, the vertex operator corresponding to the $\widetilde{\mu}$ deformation is $-V$.

The DDK-KPZ [319, 320, 321] scaling, that follows from the shift of the zero mode of the Liouville field in the action (9.13), implies that the partition function depends on $\widetilde{\mu}$ and g_s through the combination $g_s^{-1}\widetilde{\mu}^{Q/(2b)}$. Therefore we can take

$$g_s^{-1}A(\vec{t}) = -g_s^{-1}\widetilde{\mu}^{Q/(2b)}\,, \tag{9.38}$$

$$\frac{1}{2}\log g_s + B(\vec{t}) = \frac{1}{2}\log g_s - \frac{Q}{4b}\log\widetilde{\mu} + B_0\,, \tag{9.39}$$

where B_0 is a constant that is independent of $\widetilde{\mu}$ and g_s. As already mentioned, we normalize g_s so that the instanton action at $\widetilde{\mu} = 1$ equals $-1/g_s$. Using these results in (9.37) and denoting the f_{ij} and g_i for $t_i = t_j = \widetilde{\mu} - 1$ by f and g respectively, we get,

$$f = \frac{\partial^2 A}{\partial \widetilde{\mu}^2} \Big/ \left(\frac{\partial A}{\partial \widetilde{\mu}}\right)^2 \Big|_{\widetilde{\mu}=1} = \frac{2b}{Q} - 1, \qquad g = \frac{\partial B}{\partial \widetilde{\mu}} \Big/ \frac{\partial A}{\partial \widetilde{\mu}} \Big|_{\widetilde{\mu}=1} = \frac{1}{2}\,. \tag{9.40}$$

Our goal will be to verify these relations by explicit worldsheet computations, using string field theory to regularize divergences from the boundaries of moduli space.

We remind the reader that $g_s f$ is the ratio of the disk two-point function to the square of the disk one-point function, and $g_s g$ is the ratio of the annulus one-point function to the disk one-point function. In particular the mismatch that was observed in [307] is in the quantity g. Here, we have a simple prediction that $g = 1/2$, and this will serve as our lamppost to fix the mismatch. In the end, the direct worldsheet computation, aided by string field theory, leads to perfect agreement with both the predictions $f = 2b/Q - 1$ and $g = 1/2$.

As a preliminary sanity check, let us verify that the worldsheet formula (9.4) gives us the disk one-point function of $V = e^{2b\phi}$ that we expect based on the analysis in this section. We can use (9.33) and (9.38) to get the one-point function of V on the disk, and so we have the prediction

$$A_{\text{disk}}(V) = -g_s^{-1} \frac{\partial A}{\partial \widetilde{\mu}}\Big|_{\widetilde{\mu}=1} = g_s^{-1}\,\frac{Q}{2b}\,. \tag{9.41}$$

On the other hand, using (9.27) and (9.2), the formula (9.4) with $\psi_c = c\overline{c}V$ yields $A_{\text{disk}}(V) = \frac{1}{4g_s} \times \frac{Q}{4b} \times 4 \times 2 = g_s^{-1}\,\frac{Q}{2b}$, as expected. (The final factor of two is due to the fact that the two terms in (9.4) involving ∂c and $\overline{\partial}\overline{c}$ give equal contributions.)

9.4 The disk two-point function

In this section we compute the disk two-point of the cosmological constant operator $V = e^{2b\phi}$ directly from the worldsheet correlation function and show that we reproduce the value of f given in (9.40).

Using (9.12) we write the disk two-point amplitude as

$$A_{\text{disk}}(VV) = \frac{\mathrm{i}}{2g_s} \int_0^1 \mathrm{d}y\, \langle c\overline{c}V(\mathrm{i})\,(c(z) + \overline{c}(\overline{z}))V(z,\overline{z})\rangle_{\text{UHP}}\,, \tag{9.42}$$

where it is understood that the second insertion is at $z = \mathrm{i}y$. We shall analyze this by dividing the integration region over y into two parts: the range $\epsilon \le y \le 1$ and the range $0 \le y \le \epsilon$ for some small number ϵ. We treat the $0 \le y \le \epsilon$ region using string field theory Feynman diagrams to deal with the potential divergence from the $y \to 0$ region. Let us call these two contributions $A^{(1)}_{\text{disk}}(VV)$ and $A^{(2)}_{\text{disk}}(VV)$, respectively.

First we consider the contribution $A^{(1)}_{\rm disk}(VV)$ from the region $y \geq \epsilon$. We use the equation of motion (9.17) and holomorphicity of c to write this as

$$A^{(1)}_{\rm disk}(VV) = \frac{\mathrm{i}}{2bg_s}\int_\epsilon^1 \mathrm{d}y\, \langle c\overline{c}V(\mathrm{i})\, \{\, \overline{\partial}(c\partial\phi(z,\overline{z})) + \partial(\overline{c}\overline{\partial}\phi(z,\overline{z}))\, \}\rangle_{\rm UHP} \tag{9.43}$$

$$= \frac{\mathrm{i}}{4bg_s}\int_\epsilon^1 \mathrm{d}y\, \big\langle c\overline{c}V(\mathrm{i})\, \{\, \partial_x(c\partial\phi(z,\overline{z}) + \overline{c}\overline{\partial}\phi(z,\overline{z})) + \mathrm{i}\,\partial_y(c\partial\phi(z,\overline{z}) - \overline{c}\overline{\partial}\phi(z,\overline{z}))\, \}\big\rangle_{\rm UHP} \tag{9.44}$$

where we have converted to Cartesian derivatives in the second line. The term involving ∂_y can be converted to a total derivative, but we need to be a bit more careful with the term involving ∂_x.

For this, note that the $\mathrm{PSL}(2,\mathbb{R})$ transformation $z \to \frac{z-a}{1+az}$ fixes the puncture at i but, for small a, moves the puncture at $(0,y)$ to $(-a(1-y^2),y)$. That is, it moves the second puncture in the x-direction. If $\partial\phi$ and $\bar\partial\phi$ had been primaries of dimension $(0,1)$ and $(1,0)$ respectively, then $c\partial\phi$ and $\bar c\bar\partial\phi$ would have both been dimension zero primaries, and so $\mathrm{PSL}(2,\mathbb{R})$ invariance of the correlation function would imply that the x derivative term in (9.44) would vanish. However, the term proportional to Q in (9.18) spoils this argument, since the second derivative with respect to z of $\frac{z-a}{1+az}$ does not vanish for $z = \mathrm{i}y$.

We could fix this problem by taking into account the Q-dependent terms in (9.18) for $f(z) = \frac{z-a}{1+az}$, but we shall follow a slightly different approach. Imagine starting with the disk geometry with the coordinate $w = \frac{1+\mathrm{i}z}{1-\mathrm{i}z}$. Also, let $w = re^{\mathrm{i}\theta}$ in polar coordinates on the disk. In this geometry, one puncture is located at $w = 0$ while the second is placed on the real-w axis at $w = \frac{1-y}{1+y}$. On the disk geometry, the $\mathrm{PSL}(2,\mathbb{R})$ transformation that moves the second puncture off the real axis while keeping the first puncture at the origin fixed is simply a rotation of w. Since this is linear in w, the inhomogeneous term in (9.18) vanishes, and hence the θ derivative of the correlation function of dimension zero fields vanishes. So we can first transform (9.42) to the w-coordinate system using the fact that V is a dimension $(1,1)$ primary, use manipulations analogous to (9.43) and (9.44) to express the result in the (r,θ) coordinates, drop the θ derivatives, and finally transform it back to the upper half plane using $w = \frac{1+\mathrm{i}z}{1-\mathrm{i}z}$. Using (9.18), we get

$$c\,\partial\phi(w,\overline{w}) = c\,\partial\phi(z,\overline{z}) + \frac{Q}{z+\mathrm{i}}\,c(z)\,, \tag{9.45}$$

$$\overline{c}\,\overline{\partial}\phi(w,\overline{w}) = \overline{c}\,\overline{\partial}\phi(z,\overline{z}) + \frac{Q}{\overline{z}-\mathrm{i}}\,\overline{c}(\overline{z})\,. \tag{9.46}$$

Plugging these back into the analog of (9.44) in the w-coordinate system, we get

$$A^{(1)}_{\rm disk}(VV) = -\frac{1}{4bg_s}\int_\epsilon^1 {\rm d}y \left\langle c\overline{c}V({\rm i})\,\partial_y\Bigg(c\partial\phi(z,\overline{z}) + \frac{Q}{z+{\rm i}}\,c(z) - \overline{c}\overline{\partial}\phi(z,\overline{z}) - \frac{Q}{\overline{z}-{\rm i}}\,\overline{c}(\overline{z})\Bigg)\right\rangle_{\rm UHP} \tag{9.47}$$

Now we carry out the y-integral in $A^{(1)}_{\rm disk}(VV)$ by computing the two boundary terms. The contribution from the $y=1$ boundary is given only by the $c\partial\phi$ and the $\overline{c}\overline{\partial}\phi$ terms since only these contain the pole necessary to cancel the zero from the OPE of $c({\rm i})c(z)$. Thus, using the OPE (9.19), we get

$$A^{(1)}_{\rm disk}(VV)\Big|_{y=1} = -\frac{1}{4bg_s}\lim_{z\to{\rm i}}\left\langle c\overline{c}({\rm i})\left(c\,\partial\phi(z,\overline{z})V({\rm i}) - \overline{c}\overline{\partial}\phi(z,\overline{z})V({\rm i})\right)\right\rangle_{\rm UHP} \tag{9.48}$$

$$= \frac{1}{4g_s}\left\langle c\overline{c}\left(\partial c - \overline{\partial}\overline{c}\right)V\right\rangle_{\rm UHP}, \tag{9.49}$$

where all the insertions in the second line are understood to be at $z={\rm i}$. We can evaluate this correlator using (9.27) and (9.2) to get

$$A^{(1)}_{\rm disk}(VV)\Big|_{y=1} = g_s^{-1}\,\frac{Q}{2b}\,. \tag{9.50}$$

The contribution from the $y=\epsilon$ boundary contains two pieces. There is a finite piece due to the second and fourth terms in (9.47):

$$A^{(1)}_{\rm disk}(VV)\Big|_{y=\epsilon,\ \rm finite} = \frac{1}{4bg_s}\cdot\frac{Q}{4b}\cdot\frac{Q}{\rm i}\cdot(-2{\rm i})\times 2 = -g_s^{-1}\,\frac{Q^2}{4b^2}\,, \tag{9.51}$$

where we have again used (9.27) and (9.2). Finally, the contribution from the $y=\epsilon$ boundary contains a divergent piece due to the first and third terms in (9.47). We use the bulk boundary OPE (9.25), (9.26) together with (9.27) and (9.2) to get

$$A^{(1)}_{\rm disk}(VV)\Big|_{y=\epsilon,\ \rm div} = \frac{1}{4bg_s}\cdot\frac{Q}{4b}\cdot\left(-\frac{Q}{2{\rm i}\epsilon}\right)\cdot(-2{\rm i})\times 2 + O(\epsilon) = \epsilon^{-1}\,g_s^{-1}\,\frac{Q^2}{8b^2}\,. \tag{9.52}$$

Note that we do not get any order ϵ^0 contribution because of the lack of $O((z-\overline{z})^0)$ terms in the bulk-boundary OPE (9.25), (9.26).

We now analyze the contribution $A^{(2)}_{\rm disk}(VV)$ that comes from the region $0\le y\le\epsilon$. As already mentioned, we shall regard this as the contribution from a Feynman diagram of open-closed string field theory where a pair of open-closed string interaction vertices are joined by an open string propagator. This Feynman diagram is shown in figure 9.1(a).[6]

[6]The Feynman diagram in figure 9.1(b) yields the sum of (9.50), (9.51) and (9.52).

(a) (b)

Figure 9.1: The two Feynman diagrams that contribute to the disk two-point amplitude. The thick lines denote closed strings, while the thin line denotes an open string. The first diagram gives the moduli space integral over the range $0 \leq y \leq \epsilon$, and the second diagram gives the contribution from the range $\epsilon \leq y \leq 1$. Figure reproduced from [307].

The two relevant open string states are the tachyon $c_1|0\rangle$ with $L_0 = -1$, and the out-of-Siegel-gauge mode $ic_0|0\rangle$ with $L_0 = 0$ [307]. Quite generally, in string field theory we expect that the tachyon exchange contribution cancels the divergent piece (9.52). We verify this explicitly in the next subsection which also serves as a simple illustration of the mechanism by which string field theory cancels such divergences. The contribution from the exchange of $c_0|0\rangle$ vanishes since the relevant open-closed vertex, being proportional to the correlator $\langle c\bar{c}V(\mathrm{i})\,\partial c(0)\rangle_{\mathrm{UHP}}$, vanishes (as can be seen from (9.2)). The contribution from all other states with $L_0 > 0$ vanishes in the limit $\epsilon \to 0$.

Thus, putting together (9.50) and (9.51) we get

$$A_{\mathrm{disk}}(VV) = g_s^{-1}\frac{Q^2}{4b^2}\left(\frac{2b}{Q} - 1\right) . \tag{9.53}$$

Recalling the disk one-point amplitude (9.41) and the definition of $g_s f$, we get

$$g_s f = \frac{A_{\mathrm{disk}}(VV)}{A_{\mathrm{disk}}(V)^2} = g_s\left(\frac{2b}{Q} - 1\right) . \tag{9.54}$$

Thus, we find perfect agreement with the prediction in (9.40).

Tachyon exchange contribution to the disk two-point function

The goal of this subsection is to show that the tachyon exchange explicitly cancels the divergent term in (9.52). The open-closed interaction vertex is associated with an UHP two-point function, with one closed string at i and one open open string at 0. Let us denote by z and z' the coordinates on the two UHP coordinates representing the two vertices respectively. The closed strings are inserted at $z = \mathrm{i}$ and $z' = \mathrm{i}$, while the open strings are inserted at $z = 0$ and $z' = 0$. Since the open string insertions are part of the internal open string propagator, they are in general off-shell and we need to specify the local coordinates w and w' around the insertion points $z = 0$ and $z' = 0$. We take [307]

$$w = \lambda z, \qquad w' = \lambda z' , \tag{9.55}$$

for some large constant λ. Then the string field theory Feynman diagram produces part of the world-sheet moduli space where we sew the two upper half planes by the relation

$$ww' = -q, \qquad 0 \le q \le 1\,. \tag{9.56}$$

Using (9.55) we get the relation $z = -q/(\lambda^2 z')$, so that the two closed-string vertex operators are inserted in the z-plane at $z = \mathrm{i}$ and $z = \mathrm{i}q/\lambda^2$. Calling the second position $\mathrm{i}y$ we see that the range $0 \le q \le 1$ translates to $0 \le y \le \lambda^{-2}$. Since the desired range in Section 9.4 is $0 \le y \le \epsilon$, we see that we should choose

$$\lambda^2 = 1/\epsilon\,. \tag{9.57}$$

Once we have determined the relation between the parameters ϵ and λ, we shall forget the Schwinger parameter representation of the propagator and directly calculate the contribution from various open string exchange diagrams. Due to the relation (9.55) between the local and global coordinates, the coupling of an internal open string state of conformal weight $L_0 = h$ is scaled by a factor of λ^{-h}. Taking into account that we have two upper half plane amplitudes connected by an open string propagator, we get a net factor of $\lambda^{-2h} = \epsilon^h$.

The leading contribution, associated with the exchange of the open string tachyon $c_1|0\rangle = c(0)|0\rangle$ with $L_0 = -1$, is given by,

$$\epsilon^{-1} \cdot \frac{\mathrm{i}\pi}{g_s}\langle c\bar{c}V(\mathrm{i})c(0)\rangle_{\mathrm{UHP}} \cdot \frac{g_o^2}{(-1)} \cdot \frac{\mathrm{i}\pi}{g_s}\langle c\bar{c}V(\mathrm{i})c(0)\rangle_{\mathrm{UHP}}\,. \tag{9.58}$$

The two $\mathrm{i}\pi g_s^{-1}\langle c\bar{c}V(\mathrm{i})c(0)\rangle_{\mathrm{UHP}}$ factors are the disk correlators describing the open-closed interaction vertex, with conventions as in (9.5). The factor of g_o^2 can be regarded either as part of the propagator in the convention in which g_o^{-2} appears as an overall factor in the open string field theory action, or from the two open-closed string vertices if we normalize the open string field so that kinetic term has no g_o dependence. The -1 in the denominator of the middle term is a reflection of the open string tachyon having mass$^2 = -1$. Using (9.27) and (9.2) we have

$$\langle c\bar{c}V(\mathrm{i})c(0)\rangle_{\mathrm{UHP}} = \frac{Q}{4b} \cdot (-2\mathrm{i}) = -\mathrm{i}\,\frac{Q}{2b}\,. \tag{9.59}$$

Using the relationship $1/(2\pi^2 g_o^2) = 1/g_s$ [266, 287, 267, 288], we can simplify (9.58) to

$$-\epsilon^{-1}\, g_s^{-1}\, \frac{Q^2}{8b^2}\,. \tag{9.60}$$

So we conclude that the exchange of the open string tachyon precisely cancels the divergent contribution in (9.52).

Finally, we note that we could work with a more general choice of local coordinates w, w' instead of (9.55), for instance $w = \frac{\lambda z}{1-\gamma z}, w' = \frac{\lambda z'}{1-\gamma z'}$, for some constant γ. In this case, the tachyon exchange contribution will be modified, but there will also be an extra contribution from the exchange of the out-of-Siegel-gauge mode ψ multiplying the state $\mathrm{i}c_0|0\rangle$. As in [307], the sum of the two contributions, expressed as a function of ϵ, is independent of the choice of local coordinates w, w'.

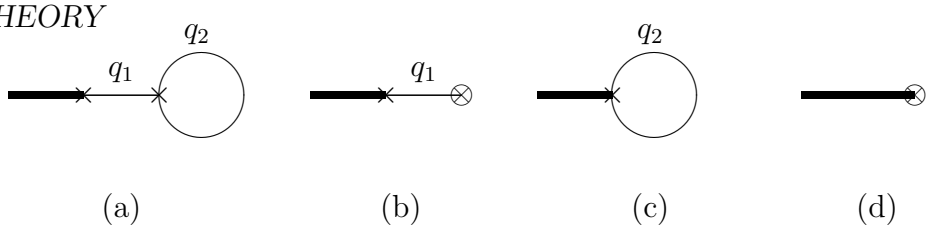

Figure 9.2: The four Feynman diagrams that contribute to the annulus one-point amplitude. The thick line denotes a closed string, while thin lines denote open strings. The $\times$ denotes a vertex on the upper half plane, whereas $\otimes$ denotes a vertex on the annulus. The variables q_1 and q_2 are the plumbing fixture variables associated with the corresponding propagators. Figure reproduced from [307].

9.5 The annulus one-point function

This section is devoted to analyzing the annulus one-point function of the cosmological constant operator V and deriving the result $g = \frac{1}{2}$ in (9.40) by directly integrating over the moduli space.

We parametrize the annulus with a complex coordinate $w = 2\pi(x + \mathrm{i}y)$, with the flat metric $\mathrm{d}w\mathrm{d}\overline{w}$. As in Section 9.2, we let $2\pi t$ be the Euclidean time in the open string channel, which means that y is periodic with period t. We can fix the translation symmetry along the y-axis by setting the y-coordinate of the vertex operator to zero. Thus, we are left with a two-dimensional moduli space, labeled by $v = e^{-2\pi t}$ and x. The range of v is $0 \leq v \leq 1$. The measure for v integration is proportional to $\mathrm{d}t$ or $\frac{\mathrm{d}v}{v}$, unlike $\frac{\mathrm{d}t}{t}$ for the empty annulus in (9.21), since the translation symmetry in the y-direction has been fixed. The open string has length π, so x spans the range $0 \leq x \leq \frac{1}{2}$. However, note that $w \to \pi - w$ is a diffeomorphism of the annulus, since both boundaries lie on the same instanton. We need to quotient by diffeomorphisms, and so the range of integration of x is in fact $0 \leq x \leq \frac{1}{4}$.

Recall that $g_s g$ is defined as the ratio of the annulus one-point amplitude to the disk one-point amplitude. By general principles, we have[7]

$$g_s\, g = \int_0^1 \mathrm{d}v \int_0^{\frac{1}{4}} \mathrm{d}x\, F(v,x) = g_s\, \frac{4b}{Q} \int_0^1 \mathrm{d}v \int_0^{\frac{1}{4}} \mathrm{d}x\ \mathrm{Tr}\left[V(w,\bar{w})\, b_0\, c_0\, v^{L_0-1}\right] . \tag{9.61}$$

The nontrivial proportionality constant in the final expression is determined in the next subsection. The coordinate w should not be confused with the local coordinates around the punctures for which we use the same symbol.

The integral (9.61) has divergences for small v and small x. As explained in detail in [307], we need to interpret the contributions from these regions as string field theory Feynman diagrams with internal propagators. These Feynman diagrams are shown in figure

[7]See, for example, section 7.3 of [265] for the analogous statement for the torus amplitude with external closed string states.

9.2 and the corresponding regions in the moduli space are shown in figure 9.3. The Feynman diagram (d) represents the contributions from the "bulk" of moduli space where there is no degeneration. Feynman diagram (c) has one internal propagator and corresponds to small v with finite x. Feynman diagram (b) also has one internal propagator, but corresponds to small x with finite v. Finally, Feynman diagram (a) has two internal propagators and corresponds to small v *and* small x.

Normalization of the worldsheet contribution to the annulus one-point function

The goal of this appendix is to derive the proportionality constant in (9.61), and also to write precise expressions for the small-v and small-x behavior of the integrand.

Recall that we can write $g_s g$ as

$$g_s\, g = \int_0^1 \mathrm{d}v \int_0^{\frac{1}{4}} \mathrm{d}x\, F(v,x)\,, \quad \text{with} \tag{9.62}$$

$$F(v,x) = C\ \mathrm{Tr}\left[V(w,\bar{w})\, b_0\, c_0\, v^{L_0-1}\right]\,, \quad w := 2\pi(x+\mathrm{i}y)\,, \tag{9.63}$$

where C is the normalization constant that we want to determine. Recalling the argument near (9.92), we can also write $F(v,x)$ as

$$F(v,x) = \partial_x G(v,x)\,, \quad G(v,x) := \frac{C}{16\pi^2 b}\,\mathrm{Tr}\left[\partial_x\phi(w,\overline{w})\, b_0\, c_0\, v^{L_0-1}\right]\,. \tag{9.64}$$

Our strategy for determining C will be to compare the integrand to the contribution from the Feynman diagram in figure 9.2 (a) for small v and small x. We would also like to compute $G(v,x)$ and $F(v,x)$ in the regions of small v or small x (with the second variable being not necessarily small).

Recall that w is the coordinate on the strip $0 \le \mathrm{Re}\,[w] \le \pi$, with $\mathrm{Re}\,[w] = 2\pi x$. We can map this to the upper half plane by the map $z = e^{\mathrm{i}w}$. The annulus is obtained from this via the identification $z \equiv vz$. The transformation of $\partial\phi$ is given in (9.18), with a similar transformation for $\overline{\partial}\phi$. We get

$$\partial_w\phi(w,\overline{w}) = \mathrm{i}\frac{Q}{2} + \mathrm{i}z\,\partial_z\phi(z,\overline{z})\,, \tag{9.65}$$

$$\partial_{\overline{w}}\phi(w,\overline{w}) = -\mathrm{i}\frac{Q}{2} - \mathrm{i}\overline{z}\,\partial_{\overline{z}}\phi(z,\overline{z})\,. \tag{9.66}$$

Thus, for small x, we can use the bulk-boundary OPEs (9.25), (9.26) to get

$$\partial_x\phi(w,\overline{w}) = 2\pi(\partial_w\phi(w,\overline{w}) + \partial_{\overline{w}}\phi(w,\overline{w})) = 2\pi\mathrm{i}\,(z\partial_z\phi(z,\overline{z}) - \overline{z}\partial_{\overline{z}}\phi(z,\overline{z})) \approx -\frac{Q}{x}\,. \tag{9.67}$$

The definition of $G(v,x)$ in (9.64) now gives

$$G(v,x) \approx -C\,\frac{Q}{b}\,\frac{1}{16\pi^2 x}\,\mathrm{Tr}\left[b_0\,c_0\,v^{L_0-1}\right] = -C\,\frac{Q}{b}\,\frac{1}{16\pi^2 x}\,\frac{Z(v)}{v}\,, \tag{9.68}$$

$$F(v,x) \approx C\,\frac{Q}{b}\,\frac{1}{16\pi^2 x^2}\,\frac{Z(v)}{v}\,. \tag{9.69}$$

Here $Z(v)$ is the annulus partition function, given in (9.22).

Next, we consider the small-v, finite-x region. We can evaluate this correlation function by separating out the matter and ghost contributions. In the ghost sector, the leading and subleading contributions to the trace are as in (9.23). In the matter sector the leading and subleading contributions for small v come from just the vacuum state $|0\rangle$. Therefore

$$\mathrm{Tr}\left[\partial_x\phi(w,\overline{w})\,b_0\,c_0\,v^{L_0-1}\right] \approx (v^{-2}-2v^{-1}+O(1))\,\langle 0|\partial_x\phi(w,\bar{w})|0\rangle \qquad \text{for small } v\,. \tag{9.70}$$

Since we do not have a trace in the Liouville sector, we no longer need the identification $z \equiv vz$. Using (9.65) and (9.66), and $\langle\partial_z\phi(z,\overline{z})\rangle_{\mathrm{UHP}} = -\frac{Q}{z-\overline{z}}$ as given in (9.28), we get

$$\langle 0|\partial_x\phi(w,\bar{w})|0\rangle = -\mathrm{i}\,2\pi Q\,\frac{z+\overline{z}}{z-\overline{z}} = -2\pi Q\,\cot(2\pi x)\,. \tag{9.71}$$

Thus, from (9.64), we get

$$G(v,x) \approx -C\,\frac{Q}{8\pi b}(v^{-2}-2v^{-1}+O(1))\cot(2\pi x)\,, \tag{9.72}$$

$$F(v,x) \approx C\,\frac{Q}{b}\,(v^{-2}-2v^{-1}+O(1))\,\frac{1}{4\sin^2(2\pi x)} \quad \text{for small } v\,. \tag{9.73}$$

We shall now fix the constant C by comparing (9.69) or (9.73) with the result $g^{(a)}$ of the Feynman diagram in figure 9.2(a), which corresponds to small v and small x. For this, we first rewrite $F(v,x)$ in the (q_1,q_2) coordinates using eqs (4.73) and (4.81) of [307] for small v and small x:

$$v \approx \frac{q_2}{\alpha^2}, \qquad x = \frac{q_1}{2\pi\widetilde{\lambda}}\,. \tag{9.74}$$

This yields

$$F(v,x)\,\mathrm{d}v\,\mathrm{d}x \approx C\,\frac{Q}{b}\,\frac{1}{16\pi^2}\,\frac{\mathrm{d}v\,\mathrm{d}x}{v^2\,x^2} \approx C\,\frac{Q}{b}\,\frac{\widetilde{\lambda}\alpha^2}{8\pi}\,\frac{\mathrm{d}q_2}{q_2^2}\,\frac{\mathrm{d}q_1}{q_1^2}\,. \tag{9.75}$$

The Feynman diagram of figure 9.2(a) can be analyzed as follows. The leading contribution for small v and small x comes from the propagation of the open string tachyon along both propagators, producing the factor $\int \mathrm{d}q_2\,q_2^{-2}\,\mathrm{d}q_1\,q_1^{-2}$. Since the tachyon vertex operator c is a primary of dimension -1, the open-closed and open-open-open interaction vertices produce factors of λ and α^3, respectively. The three open string vertex produces a factor of

the open string coupling constant g_o. The ratio of the open-closed vertex (9.5) to the disk one-point function (9.4) is given by

$$g_o \, \frac{\mathrm{i}\pi \, \langle c(0) c\bar{c}(\mathrm{i}) \rangle_{\mathrm{UHP}}}{\frac{1}{4} \langle (\partial c - \bar{\partial}\bar{c}) c\bar{c}(\mathrm{i}) \rangle_{\mathrm{UHP}}} = \pi g_o \, . \tag{9.76}$$

The factor of g_o arises due to the presence of the extra open string. We have evaluated the ghost correlators using (9.2). Putting all the factors together we get the following result for $g_s g^{(a)}$:

$$g_s g^{(a)} = \int\int \frac{\mathrm{d}q_2}{q_2^2} \, \frac{\mathrm{d}q_1}{q_1^2} \, \lambda \, \alpha^3 \, \pi \, g_o^2 \, = \int\int \frac{\mathrm{d}q_2}{q_2^2} \, \frac{\mathrm{d}q_1}{q_1^2} \, \frac{\tilde{\lambda}\alpha^2}{2\pi} \, g_s \, . \tag{9.77}$$

In going to the second expression, we have used $\tilde{\lambda} = \lambda\alpha$, and also the fact that $1/(2\pi^2 g_o^2) = 1/g_s$ [266, 287, 267, 288]. Comparing (9.75) and (9.77), we get,

$$C = \frac{4b}{Q} \, g_s \, . \tag{9.78}$$

Plugging this value of C into (9.63) and (9.62), we get the desired result (9.61).

For later use, we also rewrite (9.68), (9.69), (9.72) and (9.73) using (9.78):

$$G(v,x) \approx \begin{cases} -\frac{g_s}{2\pi} \, \cot(2\pi x) \, \{v^{-2} - 2v^{-1} + O(1)\} & \text{for small } v \\ -\frac{g_s}{4\pi^2 x} \, \frac{Z(v)}{v} & \text{for small } x \, . \end{cases} \tag{9.79}$$

$$F(v,x) \approx \begin{cases} \frac{g_s}{\sin^2(2\pi x)} \, \{v^{-2} - 2v^{-1} + O(1)\} & \text{for small } v \\ \frac{g_s}{4\pi^2 x^2} \, \frac{Z(v)}{v} & \text{for small } x \, . \end{cases} \tag{9.80}$$

Brief review of the construction of vertices

Before diving into the computational details, we give an overview of the construction of the various vertices that we will need. We will be brief since all the details were explained in [307].

We will discuss the five different types of vertices that appear in figure 9.2: (1) the upper half plane C-O vertex, (2) the upper half plane O-O-O vertex, (3) the upper half plane C-O-O vertex, (4) the annulus O vertex, and (5) the annulus C vertex. Here C and O stand respectively for closed and open strings.

The C-O vertex is described by the upper half plane geometry with complex coordinate z. The closed string puncture is inserted at $z = \mathrm{i}$ and the open string puncture is inserted at $z = 0$. There are no moduli. The local coordinate w around the open string puncture is taken to be $w = \lambda z$, with λ being a large, fixed real number.

The O-O-O vertex is described by the upper half plane geometry. Let's again denote the complex coordinate on the upper half plane by z, with the three open string punctures inserted at $z = 0$, $z = 1$ and $z = \infty$. There are no moduli, but in computing a physical amplitude, one needs to sum over the two distinct cyclic permutations of the three points. Let

α be another large, fixed real parameter. The local coordinates around the three punctures are chosen to be

$$w_1 = \alpha \frac{2z}{2-z}\,, \quad w_2 = \alpha \frac{2(z-1)}{z+1}\,, \quad w_3 = \alpha \frac{2}{1-2z}\,. \tag{9.81}$$

Next, we discuss the C-O-O vertex, which appears in figure 9.2(c). The C-O-O amplitude on the upper half plane has a one-dimensional moduli space, and provides an example of how the boundaries of moduli space are assigned to Feynman diagrams with internal propagators. Denoting the complex coordinate on the upper half plane by z, we insert the closed string puncture at $z = \mathrm{i}$ and the two open string punctures at $z = \pm\beta$. Here β is a positive real number that can be taken to be the coordinate on the one-dimensional moduli space. The $\mathrm{PSL}(2,\mathbb{R})$ transformation $z \to -1/z$ keeps the puncture at $z = \mathrm{i}$ fixed, but sends $\beta \to -1/\beta$. So we can restrict β to lie in the range $0 \le \beta \le 1$, while summing over the two permutations of the two open string punctures. The region of small β, when the two open string punctures collide, is covered by the Feynman diagram that consists of an upper half plane C-O vertex (with coordinate z) joined to an upper half plane O-O-O vertex (with coordinate $\widetilde{z}$) with an open string propagator. The joining happens via the plumbing fixture relation $\lambda z \cdot \alpha \frac{2\widetilde{z}}{2-\widetilde{z}} = -q_1$, with $0 \le q_1 \le 1$. Now define

$$\tilde{\lambda} := \lambda\alpha\,. \tag{9.82}$$

The open string puncture at $\widetilde{z} = 1$ gets mapped to $z = -\frac{q_1}{2\tilde{\lambda}}$, while the one at $\widetilde{z} = \infty$ gets mapped to $z = +\frac{q_1}{2\tilde{\lambda}}$. Thus, we see that $\beta = \frac{q_1}{2\tilde{\lambda}}$. Since the range of q_1 is $0 \le q_1 \le 1$, we see that this Feynman diagram covers the region $0 \le \beta \le \frac{1}{2\tilde{\lambda}}$. Note that $\tilde{\lambda}$ is large, so this is the region of small β, where the two open-string punctures are close to each other. The upper half plane C-O-O vertex is then assigned to cover the remaining region $\frac{1}{2\tilde{\lambda}} \le \beta \le 1$. For the range $0 \le \beta \le \frac{1}{2\tilde{\lambda}}$, the local coordinates around the two open string punctures are induced by the choice of local coordinates in the C-O and O-O-O vertices described above. For the range $\frac{1}{2\tilde{\lambda}} \le \beta \le 1$, we need to pick a choice of local coordinates that, at $\beta = \frac{1}{2\tilde{\lambda}}$, match the ones from the $\beta \le \frac{1}{2\tilde{\lambda}}$ region. The choice made in equation (4.12) of [307] involved a real-valued function $f(\beta)$ that is only constrained by the following

$$f\left(\frac{1}{2\tilde{\lambda}}\right) = \frac{4\tilde{\lambda}^2 - 3}{8\tilde{\lambda}^2}\,, \quad f(1) = 0\,, \quad f(-\beta) = -f(\beta)\,. \tag{9.83}$$

From now on, we shall work in the limit of large α and $\widetilde{\lambda}$ and ignore terms that are suppressed by inverse powers of either α or $\widetilde{\lambda}$. Of course, the final result is guaranteed to be independent of α, $\widetilde{\lambda}$ and the function $f(\beta)$.

Next, we discuss the vertex that corresponds to one open string puncture on the annulus. This appears as one of the vertices in figure 9.2(b). There is one modulus, the quantity v defined in (9.20). The full range of v is $0 \le v \le 1$. As discussed in [307], the region $0 \le v \le (\alpha^2 - \frac{1}{2})^{-1}$ of small v corresponds to the upper half plane O-O-O vertex with

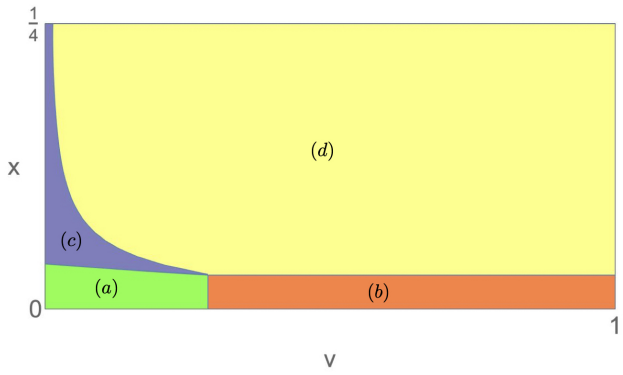

Figure 9.3: The division of moduli space of the annulus with one bulk puncture into four regions corresponding to the four Feynman diagrams in figure 9.2. The green region describes the Feynman diagram in figure 9.2(a) and is given in (9.84). The red region describes the Feynman diagram in figure 9.2(b) and is given in (9.86). The blue region describes the Feynman diagram in figure 9.2(c) and is given in (9.88)-(9.90). The remaining yellow region describes the Feynman diagram in figure 9.2(d), and covers the bulk of the (v, x) moduli space. We have taken $\tilde{\lambda} = 4$, $\alpha = 2$ and $f(\beta) = \frac{4\tilde{\lambda}^3 - 3\tilde{\lambda}}{4\tilde{\lambda}^2 - 1}\beta(1-\beta^2)$ for the purposes of plotting this figure.

two of the three open string punctures joined with a propagator. The remaining range $(\alpha^2 - \frac{1}{2})^{-1} \leq v \leq 1$ is assigned to the annulus O vertex. The choice of the local coordinate around the open string puncture has been described in [307].

Finally, we come to the C amplitude on the annulus. As already explained, in this case there is a two-dimensional moduli space parametrized by v and x. We need to divide this moduli space into four regions [307], which correspond to the four Feynman diagrams in figure 9.2. See also figure 9.3. The Feynman diagram in figure 9.2(a) corresponds to the region (shown in green in figure 9.3)

$$0 \leq v \leq \left(\alpha^2 - \frac{1}{2}\right)^{-1}, \quad 0 \leq 2\pi x \leq \tilde{\lambda}^{-1}\,\frac{2-v}{2+v}\,, \tag{9.84}$$

with (v, x) related to the plumbing fixture variables (q_1, q_2) as

$$v = \frac{q_2}{\alpha^2}\left(1 - \frac{q_2}{2\alpha^2}\right)^{-1}, \quad 2\pi x = \frac{q_1}{\tilde{\lambda}}\left(1 - \frac{q_2}{\alpha^2}\right). \tag{9.85}$$

The plumbing fixture variables always vary in the range $[0, 1]$. The Feynman diagram in figure 9.2(b) corresponds to the region (shown in red in figure 9.3)

$$\left(\alpha^2 - \frac{1}{2}\right)^{-1} \leq v \leq 1\,, \quad 0 \leq 2\pi x \leq \tilde{\lambda}^{-1}(1 - \alpha^{-2})\,, \tag{9.86}$$

with x related to the plumbing fixture variable q_1 as

$$2\pi x = \frac{q_1}{\tilde{\lambda}}\left(1-\frac{1}{\alpha^2}\right) . \tag{9.87}$$

The Feynman diagram in figure 9.2(c) corresponds to the region in the (v,x) plane parameterized as

$$\frac{1}{2\tilde{\lambda}} \le \beta \le 1\,, \quad 0 \le u \le \alpha^{-2}\left(1+\frac{1}{4\tilde{\lambda}^2}\right)^{-2}\,, \quad \text{with} \tag{9.88}$$

$$2\pi x(\beta,u) = 2\tan^{-1}(\beta) - \frac{u}{\beta\tilde{\lambda}^2}\left(1-\beta^2-2\beta f(\beta)\tilde{\lambda}\right) \quad \text{and} \tag{9.89}$$

$$v(\beta,u) = u\frac{(1+\beta^2)^2}{4\beta^2\tilde{\lambda}^2}\left(1+\frac{u}{2\beta^2\tilde{\lambda}^2}\left(1-\beta^2-2\beta f(\beta)\tilde{\lambda}\right)^2\right) . \tag{9.90}$$

The parameter u is related to the plumbing fixture variable q_2 via $u = q_2\alpha^{-2}(1+\frac{1}{4\tilde{\lambda}^2})^{-2}$. Note that this corresponds to small v but finite x region, and is shown in blue in figure 9.3. The Feynman diagram in figure 9.2(d) covers the remaining (v,x) region, not included in the three cases above; it is shown in yellow in figure 9.3.

We will need to integrate a total derivative on region (d), and so we need to discuss the boundaries of region (d). There are four boundary components, see figure 9.3. The boundary between regions (d) and (b) lies at fixed $x = (2\pi\tilde{\lambda})^{-1}(1-\alpha^{-2})$ and is parametrized by v in the range given in (9.86). The boundary between regions (d) and (c) is parametrized by β in the range given in (9.88), with fixed $u = \alpha^{-2}(1+\frac{1}{4\tilde{\lambda}^2})^{-2}$ and x, v given by (9.89), (9.90). The top boundary lies at $x = \frac{1}{4}$, with $(\tilde{\lambda}\alpha)^{-2}(1+\frac{1}{4\tilde{\lambda}^2})^{-2} \le v \le 1$. Finally, the right boundary lies at $v = 1$ with $(2\pi\tilde{\lambda})^{-1}(1-\alpha^{-2}) \le x \le \frac{1}{4}$.

We end this subsection with a couple of important remarks. First, in doing the computations, we will be expanding various expressions for large α and large $\tilde{\lambda}$. In doing so, we can drop all terms that contain negative powers of either variable α or $\tilde{\lambda}$, since these cannot contribute to the final answer [307]. The reason is that the α and $\tilde{\lambda}$ dependent terms are supposed to cancel in the end, and if a term contains a negative power of one large variable, there is no way for it to give a α and $\tilde{\lambda}$ independent term at higher orders. Second, for diagrams that contain an internal propagator, we need the string field theory replacement rules [307]

$$\int_0^1 \mathrm{d}q\, q^{-2} \to -1\,, \quad \int_0^1 \mathrm{d}q\, q^{-1} \to 0\,. \tag{9.91}$$

Here q is the parameter that enters in the plumbing fixture relation. The first replacement rule comes from the formal Schwinger parameter representation of the propagator of a field with $L_0 = -1$. The second replacement rule comes from the fact that the Siegel gauge zero modes are not part of the SFT path integral. They are replaced by the ψ field that multiples $\mathrm{i}c_0|0\rangle$, and the contribution of ψ exchanges is taken into account separately.

The worldsheet contribution

In this subsection, we will compute the worldsheet contribution to g. There are two other contributions, which we shall compute in the subsequent subsections.

Let us begin by computing the contribution from the "bulk" region of moduli space, corresponding to the Feynman diagram in figure 9.2(d). Let us denote the region of the (v, x)-plane covered by this diagram by S. We choose S to have the orientation given by the two-form $\mathrm{d}v \wedge \mathrm{d}x$. We use the equation of motion (9.17) with $\widetilde{\mu} = 1$ to replace V in (9.61) by $\frac{1}{b}\partial_w\partial_{\overline{w}}\phi$, or $\frac{1}{16\pi^2 b}(\partial_x^2 + \partial_y^2)\phi$. The $\partial_y^2\phi$ term does not contribute, since the transformation that moves the vertex operator insertion in the y-direction is a simple translation for which the anomaly term in the transformation of $\partial\phi$ (9.18) vanishes. Thus

$$g^{(d)} = \frac{1}{4\pi^2 Q}\int_S \mathrm{d}v\,\mathrm{d}x\,\partial_x\,\mathrm{Tr}\left[\partial_x\phi(w,\overline{w})\,b_0\,c_0\,v^{L_0-1}\right] = g_s^{-1}\int dv\,dx\,\partial_x G(v,x)\,, \tag{9.92}$$

where $G(v, x)$ has been defined in (9.64), (9.78). Since the right hand side of this equation is a total derivative, the computation reduces to integrating $\mathrm{Tr}\left[\partial_x\phi(w,\overline{w})\,b_0\,c_0\,v^{L_0-1}\right]$ along the boundary of S.

The boundary of S has four components, as discussed at the end of the previous subsection. The top boundary at $x = \frac{1}{4}$ does not contribute since the symmetry $w \to \pi - w$ implies that $\langle\partial_x\phi(w = \frac{\pi}{2})\rangle_{\text{annulus}} = 0$. There are no divergences at the $v = 1$ boundary, and since we are integrating $\partial_x(\ldots)$ on S, via Stokes's theorem, this boundary also does not contribute. So we only need to consider the two remaining boundaries: the boundary between regions (d) and (c), and the boundary between regions (d) and (b).

Let us first consider the boundary between regions (d) and (b), and denote the contribution as $g^{(b)\text{-}(d)}$. This boundary lies at constant small x, namely $x = \frac{1-\alpha^{-2}}{2\pi\widetilde{\lambda}}$, with v lying in the range given in the first part of (9.86). The small-x, finite-v behavior can be found from (9.79) and yields,

$$g^{(b)\text{-}(d)} = \frac{1}{2\pi}\,\widetilde{\lambda}\,(1-\alpha^{-2})^{-1}\int_{(\alpha^2-\frac{1}{2})^{-1}}^{1}\mathrm{d}v\,\frac{Z(v)}{v}\,. \tag{9.93}$$

We could evaluate this using the known form of $Z(v)$, but we note that this contribution will be exactly cancelled by the contribution $g^{(b)}$ of the Feynman diagram in figure 9.2(b).[8] Physically, this happens because there are no $L_0 = 1$ states in the Liouville open string sector that can leave an order-one contribution, and because the relation between x and q_1 in (9.87) is linear. More precisely, to evaluate the Feynman diagram in figure 9.2(b), we use the second line of (9.80), write x in terms of q_1 using (9.87), and use the replacement rule $\int_0^1 \frac{\mathrm{d}q_1}{q_1^2} \to -1$.

Now let us consider the boundary between regions (d) and (c), and denote the contribution as $g^{(c)\text{-}(d)}$. As discussed at the end of the previous subsection, the boundary between

[8] This is analogous to a similar argument made in appendix D of [307].

regions (d) and (c) is parametrized by $(v(\beta,u),x(\beta,u))$ given in (9.89) and (9.90), with $\frac{1}{2\tilde{\lambda}} \le \beta \le 1$ and u fixed to be $u = \alpha^{-2}(1+\frac{1}{4\tilde{\lambda}^2})^{-2}$. Let us denote (9.89) and (9.90) with this fixed value of u by $(v(\beta),x(\beta))$. Since v is small along this boundary, we need to understand the small-v behavior of $G(v,x)$. This has been given in (9.79), using which we get

$$g^{(c)\text{-}(d)} = -\frac{1}{2\pi}\int \mathrm{d}v\,(v^{-2}-2v^{-1})\cot(2\pi x)\,, \tag{9.94}$$

with the direction of integration being the direction of increasing β, that is, upwards along the boundary of the blue and yellow regions in figure 9.3. To do the integral in (9.94), it is helpful to first rewrite it as

$$g^{(c)\text{-}(d)} = \frac{1}{2\pi}\int_{(2\tilde{\lambda})^{-1}}^{1} \mathrm{d}\beta\,\frac{\partial}{\partial\beta}\left(v(\beta)^{-1}+2\log v(\beta)\right)\cot(2\pi x(\beta))\,. \tag{9.95}$$

Then carrying out the integrations using the known expressions for $v(\beta)$ and $x(\beta)$ given above, we get

$$g^{(c)\text{-}(d)} = \frac{\alpha^2\widetilde{\lambda}^2}{4} - \frac{\alpha^2\widetilde{\lambda}}{\pi} - \frac{3\widetilde{\lambda}}{4\pi} + \frac{\alpha^2}{8} - \frac{2\widetilde{\lambda}^2}{\pi}\int_{(2\tilde{\lambda})^{-1}}^{1}\mathrm{d}\beta\,\frac{f(\beta)^2}{1+\beta^2} + \frac{1}{2}\,. \tag{9.96}$$

Now, let us evaluate the contribution from the Feynman diagram in figure 9.2(c). This diagram corresponds to small v but finite x, the precise domain has been specified in (9.88)-(9.90). Using (9.89) and (9.90) we get the transformation of the measure

$$\mathrm{d}v\,\mathrm{d}x = \left(\frac{1+\beta^2}{4\pi\beta^2\tilde{\lambda}^2}+O(u)\right)\mathrm{d}\beta\,\mathrm{d}u, \tag{9.97}$$

and so, using (9.61) and the first line of (9.80), we have

$$\begin{aligned} g^{(c)} &= \int_{(2\tilde{\lambda})^{-1}}^{1}\mathrm{d}\beta\int_0^{\alpha^{-2}(1+(4\tilde{\lambda}^2)^{-1})^{-2}}\mathrm{d}u\,\left(\frac{1+\beta^2}{4\pi\beta^2\tilde{\lambda}^2}+O(u)\right)\frac{1}{\sin^2(2\pi x)}\left(v^{-2}-2v^{-1}+O(v^0)\right)\\ &\to -\alpha^2\left(1+\frac{1}{4\tilde{\lambda}^2}\right)^2\int_{(2\tilde{\lambda})^{-1}}^{1}\mathrm{d}\beta\,\frac{\tilde{\lambda}^2}{\pi(1+\beta^2)} \approx -\frac{\alpha^2\tilde{\lambda}^2}{4}+\frac{\alpha^2\tilde{\lambda}}{2\pi}-\frac{\alpha^2}{8}\,. \end{aligned} \tag{9.98}$$

In the second step, we used (9.89) and (9.90), replaced u by $q_2\alpha^{-2}(1+\frac{1}{4\tilde{\lambda}^2})^{-2}$, applied the replacement rule (9.91) for the plumbing fixture variable q_2, simplified a bit and ignored terms containing inverse powers of either α or $\tilde{\lambda}$. The $O(u)$ term from the measure can combine with the v^{-2} term to give an $O(1)$ expression proportional to $\int du/u = \int dq_2/q_2$, but this is set to zero using the replacement rule (9.91).

The contribution from the Feynman diagram in figure 9.2(a) can be obtained by using the expression for $F(v,x)$ in (9.80) for small v and small x, rewriting the answer in terms of

(a) (b)

Figure 9.4: The two Feynman diagrams involving the loop of the out-of-Siegel-gauge mode ψ. They both involve the upper half plane C-O-O amplitude; (a) corresponds to small β while (b) corresponds to finite β. Figure adapted from [307].

the plumbing fixture variables q_1 and q_2 using (9.85), and then using the first replacement rule in (9.91) for both q_1 and q_2. We get

$$g^{(a)} = \frac{1}{2\pi}\tilde{\lambda}\,\alpha^2\,. \tag{9.99}$$

Putting together all the Feynman diagrams in figure 9.2 using equations (9.99), (9.98), (9.96), and the fact that $g^{(b)} + g^{(b)\text{-}(d)} = 0$, we get the total worldsheet contribution to g as

$$g_{\text{ws}} = g^{(a)} + g^{(b)} + g^{(c)} + \left(g^{(b)\text{-}(d)} + g^{(c)\text{-}(d)}\right) \tag{9.100}$$

$$= \frac{1}{2} - \frac{3\tilde{\lambda}}{4\pi} - \frac{2\tilde{\lambda}^2}{\pi}\int_{(2\tilde{\lambda})^{-1}}^{1} \mathrm{d}\beta\,\frac{f(\beta)^2}{1+\beta^2}\,. \tag{9.101}$$

Contribution from ψ exchange

Since the two Siegel-gauge zero modes get replaced by the out-of-Siegel gauge mode ψ that multiplies the state $\mathrm{i}c_0|0\rangle = \mathrm{i}\partial c(0)|0\rangle$, we need to take into account the contribution from the diagrams involving ψ propagators explicitly [307]. This is a contribution that is not captured by the string worldsheet.

As mentioned in Section 9.4, the one-point C-O disk amplitude with one on-shell closed string and the open string puncture corresponding to ψ vanishes. So, we only need to consider the two Feynman diagrams shown in figure 9.4; they are analogous to figure 9.2(a) and 9.2(c). Both diagrams involve an upper-half-plane amplitude with one closed string puncture, and two open string punctures joined with a ψ propagator. Following the discussion of the upper half plane C-O-O amplitude, we see that the region $0 \le \beta \le \frac{1}{2\tilde{\lambda}}$ corresponds to figure 9.4(a), while the region $\frac{1}{2\tilde{\lambda}} \le \beta \le 1$ corresponds to figure 9.4(b). As earlier, the ψ propagator equals $\frac{1}{2}$ in our conventions.

The geometry of the upper half plane C-O-O amplitude has been discussed earlier. We represent the upper half plane with complex coordinate z, insert the closed string puncture at $z = \mathrm{i}$ and insert the two open string punctures at $z_1 = -\beta$ and $z_2 = \beta$. Let w_a, with $a \in \{1, 2\}$ denote the local coordinates around the two open string punctures, which we

relate to z as

$$z = F_a(w_a, \beta) = z_a + g_a(\beta) w_a + \frac{1}{2} h_a(\beta) w_a^2 + O(w_a^3)\,. \tag{9.102}$$

The actual amplitude, normalized to directly give the contribution to g, is given by [322, 323, 324]

$$g_\psi = -K_1 \int \mathrm{d}\beta \sum_{a=1}^{2} \oint_a \frac{\mathrm{d}z}{2\pi \mathrm{i}} \frac{\partial F_a}{\partial \beta} \left\langle b(z) F_1 \circ \mathrm{i}\partial c(0)\, F_2 \circ \mathrm{i}\partial c(0)\, c\bar{c} V(\mathrm{i}) \right\rangle_{\mathrm{UHP}}\,, \tag{9.103}$$

where $\oint_a$ represents an anticlockwise contour around z_a, and $F_a \circ \mathrm{i}\partial c(0)$ denotes the conformal transformation of the operator $\mathrm{i}\partial c$ by the function F_a. The constant K_1 is a normalization constant that we determine in the next subsection by comparing the right hand side of (9.103), with ψ replaced by the tachyon, to the result for either figure 9.2(c) or 9.2(a), which were given in (9.98), (9.99). The result is $K_1 = \frac{\mathrm{i}b}{2\pi Q}$. This includes the contribution of the ψ propagator. The β integral captures the effect of the Schwinger parameter integral associated with the horizontal open string propagator in figure 9.4(a), and the intrinsic integration parameter of the C-O-O vertex in figure 9.4(b).

Explicitly, the local coordinates around the open string punctures are [307]

$$F_1(w_1, \beta) = -\beta + \frac{2\beta}{\alpha} w_1 - \frac{\beta}{\alpha^2} w_1^2 + O(w_1^3) \tag{9.104}$$

$$F_2(w_2, \beta) = \beta + \frac{2\beta}{\alpha} w_2 + \frac{\beta}{\alpha^2} w_2^2 + O(w_2^3) \tag{9.105}$$

for $0 \le \beta \le \frac{1}{2\tilde{\lambda}}$, and

$$F_1(w_1, \beta) = -\beta + \frac{4\tilde{\lambda}(1+\beta^2)}{\alpha(4\tilde{\lambda}^2+1)} w_1 - \frac{16\tilde{\lambda}^2(1+\beta^2)(\beta + \tilde{\lambda} f(\beta))}{\alpha^2(4\tilde{\lambda}^2+1)^2} w_1^2 + O(w_1^3) \tag{9.106}$$

$$F_2(w_2, \beta) = \beta + \frac{4\tilde{\lambda}(1+\beta^2)}{\alpha(4\tilde{\lambda}^2+1)} w_2 + \frac{16\tilde{\lambda}^2(1+\beta^2)(\beta + \tilde{\lambda} f(\beta))}{\alpha^2(4\tilde{\lambda}^2+1)^2} w_2^2 + O(w_2^3) \tag{9.107}$$

for $\frac{1}{2\tilde{\lambda}} \le \beta \le 1$.

The evaluation of g_ψ given in (9.103) involves simplifying the right hand side using the bc OPE, the explicit form of the local coordinates given above, and using (9.2) and (9.27) to calculate the correlator. Using $K_1 = \frac{\mathrm{i}b}{2\pi Q}$, we find

$$g_\psi = \frac{\tilde{\lambda}}{4\pi} + \frac{2\tilde{\lambda}^2}{\pi} \int_{(2\tilde{\lambda})^{-1}}^{1} \mathrm{d}\beta\, \frac{f(\beta)^2}{1+\beta^2}\,. \tag{9.108}$$

The first term is the contribution from the Feynman diagram in figure 9.4(a), and the second term is the contribution from the Feynman diagram in figure 9.4(b).

Normalization of the ψ exchange contribution

Our goal in this subsection is to compute the normalization constant appearing in (9.103).

The strategy to determine K_1 is to compute the Feynman diagram in figure 9.4(b), but with the tachyon running in the loop instead of the ψ field, and compare the result with (9.98). Recall that figure 9.4(b) corresponds to $\frac{1}{2\tilde{\lambda}} \le \beta \le 1$, in which the two open string punctures are not close to each other. Evaluating the Feynman diagram in figure 9.4(b) with the tachyon in the open string loop requires evaluating the right hand side of (9.103) with two c operators instead of the two $\mathrm{i}\partial c$ operators. The propagator of the tachyon field equals -1 in our normalization as opposed to $1/2$ for the ψ propagator. This yields

$$g^{(c)} = 2\,K_1 \int_{(2\tilde{\lambda})^{-1}}^{1} \mathrm{d}\beta \sum_{a=1}^{2} \oint_a \frac{\mathrm{d}z}{2\pi\mathrm{i}} \frac{\partial F_a}{\partial\beta} \langle b(z) F_1 \circ c(0)\, F_2 \circ c(0)\, c\bar{c} V(\mathrm{i})\rangle_{\mathrm{UHP}} \tag{9.109}$$

$$= 2\,K_1\, \frac{\mathrm{i}Q}{b}\, \alpha^2 \tilde{\lambda}^2 \left(1 + \frac{1}{4\tilde{\lambda}^2}\right)^2 \int_{(2\tilde{\lambda})^{-1}}^{1} \frac{\mathrm{d}\beta}{1+\beta^2}\,. \tag{9.110}$$

To get to the second line, we used the bc OPE, the explicit form of F_a given in (9.106), (9.107), and the correlators (9.2), (9.27). Comparing (9.110) to the first expression in the second line of (9.98), we find

$$K_1 = \frac{\mathrm{i}b}{2\pi Q}\,. \tag{9.111}$$

We can find the same result if we study the figure 9.4(a) with the tachyon running in the loop and comparing the result to (9.99).

Gauge parameter redefinition

Finally, we also need to take into account the relation between the string field theory gauge transformation parameter θ appearing in (9.24) and the rigid $U(1)$ transformation parameter $\widetilde{\theta}$ under which an open string with one end on the instanton picks up a phase $e^{\mathrm{i}\widetilde{\theta}}$. The gauge transformation parameter θ is the one that multiplies the vacuum state $\mathrm{i}|0\rangle$. Once this relation is found, we can evaluate the denominator of (9.24) using the fact that $\widetilde{\theta}$ has period 2π.

In order to study the gauge transformation properties, it is useful to introduce a spectator instanton. A fundamental property of the BV formalism is that the gauge transformation laws are encoded in the coupling terms in the master action. Let ξ be the field that multiplies the vacuum $|0\rangle$ in the expansion of the string field with Chan-Paton factor $\begin{pmatrix} 0 & 1 \\ 0 & 0 \end{pmatrix}$. Its conjugate anti-field ξ^* has the vertex operator $c\partial c\partial^2 c/2$ and carries the Chan-Paton factor $\begin{pmatrix} 0 & 0 \\ 1 & 0 \end{pmatrix}$. Let ψ_2 be the field that multiplies the vacuum $i|0\rangle$ but with Chan-Paton factor

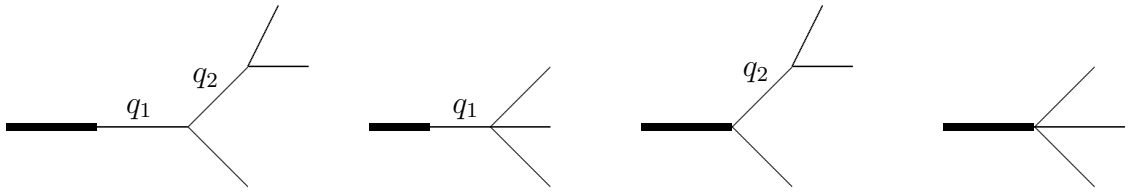

Figure 9.5: The four Feynman diagrams that contribute to the C-O-O-O amplitude. This is needed to evaluate the field-dependent relationship between the string field theory gauge parameter and the rigid gauge parameter that rotates the phase of an open string field with one end on the instanton. Figure adapted from [307].

$\begin{pmatrix} 1 & 0 \\ 0 & 0 \end{pmatrix}$. Computing the trilinear coupling of ξ-$\xi^\star$-ψ_2 using the correlator (9.2), we find the following term in the SFT path integral [307, 257]:

$$\exp(\mathrm{i}\, g_o\, \xi\xi^\star\psi_2)\,. \tag{9.112}$$

This coupling determines the infinitesimal gauge transformation of ξ to be $\delta\xi = \mathrm{i}g_o\theta\xi$ and, in turn, gives the relationship between θ and $\widetilde{\theta}$ to be $\mathrm{d}\theta = g_o^{-1}\mathrm{d}\widetilde{\theta}$. This is needed for a precise computation of the one-loop normalization factor (the exponential of the empty annulus) that accompanies D-instanton amplitudes [257].

However, we are working at the first sub-leading order in g_s, and the relation between θ and $\widetilde{\theta}$ could receive corrections that are, in general, field-dependent. Let Φ be the tachyon field that multiplies the cosmological constant operator V in the expansion of the string field, and let $\mathrm{i}\mathcal{A}$ be the C-O-O-O disk amplitude with the closed string insertion being Φ and the three open string insertions being ξ, $\xi^\star$ and ψ_2. Following [307], we note that this leads to the following field-dependent relationship between θ and $\widetilde{\theta}$:

$$\mathrm{d}\widetilde{\theta} = g_o\,(1+\mathcal{A}\Phi)\,\mathrm{d}\theta\,. \tag{9.113}$$

Substituting this in the denominator of (9.24), and writing $(1+\mathcal{A}\Phi) \approx e^{\mathcal{A}\Phi}$, we see that the path integral contains the extra term $\exp(\mathcal{A}\Phi)$. This leads to an additional contribution to the one-point function of Φ proportional to $\mathcal{A}$. Since this is of the same order as the annulus one-point function, after dividing it by the disk one-point function and g_s, we can interpret this as an additive contribution to g proportional to $\mathcal{A}$, which we call $g_{\rm ghost}$.

So, now we turn our attention to the computation of $g_{\rm ghost}$. The upper half plane C-O-O-O amplitude has two real moduli. We insert the cosmological constant operator at $z = \mathrm{i}$, and the three open string vertex operators I, $\frac{1}{2}c\partial c\partial^2 c$, I are inserted at z_1, z_2 and z_3, respectively. We only consider one cyclic ordering of I, $\frac{1}{2}c\partial c\partial^2 c$, I, which is the order in which we just wrote them. The other cyclic ordering vanishes due to the trace over the Chan-Paton factors.

Up to permutations of the external legs, there are four Feynman diagrams contributing to this amplitude; they are shown in figure 9.5.

Let β_1 and β_2 be the coordinates on the moduli space, and denote $\vec{\beta} = (\beta_1, \beta_2)$. This means that the locations z_1, z_2, z_3 of the open string punctures are functions of $\vec{\beta}$. Let the local coordinates w_1, w_2, w_3 around the three punctures be related to the UHP coordinate z via

$$z = F_a(w_a, \vec{\beta}) = f_a(\vec{\beta}) + g_a(\vec{\beta}) w_a + \frac{1}{2} h_a(\vec{\beta}) w_a^2 + O(w_a^3)\,. \tag{9.114}$$

Then, by the general rules of [322, 323, 324], we have

$$\begin{aligned} g_{\text{ghost}} = K_3 \int \mathrm{d}\beta_1 \wedge \mathrm{d}\beta_2 \Bigg\langle & \left\{ \sum_{a=1}^{3} \oint \frac{\mathrm{d}z}{2\pi \mathrm{i}} \frac{\partial F_a}{\partial \beta_1} b(z) \right\} \\ & \times \left\{ \sum_{a=1}^{3} \oint \frac{\mathrm{d}z}{2\pi \mathrm{i}} \frac{\partial F_a}{\partial \beta_2} b(z) \right\} \left\{ \frac{1}{2} c\partial c \partial^2 c(z_2) \right\} c\bar{c}V(\mathrm{i}) \Bigg\rangle\,, \end{aligned} \tag{9.115}$$

where we used the fact that all three open string insertions, being dimension zero primaries, are unaffected by the conformal transformations F_a. The constant K_3 is a constant of proportionality that will be explicitly computed in the next subsection but the result is $K_3 = -\frac{\mathrm{i}b}{\pi Q}$.[9] Using (9.115) together with (9.114), the bc OPE, and equations (9.27), (9.2), one finds

$$g_{\text{ghost}} = -\frac{1}{4\pi} \int \left[(1+f_2^2) g_2^{-3} \mathrm{d}h_2 \wedge \mathrm{d}g_2 - 2 f_2 g_2^{-2} \mathrm{d}h_2 \wedge \mathrm{d}f_2 + (2 f_2 h_2 g_2^{-3} + 2 g_2^{-1}) \mathrm{d}g_2 \wedge \mathrm{d}f_2 \right]\,. \tag{9.116}$$

Note that only (f_2, g_2, h_2) appear in the above expression since the insertions at z_1 and z_3 are the identity operator.

Next, we note that the two-form that appears in (9.116) is exact, and so g_{ghost} can be written as

$$g_{\text{ghost}} = -\frac{1}{2\pi} \int \mathrm{d}J \tag{9.117}$$

$$J := -f_2 g_2^{-1} \mathrm{d}g_2 - \frac{1}{2}(1+f_2^2) h_2 g_2^{-3} \mathrm{d}g_2 + \frac{1}{2}(1+f_2^2) g_2^{-2} \mathrm{d}h_2 + \mathrm{d}f_2 - \frac{2}{1+f_2^2}\, \mathrm{d}f_2\,. \tag{9.118}$$

The final two terms vanish when we compute $\mathrm{d}J$, but they are necessary. The $\mathrm{d}f_2$ term has been chosen so that J is invariant under the $\mathrm{PSL}(2,\mathbb{R})$ transformation $z \to \frac{z-c}{1+cz}$ that keeps the closed string puncture at the point $z = \mathrm{i}$ fixed but moves the three open string

[9] Integration over β_1 and β_2 includes integration over the Schwinger parameters of all the propagators appearing in figure 9.5, so unlike in the case of K_1 appearing in (9.103), we do not need to include any propagator factors in the definition of K_3.

punctures. This ensures that there are no special contributions from the region of moduli where the open string punctures go to infinity along the real axis. The final term in (9.118) is $\mathrm{PSL}(2,\mathbb{R})$ invariant by itself and has been chosen so that the contraction of J with the vector $(\delta f_2, \delta g_2, \delta h_2) = (1+f_2^2, 2f_2g_2, 2g_2^2+2f_2h_2)$ that generates the above $\mathrm{PSL}(2,\mathbb{R})$ transformation vanishes. This final term was missing in the analysis of [307]. Without this term J will not be a well-defined one-form in the two-dimensional moduli space parametrized by β_1, β_2, and we cannot apply Stokes's theorem to evaluate the right hand side of (9.117) as a boundary term.

Let us elaborate a bit more about this point. One could fix the $\mathrm{PSL}(2,\mathbb{R})$ transformation above by working with local coordinates such that, say, $f_2 = 0$. We can do this by making the transformation $\widetilde{z} = \frac{z-f_2}{1+f_2 z}$. Applying this transformation to (9.114), we find the new local coordinate around the second puncture to be

$$\widetilde{z} = \frac{g_2}{1+f_2^2}\, w_2 + \frac{1}{2}\frac{h_2 + h_2 f_2^2 - 2 f_2 g_2^2}{(1+f_2^2)^2}\, w_2^2 + O(w_2^3) =: \widetilde{g}_2\, w_2 + \frac{1}{2}\widetilde{h}_2\, w_2^2 + O(w_2^3)\,, \qquad (9.119)$$

where the last equality serves to define the quantities $\widetilde{g}_2$ and $\widetilde{h}_2$. In this 'gauge', both the terms proportional to $\mathrm{d}\widetilde{f}_2$ in (9.118) drop out and one gets $J = -\frac{1}{2}\widetilde{h}_2\widetilde{g}_2^{-3}\mathrm{d}\widetilde{g}_2 + \frac{1}{2}\widetilde{g}_2^{-2}\mathrm{d}\widetilde{h}_2$. Now, using the definitions of $\widetilde{g}_2$ and $\widetilde{h}_2$ from (9.119), we can transform back to the (f_2, g_2, h_2) variables, and one finds (9.118).

The benefit of using (9.118) is that since all the open string punctures are treated in the same way, the three different orderings of the open string punctures on the real line (preserving the cyclic ordering) that need to be summed can be obtained by a simple permutation of the labels. We have checked that using the gauge-fixed form of J and summing over the three orderings gives the same final answer.

Normalization of the C-O-O-O amplitude

In this appendix, we determine the normalization constant K_3 appearing in (9.115). Our strategy to determine K_3 is to study the Feynman diagram in figure 9.5(c), but with all three open string insertions being the tachyon field, with Chan-Paton factors kept the same as in the previous subsection. The consistency condition between two different ways of computing this diagram will yield the value of K_3. Let us denote the amplitude computed using (9.115) with all the external states taken as c by $\widetilde{A}$, and let $\widetilde{A}_c$ denote the contribution to this amplitude from figure 9.5(c) (with just one of the three possible assignments of the external operators to the external legs).

First, note that figure 9.5(c) with the internal propagator also being the tachyon, is the product of three factors: the C-O-O amplitude (with the closed string puncture being V and the two open string punctures being tachyons), the tachyon propagator, and the O-O-O three tachyon amplitude. The product of the C-O-O amplitude and the tachyon propagator

appears also in figure 9.2(c) and is given by (9.98).[10] The O-O-O tachyon vertex can be computed using the local coordinates in (9.81) and the ghost correlator in (9.2) to be α^3. So we find

$$\widetilde{A}_c = -\frac{1}{\pi}\,\tilde{\lambda}^2\alpha^5\left(1+\frac{1}{4\tilde{\lambda}^2}\right)^2\int_{(2\tilde{\lambda})^{-1}}^{1}\frac{\mathrm{d}\beta}{1+\beta^2}\,. \tag{9.120}$$

The second way of computing this amplitude is to start with the expression analogous to (9.115). Using $F_a\circ c(0) = g_a^{-1}c(z_a)$, we get the following expression:

$$\begin{aligned}\widetilde{A} = K_3\int \mathrm{d}\beta_1\wedge\mathrm{d}\beta_2\Bigg\langle &\left\{\sum_{a=1}^{3}\oint\frac{\mathrm{d}z}{2\pi\mathrm{i}}\frac{\partial F_a}{\partial\beta_1}b(z)\right\}\left\{\sum_{a=1}^{3}\oint\frac{\mathrm{d}z}{2\pi\mathrm{i}}\frac{\partial F_a}{\partial\beta_2}b(z)\right\}\\ &\times(g_1g_2g_3)^{-1}c(z_1)c(z_2)c(z_3)\,c\bar{c}V(\mathrm{i})\Bigg\rangle\\ = -\frac{\mathrm{i}Q}{2b}K_3\int(g_1g_2g_3)^{-1}&[(1+f_3^2)\,\mathrm{d}f_2\wedge\mathrm{d}f_1+(1+f_1^2)\,\mathrm{d}f_3\wedge\mathrm{d}f_2+(1+f_2^2)\,\mathrm{d}f_1\wedge\mathrm{d}f_3]\,.\end{aligned} \tag{9.121}$$

We used the bc OPE and equations (9.2), (9.27), (9.114) to get to the second line. Let us use this expression to evaluate $\widetilde{A}_c$. Using the explicit form of f_a, g_a and h_a suitable for the region corresponding to figure 9.5(c) given in equation (D.24) of [307], we find

$$\widetilde{A}_c = \frac{\mathrm{i}Q}{2b}K_3\cdot 2\tilde{\lambda}^2\alpha^5\left(1+\frac{1}{4\tilde{\lambda}^2}\right)^2\int_{(2\tilde{\lambda})^{-1}}^{1}\frac{\mathrm{d}\beta}{1+\beta^2}\int_0^1\frac{\mathrm{d}q_2}{q_2^2} \tag{9.122}$$

$$\to -\frac{\mathrm{i}Q}{b}K_3\,\tilde{\lambda}^2\alpha^5\left(1+\frac{1}{4\tilde{\lambda}^2}\right)^2\int_{(2\tilde{\lambda})^{-1}}^{1}\frac{\mathrm{d}\beta}{1+\beta^2}\,, \tag{9.123}$$

where we used the replacement rule $\int_0^1\frac{\mathrm{d}q_2}{q_2^2}\to -1$ for the plumbing fixture variable q_2 appearing in the internal propagator in figure 9.5(c).

Comparing (9.120) and (9.123) we get

$$K_3 = -\frac{\mathrm{i}b}{\pi Q}\,. \tag{9.124}$$

The C-O-O-O amplitude contribution

We now turn to the computation of the four Feynman diagrams in figure 9.5. The corresponding regions in moduli space are shown in figure 9.6. Except for the overall normalization and

[10] Note that (9.98) includes division by g_s and the disk one point function; so the normalization of the amplitude determined this way directly yields the contribution to g.

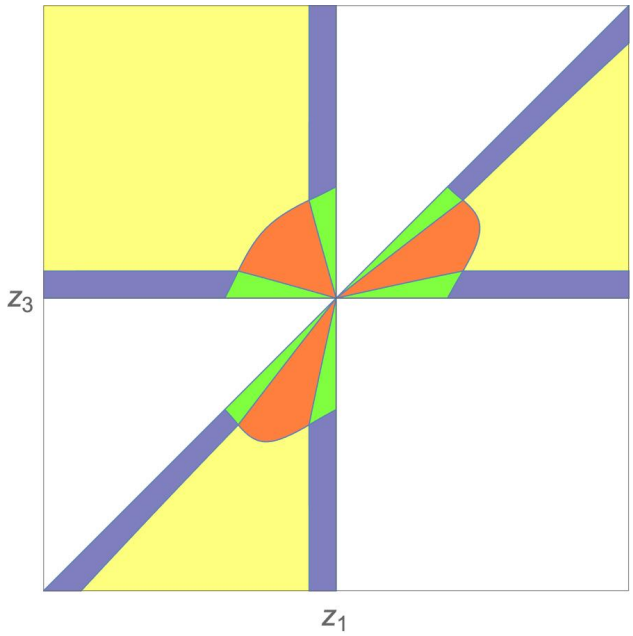

Figure 9.6: The regions of moduli space of the C-O-O-O amplitude (with a fixed cyclic ordering) corresponding to the four Feynman diagrams in figure 9.5. For this figure, we have set the location of the second puncture $z_2 = 0$. The green region corresponds to figure 9.5(a), the red region to figure 9.5(b), the blue region to figure 9.5(c), and the bulk of the moduli space, shown in yellow, corresponds to figure 9.5(d). The chosen cyclic ordering $(z_1, 0, z_3)$ gives rise to three linear orderings, namely, $z_1 \leq 0 \leq z_3$, $0 \leq z_3 \leq z_1$ and $z_3 \leq z_1 \leq 0$, which can be clearly identified. The same color is used to label different regions of the moduli space related by cyclic permutation of external open string states.

the last term in (9.118), the analysis is identical to that in appendix D of [307]. Therefore we shall be brief.

The Feynman diagrams in figure 9.5(a) and 9.5(c) vanish. This is because, given the choice of the three open string vertex operators, neither the tachyon nor the out-of-Siegel gauge mode ψ can propagate along the propagator labeled by q_2 in figure 9.5. The propagation of other $L_0 = 0$ Siegel gauge states are prevented by the replacement rule (9.91), and contributions from the $L_0 > 0$ states are suppressed in the limit of large λ and α.

Since the integrand in (9.117) is a total derivative, we can evaluate the Feynman diagram corresponding to the bulk of moduli space, i.e. figure 9.5(d), via Stokes's theorem. This region shares one boundary with the region corresponding to figure 9.5(b) (the yellow-red boundary in figure 9.6), and one boundary with the region corresponding to figure 9.5(c) (the yellow-blue boundary in figure 9.6). Let us denote these two contributions as $g_{\rm ghost}^{(b)\text{-}(d)}$ and $g_{\rm ghost}^{(c)\text{-}(d)}$, respectively.

Next, we observe that [307]

$$g_{\rm ghost}^{(b)\text{-}(d)} + g_{\rm ghost}^{(b)} = 0\,. \tag{9.125}$$

This is because if we denote the relevant part of the $\int \mathrm{d}J$ in region (b) as $\int q_1^{-2}\mathrm{d}q_1 \wedge f(\tau)\mathrm{d}\tau$, where τ is the modular parameter in the O-O-O-O vertex, then our choice of J gives $\int J = \int f(\tau)\mathrm{d}\tau$ from the (b)-(d) boundary.[11] Evaluating the contribution from figure 9.5(b) using the replacement rule (9.91), we get $-\int \mathrm{d}\tau f(\tau)$, which cancels the contribution of $\int J$ from the (b)-(d) boundary. This is similar to the cancellations we saw when we computed the worldsheet contribution.

Thus the only contribution to $g_{\rm ghost}$ comes from $g_{\rm ghost}^{(c)\text{-}(d)}$. This is the boundary between the yellow and blue regions of figure 9.6, which consists of six segments. Each of these six segments lies at $q_2 = 1$ and can be parametrized by the quantity β that appears in the definition of the C-O-O vertex in the range $\frac{1}{2\tilde\lambda} \le \beta \le 1$. Explicit expressions for f_2, g_2 and h_2 for each segment can be found in equations (D.24)-(D.26) of [307]. Apart from the normalization constant discussed above, the only change compared to [307] is due to the final term $-\frac{2\mathrm{d}f_2}{1+f_2^2}$ in the one-form J (9.118). This term precisely cancels the $O(1)$ contribution to $g_{\rm ghost}$ in [307]. The conclusion is that

$$g_{\rm ghost} = g_{\rm ghost}^{(c)\text{-}(d)} = -\frac{1}{\pi}\cdot\tilde\lambda\int_{(2\tilde\lambda)^{-1}}^{1}\mathrm{d}\beta\, f'(\beta) = \frac{\tilde\lambda}{2\pi}\,. \tag{9.126}$$

We have added together the contribution from the six boundary segments and used (9.83) to get to the final expression.

For comparison, note that the result of [307] was $g_{\rm ghost} = \frac{\tilde\lambda}{2\pi} - \frac{1}{2}$. With the modification to J that we have discussed, the function $g(\omega)$ computed in [307] will have an extra contribution $+\frac{1}{2}$. This precisely resolves the mismatch with the matrix model results of [25, 310].

Final result and remarks

Adding together the worldsheet contribution (9.101), the ψ-exchange contribution (9.108), and the contribution (9.126), we find

$$g = g_{\rm ws} + g_\psi + g_{\rm ghost} = \frac{1}{2}\,, \tag{9.127}$$

in perfect agreement with the general prediction (9.40).

As already mentioned, if we use the corrected form of J in (9.118) for the computation in [307] of the annulus one-point function in $c = 1$ string theory, we also find a perfect match

[11] This was verified in [307] for the choice of J in which the last term in (9.118) was absent. We have checked that the extra term does not affect the result. This is a consequence of the fact that, for figure 9.5(b), all the open string vertex operators remain close to the origin of the UHP, and hence the change in f_2 along the (b)-(d) boundary is small for large $\widetilde\lambda$ and α.

with the results of Balthazar, Rodriguez, and Yin [25, 310]. In the notation of [307], this would mean that $A_g = 0$.

We conclude this article with a remark about the quantity $C = \widetilde{C}$ in (9.37), which represents $O(g_s)$ corrections to the instanton action. Corrections to this order have been computed in one-matrix integrals [282, 283]. It would be interesting to compute this quantity directly from the worldsheet of the $(2, p)$ minimal string and check that it agrees with the prediction from the dual one-matrix integral. The main technical challenge seems to be that the moduli spaces of the relevant Riemann surfaces, the disk with a handle, and the three-holed sphere, are three-dimensional, which is one higher than the ones that we have analyzed.

Bibliography

[1] Stephen Hawking. "Breakdown of Predictability in Gravitational Collapse". In: *Phys. Rev. D* 14 (1976), pp. 2460–2473. DOI: 10.1103/PhysRevD.14.2460.

[2] Ahmed Almheiri et al. "Black Holes: Complementarity or Firewalls?" In: *JHEP* 02 (2013), p. 062. DOI: 10.1007/JHEP02(2013)062. arXiv: 1207.3123 [hep-th].

[3] Ahmed Almheiri, Xi Dong, and Daniel Harlow. "Bulk locality and quantum error correction in AdS/CFT". In: *JHEP* 04 (2015), p. 163. DOI: 10.1007/JHEP04(2015)163. arXiv: 1411.7041 [hep-th].

[4] Gerard 't Hooft. "Dimensional reduction in quantum gravity". In: *Conf. Proc. C* 930308 (1993), pp. 284–296. arXiv: gr-qc/9310026.

[5] Leonard Susskind. "The World as a hologram". In: *J. Math. Phys.* 36 (1995), pp. 6377–6396. DOI: 10.1063/1.531249. arXiv: hep-th/9409089.

[6] Juan Maldacena. "The Large N limit of superconformal field theories and supergravity". In: *Int. J. Theor. Phys.* 38 (1999). [Adv. Theor. Math. Phys. 2, 231 (1998)], pp. 1113–1133. DOI: 10.1023/A:1026654312961,10.4310/ATMP.1998.v2.n2.a1. arXiv: hep-th/9711200 [hep-th].

[7] Edward Witten. "Anti-de Sitter space and holography". In: *Adv. Theor. Math. Phys.* 2 (1998), pp. 253–291. DOI: 10.4310/ATMP.1998.v2.n2.a2. arXiv: hep-th/9802150 [hep-th].

[8] Steven Gubser, Igor Klebanov, and Alexander Polyakov. "Gauge theory correlators from noncritical string theory". In: *Phys. Lett.* B428 (1998), pp. 105–114. DOI: 10.1016/S0370-2693(98)00377-3. arXiv: hep-th/9802109 [hep-th].

[9] Shinsei Ryu and Tadashi Takayanagi. "Holographic derivation of entanglement entropy from AdS/CFT". In: *Phys. Rev. Lett.* 96 (2006), p. 181602. DOI: 10.1103/PhysRevLett.96.181602. arXiv: hep-th/0603001 [hep-th].

[10] Shinsei Ryu and Tadashi Takayanagi. "Aspects of Holographic Entanglement Entropy". In: *JHEP* 08 (2006), p. 045. DOI: 10.1088/1126-6708/2006/08/045. arXiv: hep-th/0605073 [hep-th].

[11] Veronika Hubeny, Mukund Rangamani, and Tadashi Takayanagi. "A Covariant holographic entanglement entropy proposal". In: *JHEP* 07 (2007), p. 062. DOI: 10.1088/1126-6708/2007/07/062. arXiv: 0705.0016 [hep-th].

[12] Thomas Faulkner, Aitor Lewkowycz, and Juan Maldacena. "Quantum corrections to holographic entanglement entropy". In: *JHEP* 11 (2013), p. 074. DOI: 10.1007/JHEP11(2013)074. arXiv: 1307.2892 [hep-th].

[13] Netta Engelhardt and Aron C. Wall. "Quantum Extremal Surfaces: Holographic Entanglement Entropy beyond the Classical Regime". In: *JHEP* 01 (2015), p. 073. DOI: 10.1007/JHEP01(2015)073. arXiv: 1408.3203 [hep-th].

[14] Daniel Jafferis et al. "Relative entropy equals bulk relative entropy". In: *JHEP* 06 (2016), p. 004. DOI: 10.1007/JHEP06(2016)004. arXiv: 1512.06431 [hep-th].

[15] Xi Dong, Daniel Harlow, and Aron C. Wall. "Reconstruction of bulk operators within the entanglement wedge in gauge-gravity duality". In: *Phys. Rev. Lett.* 117.2 (2016), p. 021601. DOI: 10.1103/PhysRevLett.117.021601. arXiv: 1601.05416 [hep-th].

[16] Geoffrey Penington. "Entanglement Wedge Reconstruction and the Information Paradox". In: (2019). arXiv: 1905.08255 [hep-th].

[17] Ahmed Almheiri et al. "The entropy of bulk quantum fields and the entanglement wedge of an evaporating black hole". In: *JHEP* 12 (2019), p. 063. DOI: 10.1007/JHEP12(2019)063. arXiv: 1905.08762 [hep-th].

[18] Chitraang Murdia et al. "Comments on holographic entanglement entropy in TT deformed conformal field theories". In: *Phys. Rev.* D100.2 (2019), p. 026011. DOI: 10.1103/PhysRevD.100.026011. arXiv: 1904.04408 [hep-th].

[19] Chitraang Murdia, Yasunori Nomura, and Pratik Rath. "Coarse-Graining Holographic States: A Semiclassical Flow in General Spacetimes". In: *Phys. Rev. D* 102.8 (2020), p. 086001. DOI: 10.1103/PhysRevD.102.086001. arXiv: 2008.01755 [hep-th].

[20] Masamichi Miyaji and Chitraang Murdia. "Holographic BCFT with a Defect on the End-of-the-World brane". In: *JHEP* 11 (2022), p. 123. DOI: 10.1007/JHEP11(2022)123. arXiv: 2208.13783 [hep-th].

[21] Kevin Langhoff, Chitraang Murdia, and Yasunori Nomura. "The Multiverse in an Inverted Island". In: (June 2021). arXiv: 2106.05271 [hep-th].

[22] Jorrit Kruthoff, Raghu Mahajan, and Chitraang Murdia. "Free fermion entanglement with a semitransparent interface: the effect of graybody factors on entanglement islands". In: *SciPost Phys.* 11 (2021), p. 063. DOI: 10.21468/SciPostPhys.11.3.063. arXiv: 2106.10287 [hep-th].

[23] Dan Stefan Eniceicu et al. "Normalization of ZZ instanton amplitudes in minimal string theory". In: (Feb. 2022). arXiv: 2202.03448 [hep-th].

[24] Dan Stefan Eniceicu et al. "Multi-instantons in minimal string theory and in matrix integrals". In: *JHEP* 10 (2022), p. 065. DOI: 10.1007/JHEP10(2022)065. arXiv: 2206.13531 [hep-th].

[25] Bruno Balthazar, Victor A. Rodriguez, and Xi Yin. "ZZ instantons and the non-perturbative dual of c = 1 string theory". In: *JHEP* 05 (2023), p. 048. DOI: 10.1007/JHEP05(2023)048. arXiv: 1907.07688 [hep-th].

[26] Ashoke Sen. "Fixing an Ambiguity in Two Dimensional String Theory Using String Field Theory". In: *JHEP* 03 (2020), p. 005. DOI: 10.1007/JHEP03(2020)005. arXiv: 1908.02782 [hep-th].

[27] Dan Stefan Eniceicu et al. "The ZZ annulus one-point function in non-critical string theory: A string field theory analysis". In: *JHEP* 12 (2022), p. 151. DOI: 10.1007/JHEP12(2022)151. arXiv: 2210.11473 [hep-th].

[28] Lauren McGough, Márk Mezei, and Herman Verlinde. "Moving the CFT into the bulk with $T\overline{T}$". In: *JHEP* 04 (2018), p. 010. DOI: 10.1007/JHEP04(2018)010. arXiv: 1611.03470 [hep-th].

[29] Marika Taylor. "TT deformations in general dimensions". In: (). arXiv: 1805.10287 [hep-th].

[30] Thomas Hartman et al. "Holography at finite cutoff with a T^2 deformation". In: *JHEP* 03 (2019), p. 004. DOI: 10.1007/JHEP03(2019)004. arXiv: 1807.11401 [hep-th].

[31] Aitor Lewkowycz and Juan Maldacena. "Generalized gravitational entropy". In: *JHEP* 08 (2013), p. 090. DOI: 10.1007/JHEP08(2013)090. arXiv: 1304.4926 [hep-th].

[32] Soumangsu Chakraborty et al. "Entanglement beyond AdS". In: *Nucl. Phys.* B935 (2018), pp. 290–309. DOI: 10.1016/j.nuclphysb.2018.08.011. arXiv: 1805.06286 [hep-th].

[33] William Donnelly and Vasudev Shyam. "Entanglement entropy and $T\overline{T}$ deformation". In: *Phys. Rev. Lett.* 121.13 (2018), p. 131602. DOI: 10.1103/PhysRevLett.121.131602. arXiv: 1806.07444 [hep-th].

[34] Bin Chen, Lin Chen, and Peng-Xiang Hao. "Entanglement Entropy in $T\overline{T}$-Deformed CFT". In: (). arXiv: 1807.08293 [hep-th].

[35] Victor Gorbenko, Eva Silverstein, and Gonzalo Torroba. "dS/dS and $T\overline{T}$". In: *JHEP* 03 (2019), p. 085. DOI: 10.1007/JHEP03(2019)085. arXiv: 1811.07965 [hep-th].

[36] Chanyong Park. "Holographic Entanglement Entropy in Cutoff AdS". In: *Int. J. Mod. Phys.* A33.36 (2019), p. 1850226. DOI: 10.1142/S0217751X18502263. arXiv: 1812.00545 [hep-th].

[37] Pawel Caputa, Shouvik Datta, and Vasudev Shyam. "Sphere partition functions & cut-off AdS". In: *JHEP* 05 (2019), p. 112. DOI: 10.1007/JHEP05(2019)112. arXiv: 1902.10893 [hep-th].

[38] Aritra Banerjee, Arpan Bhattacharyya, and Soumangsu Chakraborty. "Entanglement Entropy for TT deformed CFT in general dimensions". In: *Nucl. Phys.* B948 (2019), p. 114775. DOI: 10.1016/j.nuclphysb.2019.114775. arXiv: 1904.00716 [hep-th].

[39] Zohar Komargodski. "Aspects of renormalization group flows". In: *Lecture Notes of the Les Houches Summer School, Session XCVII, Oxford university Press* (2015). p. 255.

[40] Ling-Yan Hung, Robert C. Myers, and Michael Smolkin. "Some Calculable Contributions to Holographic Entanglement Entropy". In: *JHEP* 08 (2011), p. 039. DOI: 10.1007/JHEP08(2011)039. arXiv: 1105.6055 [hep-th].

[41] Hong Liu and Mark Mezei. "A Refinement of entanglement entropy and the number of degrees of freedom". In: *JHEP* 04 (2013), p. 162. DOI: 10.1007/JHEP04(2013)162. arXiv: 1202.2070 [hep-th].

[42] Marika Taylor and William Woodhead. "Renormalized entanglement entropy". In: *JHEP* 08 (2016), p. 165. DOI: 10.1007/JHEP08(2016)165. arXiv: 1604.06808 [hep-th].

[43] J. David Brown and James W. York Jr. "Quasilocal energy and conserved charges derived from the gravitational action". In: *Phys. Rev.* D47 (1993), pp. 1407–1419. DOI: 10.1103/PhysRevD.47.1407. arXiv: gr-qc/9209012 [gr-qc].

[44] Vijay Balasubramanian and Per Kraus. "A Stress tensor for Anti-de Sitter gravity". In: *Commun. Math. Phys.* 208 (1999), pp. 413–428. DOI: 10.1007/s002200050764. arXiv: hep-th/9902121 [hep-th].

[45] Kostas Skenderis. "Lecture notes on holographic renormalization". In: *Class. Quant. Grav.* 19 (2002), pp. 5849–5876. DOI: 10.1088/0264-9381/19/22/306. arXiv: hep-th/0209067 [hep-th].

[46] Joan Camps and William R. Kelly. "Generalized gravitational entropy without replica symmetry". In: *JHEP* 03 (2015), p. 061. DOI: 10.1007/JHEP03(2015)061. arXiv: 1412.4093 [hep-th].

[47] Xi Dong. "The Gravity Dual of Renyi Entropy". In: *Nature Commun.* 7 (2016), p. 12472. DOI: 10.1038/ncomms12472. arXiv: 1601.06788 [hep-th].

[48] Xi Dong. "Holographic Entanglement Entropy for General Higher Derivative Gravity". In: *JHEP* 01 (2014), p. 044. DOI: 10.1007/JHEP01(2014)044. arXiv: 1310.5713 [hep-th].

[49] Masamichi Miyaji and Tadashi Takayanagi. "Surface/State Correspondence as a Generalized Holography". In: *PTEP* 2015.7 (2015), 073B03. DOI: 10.1093/ptep/ptv089. arXiv: 1503.03542 [hep-th].

[50] Fabio Sanches and Sean J. Weinberg. "Holographic entanglement entropy conjecture for general spacetimes". In: *Phys. Rev.* D94.8 (2016), p. 084034. DOI: 10.1103/PhysRevD.94.084034. arXiv: 1603.05250 [hep-th].

[51] Yasunori Nomura et al. "Toward a Holographic Theory for General Spacetimes". In: *Phys. Rev.* D95.8 (2017), p. 086002. DOI: 10.1103/PhysRevD.95.086002. arXiv: 1611.02702 [hep-th].

[52] Yasunori Nomura, Pratik Rath, and Nico Salzetta. "Classical Spacetimes as Amplified Information in Holographic Quantum Theories". In: *Phys. Rev.* D97.10 (2018), p. 106025. DOI: 10.1103/PhysRevD.97.106025. arXiv: 1705.06283 [hep-th].

[53] Yasunori Nomura, Pratik Rath, and Nico Salzetta. "Spacetime from Unentanglement". In: *Phys. Rev.* D97.10 (2018), p. 106010. DOI: 10.1103/PhysRevD.97.106010. arXiv: 1711.05263 [hep-th].

[54] Yasunori Nomura, Pratik Rath, and Nico Salzetta. "Pulling the Boundary into the Bulk". In: *Phys. Rev.* D98.2 (2018), p. 026010. DOI: 10.1103/PhysRevD.98.026010. arXiv: 1805.00523 [hep-th].

[55] Leonard Susskind and Edward Witten. "The Holographic bound in anti-de Sitter space". In: (). arXiv: hep-th/9805114 [hep-th].

[56] Mark Van Raamsdonk. "Building up spacetime with quantum entanglement". In: *Gen. Rel. Grav.* 42 (2010), pp. 2323–2329. DOI: 10.1142/S0218271810018529. arXiv: 1005.3035 [hep-th].

[57] Brian Swingle. "Entanglement Renormalization and Holography". In: *Phys. Rev.* D86 (2012), p. 065007. DOI: 10.1103/PhysRevD.86.065007. arXiv: 0905.1317 [cond-mat.str-el].

[58] Bartlomiej Czech et al. "The Gravity Dual of a Density Matrix". In: *Class. Quant. Grav.* 29 (2012), p. 155009. DOI: 10.1088/0264-9381/29/15/155009. arXiv: 1204.1330 [hep-th].

[59] Aron C. Wall. "Maximin Surfaces, and the Strong Subadditivity of the Covariant Holographic Entanglement Entropy". In: *Class. Quant. Grav.* 31.22 (2014), p. 225007. DOI: 10.1088/0264-9381/31/22/225007. arXiv: 1211.3494 [hep-th].

[60] Matthew Headrick et al. "Causality & holographic entanglement entropy". In: *JHEP* 12 (2014), p. 162. DOI: 10.1007/JHEP12(2014)162. arXiv: 1408.6300 [hep-th].

[61] Jordan Cotler et al. "Entanglement Wedge Reconstruction via Universal Recovery Channels". In: *Phys. Rev.* X9.3 (2019), p. 031011. DOI: 10.1103/PhysRevX.9.031011. arXiv: 1704.05839 [hep-th].

[62] Masamichi Miyaji et al. "Continuous Multiscale Entanglement Renormalization Ansatz as Holographic Surface-State Correspondence". In: *Phys. Rev. Lett.* 115.17 (2015), p. 171602. DOI: 10.1103/PhysRevLett.115.171602. arXiv: 1506.01353 [hep-th].

[63] Mohsen Alishahiha et al. "The dS/dS correspondence". In: *AIP Conf. Proc.* 743.1 (2004). Ed. by R.E. Allen, Dimitri V. Nanopoulos, and C.N. Pope, pp. 393–409. DOI: 10.1063/1.1848341. arXiv: hep-th/0407125.

[64] Xi Dong et al. "FRW solutions and holography from uplifted AdS/CFT". In: *Phys. Rev. D* 85 (2012), p. 104035. DOI: 10.1103/PhysRevD.85.104035. arXiv: 1108.5732 [hep-th].

[65] Sam Leuven, Erik Verlinde, and Manus Visser. "Towards non-AdS Holography via the Long String Phenomenon". In: *JHEP* 06 (2018), p. 097. DOI: 10.1007/JHEP06(2018)097. arXiv: 1801.02589 [hep-th].

[66] Xi Dong, Eva Silverstein, and Gonzalo Torroba. "De Sitter Holography and Entanglement Entropy". In: *JHEP* 07 (2018), p. 050. DOI: 10.1007/JHEP07(2018)050. arXiv: 1804.08623 [hep-th].

[67] Sean Cooper et al. "Black Hole Microstate Cosmology". In: *JHEP* 07 (2019), p. 065. DOI: 10.1007/JHEP07(2019)065. arXiv: 1810.10601 [hep-th].

[68] Hao Geng. "Non-local Entanglement and Fast Scrambling in De-Sitter Holography". In: (Apr. 2020). arXiv: 2005.00021 [hep-th].

[69] Fernando Pastawski et al. "Holographic quantum error-correcting codes: Toy models for the bulk/boundary correspondence". In: *JHEP* 06 (2015), p. 149. DOI: 10.1007/JHEP06(2015)149. arXiv: 1503.06237 [hep-th].

[70] Patrick Hayden et al. "Holographic duality from random tensor networks". In: *JHEP* 11 (2016), p. 009. DOI: 10.1007/JHEP11(2016)009. arXiv: 1601.01694 [hep-th].

[71] William Donnelly et al. "Living on the Edge: A Toy Model for Holographic Reconstruction of Algebras with Centers". In: *JHEP* 04 (2017), p. 093. DOI: 10.1007/JHEP04(2017)093. arXiv: 1611.05841 [hep-th].

[72] Xiao-Liang Qi, Zhao Yang, and Yi-Zhuang You. "Holographic coherent states from random tensor networks". In: *JHEP* 08 (2017), p. 060. DOI: 10.1007/JHEP08(2017)060. arXiv: 1703.06533 [hep-th].

[73] Raphael Bousso et al. "Quantum focusing conjecture". In: *Phys. Rev.* D93.6 (2016), p. 064044. DOI: 10.1103/PhysRevD.93.064044. arXiv: 1506.02669 [hep-th].

[74] Raphael Bousso and Netta Engelhardt. "Generalized Second Law for Cosmology". In: *Phys. Rev.* D93.2 (2016), p. 024025. DOI: 10.1103/PhysRevD.93.024025. arXiv: 1510.02099 [hep-th].

[75] Aron C. Wall. "A Survey of Black Hole Thermodynamics". In: (2018). arXiv: 1804.10610 [gr-qc].

[76] Raphael Bousso, Venkatesa Chandrasekaran, and Arvin Shahbazi-Moghaddam. "From black hole entropy to energy-minimizing states in QFT". In: *Phys. Rev.* D101.4 (2020), p. 046001. DOI: 10.1103/PhysRevD.101.046001. arXiv: 1906.05299 [hep-th].

[77] Raphael Bousso, Arvin Shahbazi-Moghaddam, and Marija Tomasevic. "Quantum Penrose Inequality". In: *Phys. Rev. Lett.* 123.24 (2019), p. 241301. DOI: 10.1103/PhysRevLett.123.241301. arXiv: 1908.02755 [hep-th].

[78] Daniel Harlow. "The Ryu-Takayanagi formula from quantum error correction". In: *Commun. Math. Phys.* 354.3 (2017), pp. 865–912. DOI: 10.1007/s00220-017-2904-z. arXiv: 1607.03901 [hep-th].

[79] Chris Akers and Pratik Rath. "Holographic Renyi entropy from quantum error correction". In: *JHEP* 05 (2019), p. 052. DOI: 10.1007/JHEP05(2019)052. arXiv: 1811.05171 [hep-th].

[80] Xi Dong, Daniel Harlow, and Donald Marolf. "Flat entanglement spectra in fixed-area states of quantum gravity". In: *JHEP* 10 (2019), p. 240. DOI: 10.1007/JHEP10(2019)240. arXiv: 1811.05382 [hep-th].

[81] Raphael Bousso. "The Holographic principle". In: *Rev. Mod. Phys.* 74 (2002), pp. 825–874. DOI: 10.1103/RevModPhys.74.825. arXiv: hep-th/0203101.

[82] Matthew Headrick and Tadashi Takayanagi. "A Holographic proof of the strong subadditivity of entanglement entropy". In: *Phys. Rev.* D76 (2007), p. 106013. DOI: 10.1103/PhysRevD.76.106013. arXiv: 0704.3719 [hep-th].

[83] Patrick Hayden, Matthew Headrick, and Alexander Maloney. "Holographic Mutual Information is Monogamous". In: *Phys. Rev.* D87.4 (2013), p. 046003. DOI: 10.1103/PhysRevD.87.046003. arXiv: 1107.2940 [hep-th].

[84] Ning Bao et al. "The Holographic Entropy Cone". In: *JHEP* 09 (2015), p. 130. DOI: 10.1007/JHEP09(2015)130. arXiv: 1505.07839 [hep-th].

[85] Leonard Susskind and John Uglum. "Black hole entropy in canonical quantum gravity and superstring theory". In: *Phys. Rev.* D50 (1994), pp. 2700–2711. DOI: 10.1103/PhysRevD.50.2700. arXiv: hep-th/9401070 [hep-th].

[86] Sergey N. Solodukhin. "Entanglement entropy of black holes". In: *Living Rev. Rel.* 14 (2011), p. 8. DOI: 10.12942/lrr-2011-8. arXiv: 1104.3712 [hep-th].

[87] Chris Akers et al. "Quantum maximin surfaces". In: (2019). arXiv: 1912.02799 [hep-th].

[88] Ahmed Almheiri et al. "The Page curve of Hawking radiation from semiclassical geometry". In: (2019). arXiv: 1908.10996 [hep-th].

[89] Geoff Penington et al. "Replica wormholes and the black hole interior". In: (2019). arXiv: 1911.11977 [hep-th].

[90] Ahmed Almheiri et al. "Replica wormholes and the entropy of Hawking radiation". In: (2019). arXiv: 1911.12333 [hep-th].

[91] Aitor Lewkowycz et al. "$T\bar{T}$ and EE, with implications for (A)dS subregion encodings". In: (2019). arXiv: 1909.13808 [hep-th].

[92] Ning Bao et al. "Beyond Toy Models: Distilling Tensor Networks in Full AdS/CFT". In: *JHEP* 11 (2019), p. 069. DOI: 10.1007/JHEP11(2019)069. arXiv: 1812.01171 [hep-th].

[93] Ning Bao et al. "Holographic Tensor Networks in Full AdS/CFT". In: (2019). arXiv: 1902.10157 [hep-th].

[94] Tadashi Takayanagi and Koji Umemoto. "Entanglement of purification through holographic duality". In: *Nature Phys.* 14.6 (2018), pp. 573–577. DOI: 10.1038/s41567-018-0075-2. arXiv: 1708.09393 [hep-th].

[95] Phuc Nguyen et al. "Entanglement of purification: from spin chains to holography". In: *JHEP* 01 (2018), p. 098. DOI: 10.1007/JHEP01(2018)098. arXiv: 1709.07424 [hep-th].

[96] Souvik Dutta and Thomas Faulkner. "A canonical purification for the entanglement wedge cross-section". In: (2019). arXiv: 1905.00577 [hep-th].

[97] Thomas Hartman, Edgar Shaghoulian, and Andrew Strominger. "Islands in Asymptotically Flat 2D Gravity". In: *JHEP* 07 (2020), p. 022. DOI: 10.1007/JHEP07(2020)022. arXiv: 2004.13857 [hep-th].

[98] Thomas Hartman, Yikun Jiang, and Edgar Shaghoulian. "Islands in cosmology". In: (Aug. 2020). arXiv: 2008.01022 [hep-th].

[99] Yasunori Nomura. "Reanalyzing an Evaporating Black Hole". In: *Phys. Rev. D* 99.8 (2019), p. 086004. DOI: 10.1103/PhysRevD.99.086004. arXiv: 1810.09453 [hep-th].

[100] Yasunori Nomura. "Spacetime and Universal Soft Modes — Black Holes and Beyond". In: *Phys. Rev. D* 101.6 (2020), p. 066024. DOI: 10.1103/PhysRevD.101.066024. arXiv: 1908.05728 [hep-th].

[101] Yasunori Nomura. "The Interior of a Unitarily Evaporating Black Hole". In: *Phys. Rev. D* 102.2 (2020), p. 026001. DOI: 10.1103/PhysRevD.102.026001. arXiv: 1911.13120 [hep-th].

[102] Patrick Hayden and Geoffrey Penington. "Learning the Alpha-bits of Black Holes". In: *JHEP* 12 (2019), p. 007. DOI: 10.1007/JHEP12(2019)007. arXiv: 1807.06041 [hep-th].

[103] Chris Akers, Stefan Leichenauer, and Adam Levine. "Large breakdowns of entanglement wedge reconstruction". In: *Phys. Rev.* D100.12 (2019), p. 126006. DOI: 10.1103/PhysRevD.100.126006. arXiv: 1908.03975 [hep-th].

[104] Andreas Karch and Lisa Randall. "Open and closed string interpretation of SUSY CFT's on branes with boundaries". In: *JHEP* 06 (2001), p. 063. DOI: 10.1088/1126-6708/2001/06/063. arXiv: hep-th/0105132.

[105] Tadashi Takayanagi. "Holographic Dual of BCFT". In: *Phys. Rev. Lett.* 107 (2011), p. 101602. DOI: 10.1103/PhysRevLett.107.101602. arXiv: 1105.5165 [hep-th].

[106] Mitsutoshi Fujita, Tadashi Takayanagi, and Erik Tonni. "Aspects of AdS/BCFT". In: *JHEP* 11 (2011), p. 043. DOI: 10.1007/JHEP11(2011)043. arXiv: 1108.5152 [hep-th].

[107] John L. Cardy. "Conformal Invariance and Surface Critical Behavior". In: *Nucl. Phys. B* 240 (1984), pp. 514–532. DOI: 10.1016/0550-3213(84)90241-4.

[108] John L. Cardy. "Boundary conformal field theory". In: (Nov. 2004). arXiv: hep-th/0411189.

[109] Masahiro Nozaki, Tadashi Takayanagi, and Tomonori Ugajin. "Central Charges for BCFTs and Holography". In: *JHEP* 06 (2012), p. 066. DOI: 10.1007/JHEP06(2012)066. arXiv: 1205.1573 [hep-th].

[110] Marco Chiodaroli, Eric D'Hoker, and Michael Gutperle. "Simple Holographic Duals to Boundary CFTs". In: *JHEP* 02 (2012), p. 005. DOI: 10.1007/JHEP02(2012)005. arXiv: 1111.6912 [hep-th].

[111] Ofer Aharony et al. "Near-horizon solutions for D3-branes ending on 5-branes". In: *Phys. Rev. D* 84 (2011), p. 126003. DOI: 10.1103/PhysRevD.84.126003. arXiv: 1106.1870 [hep-th].

[112] Marco Chiodaroli, Eric D'Hoker, and Michael Gutperle. "Holographic duals of Boundary CFTs". In: *JHEP* 07 (2012), p. 177. DOI: 10.1007/JHEP07(2012)177. arXiv: 1205.5303 [hep-th].

[113] Hong Zhe Chen et al. "Quantum Extremal Islands Made Easy, Part II: Black Holes on the Brane". In: *JHEP* 12 (2020), p. 025. DOI: 10.1007/JHEP12(2020)025. arXiv: 2010.00018 [hep-th].

[114] Mir Afrasiar et al. "Islands for Entanglement Negativity in Communicating Black Holes". In: (May 2022). arXiv: 2205.07903 [hep-th].

[115] Moshe Rozali et al. "Information radiation in BCFT models of black holes". In: *JHEP* 05 (2020), p. 004. DOI: 10.1007/JHEP05(2020)004. arXiv: 1910.12836 [hep-th].

[116] Hong Zhe Chen et al. "Information Flow in Black Hole Evaporation". In: *JHEP* 03 (2020), p. 152. DOI: 10.1007/JHEP03(2020)152. arXiv: 1911.03402 [hep-th].

[117] Hao Geng and Andreas Karch. "Massive islands". In: *JHEP* 09 (2020), p. 121. DOI: 10.1007/JHEP09(2020)121. arXiv: 2006.02438 [hep-th].

[118] Hong Zhe Chen et al. "Quantum Extremal Islands Made Easy, Part I: Entanglement on the Brane". In: *JHEP* 10 (2020), p. 166. DOI: 10.1007/JHEP10(2020)166. arXiv: 2006.04851 [hep-th].

[119] Lisa Randall and Raman Sundrum. "A Large mass hierarchy from a small extra dimension". In: *Phys. Rev. Lett.* 83 (1999), pp. 3370–3373. DOI: 10.1103/PhysRevLett.83.3370. arXiv: hep-ph/9905221.

[120] Lisa Randall and Raman Sundrum. "An Alternative to compactification". In: *Phys. Rev. Lett.* 83 (1999), pp. 4690–4693. DOI: 10.1103/PhysRevLett.83.4690. arXiv: hep-th/9906064.

[121] Andreas Karch and Lisa Randall. "Locally localized gravity". In: *JHEP* 05 (2001). Ed. by Michael J. Duff, J. T. Liu, and J. Lu, p. 008. DOI: 10.1088/1126-6708/2001/05/008. arXiv: hep-th/0011156.

[122] Steven B. Giddings, Emanuel Katz, and Lisa Randall. "Linearized gravity in brane backgrounds". In: *JHEP* 03 (2000), p. 023. DOI: 10.1088/1126-6708/2000/03/023. arXiv: hep-th/0002091.

[123] Wyatt Reeves et al. "Looking for (and not finding) a bulk brane". In: *JHEP* 12 (2021), p. 002. DOI: 10.1007/JHEP12(2021)002. arXiv: 2108.10345 [hep-th].

[124] Masamichi Miyaji, Tadashi Takayanagi, and Tomonori Ugajin. "Spectrum of End of the World Branes in Holographic BCFTs". In: *JHEP* 06 (2021), p. 023. DOI: 10.1007/JHEP06(2021)023. arXiv: 2103.06893 [hep-th].

[125] Hao Geng et al. "Holographic BCFTs and Communicating Black Holes". In: *jhep* 08 (2021), p. 003. DOI: 10.1007/JHEP08(2021)003. arXiv: 2104.07039 [hep-th].

[126] Taishi Kawamoto et al. "Holographic local operator quenches in BCFTs". In: *JHEP* 05 (2022), p. 060. DOI: 10.1007/JHEP05(2022)060. arXiv: 2203.03851 [hep-th].

[127] Yuya Kusuki. "Analytic bootstrap in 2D boundary conformal field theory: towards braneworld holography". In: *JHEP* 03 (2022), p. 161. DOI: 10.1007/JHEP03(2022)161. arXiv: 2112.10984 [hep-th].

[128] Yuya Kusuki. "Semiclassical Gravity from Averaged Boundaries in two-dimensional BCFTs". In: (June 2022). arXiv: 2206.03035 [hep-th].

[129] Yuya Kusuki and Zixia Wei. "AdS/BCFT from Conformal Bootstrap: Construction of Gravity with Branes and Particles". In: (Oct. 2022). arXiv: 2210.03107 [hep-th].

[130] John L. Cardy. "Conformal invariance and statistical mechanics". In: *Les Houches Summer School in Theoretical Physics: Fields, Strings, Critical Phenomena*. Jan. 1989.

[131] Yosuke Imamura, Hiroshi Isono, and Yutaka Matsuo. "Boundary states in open string channel and CFT near corner". In: *Prog. Theor. Phys.* 115 (2006), pp. 979–1002. DOI: 10.1143/PTP.115.979. arXiv: hep-th/0512098.

[132] Yiming Chen, Victor Gorbenko, and Juan Maldacena. "Bra-ket wormholes in gravitationally prepared states". In: *JHEP* 02 (2021), p. 009. DOI: 10.1007/JHEP02(2021)009. arXiv: 2007.16091 [hep-th].

[133] Masamichi Miyaji. "Island for gravitationally prepared state and pseudo entanglement wedge". In: *JHEP* 12 (2021), p. 013. DOI: 10.1007/JHEP12(2021)013. arXiv: 2109.03830 [hep-th].

[134] Yoshifumi Nakata et al. "New holographic generalization of entanglement entropy". In: *Phys. Rev. D* 103.2 (2021), p. 026005. DOI: 10.1103/PhysRevD.103.026005. arXiv: 2005.13801 [hep-th].

[135] Ian Affleck and Andreas W. W. Ludwig. "Universal noninteger 'ground state degeneracy' in critical quantum systems". In: *Phys. Rev. Lett.* 67 (1991), pp. 161–164. DOI: 10.1103/PhysRevLett.67.161.

[136] Tatsuo Azeyanagi et al. "Holographic calculation of boundary entropy". In: *JHEP* 03 (2008), p. 054. DOI: 10.1088/1126-6708/2008/03/054. arXiv: 0712.1850 [hep-th].

[137] G. Hayward. "Gravitational action for space-times with nonsmooth boundaries". In: *Phys. Rev. D* 47 (1993), pp. 3275–3280. DOI: 10.1103/PhysRevD.47.3275.

[138] Tadashi Takayanagi and Kotaro Tamaoka. "Gravity Edges Modes and Hayward Term". In: *JHEP* 02 (2020), p. 167. DOI: 10.1007/JHEP02(2020)167. arXiv: 1912.01636 [hep-th].

[139] Ibrahim Akal et al. "Codimension two holography for wedges". In: *Phys. Rev. D* 102.12 (2020), p. 126007. DOI: 10.1103/PhysRevD.102.126007. arXiv: 2007.06800 [hep-th].

[140] Tokiro Numasawa and Ioannis Tsiares. "Universal dynamics of heavy operators in boundary CFT_2". In: *JHEP* 08 (2022), p. 156. DOI: 10.1007/JHEP08(2022)156. arXiv: 2202.01633 [hep-th].

[141] Matthew M. Roberts. "Time evolution of entanglement entropy from a pulse". In: *JHEP* 12 (2012), p. 027. DOI: 10.1007/JHEP12(2012)027. arXiv: 1204.1982 [hep-th].

[142] Sebastian de Haro, Sergey N. Solodukhin, and Kostas Skenderis. "Holographic reconstruction of space-time and renormalization in the AdS / CFT correspondence". In: *Commun. Math. Phys.* 217 (2001), pp. 595–622. DOI: 10.1007/s002200100381. arXiv: hep-th/0002230.

[143] Alexander B. Zamolodchikov and Alexei B. Zamolodchikov. "Liouville field theory on a pseudosphere". In: (Jan. 2001). Ed. by Evgeny A. Ivanov and Boris M. Zupnik. arXiv: hep-th/0101152.

[144] Pasquale Calabrese and John L. Cardy. "Evolution of entanglement entropy in one-dimensional systems". In: *J. Stat. Mech.* 0504 (2005), P04010. DOI: 10.1088/1742-5468/2005/04/P04010. arXiv: cond-mat/0503393.

[145] Pasquale Calabrese and John Cardy. "Entanglement entropy and conformal field theory". In: *J. Phys. A* 42 (2009), p. 504005. DOI: 10.1088/1751-8113/42/50/504005. arXiv: 0905.4013 [cond-mat.stat-mech].

[146] James Sully, Mark Van Raamsdonk, and David Wakeham. "BCFT entanglement entropy at large central charge and the black hole interior". In: *JHEP* 03 (2021), p. 167. DOI: 10.1007/JHEP03(2021)167. arXiv: 2004.13088 [hep-th].

[147] Ping Gao, Daniel Louis Jafferis, and Aron C. Wall. "Traversable Wormholes via a Double Trace Deformation". In: *JHEP* 12 (2017), p. 151. DOI: 10.1007/JHEP12(2017)151. arXiv: 1608.05687 [hep-th].

[148] Juan Maldacena and Xiao-Liang Qi. "Eternal traversable wormhole". In: (Apr. 2018). arXiv: 1804.00491 [hep-th].

[149] Johanna Erdmenger, Mario Flory, and Max-Niklas Newrzella. "Bending branes for DCFT in two dimensions". In: *JHEP* 01 (2015), p. 058. DOI: 10.1007/JHEP01(2015)058. arXiv: 1410.7811 [hep-th].

[150] Johanna Erdmenger et al. "Entanglement Entropy in a Holographic Kondo Model". In: *Fortsch. Phys.* 64 (2016), pp. 109–130. DOI: 10.1002/prop.201500099. arXiv: 1511.03666 [hep-th].

[151] Ahmed Almheiri et al. "The entropy of Hawking radiation". In: (June 2020). arXiv: 2006.06872 [hep-th].

[152] Yasunori Nomura. "From the Black Hole Conundrum to the Structure of Quantum Gravity". In: *Mod. Phys. Lett. A* 36.08 (2021), p. 2130007. DOI: 10.1142/S021773232130007X. arXiv: 2011.08707 [hep-th].

[153] Suvrat Raju. "Lessons from the Information Paradox". In: (Dec. 2020). arXiv: 2012.05770 [hep-th].

[154] Kyriakos Papadodimas and Suvrat Raju. "An Infalling Observer in AdS/CFT". In: *JHEP* 10 (2013), p. 212. DOI: 10.1007/JHEP10(2013)212. arXiv: 1211.6767 [hep-th].

[155] Kyriakos Papadodimas and Suvrat Raju. "State-Dependent Bulk-Boundary Maps and Black Hole Complementarity". In: *Phys. Rev. D* 89.8 (2014), p. 086010. DOI: 10.1103/PhysRevD.89.086010. arXiv: 1310.6335 [hep-th].

[156] Kyriakos Papadodimas and Suvrat Raju. "Remarks on the necessity and implications of state-dependence in the black hole interior". In: *Phys. Rev. D* 93.8 (2016), p. 084049. DOI: 10.1103/PhysRevD.93.084049. arXiv: 1503.08825 [hep-th].

[157] Yasunori Nomura. "Black Hole Interior in Unitary Gauge Construction". In: *Phys. Rev. D* 103.6 (2021), p. 066011. DOI: 10.1103/PhysRevD.103.066011. arXiv: 2010.15827 [hep-th].

[158] Chitraang Murdia, Yasunori Nomura, and Kyle Ritchie. "Black hole and de Sitter microstructures from a semiclassical perspective". In: *Phys. Rev. D* 107.2 (2023), p. 026016. DOI: 10.1103/PhysRevD.107.026016. arXiv: 2207.01625 [hep-th].

[159] Juan Maldacena and Leonard Susskind. "Cool horizons for entangled black holes". In: *Fortsch. Phys.* 61 (2013), pp. 781–811. DOI: 10.1002/prop.201300020. arXiv: 1306.0533 [hep-th].

[160] Marios Christodoulou and Carlo Rovelli. "How big is a black hole?" In: *Phys. Rev. D* 91.6 (2015), p. 064046. DOI: 10.1103/PhysRevD.91.064046. arXiv: 1411.2854 [gr-qc].

[161] Marios Christodoulou and Tommaso De Lorenzo. "Volume inside old black holes". In: *Phys. Rev. D* 94.10 (2016), p. 104002. DOI: 10.1103/PhysRevD.94.104002. arXiv: 1604.07222 [gr-qc].

[162] Kevin Langhoff and Yasunori Nomura. "Ensemble from Coarse Graining: Reconstructing the Interior of an Evaporating Black Hole". In: *Phys. Rev. D* 102.8 (2020), p. 086021. DOI: 10.1103/PhysRevD.102.086021. arXiv: 2008.04202 [hep-th].

[163] Daniel Louis Jafferis. "Bulk reconstruction and the Hartle-Hawking wavefunction". In: (Mar. 2017). arXiv: 1703.01519 [hep-th].

[164] Donald Marolf and Henry Maxfield. "Transcending the ensemble: baby universes, spacetime wormholes, and the order and disorder of black hole information". In: *JHEP* 08 (2020), p. 044. DOI: 10.1007/JHEP08(2020)044. arXiv: 2002.08950 [hep-th].

[165] Joydeep Chakravarty. "Overcounting of interior excitations: A resolution to the bags of gold paradox in AdS". In: *JHEP* 02 (2021), p. 027. DOI: 10.1007/JHEP02(2021)027. arXiv: 2010.03575 [hep-th].

[166] Yasunori Nomura. "Physical Theories, Eternal Inflation, and Quantum Universe". In: *JHEP* 11 (2011), p. 063. DOI: 10.1007/JHEP11(2011)063. arXiv: 1104.2324 [hep-th].

[167] Raphael Bousso and Leonard Susskind. "The Multiverse Interpretation of Quantum Mechanics". In: *Phys. Rev. D* 85 (2012), p. 045007. DOI: 10.1103/PhysRevD.85.045007. arXiv: 1105.3796 [hep-th].

[168] Yasunori Nomura. "Quantum Mechanics, Spacetime Locality, and Gravity". In: *Found. Phys.* 43 (2013), pp. 978–1007. DOI: 10.1007/s10701-013-9729-1. arXiv: 1110.4630 [hep-th].

[169] Alan H. Guth. "Inflation and eternal inflation". In: *Phys. Rept.* 333 (2000), pp. 555–574. DOI: 10.1016/S0370-1573(00)00037-5. arXiv: astro-ph/0002156.

[170] Alexander Vilenkin. "A Measure of the multiverse". In: *J. Phys. A* 40 (2007). Ed. by Joan Sola, p. 6777. DOI: 10.1088/1751-8113/40/25/S22. arXiv: hep-th/0609193.

[171] Andrei Linde. "Inflationary Cosmology after Planck 2013". In: *100e Ecole d'Ete de Physique: Post-Planck Cosmology*. 2015, pp. 231–316. DOI: 10.1093/acprof:oso/9780198728856.003.0006. arXiv: 1402.0526 [hep-th].

[172] Ben Freivogel. "Making predictions in the multiverse". In: *Class. Quant. Grav.* 28 (2011), p. 204007. DOI: 10.1088/0264-9381/28/20/204007. arXiv: 1105.0244 [hep-th].

[173] Arthur Hebecker. "Lectures on Naturalness, String Landscape and Multiverse". In: (Aug. 2020). arXiv: 2008.10625 [hep-th].

[174] Xi Dong et al. "Effective entropy of quantum fields coupled with gravity". In: *JHEP* 10 (2020), p. 052. DOI: 10.1007/JHEP10(2020)052. arXiv: 2007.02987 [hep-th].

[175] Sayantan Choudhury et al. "Circuit Complexity from Cosmological Islands". In: *Symmetry* 13.7 (2021), p. 1301. DOI: 10.3390/sym13071301. arXiv: 2012.10234 [hep-th].

[176] Hao Geng, Yasunori Nomura, and Hao-Yu Sun. "An Information Paradox and Its Resolution in de Sitter Holography". In: (Mar. 2021). arXiv: 2103.07477 [hep-th].

[177] Lars Aalsma and Watse Sybesma. "The Price of Curiosity: Information Recovery in de Sitter Space". In: *JHEP* 05 (2021), p. 291. DOI: 10.1007/JHEP05(2021)291. arXiv: 2104.00006 [hep-th].

[178] Chethan Krishnan. "Critical Islands". In: *JHEP* 01 (2021), p. 179. DOI: 10.1007/JHEP01(2021)179. arXiv: 2007.06551 [hep-th].

[179] Vijay Balasubramanian, Arjun Kar, and Tomonori Ugajin. "Islands in de Sitter space". In: *JHEP* 02 (2021), p. 072. DOI: 10.1007/JHEP02(2021)072. arXiv: 2008.05275 [hep-th].

[180] Watse Sybesma. "Pure de Sitter space and the island moving back in time". In: *Class. Quant. Grav.* 38.14 (2021), p. 145012. DOI: 10.1088/1361-6382/abff9a. arXiv: 2008.07994 [hep-th].

[181] A. Manu, K. Narayan, and Partha Paul. "Cosmological singularities, entanglement and quantum extremal surfaces". In: (Dec. 2020). arXiv: 2012.07351 [hep-th].

[182] Ben Freivogel et al. "A Holographic framework for eternal inflation". In: *Phys. Rev. D* 74 (2006), p. 086003. DOI: 10.1103/PhysRevD.74.086003. arXiv: hep-th/0606204.

[183] Leonard Susskind. "The Census taker's hat". In: (Oct. 2007). arXiv: 0710.1129 [hep-th].

[184] Yasuhiro Sekino and Leonard Susskind. "Census Taking in the Hat: FRW/CFT Duality". In: *Phys. Rev. D* 80 (2009), p. 083531. DOI: 10.1103/PhysRevD.80.083531. arXiv: 0908.3844 [hep-th].

[185] Alexander Vilenkin. "A quantum measure of the multiverse". In: *JCAP* 05 (2014), p. 005. DOI: 10.1088/1475-7516/2014/05/005. arXiv: 1312.0682 [hep-th].

[186] James Hartle and Thomas Hertog. "One Bubble to Rule Them All". In: *Phys. Rev. D* 95.12 (2017), p. 123502. DOI: 10.1103/PhysRevD.95.123502. arXiv: 1604.03580 [hep-th].

[187] J. R. Gott. "Creation of Open Universes from de Sitter Space". In: *Nature* 295 (1982), pp. 304–307. DOI: 10.1038/295304a0.

[188] Alan H. Guth and Erick J. Weinberg. "Could the Universe Have Recovered from a Slow First Order Phase Transition?" In: *Nucl. Phys. B* 212 (1983), pp. 321–364. DOI: 10.1016/0550-3213(83)90307-3.

[189] Raphael Bousso and Joseph Polchinski. "Quantization of four form fluxes and dynamical neutralization of the cosmological constant". In: *JHEP* 06 (2000), p. 006. DOI: 10.1088/1126-6708/2000/06/006. arXiv: hep-th/0004134.

[190] Shamit Kachru et al. "De Sitter vacua in string theory". In: *Phys. Rev. D* 68 (2003), p. 046005. DOI: 10.1103/PhysRevD.68.046005. arXiv: hep-th/0301240.

[191] Leonard Susskind. "The Anthropic landscape of string theory". In: (Feb. 2003). Ed. by Bernard J. Carr, pp. 247–266. arXiv: hep-th/0302219.

[192] Michael R. Douglas. "The Statistics of string / M theory vacua". In: *JHEP* 05 (2003), p. 046. DOI: 10.1088/1126-6708/2003/05/046. arXiv: hep-th/0303194.

[193] Sidney R. Coleman and Frank De Luccia. "Gravitational Effects on and of Vacuum Decay". In: *Phys. Rev. D* 21 (1980), p. 3305. DOI: 10.1103/PhysRevD.21.3305.

[194] S. W. Hawking and I. G. Moss. "Supercooled Phase Transitions in the Very Early Universe". In: *Phys. Lett. B* 110 (1982), pp. 35–38. DOI: 10.1016/0370-2693(82)90946-7.

[195] Erick J. Weinberg. "Hawking-Moss bounces and vacuum decay rates". In: *Phys. Rev. Lett.* 98 (2007), p. 251303. DOI: 10.1103/PhysRevLett.98.251303. arXiv: hep-th/0612146.

[196] Steven Weinberg. "Anthropic Bound on the Cosmological Constant". In: *Phys. Rev. Lett.* 59 (1987), p. 2607. DOI: 10.1103/PhysRevLett.59.2607.

[197] Tom Banks. "T C P, Quantum Gravity, the Cosmological Constant and All That..." In: *Nucl. Phys. B* 249 (1985), pp. 332–360. DOI: 10.1016/0550-3213(85)90020-3.

[198] Andrei D. Linde. "The Inflationary Universe". In: *Rept. Prog. Phys.* 47 (1984), pp. 925–986. DOI: 10.1088/0034-4885/47/8/002.

[199] W. G. Unruh. "Notes on black hole evaporation". In: *Phys. Rev. D* 14 (1976), p. 870. DOI: 10.1103/PhysRevD.14.870.

[200] William G. Unruh and Robert M. Wald. "What happens when an accelerating observer detects a Rindler particle". In: *Phys. Rev. D* 29 (1984), pp. 1047–1056. DOI: 10.1103/PhysRevD.29.1047.

[201] R. Brout et al. "A Primer for black hole quantum physics". In: *Phys. Rept.* 260 (1995), pp. 329–454. DOI: 10.1016/0370-1573(95)00008-5. arXiv: 0710.4345 [gr-qc].

[202] Ibrahim Akal et al. "Entanglement Entropy in a Holographic Moving Mirror and the Page Curve". In: *Phys. Rev. Lett.* 126.6 (2021), p. 061604. DOI: 10.1103/PhysRevLett.126.061604. arXiv: 2011.12005 [hep-th].

[203] Ignacio A. Reyes. "Moving Mirrors, Page Curves, and Bulk Entropies in AdS2". In: *Phys. Rev. Lett.* 127.5 (2021), p. 051602. DOI: 10.1103/PhysRevLett.127.051602. arXiv: 2103.01230 [hep-th].

[204] S. W. Hawking. "Particle Creation by Black Holes". In: *Commun. Math. Phys.* 43 (1975). Ed. by G. W. Gibbons and S. W. Hawking. [Erratum: Commun.Math.Phys. 46, 206 (1976)], pp. 199–220. DOI: 10.1007/BF02345020.

[205] Viatcheslav F. Mukhanov and G. V. Chibisov. "Quantum Fluctuations and a Nonsingular Universe". In: *JETP Lett.* 33 (1981), pp. 532–535.

[206] S. W. Hawking. "The Development of Irregularities in a Single Bubble Inflationary Universe". In: *Phys. Lett. B* 115 (1982), p. 295. DOI: 10.1016/0370-2693(82)90373-2.

[207] Alexei A. Starobinsky. "Dynamics of Phase Transition in the New Inflationary Universe Scenario and Generation of Perturbations". In: *Phys. Lett. B* 117 (1982), pp. 175–178. DOI: 10.1016/0370-2693(82)90541-X.

[208] Alan H. Guth and S. Y. Pi. "Fluctuations in the New Inflationary Universe". In: *Phys. Rev. Lett.* 49 (1982), pp. 1110–1113. DOI: 10.1103/PhysRevLett.49.1110.

[209] T. S. Bunch and P. C. W. Davies. "Quantum Field Theory in de Sitter Space: Renormalization by Point Splitting". In: *Proc. Roy. Soc. Lond. A* 360 (1978), pp. 117–134. DOI: 10.1098/rspa.1978.0060.

[210] Ben Freivogel, Gary T. Horowitz, and Stephen Shenker. "Colliding with a crunching bubble". In: *JHEP* 05 (2007), p. 090. DOI: 10.1088/1126-6708/2007/05/090. arXiv: hep-th/0703146.

[211] Spencer Chang, Matthew Kleban, and Thomas S. Levi. "When worlds collide". In: *JCAP* 04 (2008), p. 034. DOI: 10.1088/1475-7516/2008/04/034. arXiv: 0712.2261 [hep-th].

[212] Raphael Bousso and Arvin Shahbazi-Moghaddam. "Island Finder and Entropy Bound". In: (Jan. 2021). arXiv: 2101.11648 [hep-th].

[213] Raphael Bousso. "A Covariant entropy conjecture". In: *JHEP* 07 (1999), p. 004. DOI: 10.1088/1126-6708/1999/07/004. arXiv: hep-th/9905177 [hep-th].

[214] Jacob D. Bekenstein. "A Universal Upper Bound on the Entropy to Energy Ratio for Bounded Systems". In: *Phys. Rev. D* 23 (1981), p. 287. DOI: 10.1103/PhysRevD.23.287.

[215] H. Casini. "Relative entropy and the Bekenstein bound". In: *Class. Quant. Grav.* 25 (2008), p. 205021. DOI: 10.1088/0264-9381/25/20/205021. arXiv: 0804.2182 [hep-th].

[216] J. Eisert, M. Cramer, and M. B. Plenio. "Area laws for the entanglement entropy - a review". In: *Rev. Mod. Phys.* 82 (2010), pp. 277–306. DOI: 10.1103/RevModPhys.82.277. arXiv: 0808.3773 [quant-ph].

[217] Edward Witten. "APS Medal for Exceptional Achievement in Research: Invited article on entanglement properties of quantum field theory". In: *Rev. Mod. Phys.* 90.4 (2018), p. 045003. DOI: 10.1103/RevModPhys.90.045003. arXiv: 1803.04993 [hep-th].

[218] Mukund Rangamani and Tadashi Takayanagi. *Holographic Entanglement Entropy*. Vol. 931. Springer, 2017. DOI: 10.1007/978-3-319-52573-0. arXiv: 1609.01287 [hep-th].

[219] H. Casini, C. D. Fosco, and M. Huerta. "Entanglement and alpha entropies for a massive Dirac field in two dimensions". In: *J. Stat. Mech.* 0507 (2005), P07007. DOI: 10.1088/1742-5468/2005/07/P07007. arXiv: cond-mat/0505563.

[220] H. Casini and M. Huerta. "Reduced density matrix and internal dynamics for multicomponent regions". In: *Class. Quant. Grav.* 26 (2009), p. 185005. DOI: 10.1088/0264-9381/26/18/185005. arXiv: 0903.5284 [hep-th].

[221] M. Mintchev and E. Tonni. "Modular Hamiltonians for the massless Dirac field in the presence of a boundary". In: *JHEP* 03 (2021), p. 204. DOI: 10.1007/JHEP03(2021)204. arXiv: 2012.00703 [hep-th].

[222] M. Mintchev and E. Tonni. "Modular Hamiltonians for the massless Dirac field in the presence of a defect". In: *JHEP* 03 (2021), p. 205. DOI: 10.1007/JHEP03(2021)205. arXiv: 2012.01366 [hep-th].

[223] Robin Forman. "Functional determinants and geometry". In: *Inventiones mathematicae* 88 (1987), pp. 447–493. DOI: 10.1007/BF01391828.

[224] H. Falomir and E. M. Santangelo. "An alternative approach to chiral bag fermionic determinants". In: *Phys. Rev. D* 43 (1991), pp. 539–543. DOI: 10.1103/PhysRevD.43.539.

[225] M. Fuentes et al. "Bosonization rules in (1/2+1)-dimensions". In: *Nucl. Phys. B* 450 (1995), pp. 603–640. DOI: 10.1016/0550-3213(95)00224-G. arXiv: cond-mat/9502076.

[226] G. C. Levine. "Entanglement Entropy in a Boundary Impurity Model". In: *Phys. Rev. Lett.* 93 (26 Dec. 2004), p. 266402. DOI: 10.1103/PhysRevLett.93.266402.

[227] Ingo Peschel. "Entanglement entropy with interface defects". In: *Journal of Physics A: Mathematical and General* 38.20 (May 2005), pp. 4327–4335. DOI: 10.1088/0305-4470/38/20/002.

[228] Kazuhiro Sakai and Yuji Satoh. "Entanglement through conformal interfaces". In: *JHEP* 12 (2008), p. 001. DOI: 10.1088/1126-6708/2008/12/001. arXiv: 0809.4548 [hep-th].

[229] Ahmed Almheiri, Raghu Mahajan, and Juan Maldacena. "Islands outside the horizon". In: (Oct. 2019). arXiv: 1910.11077 [hep-th].

[230] Samir D. Mathur. "What is the dual of two entangled CFTs?" In: (Feb. 2014). arXiv: 1402.6378 [hep-th].

[231] Ahmed Almheiri, Raghu Mahajan, and Jorge E. Santos. "Entanglement islands in higher dimensions". In: *SciPost Phys.* 9.1 (2020), p. 001. DOI: 10.21468/SciPostPhys.9.1.001. arXiv: 1911.09666 [hep-th].

[232] Fridrik Freyr Gautason et al. "Page Curve for an Evaporating Black Hole". In: *JHEP* 05 (2020), p. 091. DOI: 10.1007/JHEP05(2020)091. arXiv: 2004.00598 [hep-th].

[233] Timothy J. Hollowood and S. Prem Kumar. "Islands and Page Curves for Evaporating Black Holes in JT Gravity". In: *JHEP* 08 (2020), p. 094. DOI: 10.1007/JHEP08(2020)094. arXiv: 2004.14944 [hep-th].

[234] Vijay Balasubramanian et al. "Geometric secret sharing in a model of Hawking radiation". In: *JHEP* 01 (2021), p. 177. DOI: 10.1007/JHEP01(2021)177. arXiv: 2003.05448 [hep-th].

[235] Louise Anderson, Onkar Parrikar, and Ronak M. Soni. "Islands with Gravitating Baths". In: (Mar. 2021). arXiv: 2103.14746 [hep-th].

[236] Hao Geng et al. "Information Transfer with a Gravitating Bath". In: (Dec. 2020). arXiv: 2012.04671 [hep-th].

[237] Chethan Krishnan, Vaishnavi Patil, and Jude Pereira. "Page Curve and the Information Paradox in Flat Space". In: (May 2020). arXiv: 2005.02993 [hep-th].

[238] Koji Hashimoto, Norihiro Iizuka, and Yoshinori Matsuo. "Islands in Schwarzschild black holes". In: *JHEP* 06 (2020), p. 085. DOI: 10.1007/JHEP06(2020)085. arXiv: 2004.05863 [hep-th].

[239] Don N. Page. "Particle Emission Rates from a Black Hole: Massless Particles from an Uncharged, Nonrotating Hole". In: *Phys. Rev. D* 13 (1976), pp. 198–206. DOI: 10.1103/PhysRevD.13.198.

[240] Finn Larsen and Frank Wilczek. "Geometric entropy, wave functionals, and fermions". In: *Annals Phys.* 243 (1995), pp. 280–298. DOI: 10.1006/aphy.1995.1100. arXiv: hep-th/9408089.

[241] Daniel N. Kabat. "Black hole entropy and entropy of entanglement". In: *Nucl. Phys. B* 453 (1995), pp. 281–299. DOI: 10.1016/0550-3213(95)00443-V. arXiv: hep-th/9503016.

[242] Ralph Roskies and Fidel Schaposnik. "Comment on Fujikawa's Analysis Applied to the Schwinger Model". In: *Phys. Rev. D* 23 (1981), pp. 558–560. DOI: 10.1103/PhysRevD.23.558.

[243] Juan Maldacena, Douglas Stanford, and Zhenbin Yang. "Conformal symmetry and its breaking in two dimensional Nearly Anti-de-Sitter space". In: *PTEP* 2016.12 (2016), p. 12C104. DOI: 10.1093/ptep/ptw124. arXiv: 1606.01857 [hep-th].

[244] P. Di Francesco, Paul H. Ginsparg, and Jean Zinn-Justin. "2-D Gravity and random matrices". In: *Phys. Rept.* 254 (1995), pp. 1–133. DOI: 10.1016/0370-1573(94)00084-G. arXiv: hep-th/9306153.

[245] Phil Saad, Stephen H. Shenker, and Douglas Stanford. "JT gravity as a matrix integral". In: (Mar. 2019). arXiv: 1903.11115 [hep-th].

[246] Stephen H. Shenker. "The Strength of nonperturbative effects in string theory". In: *Cargese Study Institute: Random Surfaces, Quantum Gravity and Strings*. Aug. 1990, pp. 809–819.

[247] Joseph Polchinski. "Combinatorics of boundaries in string theory". In: *Phys. Rev. D* 50 (1994), R6041–R6045. DOI: 10.1103/PhysRevD.50.R6041. arXiv: hep-th/9407031.

[248] Francois David. "Phases of the large N matrix model and nonperturbative effects in 2-d gravity". In: *Nucl. Phys. B* 348 (1991), pp. 507–524. DOI: 10.1016/0550-3213(91)90202-9.

[249] Emil J. Martinec. "The Annular report on noncritical string theory". In: (May 2003). arXiv: hep-th/0305148.

[250] David Kutasov et al. "Annulus amplitudes and ZZ branes in minimal string theory". In: *JHEP* 08 (2004), p. 026. DOI: 10.1088/1126-6708/2004/08/026. arXiv: hep-th/0406030.

[251] P. G. Silvestrov and A. S. Yelkhovsky. "Two-dimensional gravity as analytical continuation of the random matrix model". In: *Phys. Lett. B* 251 (1990), pp. 525–529. DOI: 10.1016/0370-2693(90)90791-4.

[252] Francois David. "Nonperturbative effects in matrix models and vacua of two-dimensional gravity". In: *Phys. Lett. B* 302 (1993), pp. 403–410. DOI: 10.1016/0370-2693(93)90417-G. arXiv: hep-th/9212106.

[253] Masanori Hanada et al. "Loops versus matrices: The Nonperturbative aspects of noncritical string". In: *Prog. Theor. Phys.* 112 (2004), pp. 131–181. DOI: 10.1143/PTP.112.131. arXiv: hep-th/0405076.

[254] Nobuyuki Ishibashi and Atsushi Yamaguchi. "On the chemical potential of D-instantons in c=0 noncritical string theory". In: *JHEP* 06 (2005), p. 082. DOI: 10.1088/1126-6708/2005/06/082. arXiv: hep-th/0503199.

[255] Akira Sato and Asato Tsuchiya. "ZZ brane amplitudes from matrix models". In: *JHEP* 02 (2005), p. 032. DOI: 10.1088/1126-6708/2005/02/032. arXiv: hep-th/0412201.

[256] Nobuyuki Ishibashi, Tsunehide Kuroki, and Atsushi Yamaguchi. "Universality of nonperturbative effects in c<1 noncritical string theory". In: *JHEP* 09 (2005), p. 043. DOI: 10.1088/1126-6708/2005/09/043. arXiv: hep-th/0507263.

[257] Ashoke Sen. "Normalization of D-instanton amplitudes". In: *JHEP* 11 (2021), p. 077. DOI: 10.1007/JHEP11(2021)077. arXiv: 2101.08566 [hep-th].

[258] Raghu Mahajan, Douglas Stanford, and Cynthia Yan. "Sphere and disk partition functions in Liouville and in matrix integrals". In: *JHEP* 07 (2022), p. 132. DOI: 10.1007/JHEP07(2022)132. arXiv: 2107.01172 [hep-th].

[259] Sergei Yu. Alexandrov, Vladimir A. Kazakov, and David Kutasov. "Nonperturbative effects in matrix models and D-branes". In: *JHEP* 09 (2003), p. 057. DOI: 10.1088/1126-6708/2003/09/057. arXiv: hep-th/0306177.

[260] Vladimir A. Kazakov and Ivan K. Kostov. "Instantons in noncritical strings from the two matrix model". In: *From Fields to Strings: Circumnavigating Theoretical Physics: A Conference in Tribute to Ian Kogan*. Mar. 2004, pp. 1864–1894. DOI: 10.1142/9789812775344_0045. arXiv: hep-th/0403152.

[261] Sidney Coleman. *Aspects of Symmetry: Selected Erice Lectures*. Cambridge, U.K.: Cambridge University Press, 1985. ISBN: 978-0-521-31827-3. DOI: 10.1017/CBO9780511565045.

[262] Paolo Gregori and Ricardo Schiappa. "From Minimal Strings towards Jackiw-Teitelboim Gravity: On their Resurgence, Resonance, and Black Holes". In: (Aug. 2021). arXiv: 2108.11409 [hep-th].

[263] Gregory W. Moore, Nathan Seiberg, and Matthias Staudacher. "From loops to states in 2-D quantum gravity". In: *Nucl. Phys. B* 362 (1991), pp. 665–709. DOI: 10.1016/0550-3213(91)90548-C.

[264] Nathan Seiberg and David Shih. "Branes, rings and matrix models in minimal (super)string theory". In: *JHEP* 02 (2004), p. 021. DOI: 10.1088/1126-6708/2004/02/021. arXiv: hep-th/0312170.

[265] J. Polchinski. *String theory. Vol. 1: An introduction to the bosonic string*. Cambridge Monographs on Mathematical Physics. Cambridge University Press, Dec. 2007. DOI: 10.1017/CBO9780511816079.

[266] Ashoke Sen. "Universality of the tachyon potential". In: *JHEP* 12 (1999), p. 027. DOI: 10.1088/1126-6708/1999/12/027. arXiv: hep-th/9911116.

[267] Martin Schnabl. "Analytic solution for tachyon condensation in open string field theory". In: *Adv. Theor. Math. Phys.* 10.4 (2006), pp. 433–501. DOI: 10.4310/ATMP.2006.v10.n4.a1. arXiv: hep-th/0511286.

[268] John L. Cardy. "Boundary Conditions, Fusion Rules and the Verlinde Formula". In: *Nucl. Phys. B* 324 (1989), pp. 581–596. DOI: 10.1016/0550-3213(89)90521-X.

[269] A. Rocha-Caridi. "Vacuum Vector Representations of the Virasoro Algebra". In: *Vertex Operators in Mathematics and Physics*. Ed. by J. Lepowsky, S. Mandelstam, and I. M. Singer. New York, NY: Springer US, 1985, pp. 451–473. ISBN: 978-1-4613-9550-8.

[270] P. Di Francesco, P. Mathieu, and D. Senechal. *Conformal Field Theory*. Graduate Texts in Contemporary Physics. New York: Springer-Verlag, 1997. DOI: 10.1007/978-1-4612-2256-9.

[271] Edward Witten. "Noncommutative Geometry and String Field Theory". In: *Nucl. Phys. B* 268 (1986), pp. 253–294. DOI: 10.1016/0550-3213(86)90155-0.

[272] Michael R. Douglas. "The Two matrix model". In: *Cargese Study Institute: Random Surfaces, Quantum Gravity and Strings*. 1990.

[273] J. M. Daul, V. A. Kazakov, and I. K. Kostov. "Rational theories of 2-D gravity from the two matrix model". In: *Nucl. Phys. B* 409 (1993), pp. 311–338. DOI: 10.1016/0550-3213(93)90582-A. arXiv: hep-th/9303093.

[274] Nathan Seiberg and David Shih. "Minimal string theory". In: *Comptes Rendus Physique* 6 (2005), pp. 165–174. DOI: 10.1016/j.crhy.2004.12.007. arXiv: hep-th/0409306.

[275] Bruno Balthazar, Victor Rodriguez, and Xi Yin. "Multi-Instanton Calculus in $c = 1$ String Theory". In: (Dec. 2019). arXiv: 1912.07170 [hep-th].

[276] Bruno Balthazar, Victor A. Rodriguez, and Xi Yin. "The S-Matrix of 2D Type 0B String Theory Part 2: D-Instanton Effects". In: (Apr. 2022). arXiv: 2204.01747 [hep-th].

[277] Ashoke Sen. "Normalization of type IIB D-instanton amplitudes". In: *JHEP* 12 (2021), p. 146. DOI: 10.1007/JHEP12(2021)146. arXiv: 2104.11109 [hep-th].

[278] Sergei Alexandrov, Ashoke Sen, and Bogdan Stefański. "D-instantons in Type IIA string theory on Calabi-Yau threefolds". In: *JHEP* 11 (2021), p. 018. DOI: 10.1007/JHEP11(2021)018. arXiv: 2108.04265 [hep-th].

[279] Sergei Alexandrov, Ashoke Sen, and Bogdan Stefański. "Euclidean D-branes in type IIB string theory on Calabi-Yau threefolds". In: *JHEP* 12 (2021), p. 044. DOI: 10.1007/JHEP12(2021)044. arXiv: 2110.06949 [hep-th].

[280] Sergei Alexandrov et al. "D-instanton Induced Superpotential". In: (Apr. 2022). arXiv: 2204.02981 [hep-th].

[281] Nathan B. Agmon et al. "D-instanton Effects in Type IIB String Theory". In: (May 2022). arXiv: 2205.00609 [hep-th].

[282] Marcos Marino, Ricardo Schiappa, and Marlene Weiss. "Nonperturbative Effects and the Large-Order Behavior of Matrix Models and Topological Strings". In: *Commun. Num. Theor. Phys.* 2 (2008), pp. 349–419. DOI: 10.4310/CNTP.2008.v2.n2.a3. arXiv: 0711.1954 [hep-th].

[283] Marcos Marino, Ricardo Schiappa, and Marlene Weiss. "Multi-Instantons and Multi-Cuts". In: *J. Math. Phys.* 50 (2009), p. 052301. DOI: 10.1063/1.3097755. arXiv: 0809.2619 [hep-th].

[284] Marcos Mariño. "Lectures on non-perturbative effects in large N gauge theories, matrix models and strings". In: *Fortsch. Phys.* 62 (2014), pp. 455–540. DOI: 10.1002/prop.201400005. arXiv: 1206.6272 [hep-th].

[285] Gerald V. Dunne and Mithat Ünsal. "What is QFT? Resurgent trans-series, Lefschetz thimbles, and new exact saddles". In: *PoS* LATTICE2015 (2016), p. 010. DOI: 10.22323/1.251.0010. arXiv: 1511.05977 [hep-lat].

[286] Inês Aniceto, Gokce Basar, and Ricardo Schiappa. "A Primer on Resurgent Transseries and Their Asymptotics". In: *Phys. Rept.* 809 (2019), pp. 1–135. DOI: 10.1016/j.physrep.2019.02.003. arXiv: 1802.10441 [hep-th].

[287] Ashoke Sen and Barton Zwiebach. "Tachyon condensation in string field theory". In: *JHEP* 03 (2000), p. 002. DOI: 10.1088/1126-6708/2000/03/002. arXiv: hep-th/9912249.

[288] Theodore Erler and Carlo Maccaferri. "String field theory solution for any open string background. Part II". In: *JHEP* 01 (2020), p. 021. DOI: 10.1007/JHEP01(2020)021. arXiv: 1909.11675 [hep-th].

[289] Ashoke Sen. "SO(32) spinors of type I and other solitons on brane - anti-brane pair". In: *JHEP* 09 (1998), p. 023. DOI: 10.1088/1126-6708/1998/09/023. arXiv: hep-th/9808141.

[290] Edward Witten. "D-branes and K theory". In: *JHEP* 12 (1998), p. 019. DOI: 10.1088/1126-6708/1998/12/019. arXiv: hep-th/9810188.

[291] Nathan Berkovits, Ashoke Sen, and Barton Zwiebach. "Tachyon condensation in superstring field theory". In: *Nucl. Phys. B* 587 (2000), pp. 147–178. DOI: 10.1016/S0550-3213(00)00501-0. arXiv: hep-th/0002211.

[292] Ricardo Schiappa and Ricardo Vaz. "The Resurgence of Instantons: Multi-Cut Stokes Phases and the Painleve II Equation". In: *Commun. Math. Phys.* 330 (2014), pp. 655–721. DOI: 10.1007/s00220-014-2028-7. arXiv: 1302.5138 [hep-th].

[293] Ashoke Sen. "Muti-instanton amplitudes in type IIB string theory". In: *JHEP* 12 (2021), p. 065. DOI: 10.1007/JHEP12(2021)065. arXiv: 2104.15110 [hep-th].

[294] Marcos Marino. *Chern-Simons Theory, Matrix Models, and Topological Strings*. International series of monographs on physics. Clarendon Press, 2005. ISBN: 9780198568490.

[295] E. Brezin et al. "Planar Diagrams". In: *Commun. Math. Phys.* 59 (1978), p. 35. DOI: 10.1007/BF01614153.

[296] Jan Ambjørn et al. "Matrix model calculations beyond the spherical limit". In: *Nucl. Phys. B* 404 (1993). [Erratum: Nucl.Phys.B 449, 681–681 (1995)], pp. 127–172. DOI: 10.1016/0550-3213(93)90476-6. arXiv: hep-th/9302014.

[297] Jan Ambjorn, J. Jurkiewicz, and Yu. M. Makeenko. "Multiloop correlators for two-dimensional quantum gravity". In: *Phys. Lett. B* 251 (1990), pp. 517–524. DOI: 10.1016/0370-2693(90)90790-D.

[298] Bertrand Eynard, Taro Kimura, and Sylvain Ribault. "Random matrices". In: (Oct. 2015). arXiv: 1510.04430 [math-ph].

[299] D. Bessis, C. Itzykson, and J. B. Zuber. "Quantum field theory techniques in graphical enumeration". In: *Adv. Appl. Math.* 1 (1980), pp. 109–157. DOI: 10.1016/0196-8858(80)90008-1.

[300] Nicholas M Ercolani and KDT-R McLaughlin. "Asymptotics of the partition function for random matrices via Riemann-Hilbert techniques and applications to graphical enumeration". In: *International Mathematics Research Notices* 2003.14 (2003), pp. 755–820.

[301] Harish-Chandra. "Differential Operators on a Semisimple Lie Algebra". In: *Am. J. Math.* 79.1 (1957), p. 87. DOI: 10.2307/2372387.

[302] C. Itzykson and J. B. Zuber. "The Planar Approximation. 2." In: *J. Math. Phys.* 21 (1980), p. 411. DOI: 10.1063/1.524438.

[303] Paul Zinn-Justin and J. B. Zuber. "On some integrals over the U(N) unitary group and their large N limit". In: *J. Phys. A* 36 (2003), pp. 3173–3194. DOI: 10.1088/0305-4470/36/12/318. arXiv: math-ph/0209019.

[304] M. L. Mehta. "A Method of Integration Over Matrix Variables". In: *Commun. Math. Phys.* 79 (1981), pp. 327–340. DOI: 10.1007/BF01208498.

[305] B. Eynard. "Large N expansion of the 2 matrix model". In: *JHEP* 01 (2003), p. 051. DOI: 10.1088/1126-6708/2003/01/051. arXiv: hep-th/0210047.

[306] M. Bertola. "Free energy of the two matrix model / dToda tau function". In: *Nucl. Phys. B* 669 (2003), pp. 435–461. DOI: 10.1016/j.nuclphysb.2003.07.029. arXiv: hep-th/0306184.

[307] Ashoke Sen. "D-instantons, string field theory and two dimensional string theory". In: *JHEP* 11 (2021), p. 061. DOI: 10.1007/JHEP11(2021)061. arXiv: 2012.11624 [hep-th].

[308] Joydeep Chakravarty and Ashoke Sen. "Normalization of D instanton amplitudes in two dimensional type 0B string theory". In: *JHEP* 02 (2023), p. 170. DOI: 10.1007/JHEP02(2023)170. arXiv: 2207.07138 [hep-th].

[309] Ashoke Sen. "Infrared finite semi-inclusive cross section in two dimensional type 0B string theory". In: *JHEP* 04 (2023), p. 101. DOI: 10.1007/JHEP04(2023)101. arXiv: 2208.07385 [hep-th].

[310] Bruno Balthazar, Victor A. Rodriguez, and Xi Yin. "Unpublished". In: (2020).

[311] A. Zamolodchikov. "Higher equations of motion in Liouville field theory". In: *Int. J. Mod. Phys. A* 19S2 (2004). Ed. by A. Belavin and Edward Corrigan, pp. 510–523. DOI: 10.1142/S0217751X04020592. arXiv: hep-th/0312279.

[312] Alexei B. Zamolodchikov. "Three-point function in the minimal Liouville gravity". In: *Theor. Math. Phys.* 142 (2005), pp. 183–196. DOI: 10.1007/s11232-005-0003-3. arXiv: hep-th/0505063.

[313] Alexander Belavin and Alexei Zamolodchikov, eds. *Polyakov's string: Twenty five years after. Proceedings*. Oct. 2005. arXiv: hep-th/0510214.

[314] A. A. Belavin and A. B. Zamolodchikov. "On Correlation Numbers in 2D Minimal Gravity and Matrix Models". In: *J. Phys. A* 42 (2009), p. 304004. DOI: 10.1088/1751-8113/42/30/304004. arXiv: 0811.0450 [hep-th].

[315] A. Artemev and A. Belavin. "Five-point correlation numbers in minimal Liouville gravity and matrix models". In: *Nucl. Phys. B* 985 (2022), p. 116019. DOI: 10.1016/j.nuclphysb.2022.116019. arXiv: 2207.01665 [hep-th].

[316] Paul H. Ginsparg and Jean Zinn-Justin. "Large order behavior of nonperturbative gravity". In: *Phys. Lett. B* 255 (1991), pp. 189–196. DOI: 10.1016/0370-2693(91)90234-H.

[317] Joseph Polchinski. "Combinatorics of boundaries in string theory". In: *Phys. Rev. D* 50 (1994), R6041–R6045. DOI: 10.1103/PhysRevD.50.R6041. arXiv: hep-th/9407031.

[318] Ashoke Sen. "D-instanton Perturbation Theory". In: *JHEP* 08 (2020), p. 075. DOI: 10.1007/JHEP08(2020)075. arXiv: 2002.04043 [hep-th].

[319] F. David. "Conformal Field Theories Coupled to 2D Gravity in the Conformal Gauge". In: *Mod. Phys. Lett. A* 3 (1988), p. 1651. DOI: 10.1142/S0217732388001975.

[320] Jacques Distler and Hikaru Kawai. "Conformal Field Theory and 2D Quantum Gravity". In: *Nucl. Phys. B* 321 (1989), pp. 509–527. DOI: 10.1016/0550-3213(89)90354-4.

[321] V. G. Knizhnik, Alexander M. Polyakov, and A. B. Zamolodchikov. "Fractal Structure of 2D Quantum Gravity". In: *Mod. Phys. Lett. A* 3 (1988). Ed. by I. M. Khalatnikov and V. P. Mineev, p. 819. DOI: 10.1142/S0217732388000982.

[322] Barton Zwiebach. "Closed string field theory: Quantum action and the B-V master equation". In: *Nucl. Phys. B* 390 (1993), pp. 33–152. DOI: 10.1016/0550-3213(93)90388-6. arXiv: hep-th/9206084.

[323] Barton Zwiebach. "Oriented open - closed string theory revisited". In: *Annals Phys.* 267 (1998), pp. 193–248. DOI: 10.1006/aphy.1998.5803. arXiv: hep-th/9705241.

[324] Corinne de Lacroix et al. "Closed Superstring Field Theory and its Applications". In: *Int. J. Mod. Phys. A* 32.28n29 (2017), p. 1730021. DOI: 10.1142/S0217751X17300216. arXiv: 1703.06410 [hep-th].